ACTA UNIVERSITATIS SZEGEDIENSIS

ACTA PHYSICA ET CHEMICA

NOVA SERIES

TOMUS XXIII FASCICULUS 4

AUSHAF 23 (4) 365—524 (1977)
HU ISSN 0001—6721

SZEGED, HUNGARIA
1977

ACTA UNIVERSITATIS SZEGEDIENSIS

ACTA PHYSICA ET CHEMICA

NOVA SERIES

TOMUS XXIII FASCICULUS 4

AUSHAF 23 (4) 365—524 (1977)
HU ISSN 0001—6721

SZEGED, HUNGARIA
1977

SUBNANOSECOND RELAXATION OSCILLATIONS IN NITROGEN LASER PUMPED DYE-LASERS

By

B. RÁCZ, ZS. BOR, G. SZABÓ and CS. ZOLTÁN

Institute of Experimental Physics, Attila József University, Szeged

(Received June 1, 1977)

A four-level kinetic dye-laser model was investigated using N_2 laser pumping. The damped oscillation of dye-lasers and the generation of subnanosecond pulses are investigated theoretically and experimentally. The numerical solutions of coupled rate equations are in good qualitative agreement with experimental data.

An ever increasing number of laser applications demand light sources emitting subnanosecond pulses. The best known method to achieve subnanosecond pulses is mode-locking. In this paper a theoretical calculation is presented for studying the kinetic properties of nitrogen laser-pumped dye-lasers and conditions of damped subnanosecond oscillation are given. The rate equations of organic dye-lasers and the solutions for different cases are well known [1—3]. We are applying the equations given by ATKINSON and PACE [3]. The energy levels (involved in lasing) of an organic dye are schematically depicted in Fig. 1. (1 is the singlet ground, 2 is the first excited singlet, T and 3 are triplet states). Each electronic state consists of a set of vibrational (heavy lines) and rotational (light lines) sublevels. The radiative transitions are denoted by solid, the nonradiative transitions by wavy, and the forbidden transitions by dashed lines. The rate equations can be written as follows,

$$\frac{dn_m}{dt} = n_m\left[\left(n_2\sigma(\lambda) - n_T\sigma_{TT}(\lambda) - n_1\sigma_{ss}(\lambda)\right)\frac{Fc}{\eta} - \frac{1}{\tau_m}\right] + \frac{Fcn_2\sigma(\lambda)}{\eta V}, \tag{1}$$

$$\frac{dn_2}{dt} = W_2 n_1 - \frac{n_2}{\tau} - \sum_m n_2 n_m \sigma(\lambda)\frac{c}{\eta} + \sum_m n_1 n_m \sigma_{ss}(\lambda)\frac{c}{\eta}, \tag{2}$$

$$\frac{dn_T}{dt} = kn_2 - \frac{n_T}{\tau_T} - \sum_m n_T n_m \sigma_{TT}(\lambda)\frac{c}{\eta} + \frac{n_3}{\tau_3}, \tag{3}$$

$$\frac{dn_3}{dt} = \sum_m n_T n_m \sigma(\lambda)\frac{c}{\eta} - \frac{n_3}{\tau_3}, \tag{4}$$

$$n = n_1 + n_2 + n_T + n_3. \tag{5}$$

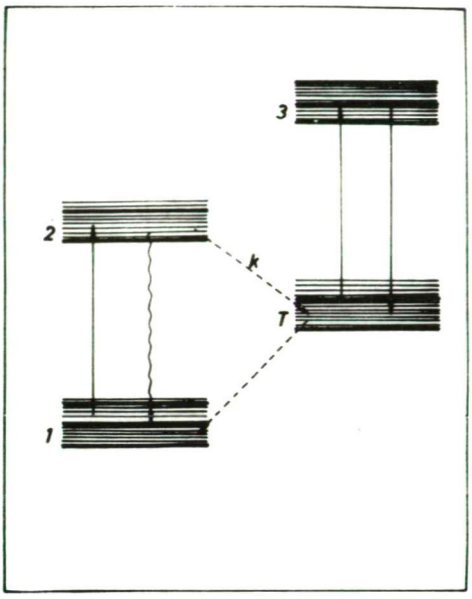

Fig. 1. Energy levels of a typical dye

Here we used the following notation: n_m is the photon number in mode m, n_1, n_2, n_T, and n_3 are the population densities of the 1, 2, T, and 3 levels, V is the volume of cavity, c is the velocity of light, η is the refractive index of the solution, $\sigma(\lambda)$, $\sigma_{ss}(\lambda)$, $\sigma_{TT}(\lambda)$ are the cross sections of stimulated emission, singlet-singlet absorbtion, and triplet-triplet absorption, τ_m is the cavity lifetime, $W_2 n_1$ is the term of optical excitation, τ, τ_T, τ_3 are lifetimes of states 2, T and 3, k is the intersystem crossing rate, n is the concentration of dye molecules.

Let us assume that densities are uniform throughout the medium, and $F \cdot V$ denotes the volume of that part of the cavity which is filled by the lasing solution. We shall rewrite Eqs. (1)—(5) because the magnitude of k is the order of 10^7 [4]. In case of N_2 laser pumping, where the pulsewidth is less than 10 nsec, the first triplet state T cannot have considerable population, consequently the triplet-triplet absorption is negligible, so Eqs. (3) and (4) and the second term $\left(n_m n_T \sigma(\lambda)_{TT} \frac{Fc}{\eta}\right)$ in Eq. (1) can be omitted. Let us further assume that the singlet-excited singlet -state absorbtion is negligible (it is a reasonable assumption in the case of many dyes), and there is no coupling between modes (in mathematical terms the differential equations are separable), and the photon number is uniformly distributed among modes.

This way we get

$$\frac{dn_m}{dt} = n_m \left(n_2 \frac{\sigma(\lambda) Fc}{\eta} - \frac{1}{\tau_m} \right) + \frac{Fc\sigma(\lambda)}{\eta V}, \tag{6}$$

$$\frac{dn_2}{dt} = W_2 n_1 - \frac{n_2}{\tau} + n_2 n_m \frac{m\sigma(\lambda) c}{\eta}. \tag{7}$$

Using the following notation

$$n_0 = \frac{1/\tau_m}{(N_m+1)\dfrac{\sigma(\lambda) Fc}{\eta}}, \quad y = \frac{n_2}{n_0}, \quad q = N_m,$$

$$b = \frac{m}{VN_0}, \quad W = \frac{W_2 n_1 \tau_m}{n_0}, \quad a = \frac{\tau_m}{\tau}, \quad x = \frac{t}{\tau_m},$$

our equations can be simply written as follows:

$$\frac{dq}{dx} = q(y-1)+y, \tag{8}$$

$$\frac{dy}{dx} = W-y(a+bq). \tag{9}$$

According to ATKINSON and PACE [3] the cavity lifetime is equal to the following expression

$$\tau_m = \frac{2L}{c\ln(R_1R_2)},$$

where R_1 and R_2 are the reflectivity of mirrors, and L is the length of the cavity. Conditions of damped-relaxation oscillation can be determined by applying small-signal analysis. If the pumping rate is constant, the laser should reach steady state, *i. e.*

$$\frac{dy}{dx} = \frac{dq}{dx} = 0 \quad \text{and} \quad q = q_0 = \frac{W_0-a}{b}, \quad y = y_0 \approx 1.$$

If the laser departs from the steady state by y^* and q^* $y^* \ll 1$, $q^* \ll q_0$ we obtain from Eqs. (8) and (9) by substituing $y=y_0+y^*$ and $q=q_0+q^*$,

$$\frac{d^2y^*}{dx^2}+W\frac{dy^*}{dx}+(W-a)y^* = 0, \tag{10}$$

$$\frac{d^2q^*}{dx^2}+W\frac{dq^*}{dx}+(W-a)q^* = 0. \tag{11}$$

These differential equations describe the damped-relaxation oscillation. Note that these differential equations have periodical solutions providing that $\omega = \sqrt{W-a\frac{W^2}{4}}$ is real. Therefore, we may write

$$y^* = A_y \exp\left(-\frac{W}{2}x\right)\cos\left[\left(\sqrt{W-a-\frac{W^2}{4}}\right)x\right]$$

A_y is determined by the initial conditions. (A similar equation holds for q^*.) For periodical solution it is necessary that $q \leqq 1$, which means: $\tau_m \leqq \tau$. The reason why relaxation oscillation did not occur was that $\frac{\tau_m}{\tau} \ll 1$ was not satisfied [1, 4]. Eqs. (8), (9) were solved by an R—40 computer with the Runge—Kutta method.

The pumping pulse was approximated as follows:

$$W = p \cdot 3.46 \cdot 10^{-4} x^{2.7} \exp(-5.18 \cdot 10^{-2} x)$$

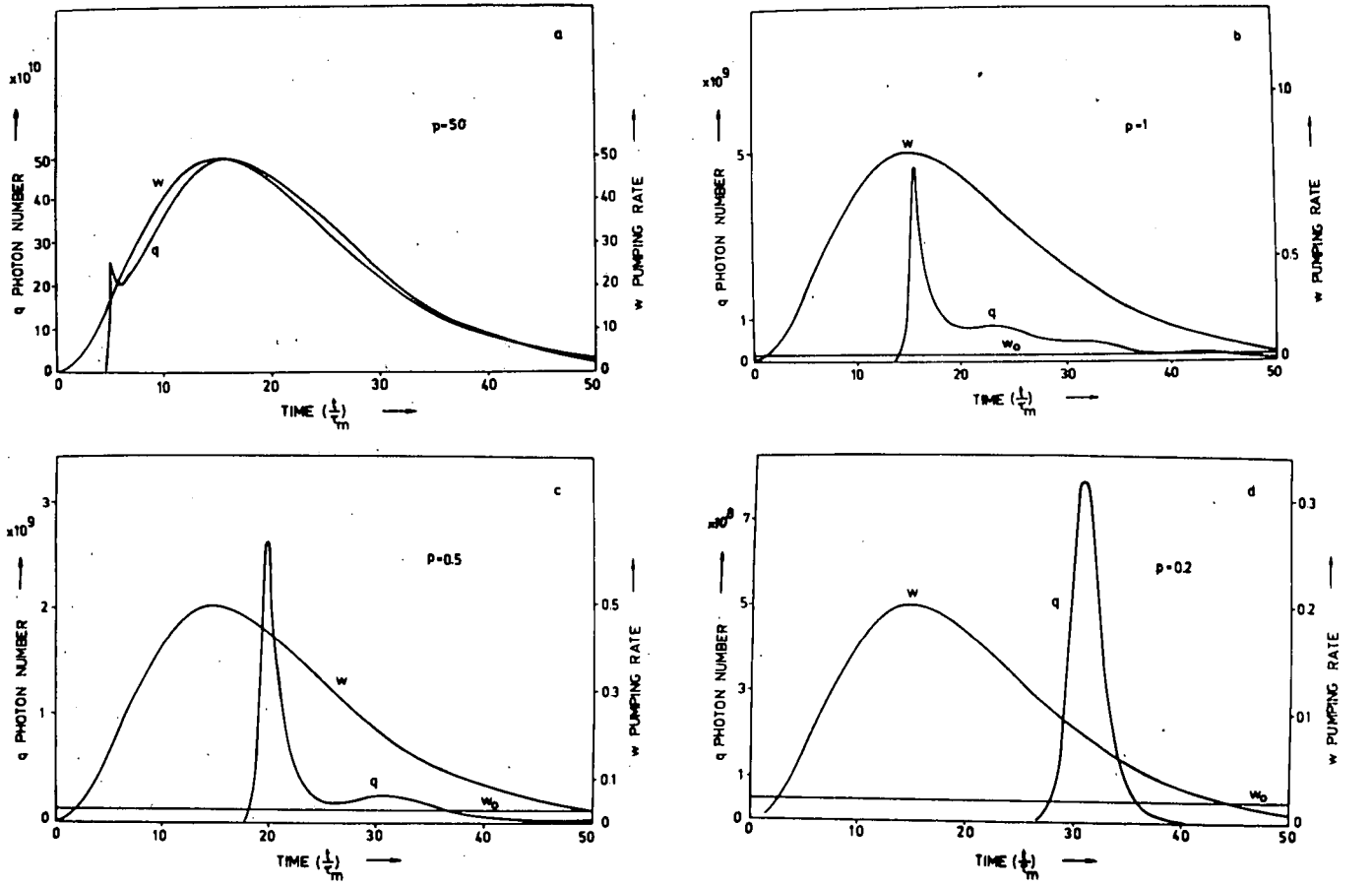

Fig. 2. Numerical solution of coupled-rate equations at the following parameters: $\tau_m = 150$ psec, $\tau = 5.5$ nsec, $b = 2.882 \cdot 10^{-10}$ and (*a*) $W_{max} = 50$, (*b*) $W_{max} = 1$, (*c*) $W_{max} = 0.5$, (*d*) $W_{max} = 0.2$

LIN carried out similar calculations approximating the pumping pulses by trapesoidal function [5]. For calculations the following parameters were used:

$$\tau_m = 150p \text{ sec} \quad p = 0.2, 0.5, 1, 50$$

$$\tau_m = 42.3p \text{ sec} \quad p = 0.05, 0.1, 0.2, 50$$

(42.3 psec was the smallest that we could realize experimentally). Fig. 2 *a* shows that, at high pumping levels, the numerical solution is in agreement with the experi-

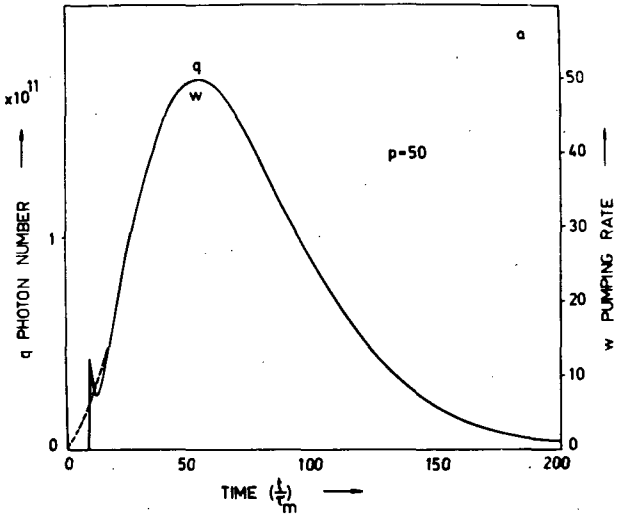

a)

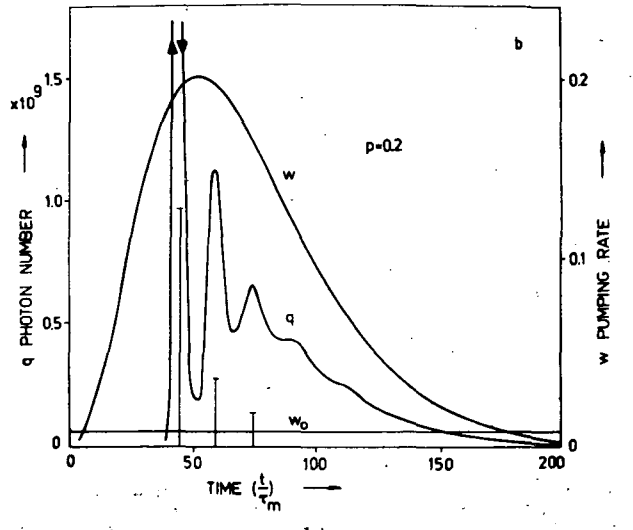

b)

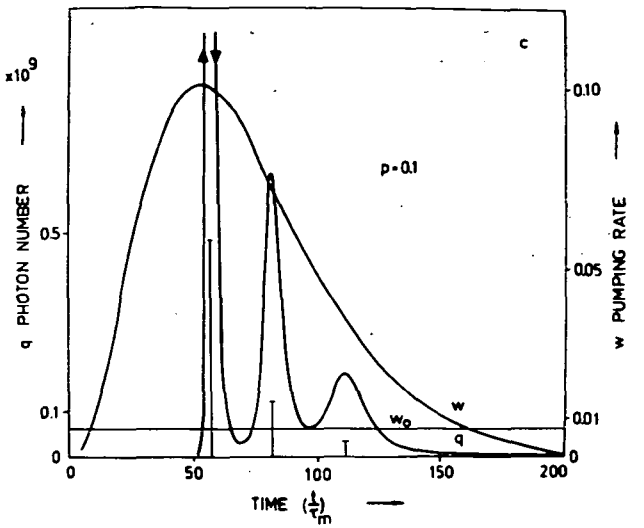

c)

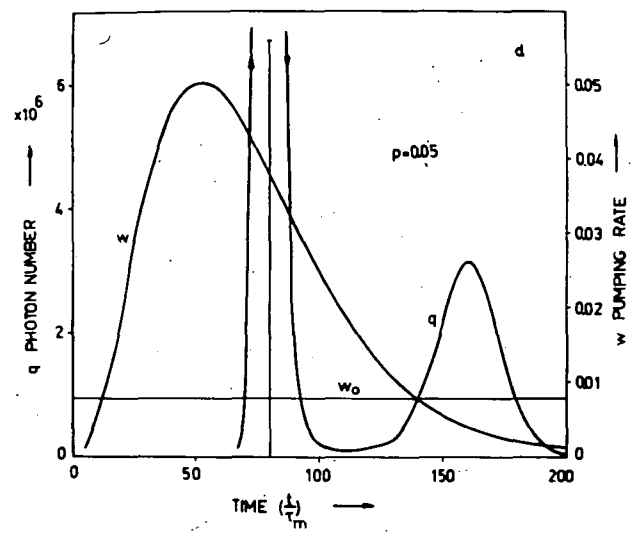

d)

Fig. 3. Numerical solutions of coupled-rate equations at the following parameters: $\tau_m = 43.2$ psec, $\tau = 5.5$ nsec, $b = 8.479 \cdot 10^{-9}$ and (*a*) $W_{max} = 50$, (*b*) $W_{max} = 0.2$, (*c*) $W_{max} = 0.1$, (*d*) $W_{max} = 0.05$

mental results [1, 2, 4]. Fig. 2*b* shows the output pulse in the case of strongly damped relaxation oscillation. As shown above damping is proportional to $W/2$. In Figs. 2*c* and 2*d* the case of small damping is given, and there is no oscillation, because the pumping intensity has been dropped before the evolution of the second pulse.

In Fig. 2*d* there is a single pulse of very low intensity. By decreasing the cavity lifetime the width of pumping pulse is relatively increased, because it is measured in τ_m units. In Figs. 3*a*–3*d* the solutions for 43.2 psec cavity lifetime are shown. Fig 3*a*, Figs. 3*b*, 3*c* how definite relaxation oscillation. It can be seen that on decreasing τ_m the pulsewidth was also decreased *e.g.* the initial pulsewidth in Fig. 2*d* is about 1.2 nsec, while in Fig. 3*b* it is about 0.4 nsec. By changing the pumping intensity and the cavity lifetime the required subnanosecond pulses could be produced [6].

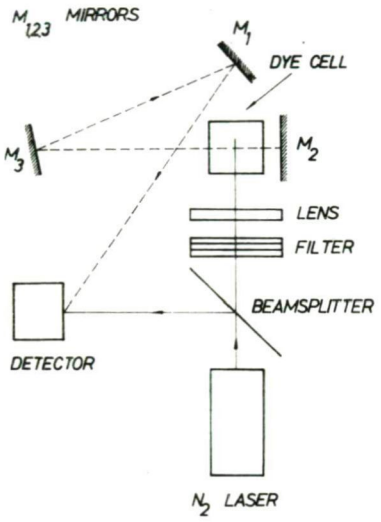

Fig. 4. Experimental arrangement

Our experimental arrangement is shown in Fig. 4. The pumping source was a N_2 laser [7] operating at 3371 Å with a typical output power of 0.2 MW, pulse duration of 6 nsec, and repetition rate of 50 pps. The pumping beam was focused by a cylindrical lens onto the front window of the dye cell, containing a $5 \cdot 10^{-3}$ mole/l ethanol solution of Rhodamine 6G. The cavity was formed by the cell wall and mirror M_3. The detector was a FEK—15 KM-type biplanar photodiode, with 500 psec risetime. The output was monitored by a I 2—7-type travelling-wave oscilloscope, or a S7—8-type sampling oscilloscope. The experimental results are summarized in Figs. 5—6. Fig. 5 shows the signal on a travelling-wave oscilloscope; here the dye laser signal was delayed by M_1 and M_2 mirrors. Peaks in the dye laser pulse can be very well seen. Fig. 6*a* shows a typical N_2 laser pulse, Figs. 6*b* and *c* shows typical dye laser pulses at high and low pumping level, respectively. These results are in good qualitative agreement with our theoretical calculations.

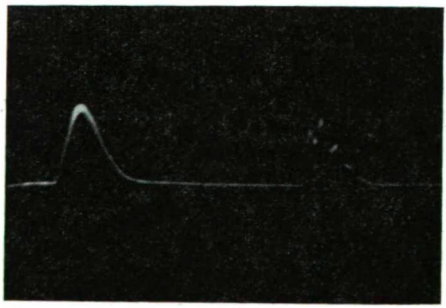

Fig. 5. Time behaviour of N_2 laser (*a*) and dye-laser oscillation (*b*)

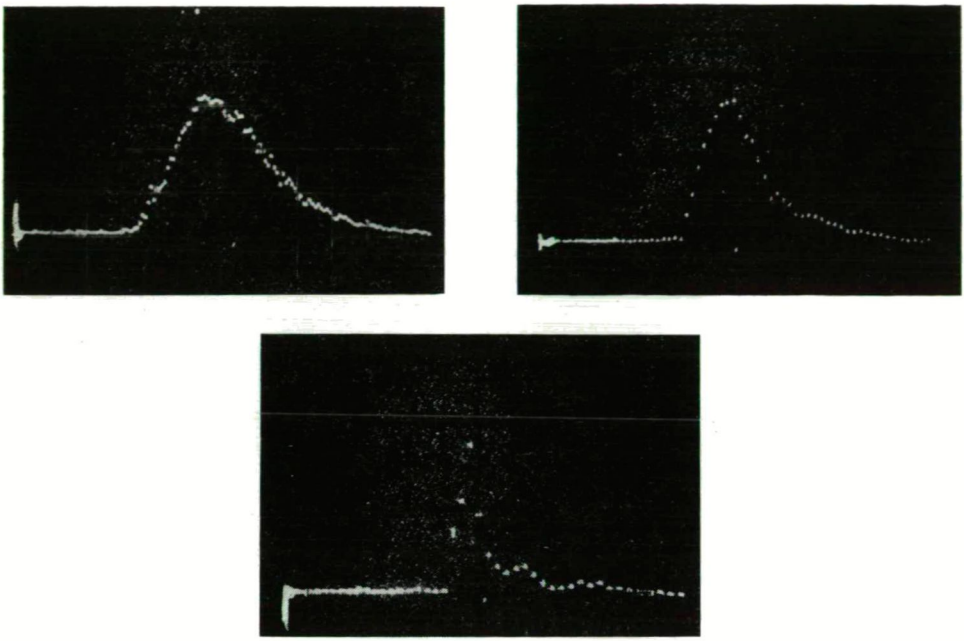

Fig. 6. Oscillograms of N_2 laser (*a*), dye laser at high pumping level (*b*) and dye laser at low pumping level (*c*). Sweep speed 2 nsec/div, risetime of photodiode 500 psec

References

[1] *Sorokin, P. P., J. R. Lankard, V. L. Moruzzi, E. C. Hammond:* J. Chem. Phys. **58,** 4726 (1967).
[2] *Weber, M. J., M. Bass:* IEEE J. Quantum Electronics **QE—5,** 175 (1969).
[3] *Atkinson, J. B., F. P. Pace:* IEEE J. Quantum Electronics **QE—9,** 569 (1973).
[4] *Schäfer, F. P.:* dye Lasers, Springer Verlag, Berlin, Heidelberg, New York, 1974.
[5] *Lin, Ch.:* IEEE J. Quantum Electronics **QE—11,** 602 (1975).
[6] *Salzmann, H., H. Strohwald:* Phys. Letters **57. A,** 41 (1976).
[7] *Ketskeméty, I., B. Rácz, Zs. Bor, L. Kozma:* Acta Tech. Hung. **80,** 55 (1975).

СУБНАНОСЕКУНДНЫЕ РЕЛАКСАЦИОННЫЕ ОСЦИЛЛЯЦИИ В ЛАЗЕРАХ НА КРАСИТЕЛЯХ ПРИ НАКАЧКЕ АЗОТНЫМ ЛАЗЕРОМ

Б. Рац, Ж. Бор, Г. Сабо и Ч. Золтан

Рассматривается кинетическая четырехуровневая модель лазера на красителе, возбуждаемого азотным лазером. Теоретически и экспериментально исследованы затухающие осцилляции и генерация субнаносекундных импульсов в лазере на красителях. Численные результаты решений уравнений скоростей и экспериментальные данные находятся в хорошем согласии.

EXCITATION ENERGY TRANSFER IN MULTI-COMPONENT LUMINESCENT SOLUTIONS

By

I. KETSKEMÉTY

Institute of Experimental Physics, Attila Jozsef University, Szeged

and

J. KUŠBA

Institute of Physics, Technical University, Gdansk, Poland

(Received April 10, 1977)

Based on the paper of BUDÓ and KETSKEMÉTY we derived a general equation which describes the shape of the fluorescence spectrum of multi-component solutions as a function of the emission-, absorption- and quantum yield spectrum of each component. Both radiative and non-radiative excitation energy transfers were taken into account. This equation is discussed for the cases of one-, two- and three-component solutions.

The problem of excitation energy transfer in luminescent multi-component solutions appears frequently in the literature. In many cases [1—7] considerable enhancement of the generated energy of dye lasers could be achieved by applying multicomponent systems. Recent experiments [8] threw light onto the excitation energy migration in the phycoerythrin — phycocyanin — chlorophyll *a* system of plant chloroplasts. More detailed chromatographic investigations revealed that some dyes, widely applied to luminescence investigations are, in fact, mixtures of several components. Thus, the problem of luminescence of multi-component solutions can be regarded as a theoretical and experimental topic [9—12].

Radiative energy transfer in multi-component solutions

The general equations which describe the shape of the fluorescence spectrum of a two- and three-component solution was given in our previous papers [9—11]. These expressions take into account the influence of reabsorption and secondary emission on the shape of the spectrum but neglect the contribution of higher order emissions as small one. Quite recently we demonstrated [12] that emission of at least third order should be additionally taken into account to obtain satisfactory agreement with certain experimental data.

These expressions can be generalized for arbitrary number of components under the same assumptions and formalism as given elsewhere [9, 13]. Let us assume that the luminescence of an n-component solution will be excited by a parallel light-

beam with a cross-section of $R^2\pi$, perpendicular to the front face of the sample. The luminescence light will be reversely directed starting from the centre of the excitation region. Its crosssection is small as compared to $R^2\pi$ and, thus, when computing the intensity of the fluorescence we can limit ourselves to the direct neighbourhood of the straight line which passes through the central point of the

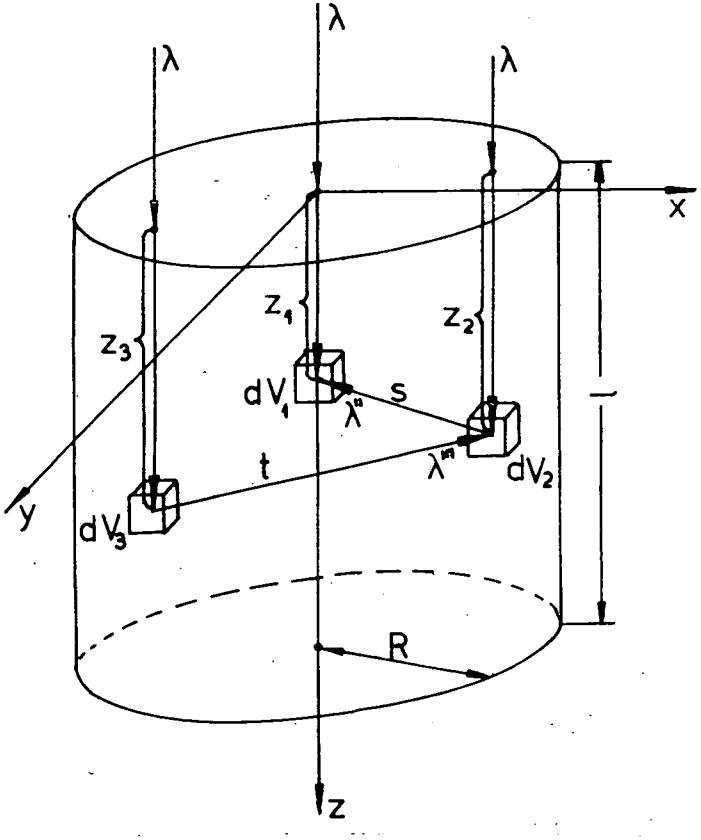

Fig. 1.

excitation region. In this case the illuminated part of the solution forms a cylinder (base radius R and height = the thickness of the sample $-l$) whose axis coincides with the z-axis of the coordinate system $Oxyz$ (Fig. 1). The exciting light which enters the solution has an intensity of E_λ at the front ($z=0$) of the sample. From this light available an arbitrary elementary volume dV at deepth z absorbs in each second the amount of quanta

$$E_\lambda k(\lambda) e^{-k(\lambda)z} dV, \qquad (1)$$

where $k(\lambda)$ is the absorption coefficient of the solution at this wavelength (λ). If no chemical reactions occur in the solution then we can assume [12] that

$$k(\lambda) = \sum_{i=1}^{n} k_i(\lambda), \tag{2}$$

where $k_i(\lambda)$ denote the absorption coefficient of each component. Let us denote the normalized true fluorescence quantum-spectrum of the successive components and their effective quantum yield* with $f_i(\lambda)$ and $\eta_i'(\lambda)$ respectively, then the magnitude and spectral distribution of the first order photoluminescence quantum flux (depending on wavelength λ') which is emitted from the volume element dV_1 can be described by the following expression:

$$d^4\varphi_P(\lambda, \lambda', z_1) = E_\lambda e^{-k(\lambda)z_1} k(\lambda) \sum_{i=1}^{n} \eta_i'(\lambda) f_i(\lambda')\, dV_1\, d\lambda' =$$

$$= E_\lambda e^{-k(\lambda)z_1} k(\lambda) \sum_{i=1}^{n} P_{ii}(\lambda, \lambda')\, dV_1\, d\lambda' \tag{3}$$

where

$$P_{ij}(\lambda, \lambda') = \eta_i'(\lambda) f_j(\lambda'). \tag{4}$$

The number of quanta emitted by first order photoluminescence, $B(\lambda, \lambda')_p d\lambda'$ in unit time and from unit area in unitary solid andle and, in the range $(\lambda', \lambda'+d\lambda')$, can be obtained by integrating expression (3) along the whole thickness of the sample. Taking into account the reabsorption of the emitted quanta inside the cuvette we obtain:

$$B(\lambda, \lambda')_P\, d\lambda' = \frac{\varrho}{4\pi n^2} E_\lambda \int_0^l e^{-[k(\lambda)+k(\lambda')]z_1} k(\lambda) \sum P_{ii}(\lambda, \lambda')\, dz_1\, d\lambda' =$$

$$= C(\lambda, \lambda') \sum_{i=1}^{n} P_{ii}(\lambda, \lambda')\, d\lambda', \tag{5}$$

where ϱ is a coefficient which takes into account the radiation losses caused by the partial reflection from the front wall of the cuvette, n is the refractive index of the solution, and $C(\lambda, \lambda')$ is defined as

$$C(\lambda, \lambda') = \frac{\varrho}{4\pi n^2} E_\lambda \frac{\alpha}{\alpha+\beta}(1-e^{-(\alpha+\beta)}), \tag{6}$$

where $\alpha = k(\lambda) \cdot l$ and $\beta = k(\lambda') \cdot l$. Similarly, the magnitude and the spectral distribution of the second order emission from the element dV_1 (appearing as a result

* Effective qunatum yield $\eta_i'(\lambda)$ means the ratio of the number of quanta if emitted from element dV by the i-th component to the number of quanta absorbed in this element by all components of the solution from the light at wavelength λ.

of radiative excitation energy transfer to this element from the other part of the excitation region) can be described by the following expression

$$d^4\varphi_s(\lambda, \lambda', z_1) = \int_{\lambda''} \int_{V_2} E_\lambda e^{-k(\lambda)z_2} k(\lambda) \sum_{i=1}^{n} P_{ii}(\lambda, \lambda'') \times$$
$$\times \frac{1}{4\pi s^2} k(\lambda'') e^{-k(\lambda'')s} \sum_{j=1}^{n} P_{jj}(\lambda'', \lambda')\, dV_2\, d\lambda''\, dV_1\, d\lambda'. \tag{7}$$

Since

$$\sum_{i=1}^{n} P_{ii}(\lambda, \lambda'') \cdot \sum_{j=1}^{n} P_{jj}(\lambda'', \lambda') \equiv \sum_{i,j=1}^{n} P_{ij}(\lambda, \lambda') P_{ji}(\lambda'', \lambda''), \tag{8}$$

we may write

$$d^4\varphi_s(\lambda, \lambda', z_1) =$$
$$E_\lambda k(\lambda) \sum_{i,j=1}^{n} \left[P_{ij}(\lambda, \lambda') \int_{\lambda''} P_{ji}(\lambda'', \lambda'') k(\lambda'') \frac{e^{-k(\lambda'')s - k(\lambda)z_2}}{4\pi s^2} dV_2\, d\lambda'' \right] dV_1\, d\lambda'. \tag{9}$$

The intensity and the spectral distribution of the second order emission $B(\lambda, \lambda')_s$ can be obtained by integration (as for $B(\lambda, \lambda')_p$)

$$B_s(\lambda, \lambda') = \frac{\varrho}{4\pi n^2} E_\lambda k(\lambda) \sum_{i,j=1}^{n} \left[P_{ij}(\lambda, \lambda') \int_{\lambda''} P_{ji}(\lambda'', \lambda'') \int_0^l e^{-k(\lambda')z_1} k(\lambda'') \times \right.$$
$$\left. \times \int_{V_2} \frac{e^{-k(\lambda'')s - k(\lambda)z_2}}{4\pi s^2} dV_2\, d\lambda'' \right] dz_1 = \frac{\varrho}{4\pi n^2} E_\lambda k(\lambda) l \sum_{i,j=1}^{n} P_{ij}(\lambda, \lambda') S_{ji}(\lambda'), \tag{10}$$

where S_{ji} denotes

$$S_{ji}(\lambda') = \int_{\lambda''} \eta'_j(\lambda'') f_i(\lambda'') \left[\frac{1}{l} \int_0^l e^{-k(\lambda')z_1} \left(\frac{k(\lambda'')}{4\pi} \int_{V_2} \frac{e^{-k(\lambda'')s - k(\lambda)z_2}}{s^2} dV_2 \right) dz_1 \right] d\lambda''. \tag{11}$$

Eq. (11) is identical with Eq. (11) from our previous paper [13]. Introducing the following notation

$$\varkappa_{ij} = \frac{\alpha + \beta}{l(1 - e^{-(\alpha+\beta)})} S_{ji}, \tag{12}$$

we obtain

$$B_s(\lambda, \lambda') = C(\lambda, \lambda') \sum_{i,j=1}^{n} P_{ij}(\lambda, \lambda') \varkappa_{ij}. \tag{13}$$

Inserting Eq. (4) to Eq. (13) we may write

$$B_s(\lambda, \lambda') = C(\lambda, \lambda') \sum_{i,j=1}^{n} \eta'_i(\lambda) \varkappa_{ij} f_j(\lambda'). \tag{14}$$

On the basis of Eqs. (16), (17), (19) and (26) from the paper [13] we can easily prove that:

$$\varkappa_{ij} = \int_0^\infty \eta'_j(\lambda'') f_i(\lambda'') M(\lambda'')\, d\lambda''. \tag{15}$$

The function $M(\lambda'')$ is given by

$$M(\lambda'') = \frac{(\alpha+\beta)(1-e^{-\alpha})(1-e^{-\beta})}{2\alpha\beta[1-e^{-(\alpha+\beta)}]}[\gamma E_i(-m\gamma)-\gamma E_i(-\gamma)]+$$
$$+\frac{1}{2[1-e^{-(\alpha+\beta)}]}[\chi(\alpha,\gamma)+\chi(\beta,\gamma)+e^{-\beta}\psi(\alpha,\gamma)+e^{-\alpha}\psi(\beta,\gamma)], \tag{16}$$

where $\gamma = k(\lambda'')l$, $m = R/l$ and

$$E_i(x) = 0.5772\ldots+\ln|x|+x+\frac{x^2}{2\cdot 2!}+\frac{x^3}{3\cdot 3!}+\ldots,$$
$$\psi(x,\gamma) = \frac{\gamma e^{-x}}{x}[G(-\gamma)-G(-\gamma+x)], \tag{17}$$
$$\chi(x,\gamma) = \frac{\gamma}{x}[G(-\gamma)-G(-\gamma-x)].$$

$G(x)$ is defined as $G(x)=E_i(x)-\ln|x|$.

A presice computation of the spectral distribution and the intensity of the third order emission of a multi-component solution is connected with great difficulties. According to BUDÓ and KETSKEMÉTY [13] this can be done by assuming that the ratio of emission intensity of the $(m+1)$ th order of the kth component (excited by the radiative energy transfer of the mth order emission of the ith component) is independent of m and this ratio is equal to the ratio of the primary and secondary emission intensities in the same system. Comparing Eqs. (5) and (14) it can be seen that this assumption is equivalent with the premise that Eq. (15) not only describes the energy transfer to secondary emission but also the energy transfer to higher order emissions. Thus, according to Eq. (14) for third order emission we may write

$$B_i(\lambda,\lambda') = C(\lambda,\lambda')\sum_{i,j,k=1}^{n}\eta_i'(\lambda)\varkappa_{ij}\varkappa_{jk}f_k(\lambda'). \tag{18}$$

The shape of the fluorescence spectrum, $B(\lambda,\lambda')$, of an n-component solution taking into account first, second and third order emissions can be given as a sum of Eqs. (5), (15) and (18)

$$B(\lambda,\lambda') \simeq C(\lambda,\lambda')\sum_{i=1}^{n}\left[\eta_i'(\lambda)+\sum_{j=1}^{n}\eta_j'(\lambda)\varkappa_{ji}+\sum_{j,k=1}^{n}\eta_k'(\lambda)\varkappa_{kj}\varkappa_{ji}\right]f_i(\lambda'). \tag{19}$$

By applying this procedure subsequently we could easily find the approximate expressions which takes into account the contributions of the emission of arbitrary order to the fluorescence spectrum of a solution of arbitrary number of components. From Eq. (19) we can see that the successive terms with $\varkappa_{ii}$ form in the expression of $B(\lambda,\lambda')$ a decreasing geometrical progression with a quotient of $\varkappa_{ii}$. Therefore, we can write another expression for $B(\lambda,\lambda')$ which is a better approximation of the real luminescence spectrum for multicomponent solutions than Eq. (19)

$$B(\lambda,\lambda') \simeq C(\lambda,\lambda')\sum_{i=1}^{n}\left[\frac{1}{1-\varkappa_{ii}}\eta_i'(\lambda)+\sum_{\substack{j=1\\(j\neq i)}}^{n}\eta_j'(\lambda)\varkappa_{ji}+\sum_{\substack{j,k=1\\(j=k\Rightarrow j\neq i)}}^{n}\eta_k'(\lambda)\varkappa_{kj}\varkappa_{ji}\right]f_i(\lambda'). \tag{20}$$

Introducing the terms of non-radiative energy transfer into the theory of radiative transfer

In the case of a solution in which the emission spectra of the acceptors does not overlap with the absorption spectra of the donors according to Eq. (16), all values $\varkappa_{ij}$ for $i>j$ vanish and then Eq. (20) becomes:

$$B(\lambda, \lambda') \simeq C(\lambda, \lambda') \sum_{i=1}^{n} \left[\frac{1}{1-\varkappa_{ii}} \eta_i'(\lambda) + \sum_{\substack{j=1 \\ (j<i)}}^{n} \eta_j(\lambda) \varkappa_{ji} + \sum_{\substack{j,k=1 \\ (j,k<i)}}^{n} \eta_k'(\lambda) \varkappa_{kj} \varkappa_{ji} \right] f_i(\lambda'). \quad (21)$$

Under these conditions we apply the definition of the effective quantum yield and denote the transition probability of the ith component molecule to the electronic excited state by $\eta_i^*(\lambda)$, and so we obtain the following expressions

$$\eta_1'(\lambda) = \frac{1}{k(\lambda)} k_1(\lambda) \eta_1^*(\lambda) K_1,$$

$$\eta_2'(\lambda) = \frac{1}{k(\lambda)} [k_2(\lambda) \eta_3^*(\lambda) K_2 + k_1(\lambda) \eta_1^*(\lambda) K_{12} K_2], \quad (22)$$

$$\eta_3'(\lambda) = \frac{1}{k(\lambda)} [k_3(\lambda) \eta_3^*(\lambda) K_3 + k_1(\lambda) \eta_1^*(\lambda) (K_{13} K_3 + K_{12} K_{23} K_3) + k_2(\lambda) \eta_2^*(\lambda) K_{23} K_3].$$

The constants K_i and K_{ik} denote the quantum yield of each component and the yield of non-radiative excitation energy transfer between the ith and kth component. We can easily see that for the effective quantum yield of the ith component the following equation holds

$$\eta_i'(\lambda) = \frac{K_i}{k(\lambda)} \left\{ k_i(\lambda) \eta_i^*(\lambda) + \sum_{\substack{j=1 \\ (j<i)}}^{n} k_j(\lambda) \eta_j^*(\lambda) \left[K_{ji} + \sum_{\substack{k=1 \\ (j<k<i)}}^{n} K_{jk} K_{ki} + \right. \right.$$
$$\left. \left. + \sum_{\substack{k,l=1 \\ (j<k<l<i)}}^{n} K_{jk} K_{kl} K_{li} + \ldots + K_{12} K_{23} \cdot \ldots \cdot K_{i-2,i-1} K_{i-1,i} \right] \right\}. \quad (23)$$

In the particular case of monocomponent solutions Eq. (21) can be written according to Eq. (25) from [13]

$$B(\lambda, \lambda') = C(\lambda, \lambda') \eta_1^*(\lambda) K_1 \frac{1}{1-\varkappa_{11}} f_1(\lambda'). \quad (24)$$

For two-component solutions we obtain:

$$B(\lambda, \lambda') = C(\lambda, \lambda') \left\{ \frac{1}{1-\varkappa_{11}} \eta_1'(\lambda) f_1(\lambda') + \left[\frac{1}{1-\varkappa_{22}} \eta_2'(\lambda) + \varkappa_{12}(1+\varkappa_{22}) \eta_1'(\lambda) \right] f_2(\lambda') \right\}. \quad (25)$$

And for three-component solutions

$$B(\lambda, \lambda') = C(\lambda, \lambda')\left\{\frac{1}{1-\varkappa_{11}}\eta_1'(\lambda)f_1(\lambda')+\left[\frac{1}{1-\varkappa_{22}}\eta_2'(\lambda)+\varkappa_{12}(1+\varkappa_{22})\eta_1'(\lambda)\right]f_2(\lambda')+\right.$$

$$\left.+\left[\frac{1}{1-\varkappa_{33}}\eta_3'(\lambda)+\varkappa_{23}(1+\varkappa_{22}+\varkappa_{33})\eta_2'(\lambda)+(\varkappa_{13}+\varkappa_{13}\varkappa_{33}+\varkappa_{12}\varkappa_{23}+\varkappa_{11}\varkappa_{13})\eta_1'(\lambda)\right]f_3(\lambda')\right\}. \tag{26}$$

This equation is identical with those published previously [12].

Substituting Eq. (22) into Eq. (16) we obtain the following expressions for the $\varkappa_{ij}$'s for one-, two- and three-component solutions:

$$\begin{aligned}
\varkappa_{11} &= K_1 R_{11},\\
\varkappa_{12} &= K_2 R_{12}+K_{12}K_2 R_{11},\\
\varkappa_{13} &= K_3 R_{13}+K_{13}K_3 R_{11}+K_{12}K_{13}K_3 R_{11}+K_{23}K_3 R_{12},\\
\varkappa_{22} &= K_2 R_{22}\\
\varkappa_{23} &= K_3 R_{23}+K_{23}K_3 R_{22}\\
\varkappa_{33} &= K_3 R_{33}
\end{aligned} \tag{27}$$

where

$$R_{ij} = \int_0^\infty \frac{k_j(\lambda'')}{k(\lambda'')}\eta_j^*(\lambda'')f_i(\lambda'')M(\lambda'')\,d\lambda''. \tag{28}$$

As seen from Eqs. (23)—(28) to the calculation of $B(\lambda, \lambda')$ values for concrete solutions, apart from the absorption-, the emission-, and the absolute quantum yield spectrum of each component, is is necessary to know the yield values K_i and K_{ij}. These yields can be computed from the expressions obtained for the non-radiative excitation energy transfer in multi-component solutions. To this problem, however, a separate paper will be devoted [14].

We should emphasize that Eq. (26) was supported by our previous experimental data [12]. The investigations were carried out on two series of three-component solutions with a constant concentration of the first and third component varying the concentration of the second component. Yields K_i and K_{ij} were computed from the expressions obtained by generalizing the non-radiative excitation energy transfer theory of BOJARSKI and DOMSTA [15] for the multi-component case. For both solution series the agreement between Eq. (26) and the experimental data was satisfactory.

* * *

This work was partially supported by the Polish Academy of Sciences under the project MR. I—9. 4.5.

References

[1] *Peterson, O. G., B. B. Snavely:* Bull. Am. Phys. Soc. **13,** 397 (1968).
[2] *Moeller, C. E., C. M. Verber and A. H. Adelman:* Appl. Phys. Lett. **18,** 278 (1971).
[3] *Rácz, B., I. Ketskeméty and L. Kozma:* Zh. Prikl. Spektroskopii **16,** 914 (1972).
[4] *Vu Thien Han:* C. R. Acad. Sci. Paris **274B,** 266 (1972).
[5] *Schmidt, W., W. Appt and N. Wittekindt:* Z. Naturforsch. **27a,** 37 (1972).
[6] *Ahmed, S. A., J. S. Gergely and D. Infante:* J. Opt. Soc. Am. **63,** 1321 (1973).
[7] *Levin, M. B., A. S. Cherkasov and V. I. Shirokov:* Optika i Spektrosk. **28,** 150 (1975).
[8] *Duysens, L.:* Nature **168,** 548 (1951).
[9] *Ketskeméty, I.:* Acta Phys. Hung. **10,** 429 (1959).
[10] *Ketskeméty, I., A. N. Shibistyi:* Zh. Prikl. Spektroskopii **18,** 843 (1973).
[11] *Shibistyi, A. N., I. Ketskeméty, L. Kozma and E. Hun:* Izw. Akad. Nauk SSSR Ser. Fiz. **37,** 763 (1973).
[12] *Ketskeméty, I., J. Kušba:* Acta Phys. et Chem. Szeged **20,** 239 (1974).
[13] *Budó, Á., I. Ketskeméty:* Acta Phys. Hung. **7,** 207 (1956).
[14] *Kušba, J., C. Bojarski* (to be published).
[15] *Bojarski, C., J. Domsta:* Acta Phys. Hung. **30,** 145 (1971).

ПЕРЕДАЧА ЭНЕРГИИ ВОЗБУЖДЕНИЯ В МНОГОКОМПОНЕНТНЫХ ЛЮМИНЕСЦЕНТНЫХ РАСТВОРАХ

И. Кечкеметн и Й. Кушба

Основаясь на работах Будо и Кечкемети представлена общая формула, описывающая смещение спектров флуоресценции, как функция эмиссионного и абсорбционного спектров и квантового выхода каждого из составляющих компонентов. Приняты во внимание как излучательные, так и безызлучательные передачи энергии возбуждения. Представленное уравнение рассмотрено для одно-, двух- и трехкомпонентных растворов.

THE INFLUENCE OF THE ENVIRONMENT ON THE LUMINESCENCE OF DISSOLVED DYE MOLECULES

By

J. HEVESI and L. KOZMA

Institute of Biophysics and Institute of Experimental Physics,
Attila József University,
Szeged

(Received September 1, 1977)

The Stepanov—Neporent—Ketskeméty relation which correlates absorption, fluorescence and solution characteristics was applied for solutions with ordered (micellar) structure and for solutions exposed to high electric field of laser light. The results show that the relation is fulfilled in both cases, although, there are exceptions for inordered solutions excited by intensive laser light. It can be concluded that the relation can give information on the interaction between excited molecules and their environment.

The absorption and fluorescence properties of luminescing molecules are significantly affected by the interaction of the environmental molecules. Important results were obtained by several authors from the investigations of the fluorescence characteristics for these interactions [1]. An appropriate way for studying the effect of the molecular environment is to test the validity of the Stepanov—Neporent—Ketskeméty relation [2] which correlates absorption $k(\nu)$, fluorescence $f_q(\nu)$, quantum yield $\eta(\nu)$ spectra, and the mean lifetime of the excited system τ, since the environmental effects may lead to the violation of this relationship. By means of this method the dissipation of the excess excitation energy to the solvent, the „local temperature" of the excited fluorescing centrum, were studied [3].

The results given below refer to systems in which the fluorescing molecules are significantly influenced by their environment, namely:

a) they are embedded into ordered structures (micelles) [4],

b) they are exposed to intense electric field (of the laser light).

In these cases the eigenstates of the molecules become significantly perturbed or/and the fluorescence is influenced by nonlinear processes. For studying these less known interactions the Stepanov—Neporent—Ketskeméty relation

$$\frac{f_q(\nu)}{k(\nu)} = \frac{8\pi n_r^2}{c^2} \frac{\tau}{\eta_m^2} \frac{\eta(\nu)}{n} \nu^2 \exp\left[-h(\nu-\nu_0)/kT\right] \tag{1}$$

was applied. The notation used: n_r — the refractive index of the solution, c — velocity of light, η_m — maximum quantum yield of the fluorescence, n — the concentration of the fluorescing molecules, ν_0 — frequency of pure electron transition, ν —

frequency of light, h and k the Planck and the Boltzmann constants, T — the absolut temperature.

a) The experiments were carried out with $5 \cdot 10^{-6}$ M solutions of Rhodamin 6G dissolved in micellar systems. The solvent was a mixture of water and sodium-laurylsulphate (SLS) detergent, in which the detergent ions form micelles of lamellar structure [4]. In this system the Rhodamin 6G molecules are adsorbed onto/into the micelles and as a consequence the energy levels of the molecules are changed. This is demonstrated by the change of the absorption and the fluorescence spectra of the system. The dye molecules bound to the same micelles interact and energy migration takes place. The quantum yield and the mean lifetime of the fluorescence are changed by these interactions, too. It was demonstrated by our earlier experiments that changes in the detergent concentration have significant influence on the mean lifetime of the fluorescence [5]. Changing detergent concentration brings about the deformation of the spectra of the solutions, too. The Stepanov relation, however, is fulfilled in all cases and the effective temperature of the excited molecules calculated from Eq. (1) decreases with increasing lifetime. This leads to the conclusion that quenching processes should occur in the system; they depend on the detergent concentration and lead to the decrease of the mean lifetime and to the increase of the effective temperature of the molecules, similarly to the processes found in mole-

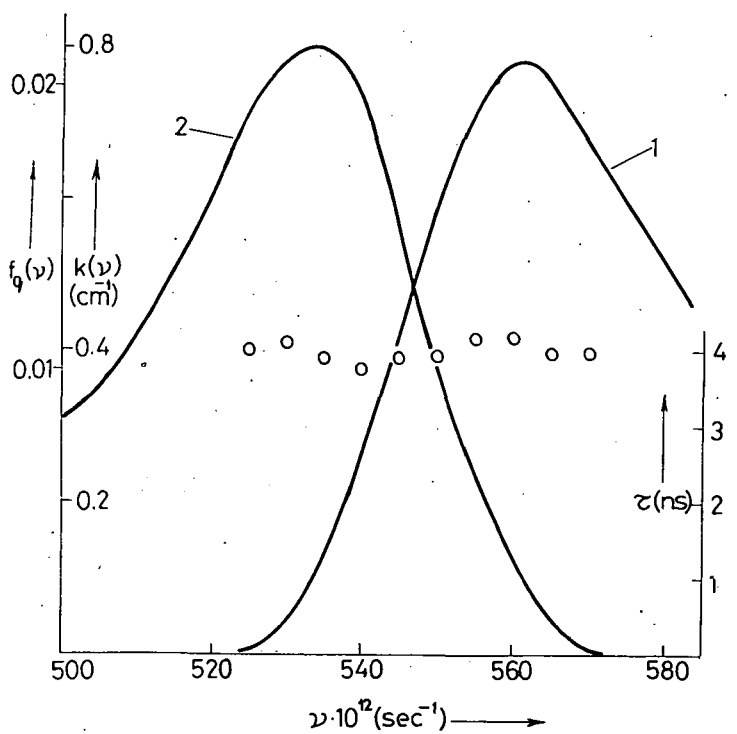

Fig. 1. Absorption (1) and fluorescence (2) spectra of $5 \cdot 10^{-6}$ M Rhodamin 6G solution and calculated values of τ *v.s.* frequency

cular solutions in the case of foreign quenching [6]. It seems plausible that the observed deformations of the spectra are caused by aggregates formed in the solution. In this case the τ mean lifetime, calculated by using Eq. (1), should depend stronly on the frequency.

The mean lifetime was calculated from fluorescence spectroscopical data of $5 \cdot 10^{-6}$ M Rhodamin 6G solutions containing SLS — detergent in different amounts according to Eq. (1), for frequencies corresponding to the overlapping region of the absorption and fluorescence spectra. The results are summarized in Table I. For demonstration the spectra used for the calculation and the calculated mean lifetime values of a particular solution are plotted in Fig. 1. It can be seen from the data and Fig. 1. that Eq. (1) is fulfilled for the luminescence characteristics of the dye molecules bound onto/into micelles similarly as for fluorescing molecules in solutions.

Table I

$\tau(\nu)_{calc}$ and τ_{meas} values (in ns) of Rhodamin 6G solutions with concentration of $5 \cdot 10^{-6}$ M vs. detergent (SLS) *concentration*

$C_{SLS}\,10^3$ (M) / $\nu \cdot 10^{-12}$ (S^{-1})	0	2.5	3	3.5	4	6
	$\tau(\nu)_{calc}$					
530	—	1.80	2.35	4.10	4.98	4.88
535	—	1.65	2.43	3.91	5.05	4.90
540	3.80	1.62	2.31	3.75	4.80	4.95
545	3.80	1.76	2.30	3.91	4.90	5.07
550	3.70	1.72	2.42	3.91	1.93	5.00
555	3.80	1.70	2.35	4.02	5.06	4.92
560	3.68	1.60	2.62	4.02	5.07	5.02
565	3.80	1.60	2.58	3.95	5.08	5.15
570	3.82	—	2.64	3.95	4.72	4.91
τ_{meas}	3.70	1.70	2.50	3.90	4.90	5.00

These results indicate that the eigenstates of dye molecules bound onto/into ordered structures are significantly perturbed due to the interaction with environment. This perturbation influences only the energy levels and the fluorescent and nonfluorescent transitions of molecules shown by the changes in $k(\nu)$, η_{fl} and τ depending on the detergent concentration. Simultaneously the position of the spectra was shifted. The applied model for describing the fundamental properties of the fluorescing centrum and the processes within it is similar to that used for fluorescent molecules in molecular solutions. This is shown by the validity of Eq. (1), which

proves that the aggregates cannot play an important role in the applied concentration region.

b) Investigations were carried out for molecular dye solutions excited by high intensity (laser) light. For this case the Stepanov relation has the form [7]:

$$\frac{f_q(\nu)}{k(\nu)} = \frac{8\pi h\nu^3 n_r^2}{c^2} \cdot \frac{1}{\frac{n_1}{n_2}\exp\left[\frac{h(\nu-\nu_0)}{kT}-1\right]} \tag{2}$$

where n_1 and n_2 is the concentration of the molecules in the ground state and in the excited states, respectively, $(n_1+n_2=n)$ is the total concentration. Note that in the case of population inversion which is necessary to the functioning of dye lasers the absorption coefficient has to be negative in the laser emission frequency region. The practical importance of Eq. (2) is, that knowing the fluorescence spectra and the number of the excited particles the amplification curve can be easily determined from Eq. (2).

To study this case calculations were carried out for fluorescing solutions applied in dye lasers. The calculated values were compared with theoretical curves calculated for quasistationary dye lasers [8]:

$$k_a(\nu) = \frac{c^2}{8\pi\tau_0\nu^2} \cdot n_2 f_q(\nu) - n_1 k(\nu)\eta(\nu), \tag{3}$$

where $k_a(\nu) = -k(\nu)$ — the amplification coefficient, τ_0 — the natural lifetime of the fluorescence.

We found that the absorption spectra calculated from Eq. (2) become negative in all cases in the laser emission frequency region. The position of the maxima of the negative absorption band depends on the population of the excited state, con-

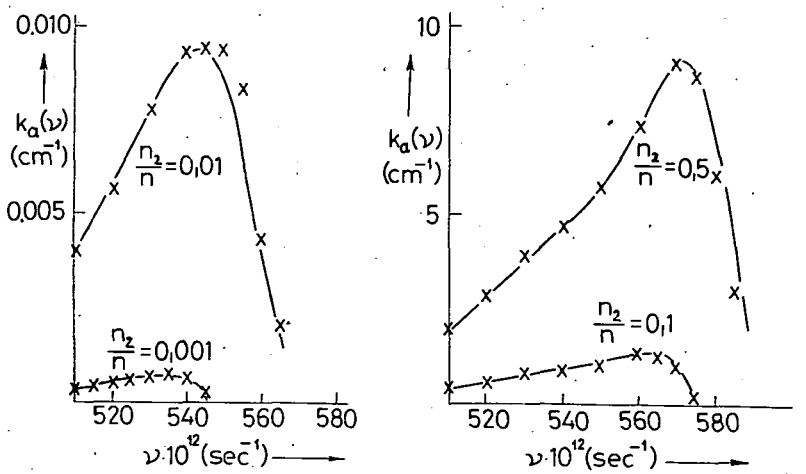

Fig. 2. Calculated values of $k_a(\nu)$ by using Eq. (3) [——] or Eq. (2) [× × ×] for different n_2/n ratios

sequently it describes well the dependence of the lasing wavelength on the output of the pumping. It has to be noted, however, that the shape of the curves calculated from Eq. (2) coincides with that of the curves calculated from Eq. (3) only in certain cases. In Fig. 2 an example is shown for $1 \cdot 10^{-4}$ M fluorescein solution.

From these results we concluded that the intense laser light with extremely high energy density does not exert deforming influence on the dye molecules as demonstrated by the rigorous fulfilment of the Stepanov relation. Any departure from this rigorous fulfilment could be observed only in special cases.

The applied method for studying the influence of the molecular environment of the excited molecules makes possible that, with further development of this method, the molecular processes of photosynthetizing systems using conventional and laser light sources can be studied.

References

[1] *Bakhshiev, A. N.:* Opt. Spectrosc. **19,** 141 (1967); *A. Jablonski:* Acta Phys. Polon. **31,** 243 (1963).
[2] *Stepanov, B. I.:* Dokl. Akad. Nauk SSSR **112,** 839 (1957); *B. S. Neporent:* Izv. Akad. Nauk SSSR **22,** 1372 (1958); *I. Ketskeméty, J. Dombi, R. Horvai:* Ann. Phys. **8,** 342 (1961).
[3] *Kozma, L., L. Szalay, J. Hevesi:* Acta Phys. et Chem. Szeged **10,** 67 (1964).
[4] *Singhal, G. S., E. Rabinowitch, J. Hevesi, V. Srinivasan:* Photochem. Photobiol. **11,** 531 (1970).
[5] *Lehoczki, E., E. Bálint, J. Hevesi, E. Bor:* Zh. Prikl. Spectrosc. **19,** 68 (1973).
[6] *Hevesi, J., L. Kozma:* Acta Phys. et Chem. Szeged: **8,** 103 (1962).
[7] *Gribkovski, V. P., B. I. Stepanov:* Dokl. Akad. Nauk SSSR **183,** 67 (1968).
[8] *Ketskeméty, I., L. Kozma:* Z. Naturforsch. **27a,** 1686 (1972).

ВЛИЯНИЕ ОКРУЖЕНИЯ НА ЛЮМИНЕСЦЕНЦИЮ РАСТВОРЕННЫХ КРАСИТЕЛЕЙ

Я. Хевеши и Л. Козма

Универсальное соотношение Степанова–Непорента–Кечкемети, выражающее связь спектров поглощения, флуоресценции и характеристик растворов, применено для растворов с неоднородной структурой (мицеллы) при обычном возбуждении и нормальных растворов, находящихся в сильном электромагнитном поле. Полученные результаты показывают, что соотношение выполняется в обоих случаях, однако при возбуждении нормальных растворов интенсивным излучением наблюдаются некоторые особенности. Сделано заключение, что универсальное соотношение может дать информацию о взаимодействии между молекулами растворенного вещества и растворителя.

ВЛИЯНИЕ ТЕМПЕРАТУРЫ НА ДЕТЕРГЕНТНЫЕ СИСТЕМЫ, СОДЕРЖАЩИЕ ОРГАНИЧЕСКИЕ КРАСИТЕЛИ

М. МОЛНАР и Я. ХЕВЕШИ
Институт экспериментальной физики и Кафедра биофизики
Университета им. Аттилы Йожефа, Сегед

(Поступило в редакцию 31 августа 1977 г.)

Физические процессы фотосинтеза могут быть легко исследованы в модельных системах *in vitro*, содержащих красители. Важным критерием применения модельных систем является их стабильность. В данной работе мы рассмотрели один из параметров, влияющих на стабильность, а именно, влияние температуры на проводимость мицеллярных систем, содержащих красители: тионин, родамин 6Ж и метиленовый голубой с концентрацией $5 \cdot 10^{-6}$ моль/л, а также влияние температуры на спектры поглощения и спектры излучения. Мы установили, что применяемые системы очень чувствительно реагируют на изменения температуры. Однако температура не вызывает спектральных изменений и не вызывает смещений максимумов поглощения и излучения систем.

Введение

Для того, чтобы понять механизм и энергетику фотосинтеза, необходимо знать, наряду с другими факторами, микро- и субмикроструктуру хлоропласта, выполняющую главную роль при приеме света, а также ее функции. Однако, экспериментальное исследование физических процессов фотосинтеза в системах *in vivo* — задача трудная. Для изучения фотофизических процессов целесообразным кажется применение модельных систем *in vitro*. Один из групп обычно применяемых модельных систем, где хлоропласт в структурном отношении легко доступен, образуют детергентные системы, содержащие красители [1]. В мицеллярных системах *in vitro* хлоропласт, начиная от определенной концентрации, названной «критической концентрацией мицеллообразования» (ККМ), соответствует ламеллам, детергент-ламеллы [2], а органические красители, как например, тионин, родамин 6Ж и метиленовый голубой, соответствуют фотосинтетическим пигментам, находящимся в хлоропласте [3—5].

При использовании эти систем в ходе спектрофотометрических исследований система подвергалась ряду внешних воздействий: часто нагревалась, освещалась. Следовательно, при их использовании важным вопросом является стабилизация их по отношению к этим влияниям. Значит, необходимо знать, в какой мере воздействуют эти влияния на спектроскопические и физические особенности применяемых мицеллярных систем. В детергентных системах, содержащих хлорофил, уже были проведены подобные исследования стабили-

зации [6], но в часто применяемых системах краситель-детергент, такие исследования еще не проводились.

В данной работе мы пытались выяснить среди прочих факторов, влияющих на особенности окрашенных детергентных систем, роль температуры.

Состав исследуемых систем, экспериментальные методы

В мицеллярной системе в качестве детергента мы применяли натрий-лаурилсульфат (SLS), а качестве органических красителей—тионин (Th), родамин 6Ж (Rh 6Ж) и метиленовый голубой (MB).

Концентрация детергента в рамках одной серии составляла: 0; $2 \cdot 10^{-3}$; $2{,}5 \cdot 10^{-3}$; $3 \cdot 10^{-3}$; $3{,}5 \cdot 10^{-3}$; $4 \cdot 10^{-3}$; $6 \cdot 10^{-3}$; и $8 \cdot 10^{-3}$ моль/л. Концентрация применяемых красителей была постоянной $5 \cdot 10^{-6}$ моль/л. Таким способом мы рассмотрели три системы: тионин + детергент (Th + SLS), родамин 6Ж + детергент (Rh 6Ж + SLS), и метиленовый голубой + детергент (MB + SLS). Наши исследования проводились при температурах: 30 °C, 50 °C и 70 °C. При этих трех температурах мы измеряли удельную проводимость, слектры поглощения и излучения растворов.

При измерении проводимости мы применяли кондуктометр типа ОК—102 (Radelkis), а также измерительную пластинку (электрод-колокол) типа ОК—902. В целях сохранения постоянной температуры мы применяли термостатированный измерительный сосуд. Термостабилизацию препаратов мы проводили с помощью термостата типа Ministat—607.

Для измерения поглощения мы применяли двухлучевый спектрофотометр типа Optica Milano CF—4 DR. Для сохранения постоянной температуры использовали термостатированную кювету и термостат типа U—10 Höpler. Для измерения спектров излучения мы применяли спектрофотометр типа ДФС —12. Измерение излучения проводили при постоянной температуре указанным методом.

Результаты экспериментов, и их обсуждение

1. Измерение электропроводности

Мы исследовали проводимость трех систем краситель-детергент, при трех разных температурах, в зависимости от концентрации детергента. Полученные результаты покозали, что величина ККМ при трех исследованных температурах составляла $3{,}5—3{,}8 \cdot 10^{-3}$ моль/л. Наши результаты покозали, что при более высокой температуре степень мицеллизации меньше. Это означает, что электрические свойства веществ чувствительно реагируют на изменение температуры.

2. Измерения спектров поглощения

В ходе исследования светопоглощения системы Th + SLS многие авторы [7, 8] указывали, что при внесении в систему детергента между детергентом и молекулами красителя имеет место взаимодействие; возникают нерастворимые в воде сложные соли. На присутствие комплексов в спектре поглощения ука-

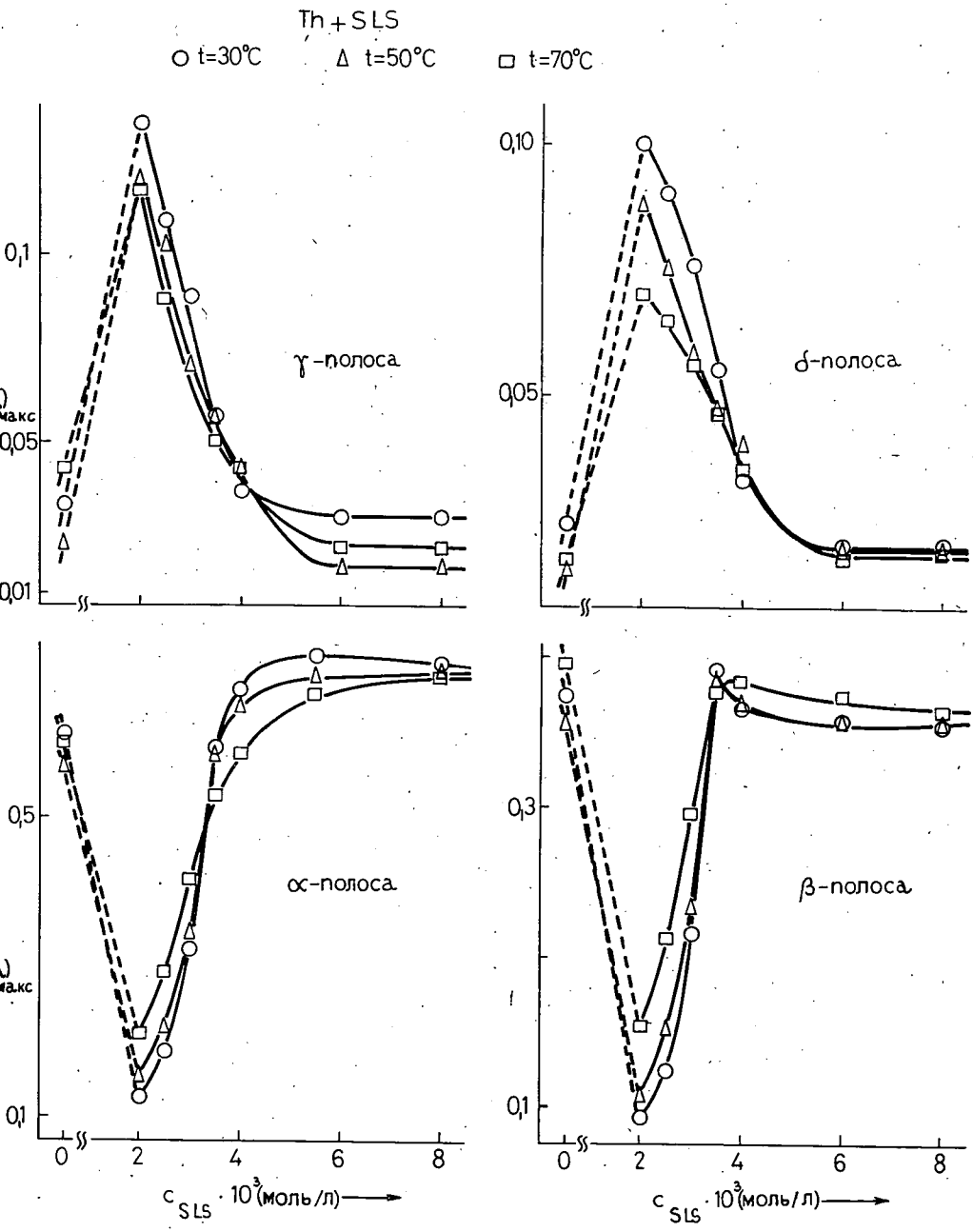
Th + SLS
○ t=30°C
△ t=50°C
□ t=70°C
γ-полоса
δ-полоса
α-полоса
β-полоса
0,1
0,05
0,01
0,10
0,5
0,3
0
2
4
6
8
$c_{SLS} \cdot 10^3$(моль/л)

Рис. 1.

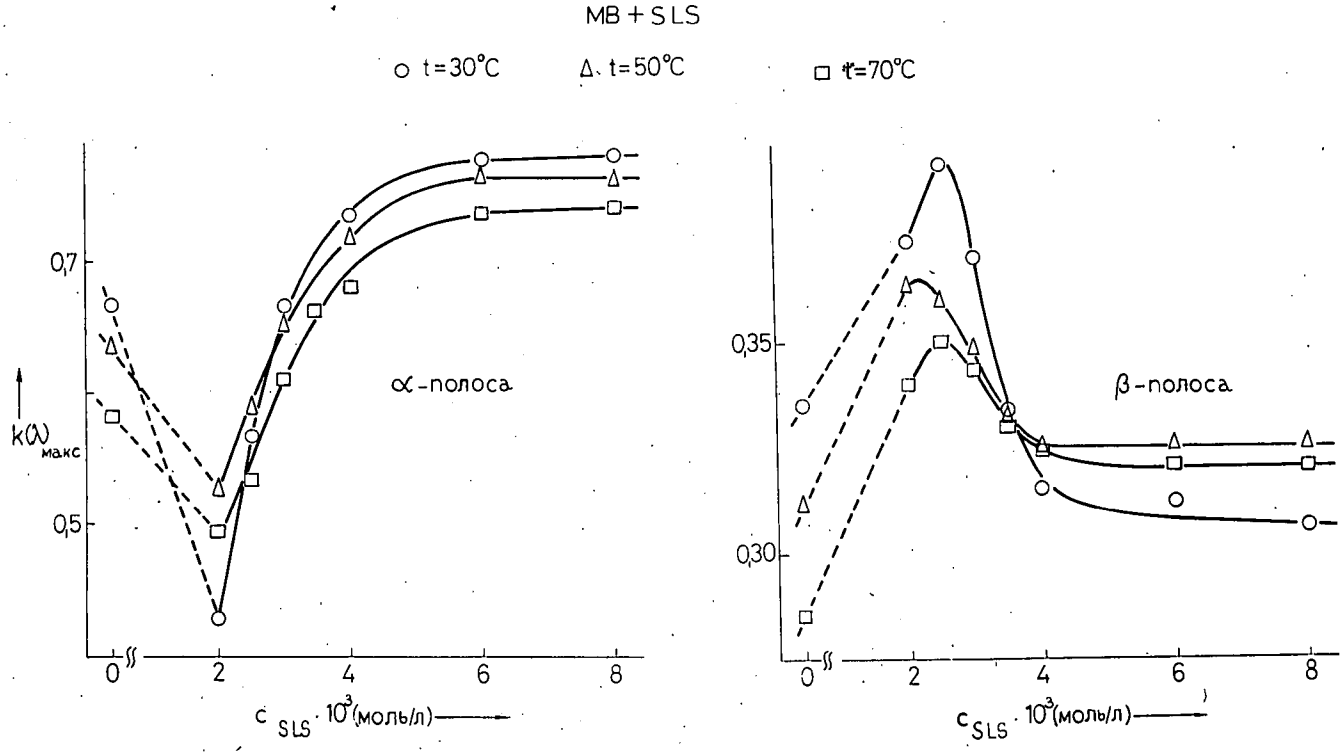
MB + SLS
○ t=30°C
Δ t=50°C
□ t=70°C
0,7
0,5
k(λ)макс
α-полоса
0
2
4
6
8
c SLS · 10³(моль/л)
0,35
0,30
β-полоса
0
2
4
6
8
c SLS · 10³(моль/л)

Рис. 2.

зывают возникающие местные максимумы. Например, появление в спектре поглощения системы Th+SLS так называемая α-полоса (около 600 нм) — красители-мономеры, β-полоса (около 565 нм) — димеры и γ-полоса (около 465 нм) — сложные соли красителя-детергента, δ-полоса (около 640 нм) — обясняются образованием агрегатов красителя более высокой степени. Величины максимума этих полос в зависимости от температуры и концентрации детергента изображены на рис. 1.

На рисунке видно, что с возрастанием температуры величины максимума α- и β-полос по сравнению с соответствующими величинами водного раствора (где ниже ККМ) немного понижается, а выше ККМ несколько превышают величины α и β водного раствора. Последнее явление объяняется тем, что при более высоких температурах агрегаты красителя образуются все труднее и труднее. Величины γ- и δ-полос с возрастанием температуры уменьшаются, *т. е.* практически исчезают. Сложные соли с возрастанием температуры все более становятся растворимыми и, таким образом, появляется возможность вхождения молекул красителей в мицеллы.

На рисунке хорошо видно, что у α-полосы кривые, полученные при трех температурах, пересекаются в одной точке. Эта точка находится при концентрации детергента $3{,}5 \cdot 10^{-3}$ моль/л, следовательно, явно приближается к величение ККМ, полученной при измерении электропроводности.

Изменение максимумов поглощения системы MB+SLS показано на рис. 2. В этой системе спектр поглощения имеет два максимума (α-полоса, возникшая из мономеров, она находится около 665 нм, и β-полоса, возникшая из димеров, эта полоса лежит около 615 нм).

Температурным изменением величин α-полосы можно установить, что величины, измеренные при $t=50\,^{\circ}C$ и $t=70\,^{\circ}C$ изменяются параллельно друг другу таким образом, что величины найденные при более высокой температуре меньшие.

Наибольшее изменение показывает кривая, полученная при $t=30\,^{\circ}C$. Величины β-полосы (ниже ККМ) уменьшаются под влиянием повышения температуры, а это в свою очередь указывает на то, что в это время сложные соли краситель-детергент (ими обьясняется частично появление β-полосы [9]) постепенно растворяются. Три кривые, показывающие температурную зависимость β-полосы, также пересекаются в одной точке, а именно, около величины ККМ.

3. Измерения спектров излучения

Результаты измерений излучения, проведенные в системе показаны на рис. 3. На рисунке мы отметили относительные величины (интенсивность растворов, не содержащих SLS, мы взяли произвольно за 100).

На рисунке видно, что при малых концентрациях детергента с возрастанием температуры интенсивность флуоресценции повышается, в то же время при больших концентрациях детергента наблюдается влияние температурного тушения. Точка пересечения кривых, изображенных на рисунке, соответствует приблизительно величине ККМ.

В таблице мы отметили, относительные значения максимумов спектров излучения и места максимумов (в нм) во всех трех исследованных системах. По этим данным видно, что изменение температуры не влияет на положение

Таблица

Значения интенсивности и положение максимумов люминесценции систем краситель-детергент

$C_{SLS} \cdot 10^3$ (моль/л)	Th+SLS			Rh 6Ж+SLS			MB+SLS		
	30 °C	50 °C	70 °C	30 °C	50 °C	70 °C	30 °C	50 °C	70 °C
0	100	100	100	100	100	100	100	100	100
	619,0	620,0	619,0	552,0	552,5	553,5	685,0	684,0	687,0
2	17,3	32,0	53,9	21,2	29,3	16,3	4,8	31,5	56,5
	618,5	621,5	623,0	558,5	561,0	555,0	685,0	684,0	685,0
2,5	24,7	37,0	58,9	44,1	41,9	19,2	7,0	45,4	70,1
	622,0	621,5	621,5	560,0	561,0	557,5	683,5	682,5	685,0
3	42,3	42,6	62,6	61,5	56,6	35,8	26,5	81,0	81,0
	621,5	621,0	621,5	559,5	5605,	559,5	683,0	682,0	683,5
3,5	76,4	73,2	71,2	82,1	66,5	45,9	62,5	102,9	104,3
	621,0	620,5	620,5	560,0	560,0	559,5	683,0	683,5	683,5
4	146,4	121,3	81,8	84,8	75,4	61,3	128,8	139,1	124,9
	621,0	619,5	620,0	559,0	559,0	558,0	682,5	681,5	683,5
6	179,4	160,7	134,9	80,6	75,8	71,9	210,0	186,9	170,0
	620,5	620,5	620,5	559,0	557,5	557,0	681,5	681,5	683,0
8	179,0	166,7	143,6	81,9	74,3	74,4	209,0	187,9	184,0
	620,5	620,0	619,5	557,0	555,0	557,0	681,5	681,0	681,0

спектров излучения. Из таблицы видно, что значительное влияние температуры на свойства излучения наблюдается в системах Rh 6Ж: с повышением температуры уже при $t = 50\ ^\circ C$ имеет место значительное температурное тушение, но в особенности это проявляется при $t = 70\ ^\circ C$. Влияние тушения наблюдается при всех коцентрациях детергента.

Влияние температуры показано и в случае систем MB+SLS. С повышением температуры (ниже ККМ) возратают и величины интенсивности флуоресценции, а выше ККМ, значительную роль играет температурное тушение.

Наши результаты показывают, что исследованные системы чувствительно реагируют на изменение температуры. Повышение температуры влечет за собой снижение степени мицелляции. Температура влияет также и на интенсивности полос поглощения. Возрастающая температура (ниже ККМ), как правило, увеличивает интенсивность флуоресценции, а при концентрациях детергента выше ККМ всегда наблюдается влияние температурного тушения. В спектре излучения изменение температуры не вызывает спектральных смещений.

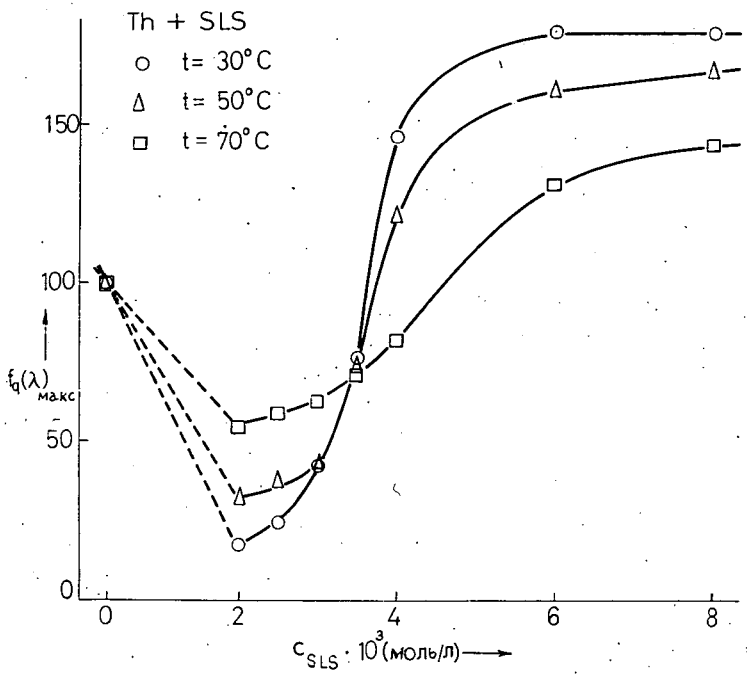

Рис. 3.

Литература

[1] *Singhal, G. S., E. Rabinowitch, J. Hevesi, V. Srinivasan:* Photochem. Photobiology **11,** 531 (1970).
[2] *Winsor, P. A.:* Chem. Rev. **68,** 1 (1968).
[3] *Хевеши, Я., Э. Лехоцки, Э. Балинт:* ЖПС. **13,** 456 (1970).
[4] *Hevesi, J., E. Bálint, E. Lehoczki:* Acta Phys. Polon. **A38,** 839 (1970).
[5] *Bálint, E., J. Hevesi, E. Lehoczki:* Acta Phys. et Chem. Szeged **17,** 119 (1971).
[6] *Wagner, B. R.:* Spektroskopische und photochemische Untersuchungen an Clorophyllhaltigen Netzmittelmizellen, Dissertation, der Eberhard-Karls-Universität zu Tübingen (1969)
[7] *Bálint, E., E. Lehoczki, J. Hevesi:* Acta Phys. et Chem. Szeged **17,** 15 (1971).
[8] *Lehoczki, E., J. Hevesi:* Acta Phys. et Chem. Szeged **18,** 11 (1972).
[9] *Rózsa, Zs.:* Dissertation, Szeged (1973).

THE EFFECT OF TEMPERATURE ON THE DYE-DETERGENT (MICELLE) SYSTEMS

M. Molnár and J. Hevesi

The physical process of photosynthesis can be investigated very well on *in vitro* dye-detergent model systems. Important criteria of the applicability of model systems is their stability. This work presents the investigation of the effect of temperature on the conductivity the absorbtion and emission spectra of micelle systems containing $5 \cdot 10^{-6}$ M Thionine; Rhodamine 6G, and Methylene Blue dyes. It has been found the used systems react sensitively to the temperature. Therefore the change of temperature does not cause spectral changes *i. e.* the wavelength of absorbtion and emission maxima does not change.

ÜBER EINIGE ELEKTRISCHE EIGENSCHAFTEN DER GRATONITEINKRISTALLE

Von

CS. LOBODA, J. KISPÉTER* und B. RIBÁR

Institut für Physik der Naturwissenschaftlich-Mathematischen Fakultät, Novi Sad (Jugoslawien)

* Institut für Experimentalphysik der Attila József Universität, Szeged (Ungarn)

(Eingegangen am 15. Juni 1977)

I—U Charakteristik und Temperaturabhängigkeit der elektrischen Leitfähigkeit bei Gratonit wurden untersucht mit Berücksichtigung der Polarisationsspannung, die in untersuchten Material auftrat. Es wurde erwiesen, daß Gratonit im Temperaturintervall von 100 K bis 400 K Halbleitereigenschaft zeigte. Die thermische Aktivierungsenergie von 0,046 eV und 1,26 eV wurde aus dem Zusammenhang $\log \sigma - \frac{1000}{T}$ bestimmt. Die Polarisationsspannung vermindert sich bei Beleuchtung.

Die Systematisierung und Strukturuntersuchung der als seltene Minerale betrachteten Sulfosalze ist vor allem von kristallographischer und kristallochemischer Bedeutung. Das Mineral Gratonit gehört nach der Klassifikation von NOWACKI [1] zur Gruppe I. c der Sulfosalze mit $3 < \varphi < 4$ $\left(\varphi = \frac{\text{Zahl der S-Atome}}{\text{Zahl der As-Atome}}\right)$. Im Fall $3 < \varphi < 4$ sind isolierte AsS_3-Pyramiden mit zusätzlichen Schwefel-Atomen im Gitter vorhanden. Die Struktur des Gratonits [2] zeigte, daß im Kristall kovalente Bindungen vorkommen. Das führte die Verfasser zu dem Gedanken, die grundlegenden elektrischen Eigenschaften dieses Minerals zu prüfen. Aus Gratonitpulver gepresste Schichten zeigten bei Messungen [3], daß das Mineral im Temperaturintervall von 293 K bis 373 K Halbleitereigenschaften besitzt, man muß aber die unter Einfluß der äußeren Spannungen entstehenden Polarisationsspannungen berücksichtigen. Elektrische Messungen an Halbleitern zeigten, daß zwischen den elektrischen Eigenschaften von Einkristallen und aus Pulver gepressten Proben wesentliche Unterschiede bestehen können. Es schien deshalb angezeigt, die elektrischen Eigenschaften der Gratonit-Einkristalle zu prüfen, weiterhin die Temperaturintervalle auf niedrigere Temperaturen auszudehnen. Über diese Prüfungen wollen wir im gegenwärtigen berichten.

Für die Untersuchungen stand uns aus Cerro de Pasco (Peru) stammendes Mineral zur Verfügung, aus dem wir duch Schneiden, Schleifen und Polieren massive Prismenartige Einkristall-Proben von ungefähr $3 \times 1{,}5 \times 0{,}5$ mm³ formierten. Auf die Oberfläche der Probe wurden im Vakuum von 5×10^{-5} torr auf 1 mm Elektrodenentfernung Goldelektroden aufgedampft. Zu dieser Prüfung wurden die Proben

in einem Vakuum-Metallkryostat mit Hilfe von Federkontakten am Nasskopf befestigt. Die Temperatur der Probe wurde mit einem Kupfer-Konstantan Thermoelement von 0,2 mm Durchmesser gemessen und die Temperatur im Intervall von 80 K bis 380 K geändert. Die Spannung Lieferte eine transistorisierte Einheit Tr—9160; der durch die Probe fließende Strom wurde mit einem Elektrometer Typ Keithley 610 C gemessen, und die zeitliche Änderung des durchfließenden Stromes durch einem Schreiber Typ Goerz Servogor 2S registriert, welcher am ausgang des Elektrometers angeschlossen war. Die Polarisationsspannung wurde auch jetzt auf die in [3] beschriebene Weise bestimmt. Die Oberfläche der Probe wurde durch das Glasfenster des Metallkryostate mit Hilfe eines Monochromators SPM—1 beleuchtet. Es muß bemerkt werden, daß die geprüften Proben photoempfindlich waren, deshalb wurden einige Messungen auch so durchgeführt, daß die Proben wärend der Messung mit monochromatischem Licht von maximaler Photoempfindlichkeit bei der gegebenen Temperatur beleuchtet wurden.

Es wurde festgestellt, daß im Gratonit-Einkristall auch eine Polarisationsspannung entsteht. Nach der Anschalten der äußeren Spannung an die Probe nimmt die durchfliessende Stromstärke, auf Einfluß des entgegengesetzten Polarisationsfeldes allmählich ab, und errecht einen Sättigungswert. Nach Aufhören der äußeren Spannung fließt in der Probe ein entgegengesetzter Kurzschlusstrom, der in Abhängigkeit von der Zeit allmählich verschwindet.

Die Messungen an Dielektriken zeigten, daß die Gleichstromleitfähigkeit dem Zusammenhang

$$\sigma(t) = at^{-n} + \sigma_0$$

gut folgt, wo $\sigma(t)$ die momentane Leitfähigkeit der Probe, σ_0 die Gleichgewichtsleitfähigkeit ist und a sowie n von Eigenschaften des Materials abhängige Konstanten bedeuten.

Die Kurzschlussleitfähigkeit ändert sich nach dem Zusammenhang

$$\sigma'(t) = -a't^{-n},$$

wo a' und n' ebenfalls von Materialeeigenschaften abhängige Konstanten sind.

Die Exponenten n und n' können Werte zwischen 0,3 und 1,2 haben [4]. Es wurde angenommen, daß die Leitfähigkeit bzw. die Änderung des Stromes bei Ein- und Ausschalten der Spannung sich auch bei den geprüften Gratonit-Einkristallen ebenfalls durch die obigen Gleichungen beschreiben läßt. Zur Bestimmung der Konstanten n, n' und a, a', wurden die berechneten Kurven den experimentellen Kurven mit Hilfe elektronischer Rechenmaschinen angepaßt. Einerseits wurde festgestell daß auch in diesem Fall die erwähnten Gleichungen gültig sind, anderseits wurden die Werte der Konstanten erhalten. Das Abklingen der Stromstärke wurde bei Ein- und Ausschalten bei Zimmertemperatur in Spannungsintervall 1 V bis 200 V, anderseits bei 10 V äußerer Spannung im Temperaturintervall 273 K bis 373 K untersucht.

Die Messresultate ergaben, daß $n = 0{,}75 \pm 0{,}03$ und $n' = 0{,}98 \pm 0{,}03$ und unabhängig von der Spannung ist. Die Werte von a bzw. a' sind bis 50 V beinahe konstant, danach nehmen sie um 60% ab. In Abhängigkeit von der Temperatur steigen die Werte der Potenzen n von 0,75 bis 1,1 linear an, während sich die Potenz n' nicht ändert. Die Werte der Koeffizienten a und a' werden mit steigender Temperatur um annähernd eine Größeordnung höher.

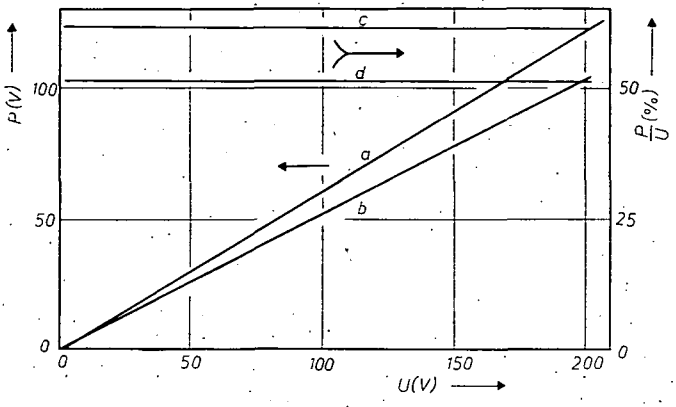

Abb. 1. Abhängigkeit der Polarisationsspannung von der äußeren Spannung. *a*: im Dunkeln *b:* bei Beleuchtung mit Licht von $\lambda = 730$ nm. Mit *c* sind den Werten *a*, mit *d* den bei Beleuchtung erhaltenen Ergebnissen entsprechende Werte bezeichnet.

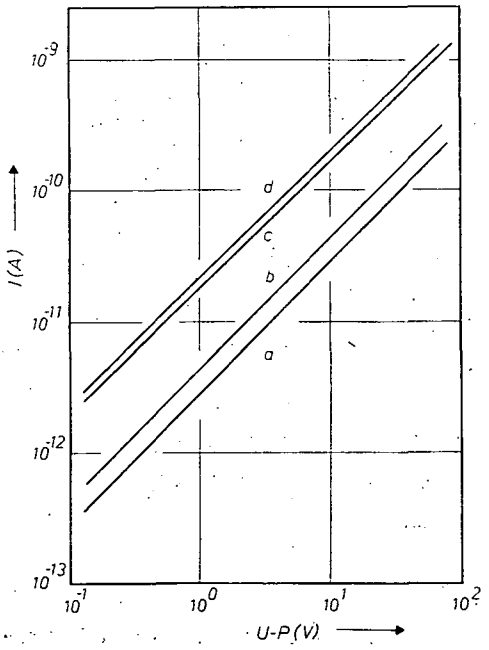

Abb. 2. Der mit der Polarisationsspannung korrigierte *I—U* Charakteristik. Bei 293 K: *a* im Dunkeln, *b* bei Beleuchtung mit Licht von der Wellenlänge $\lambda = 730$ nm; bei 333 K: *c* im Dunkeln, *d* mit Licht von $\lambda = 740$ nm beleutet.

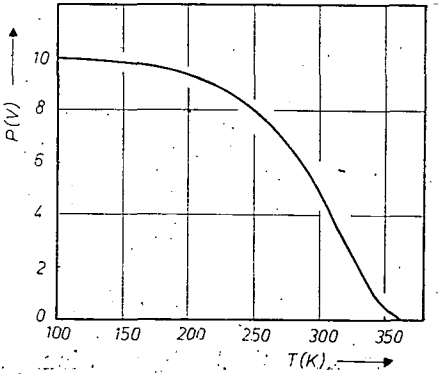

Abb. 3. Temperaturabhängigkeit der Polarisationsspannung.

Abb. 1 zeigt die Abhängigkeit der Polarisationsspannung, bzw. des Verhältnisses der Polarissationsspannung und der dazu gehörenden äußeren Spannung von der äußeren Spannung. Aus der Abb. 1 sieht man, daß die Polarisationsspannung im untersuchten Spannungsgebiet bis 200 V, wie im Dunkel Kurve *a*, ebenso unter Wirkung von Licht Kurve *b* linear ansteigt, und daß die Polarisationsspannung bei Beleuchtung abnimmt. Das Verhältnis P/U ist in beiden Fallen unabhängig von der Spannung und beträgt 60% bzw. 50%.

Mit Berücksichtigung der Polarisationsspannung läßt sich die korrigierte $I-U$ Charakteristik angeben (Abb. 2). Es ist ersichtlich, däß, wie bei 293 K, auch bei 323 K der Gang der Kurven auf eine ohmische Eigenschaft verweist, und unter Beleuchtung mit Licht von $\lambda = 730$ nm Wellenlenge die Leitfähigkeit sich in geringen Masse steigert. Aus dieser Feststellung kann man auch auf das Ausmaß der photoelektrischen Empfindlichkeit Schliessen.

Die Abhängigkeit der Polarisationsspannung von der Temperatur im Intervall zwischen 100 K und 373 K bei 10 V äußerer Spannung ist aus Abb. 3 zu sehen. Die Resultate zeigen, daß die Polarisationsspannung bis 150 K beinahe dem gleichen Wert aufweist, wie die äußere Spannung, danach allmählich abnimmt und in der Umgebung von 373 K verschwindet.

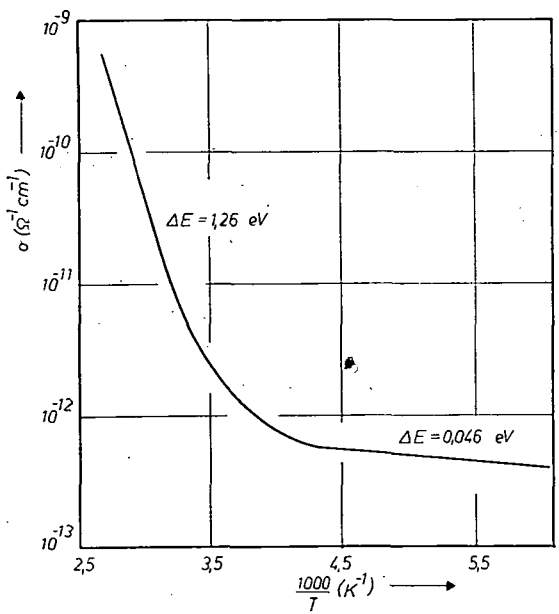

Abb. 4. Temperaturabhängigkeit der Leitfähigkeit.

In Kenntnis der Polarisationsspannung läßt sich die Abhängigkeit der Leitfähigkeit von der Temperatur bestimmen; Abb. 4 stellt das Resultat in $\log \sigma - \frac{1000}{T}$ dar. Im ganzen untersuchten Temperaturbereich zeigt die Probe Halbleitereigenschaften. Man kann zwei gerade Abschnitte unterscheiden: bei niedrigen Tempera-

turen die thermische Aktivierungsenergie, die auf Grund des Zusammenhanges $\sigma = \sigma_0 \exp(-\Delta E/kT)$ 0.046 eV ist und bei höheren Temperaturen (über 273 K) den Wert 1.26 eV hat.

Durch Vergleich der auf Einkristalle und gepresste Pulverschichten bezüglichen Meßresultate kann man feststellen daß, im Gegensatz zu den mit CdSe durchgeführten Untersuchungen [3], bei Gratonit keine bedeutenden Unterschiede nachweisbar sind. Bei Zimmertemperatur gemessene Polarisationsspannungen sind bei Einkristallen um 30% bis 50% höher, als bei gepressten Pulverschichten. Das häng auch von dem Material der benutzten Elektrode ab. (Die um 50% höheren Ergebnisse wurden mit Ionimplantierten Nickel-Elektrode erhalten.) Aus der letzteren Beobachtung sowie noch einigen weiteren Beobachtungen kann man darauf folgern, daß die Polarisationsspannung vorwiegend auf dem Grenzgebiet (der Grenzfläche) zwischen der Elektrode des untersuchten Material entsteht. Genauere Information könnte man von Messungen mit Hilfe einer Potentialsonde erwarten.

Durch den Vergleich der Temperaturabhängigkeit der Polarisationsspannung und der Leitfähigkeit kann man die Tatsache erklären, daß bei niedrigeren Temperaturen die Leitfähigkeit von der Temperatur kaum abhängig ist, *d. h.* die hohe Polarisationsspannung die Halbleitereigenschaft der Probe überdeckt.

Die Entstehung der Polarisationsspannung kann man mit Hilfe der Anwesenheit von Haftstellen in der verbotenen Zone erklären. Darauf weist auch der Umstand hin, daß die Polarisationsspannung über 373 K verschwindet und sich bei Beleuchtung vermindert.

Zur tieferen Deutung der erhaltenen Resultate bzw. zur genauen Beschreibung des Leitfähigkeitsprozesses sind noch weitere Untersuchungen nötig.

* * *

Die Verfasser sind Herrn Prof. Dr. I. KETSKEMÉTY, Direktor des Institutes für Experimenthalphysik der Universität Szeged, für sein Interesse an der Arbeit, Herrn Prof. Dr. W. NOWACKI (Bern) und Herrn Prof. Dr. G. C. AMSTUTZ (Heidelberg) für die freundliche Bereitstellung von Gratonitkristallen zu Dank verpflichtet.

Literatur

[1] *Nowacki, W.*: Schweiz. Min. Petr. Mitt. **49**, 109 (1969).
[2] *Ribár, B.*: Z. Kristallogr. **128**, 321 (1969).
[3] *Loboda. Cs., J. Kispéter, B. Ribár*: Arbeiten der Naturwissenschaftlich-Mathematischen Fakultät Novi Sad, Band **6**, 135 (1976).
[4] *Szazsin, B. I.*: Elektroprovodnoszt polimerov, Izd. Himija, Moszkva, 1964.

О НЕКОТОРЫХ ОСОБЕННОСТЯХ ЭЛЕКТРИЧЕСКИХ СВОЙСТВ МОНОКРИСТАЛЛОВ ГРАТОНИТОВ

Ч. Лобода, Й. Кишпетер и Б. Рибар

Исследованы *I—U* характеристики и зависимость проводимости от температуры на монокристаллах гратонита учитывая поляризационные напряжения, возникающие в кристалле. Показано, что гратонит обладает полупроводниковыми свойствами в области 100—400 К, из зависимости $\log \sigma$ от обратной температуры определена термическая энергия активации; соответственно 0,046 и 1,26 эВ.

ЧИСЛЕННЫЙ АНАЛИЗ ПАРАМЕТРОВ ЛАВИННО-ПРОЛЁТНЫХ ДИОДОВ НА ГЕТЕРОПЕРЕХОДЕ ГЕРМАНИЙ-АРСЕНИД ГАЛЛИЯ

К. М. ДАТИЕВ*

Факультет электронной техники, Северо-Кавказский политехнический институт г. Орджоникидзе (СССР)

(Поступило в Редакцию 1 сентября 1977 г.)

Проведен расчёт мощности генерации лавинно-пролётного диода (ЛПД) на гетеропереходе германий-арсенид галлия с однородным распределением электрического поля в слое умножения. Полученные данные позволяют определить необходимый набор параметров ЛПД и гетероперехода германий-арсенид галлия, обеспечивающий требуемые к. п. д. (мощность генерации) и оптимальную нагрузку.

В ранее опубликованных работах [1—3] были определены статические параметры двухслойной структуры запирающего слоя на основе гетероперехода Ge—GaAs для создания высокоэффективных ЛПД. В работе [4] рассмотрена взаимосвязь предельной мощности генерации ЛПД на гетеропереходе Ge—GaAs, характеризующийся линейным распределением электрического поля в слое умножения, с параметрами режима и структуры. Результаты указанных работ позволяют определить необходимый набор параметров ЛПД и двухслойной структуры запирающего слоя на основе гетероперехода Ge—GaAs, обеспечивающий требуемые к. п. д. или мощность генерации и оптимальную нагрузку.

Настоящая работа посвящена решению задачи о взаимосвязи максимальной мощности генерации ЛПД на гетеропереходе Ge—GaAs с однородным распределением электрического поля в слое умножения и параметрами режима и структуры. На рис. 1 представлена схема рассматриваемой модели ЛПД на гетеропереходе $(p^+-p)\mathrm{Ge}-(n-n^+)\mathrm{GaAs}$, распределение атомов примесей и электрического поля в запирающем слое. Такая структура описывается в общем случае шестью параметрами: концентрациями примесей N_1 и N_2 и толщинами δ_1 и δ_2 высокоомных слоёв германия и арсенида галлия соответственно и концентрациями N_3 и N_4 в низкоомных частях Ge и GaAs.

При анализе предполагается, что переходы резкие, а высокоомные слои легированы однородно. Также предполагается, что степени легирования p^+ и n^+ областей много больше, чем уровни легирования p и n слоёв и, следовательно, падением напряжения и умножением в низкоомных слоях германия и арсенида галлия можно пренебречь.

В общем случае границы области запирающего слоя X_1 и X_2 в режиме лавинного пробоя могут быть меньше толщин высокоомных слоёв δ_1 и δ_2 соответственно. При этом такая структура ЛПД, анализ которой проведен в работе [4],

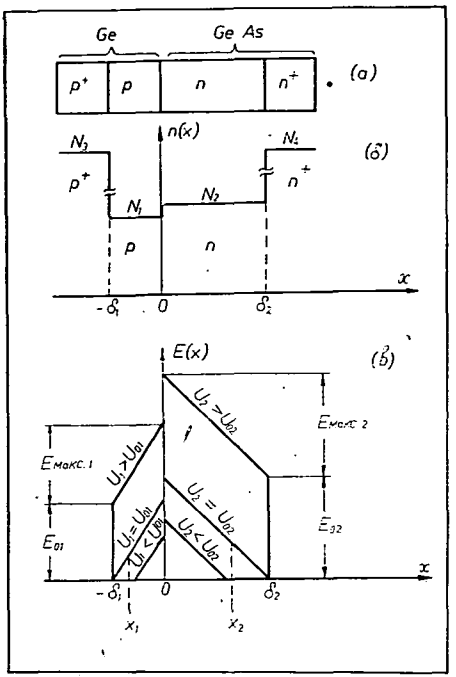

Рис. 1. Схема модели ЛПД на гетеропереходе (p^+-p)Ge$-(n-n^+)$GaAs: (а) структура диода; (б) распределение атомов примесей; (в) распределение электрического поля.

имеет линейное распределение электрического поля в области запирающего слоя.

В данной работе рассматривается структура, в которой толщины высокоомных слоёв p и n областей гетероперехода настолько малы, что до лавинного пробоя наступает режим ограниченного расширения областей запирающего слоя по обе стороны от границы раздела. Такая структура характеризуется тем, что области запирающего слоя в p и n частях перехода с ростом обратного напряжения достигают соответственно p^+ и n^+ слоёв. Очевидно, что при дальнейшем увеличении модуля обратного напряжения ширина области запирающего слоя не будет возрастать, а ёмкость перехода становится постоянной. Можно, показать, что указанный режим будет иметь место при напряжениях $U \geqq U_0$, составляющие которого U_{01} и U_{02} определяются в виде [2]

$$U_{01} = qN_1\delta_1^2/2\varepsilon_0\varepsilon_1 - \varphi_{K1}, \qquad (1)$$

$$U_{02} = qN_2\delta_2^2/2\varepsilon_0\varepsilon_2 - \varphi_{K2}, \qquad (2)$$

где φ_{K1} и φ_{K2} — составляющие контактной разности потенциалов в *1* и *2* материалах соответственно (здесь и далее: индекс *1*- германий, *2*- арсенид галлия).

Распределение электрического поля для рассматриваемой структуры будет иметь вид:

а) в p- области запирающего слоя при $-\delta_1 \leqq x \leqq 0$

$$E_1(x) = E_{\text{макс. 1}}\left(1+\frac{x}{\delta_1}\right)+E_{01}, \qquad (3)$$

где

$$E_{\text{макс. 1}} = qN_1\delta_1/\varepsilon_0\varepsilon_1, \qquad (4)$$

$$E_{01} = U_1/\delta_1 - E_{\text{макс. 1}}/2, \qquad (5)$$

$$U_1 = \int_{-\delta_1}^{0} E_1(x)\,dx - \varphi_{K1}, \qquad (6)$$

б) в n — области запирающего слоя при $0 \leqq x \leqq \delta_2$

$$E_2(x) = E_{\text{макс. 2}}\left(1-\frac{x}{\delta_2}\right)+E_{02}, \qquad (7)$$

где

$$E_{\text{макс. 2}} = qN_2\delta_2/\varepsilon_0\varepsilon_2, \tag{8}$$

$$E_{02} = U_2/\delta_2 - E_{\text{макс. 2}}/2, \tag{9}$$

$$U_2 = \int_0^{\delta_2} E_2(x)\,dx - \varphi_{K2}, \tag{10}$$

q — заряд электрона; ε_0 — диэлектрическая проницаемость вакуума; ε_1 и ε_2 — относительные проницаемости материалов; $U = U_1 + U_2$ — приложенное напряжение и его составляющие.

В работе [2] было показано, что при лавинном пробое гетеропереходов Ge—GaAs с глубокой степенью ограничения области запирающего слоя $E_{01} \gg E_{\text{макс. 1}}$ и $E_{02} \gg E_{\text{макс. 2}}$ и, следовательно, распределение электрического поля в области запирающего слоя можно считать достаточно однородным.

При анализе использовалась модель эквивалентного слоя умножения (ЭСУ) [5]. Эквивалентная схема запирающего слоя ЛПД и векторная диаграмма токов в этом слое приведены на рис. 2, где C- ёмкость запирающего слоя гетероперехода; $I_{ср.пр.}$ — генератор среднего тока проводимости; E- генератор ЭДС, описывающий пролетные эффекты в запирающем слое гетероперехода.

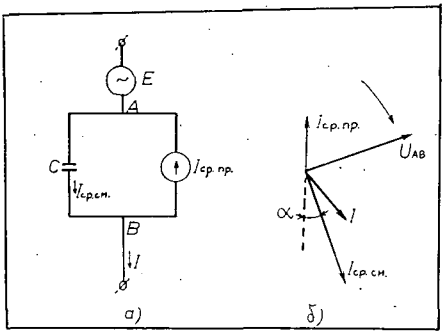

Рис. 2. Эквивалентная схема запирающего слоя ЛПД (а) и векторная диаграмма токов в этом слое (б)

Кроме того были использованы следующие общепринятые допущения:
а) смещение на диоде всегда обратное;
б) движением границ области запирающего слоя можно пренебречь, что означает как независимость сопротивления потерь диода от амплитуды колебаний, так и линейную зависимость генератора ЭДС от тока проводимости;
в) обратный ток насыщения равен нулю;
г) пролетный угол в ЭСУ подчиняется условию $\omega\tau_\lambda \leqq 1$, связанному с ограничением исходной модели ЭСУ.

В соответствии с эквивалентной схемой запирающего слоя ЛПД (рис. 2) электронный к. п. д. $\eta_{эл.}$, характеризующий мощность $P_{эл.}$, выделяющуюся в области запирающего слоя, равен [4]

$$\eta_{эл} = \frac{1}{2}\omega C \operatorname{Re} Z \cdot Y_1(K)K \cdot \cos\alpha_1(K)\left[1 - \frac{1}{\omega\tau_\lambda}\cdot\frac{Y_1(K)}{\cos\alpha_1(K)}\cdot\frac{1}{Km^{1/n}}\cdot\frac{\tau_\lambda I_o}{CU_{пр.}}\right] - \tag{11}$$

$$-\frac{1}{2}Y_1(K)K\cdot\sin\alpha_1(K)(1+\omega C \operatorname{Im} Z),$$

где Re Z, Im Z- действительная и мнимая части импеданса генератора ЭДС; τ_λ — время пролета носителей через половину ширины ЭСУ; $K = \tilde{U}_{AB}/\bar{U}_{AB}$ —

приведенная амплитуда переменной составляющей напряжения; $\overline{U}_{AB}$ — постоянная составляющая напряжения, действующего на границах ЭСУ в условиях обеднения;
$Y_1(K)=I_{ср.\,пр.}/I_o$ — приведенная амплитуда первой гармоники среднего тока проводимости;
I_0 — постоянная составляющая среднего тока проводимости, величина которой произвольно задается и определяет режим работы ЛПД;
$\alpha_1(K)$ — фаза первой гармоники среднего тока проводимости;
$U_{пр.}$ — напряжение пробоя при токе I_o и в отсутствие генерации;
$n=5{,}45$ — показатель степенной зависимости коэффициента ударной ионизации носителей в германии от поля [6];
$m=(\overline{U}_{AB}/U_{пр.})^n$ — приведенная постоянная составляющая напряжения;
ω — круговая частота.

Для двухслойной структуры ЛПД на основе гетероперехода Ge—GaAs с однородным распределением электрического поля в слое умножения выражение для импеданса генератора ЭДС можно представить в виде

$$\operatorname{Re} Z = \varphi_2/\omega C_2, \tag{12}$$

$$\operatorname{Im} Z = \psi_1/3\omega C_1 + \psi_2/\omega C_2, \tag{13}$$

где

$$\varphi_2 = (1-\cos\xi_2)/\xi_2, \tag{14}$$

$$\psi_{1,2} = (\sin\xi_{1,2}-\xi_{1,2})/\xi_{1,2}, \tag{15}$$

$$\xi_1 = \omega\tau_\lambda/2 = \omega\tau_1/6, \tag{16}$$

$$\xi_2 = \omega\tau_2, \tag{17}$$

C_1 и C_2 — составляющие полной ёмкости запирающего слоя; τ_1 — время пролета носителей через Ge — область запирающего слоя; τ_2 — время пролета носителей через GaAs — область запирающего слоя.

Для определения зависимостей $y_1(K)$ и $\alpha_1(K)$ было проведено решение уравнения лавины [5]

$$\varphi_n[U_{AB}(t)] = 1+\tau_\lambda \frac{I_{ср.\,пр.}(t-\tau_\gamma)}{I_{ср.\,пр.}(t)} - \frac{I_{обр.}}{I_{ср.\,пр.}(t)}. \tag{18}$$

В соответствии с моделью ЭСУ были определены параметры τ_λ и τ_γ и зависимость полного умножения φ_n от напряжения на запирающем слое в условиях обеднения. Для рассматриваемой двухслойной структуры запирающего слоя ЛПД на гетеропереходе Ge—GaAs с однородным распределением электрического поля в слое умножения указанные зависимости имеют вид

$$\varphi_n(U_{AB}) = (U_{AB}/U_{пр.})^n, \tag{19}$$

$$\tau_\lambda = 1/3\tau_1, \tag{20}$$

$$\tau_\gamma = -0{,}2\tau_\lambda. \tag{21}$$

Уравнение лавины было решено численным методом на ЭВМ в предположении $I_{обр.}=0$, поскольку в рабочем режиме ЛПД отношение $I_{обр.}$ к рабочему току I_0 достигает величин $10^{-4}-10^{-5}$. Результат решения уравнения лавины (18) при гармоническом напряжении, действующем на границах ЭСУ в условиях обеднения

$$U_{AB}(t) = \overline{U}_{AB}(1+K\sin\omega t) \tag{22}$$

с учетом выражений (19—21) представлен на рис. 3.

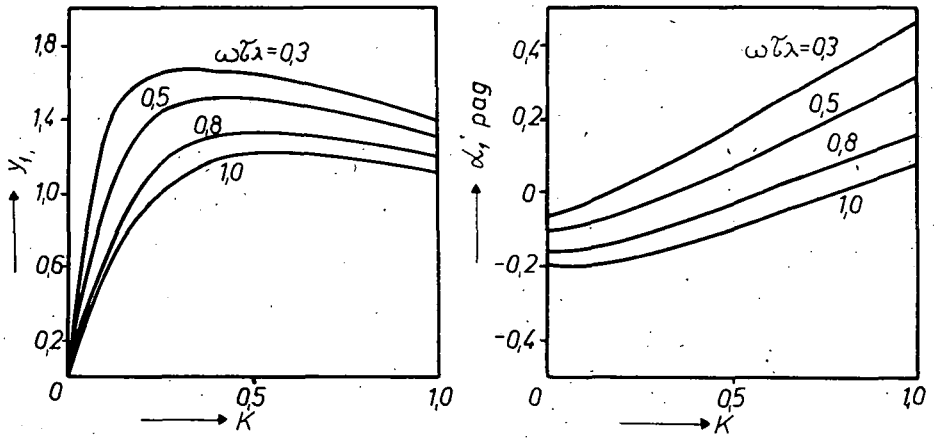

Рис. 3. Зависимость амплитуды Y_1 и её фазы α_1 от амплитуды напряжения K в диапазоне пролетных углов.

Уравнение (11) с учетом выражений (12—17) вместе с результатами решения уравнения лавины позволяет рассчитать электронный к. п. д. $\eta_{эл.}$ в зависимости от сочетания параметров K, $\omega\tau_\lambda$, $\tau_\lambda I_0/CU_{пр.}$, ξ_2. На рис. 4 представлены зависимости максимального электронного к. п. д. $\eta_{эл.макс.}$, определяемого максимумом функции $\eta_{эл.}(K)$, от пролетного угла в ЭСУ $\omega\tau_\lambda$, приведенного тока $\tau_\lambda I_0/CU_{пр.}$ и угла пролета ξ_2 в GaAs — области запирающего слоя.

Для расчета мощности $P_н$, отдаваемой в нагрузку, воспользуемся эквивалентной схемой генератора на ЛПД (ГЛПД) (рис. 5), отличающейся от эквивалентной схемы запирающего слоя ЛПД (рис. 2) включением сопротивления потерь диода R_s и сопротивления нагрузки $Z_н$, описывающий корпус диода и внешнюю цепь, присоединенную к диоду. В соответствии с рис. 5 выражение для нагрузочного к. п. д. генератора $\eta_н$, работающего на согласованную нагрузку, можно представить в виде [4]

$$\eta_н = \eta_{эл.} - \frac{1}{2}(\omega\tau_\lambda)^2 \frac{K^2 m^{1/n}}{\tau_\lambda I_0/CU_{пр.}} \left[1 - \frac{Y_1(K)}{\omega\tau_\lambda} \cdot \frac{\tau_\lambda I_0}{CU_{пр.}} \cdot \frac{1}{Km^{1/n}}\right]^2 \cdot \frac{\tau_s}{\tau_\lambda}. \tag{23}$$

На рис. 6 приведены зависимости максимального к. п. д. $\eta_{н.макс.}$, соответствующий максимальной мощности, отдаваемой в нагрузку диодом с потерями, от приведенного тока $\tau_\lambda I_0/CU_{пр.}$ для различных значений $\omega\tau_\lambda$, ξ_2, τ_s/τ_λ. На рис. 7

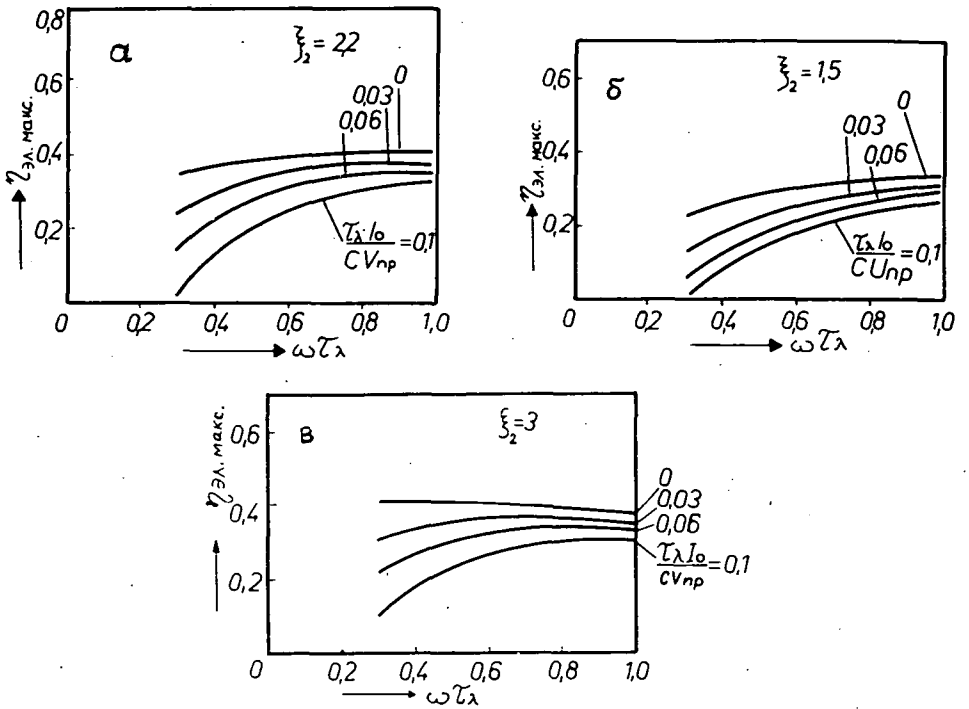

Рис. 4. Зависимость максимального электронного к. п. д. $\eta_{эл.\,макс.}$ от угла пролета $\omega\tau_\lambda$, приведенного тока $\tau_\lambda I_0/CU_{пр.}$ и ξ_2:

а – $\xi_2 = 2{,}2$; б – $\xi_2 = 1{,}5$; в – $\xi_2 = 3$.

для сравнения приведены аналогичные зависимости для германиевого ЛПД с p–i–n структурой, полученные из этих же уравнений при $\xi_1 = 0$.

Полученные результаты позволяют проанализировать влияние различных параметров ЛПД на гетеропереходе Ge—GaAs с однородным распределением электрического поля в слое умножения на к. п. д. или мощность, отдаваемую в нагрузку генератором, а также определить необходимый набор параметров ЛПД, обеспечивающий требуемые к. п. д. или мощность генерации и оптимальную нагрузку. Анализ результатов, представленных на рис. 4—7, показывает, что по к. п. д. и, следовательно мощности, отдаваемой в нагрузку, ЛПД на гетеропереходе Ge—GaAs с однородным распределением электрического поля в слое умножения более чем на порядок превосходят германиевые ЛПД с p–i–n структурой. Вместе с тем максимальные значения электронного к. п. д. ЛПД с рассмотренной двухслойной структурой запирающего слоя не достигают

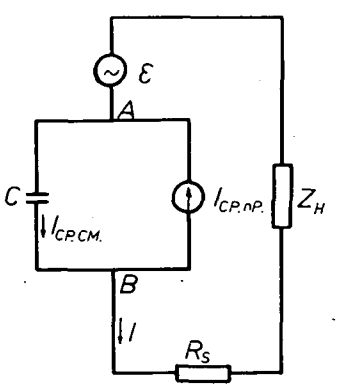

Рис. 5. Эквивалентная схема генератора на ЛПД.

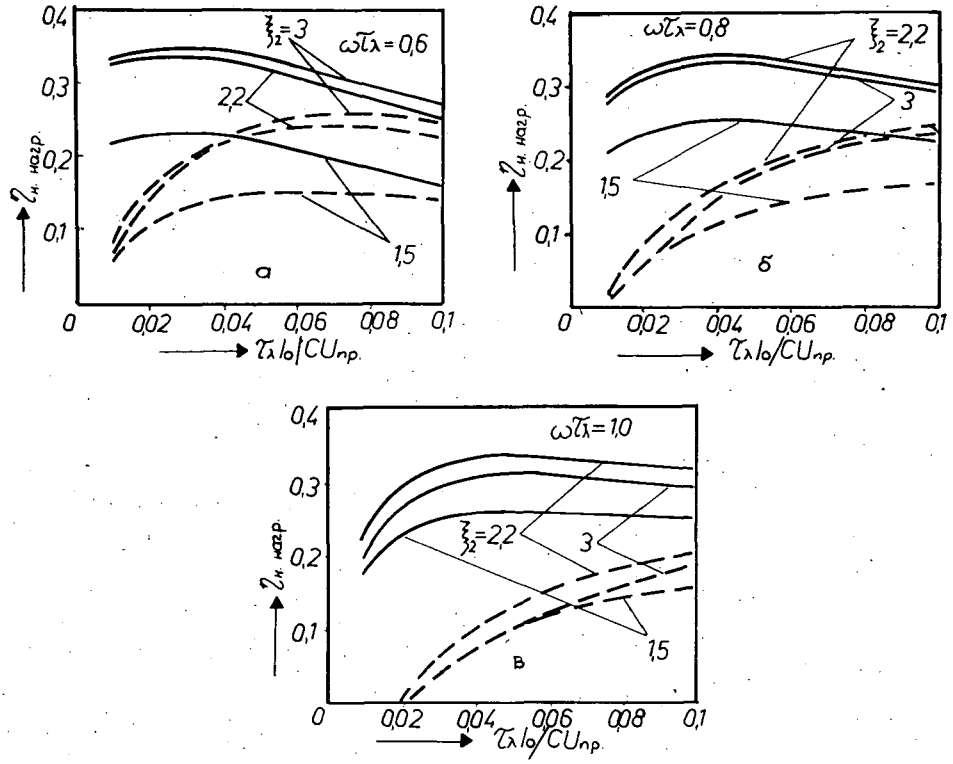

Рис. 6. Зависимость максимального к. п. д. $\eta_{н.\ макс.}$ от приведенного тока $\tau_\lambda I_0/CU_{пр.}$, угла пролета ξ_2, величины потерь τ_s/τ_λ и угла пролета $\omega\tau_\lambda$:

а – $\omega\tau_\lambda = 0{,}6$; б – $\omega\tau_\lambda = 0{,}8$; в – $\omega\tau_\lambda = 1$; ———— $\tau_s/\tau_\lambda = 0{,}005$; — — — $\tau_s/\tau_\lambda = 0{,}05$

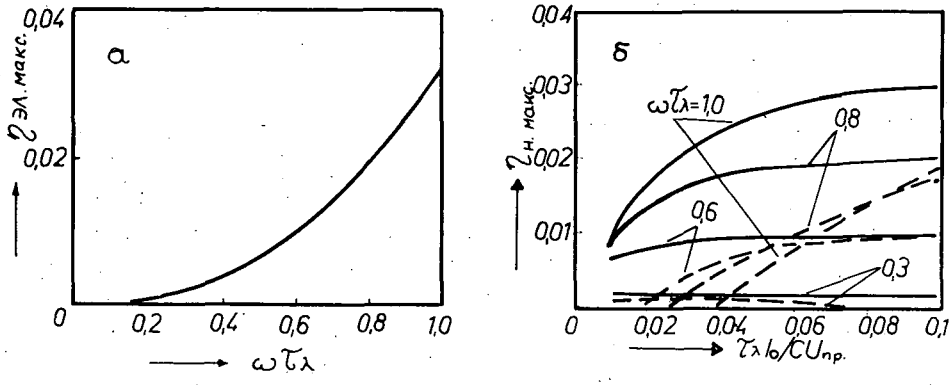

Рис. 7. Зависимости максимальный электронного $\eta_{эл.\ макс.}$ (а) и нагрузочного $\eta_{н.\ макс.}$ (б) к. п. д. для германиевого ЛПД с *p–i–n* структурой:

———— $\tau_s/\tau_\lambda = 0{,}005$; — — — $\tau_s/\tau_\lambda = 0{,}05$.

70% [7], а ограничиваются значениями40%. Это связано с тем, что оценка максимальной эффективности ЛПД с двухслойным запирающим слоем [7] была проведена без учета фазового сдвига между амплитудой первой гармоники среднего тока проводимости и амплитудой напряжения и зависимости его от последней. В то же время проведенный расчет подтвердил преимущества использования двухслойной структуры запирающего слоя в ЛПД и позволил оценить перспективы использования гетеропереходов в ЛПД.

Результаты настоящей работы, приведенные на графиках 3—4, 6 совместно с данными работы [2] позволяют определить необходимый набор параметров ЛПД и двухслойной структуры запирающего слоя на основе гетероперехода Ge—GaAs с однородным распределением электрического поля в слое умножения, обеспечивающий требуемые к. п. д. или мощность генерации и оптимальную нагрузку.

Анализ перспектив использования гетеропереходов в ЛПД позволяет сделать вывод о том, что для дальнейшего повышения к. п. д. ЛПД целесообразно использовать трёхслойную структуру запирающего слоя с двумя пролетными пространствами (материалы с высокой пробивной напряженностью электрического поля) по обе стороны от слоя умножения (материал с низкой пробивной напряженностью электрического поля). Такая структура, например, на основе (p^+-p)GaAs$-n$Ge$-(n-n^+)$GaAs позволяет повысить эффективность лавиннопролетного диода до 60—65%. Предварительные расчеты показывают, что указанная эффективность ЛПД может быть достигнута при условии, что болщины двух высокоомных слоев, в которых сосредоточен пролет носителей, тудут одинаковыми. Результаты детального анализа параметров ЛПД на основе таких структур будут представлены к печати позднее.

Выводы

1. Проведено решение уравнения лавины для двухслойной структуры запирающего слоя ЛПД на основе гетероперехода Ge—GaAs с однородным распределением электрического поля в слое умножения, позволившее определить амплитуду и фазу первой гармоники среднего тока проводимости.

2. Проведен расчет электронного и нагрузочного к. п. д. ЛПД с двухслойным запирающим слоем, позволяющий определить необходимый набор параметров ЛПД и двухслойной структуры запирающего слоя гетероперехода Ge—GaAs, обеспечивающий требуемые к. п. д. или мощность генерации и оптимальную нагрузку.

3. Предложена трёхслойная структура запирающего слоя ЛПД, позволяющая повысить максимальный к. п. д. до 60—65%.

* * *

Автор выражает благодарность сотрудникам лаборатории полупроводников Института экспериментальной физики АН ВНР за помощь в работе.

Литература

[1] *Датиев, К. М., И. М. Мартиросов, Я. А. Федотов:* Электронная техника, сер. 2 **6**, 35 (1970).
[2] *Федотов, Я. А., К. М. Датиев:* Электронная техника, сер. 2 **6**, 3 (1971).
[3] *Датиев К. М.:* Acta Phys. et Chem. Szeged **23**, 000 (1977).
[4] *Федотов, Я. А., К. М. Датиев:* Электронная техника, сер. 2 **3**, 3 (1976).
[5] *Захаров, А. Л., И. М. Мартиросов:* ФТП **1**, 1777 (1967).
[6] *Шотов, А. П.:* ЖТФ **28**, 437 (1958).
[7] *Вальд-Перлов, В. М., И. М. Мартиросов, А. С. Тагер:* Авт. Свид. СССР № 245 922, БИ 20 (1969).

NUMERICAL ANALYSIS OF Ge—GaAs IMPATT DIODES

K. M. Datiev

Calculation of generation power was done for the case of homogenous field distribution in the multiplication region of Ge—GaAs IMPATT diodes. The obtained data made possible to determine the generation efficiency and the optimum load.

CHEMISTRY IN LASERS. XIV. UTILIZATION OF NOBLE GAS HYDRIDE LASERS IN THE DISSIPATIVE CONFINEMENT OF TWO-STEP NUCLEAR FUSION OF DOUBLY ISOTOPIC BORON HYDRIDES

By

C. P. KESZTHELYI*

Department of Chemistry, University of Colorado
Boulder, Colorado 80 309, U.S.A.

(Received June 1, 1977)

The article is a continuation of the non-classical aspects of fusion (Part XI.). The utilization of doubly isotopic boron hydrides (H—2 and H—3 combined with B—11) in a two-step dissipatively controlled nuclear fusion process is proposed for energy generation, with tandem laser/e-beam pumping. To broaden the optical excitation capability, noble gas hydrides are shown to have principal advantages: lack of a bound ground electronic state (comparable with excimers), far less corrosiveness than noble gas halides (or fluorine containing laser media), wide range of tunability including the soft X-ray/VUV region, and lack of decomposition of the compounds involved upon prolonged usage (superior to dyes).

Two main experimental approaches are available to achieve controlled nuclear fusion, which in turn offers useful energy release: the charged particle accelerator, and thermonuclear fusion. Considerations of a charged particle accelerator are not stressed in this paper, but it is useful to point out the essential contrast between it and thermonuclear fusion: accelerated particles comprise a rather uniform vectorial ensemble with respect to both direction and energy, whereas in the thermonuclear approach the ensemble is normally characterized by a wide distribution of energies as well as random motion. It may also be recalled that it is necessary to distinguish, in the thermonuclear approach, between the kinetic temperature related to Maxwellian distribution, and the equivalent radiation temperature based on black body radiation; the significant differences between the two temperatures can, in the broad sense, provide the perultimate challenge that has attracted many leading scientists to fusion research in recent years.

From a practical standpoint confinement of the fusion reaction center is of paramount importance, and the magnetohydrodynamic approach seems to have taken up a perhaps disproportionate amount of available funds, leaving inertial confinement following laser excitation in the uncertain category. It is important, nevertheless, to discuss the future trend of departing from gas dynamic ablation mo-

* Visiting Faculty; permanent address: Chemistry Department, Louisiana State University, Baton Rouge, LA, U.S.A.

Present address: U.S. National Academy of Sciences — Hungarian Academy of Sciences visiting exchange scientist, SzBK, H-6701 Szeged, Hungary.

dels in using laser excitation. Up to 50% of the laser energy is transferable into pellett kinetic energy by dynamic absorption and superefficient compression, as was shown by HORE [1] in 1976. The key concept in Hore's approach is to enhance cold implosion. Once cold implosion has passed a critical stage, the system is far enough from equilibrium to be subject to that peculiar branch of non-equilibrium thermodynamics that has gained due recognition recently through the outstanding efforts of Professor Ilya PRIGOGINE and his co-workers, in particular P. GLANSDORFF, R. LEFEVER, and G. NICOLIS. Through autocatalysis or feed-back interaction the non-linear system can form an orderly assembly of new macroscopic dimensions. (The non-symmetrical design of the joint European TORUS may also facilitate such factors in confinement.) The utilization of such "dissipative structures" (popularized by the Zhabotinski-effect) for controlled nuclear fusion has been mentioned previously [2], and now we wish to propose a specific multi-step process that can provide feed-back interaction for confined, oscillatory energy release. Doubly isotopic boron hydrides (H—2 and H—3 combined with B—11), besides offering both hydrogen and boron nuclear fusion in the same molecular dimension, are fascinating chemicals on their own right. Since the first extended report [3] in 1933 on the class of compounds known as boron hydrides, some of the most exciting developments in chemistry have been tied to this area of research. Perhaps the most widely appreciated peculiarity of boron chemistry is the "electron deficiency" of some compounds like B_2H_6, or icosahedral fragments; this has led to the three-center bond concept [4—6] which enjoys general acceptance today. The charge distribution can be approximated in a simple manner from atom-atom polarizability ($\Pi(k, l)$) as:

$$\Pi(k, l) = 2 \sum_{j=1}^{m} \sum_{i=m+1}^{n} \frac{C_{ij} C_{li}}{\varepsilon_j - \varepsilon_i} [C_{kj}(SC)_{ki} + C_{ki}(SC)_{kl}], \tag{1}$$

where ε_i represent zeroth-order energies, and all levels are empty except those below n, which are doubly occupied. It is of particular interest to us that negative charges tend to be localized in the inner regions of the molecule, and in most cases with disruption of the molecular geometry. This suggests the possibility of highly inelastic interactions with e-beams, due to the availability of very long duration reaction channels (*i.e.*, molecular rearrangement). Some of these rearrangements are also significant in terms of the resurgence of chemical topology in the last few years; the pioneering work of early investigators [7] has never been extended to high energy density regions which are now of fundamental concern, and it is hoped that some effort in basic research will be devoted to this area of boron chemistry in the near future.

Nuclear fusion reactions often occur with greater ease than predicted, *i.e.* there is a discrepancy between the Coulomb barrier calculated according to classical theory, and the experimentally observed barrier penetration (which accounts for the fact that nuclear reactions do occur at detectable rates far below the Coulomb barrier, and provides a powerful argument in favor of quantum mechanics and tunnelling.) Concerning the first of the two fusion steps, it would be counterproductive to attempt to review here the development of hydrogen isotope fusion, an area of chemistry so well established that even elementary texts of recent vintage cover it in considerable detail [8]. Summarizing some of the heavy hydrogen reactions, including the "neutron

branch" (Eq. (2)), the "proton branch" (Eq. (3)), and two reactions (Eqs. (4) and (5)) of high energy yield:

$$D+D \rightarrow \underset{(0.82\ MeV)}{He^3} + \underset{(2.45\ MeV)}{n} \quad (2)$$

$$D+D \rightarrow \underset{(1.01\ MeV)}{T} + \underset{(3.02\ MeV)}{H} \quad (3)$$

$$D+T \rightarrow \underset{(3.5\ MeV)}{He^4} + \underset{(14.1\ MeV)}{n} \quad (4)$$

$$D+He^3 \rightarrow \underset{(3.6\ MeV)}{He^4} + \underset{(14.7\ MeV)}{H} \quad (5)$$

we find that about 33% of the energy liberated is carried by charged particles to be deposited internally within the reacting system for a pure deuterium target, with the neutrons making additional contributions. This energy would partially aid the next stage: fusion involving boron nuclei.

Compared to the hydrogen isotopes', boron fusion is a new and little explored area. The complete-fusion cross section of boron-11+terbium-159 was reported by KOZUB *et al.* [9] in 1974, while ZEBELMAN and co-workers reported [10] in the same year both fission and completefusion values. Evidence of an intermedate quasi-stationary state of boron-11 fusion was presented [11] by PETKOV *et al.* in 1975, and related by the same authors to fission calculations in a separate publication [12.] While only a fraction of the boron fusion effort has been fully reported in the open literature, several important advances are documented for the year 1976: (a) DAYRAS, STOCKSTAD, SWITKOWSKI and WIELAND at CIT determined fusion cross sections for $B+^{12}C$ over a 5 MeV range extending below the Coulomb barrier, and compared the results with optical model calculations [13]; (b) NAMBOODIRI and cp-workers examined fusion products of $^{12}C+^{12}C$, and considered the boron cross section too [14]; (c) DATLA *et al.* used a small θ-pinch plasma to deduce ionization rate coefficients for B(IV) as well as C(V) [15].

Among the large number of possible compounds, B_4H_{10} and B_5H_{11} are typical suitable analogs, with varying atomic ratios of the desired isotopes. In the tandem excitation process laser driven heavy hydrogen fusion is the initiator for the boron-11 fusion, which is e-beam pumped. The energetic feed-back leading to oscillatory confinement of the reaction center need not necessarily be tied to a classical reaction of nuclear chemistry, but could be due, for example, to self-focussing control of the energy release process as a function of dissipative structures. To aid the oscillatory mechanism, the energy input is of crucial importance, and several aspects can only be decibed by experiment. In the following we address ourselves to the question of upgrading laser performance.

In the quest for suitable materials to provide high output power, tunability, short wavelength, and if possible exceptional stability, various shortcomings of available laser systems become readily apparent. By resorting to the concept of strongly coupling the radiation field in an optical resonant cavity with a suitable

molecular ensemble [16], the feasibility of preparing some optimal compounds *in situ* became an evident route of novel significance. Hydrogen, the simplest chemical element, is an ideal counterpart to noble gases, due to the lack of a stable hydride with any of them. It is instructive to pursue the details of thermodynamic stability vs. instability based on known bond energetics, and the excellent and provoking text by DASENT [17] should be consulted by those unfamiliar with the field. The necessary orbital overlap for hydride formation can be produced by hyperpolarization—with varying facility as a function of the number of electrons involved, the extent of the electron cloud and its polarizability, hence as a function of atomic number or isotope in case of hydrogen. To select energy levels one needs to refer, perhaps paradoxically, not to general texts on quantum chemistry, but to Kittel's "Thermal Physics" [18]. The crucial trade-off of ordinary molecular orbitals for the alternate set available in the OR cavity is readily acceptable once an essentially relativistic treatment, based on photon-cavity interactions rather than the atomic and molecular electronic transition lines, is adopted. The soundness of the approach can be gauged from theoretical [19] as well as experimental grounds; the latter stems from Stanford University's spectacular development of a free-electron laser (yet to be published), in which a relativistic electron beam creates the energy levels for population inversion through interaction with a pulsed magnetic field.

Additional factors influencing tuneability are the overall pressure, temperature, and above all: composition. With several noble gases in the cavity, staircase tuning to short wavelengths is the obvious approach, hydride formation giving great flexibility in comparison to noble gas excimers/exciplexes only. Unlike CO_2 (which has been successfully tuned already by controlling added inert gas components and overall pressure), the decomposition products in the present system are innocuous starting materials. A TEA arrangement is promising in view of VUV laser action having been reported in pure hydrogen upon electric discharge. A similar arrangement reported in 1973 [20], based on electric discharge pumping of noble gas-scintillator dye vapor mixtures in an optical cavity, was subject to dye decomposition and slow coating of the mirrors from the cavity side—complications which are, of course, totally eliminated when rare gases and hydrogen comprise the optically active medium.

References

[1] *Hore, H.:* Proc. Eur Electro-Opt. Mark. Technol. Conf. (2nd). (1976).
[2] *Keszthelyi, C. P.:* Chemistry and Lasers **3**, 641 (1976).
[3] *Stock, A.:* "Hydrides of Boron and Silicon", Cornell University Press, Ithaca, New York, 1933.
[4] *Stitt, F.:* J. Chem. Phys. **8**, 891 (1940).
[5] *Pitzer, K. S.;* J. Amer. Chem. Soc. **67**, 1126 (1946).
[6] *Mulliken, R. S.:* Chem. Rev. **41**, 207 (1947).
[7] *Dickerson, R. E., W. N. Lipscomb:* J. Chem. Phys. **27**, 212 (1957).
[8] *Gordon, G., W. Zoller:* "Chemistry in Modern Perspective", Addison Wesley, 1973.
[9] *Kozub, R. L., D. Logan, J. M. Miller,* and *M. Zebelman:* Phys. Rev. C **10**, 214 (1974).
[10] *Zebelman, A. M., L. Kowalski, J. Miller, K. Beg, Y. Eyal, G. Jaffe, A. Kandil,* and *D. Logan:* Phys. Rev. C **10**, 200 (1974).
[11] *Petkov, I., Ya. Delchev:* Bulg. J. Phys. **2**, 293 (1975).
[12] *Delchev, Ya., I. Petkov,* and *Kh. Khristov:* Yad. Energ. **2**, 13 (1975).
[13] *Dayras, R. A., R. G. Stokstad, Z. E. Switkowski, and R. M. Wieland:* Nucl. Phys. A **A261** 478 (1976).
[14] *Namboodiri, M. N., E. T. Chulick,* and *J. B. Natowitz:* Nucl. Phys. A **A263**, 491 (1976).

[15] *Datla, R. U., L. J. Nugent,* and *Hans R. Griem:* Phys. Rev. A **14**, 979 (1976).
[16] *Keszthelyi, C. P.:* Spec. Ltrs. 3, 85 (1974).
[17] *Dasent, W. E.:* "Nonexistent Compounds", Marcel-Dekker, Inc., New York, 1965.
[18] *Kittel, C.:* "Thermal Physics", John Wiley and Sons, Inc., New York, 1969.
[19] *Wigner, E. P.:* Rev. Mod. Phys. **29**, 255 (1975).
[20] *Keszthelyi, C. P.:* Ph. D. Thesis, University of Texas at Austin, 1973.

ЛАЗЕРНАЯ ХИМИЯ, XIV. ПРИМЕНЕНИЕ ЛАЗЕРОВ НА ИНЕРТНЫХ ГАЗОВЫХ ГИДРИДАХ В ДИССИПАТИВНЫХ СТАБИЛИЗАЦИЯХ ДВУХСТУПЕНЧАТОЙ ЯДЕРНОЙ ФУЗИИ ДВОЙНЫХ ИЗОТОПОВ БОРОГИДРИДОВ

Ч. П. Кестхели

Настоящая статья является продолжением серии статей по неклассическим аспектам ядерной фузии (часть XI.). Предлагается применение двойных изотопов борогидридов (H—2 и H—3 в сочетании с B—11) в двухступенчатых контролируемых ядерных фузионных процессах для генерации энергии с помощью накачки электронного пучка тандемного лазера. Для расширения области оптической возбуждаемости, гидриды инертных газов обладают следующими принципиальными преимуществами: 1. отсуствие связного основного электронного состояния (подобно эксимерам); 2. гораздо менее коррозионные чем галиды инертных газов (или, чем лазерные материалы содержащие фтор); 3. широкая область подстройки, включая мягкие рентгеновские лучи и вакуумного ультрафиолета; 4. отсуствие разложения веществ участвующих в продолжительной эксплоатации лазера (превосходя красители)

THE SPECTRA, STEREOCHEMISTRY AND ELECTRONIC STRUCTURES OF COPPER(II) COMPLEXES

By

J. CSÁSZÁR and J. BALOG

Institute of General and Physical Chemistry, Attila József University, Szeged, Hungary

(Received 1 September 1977)

The relationships between the spectral properties of Cu(II) complexes with different symmetries and the geometries of the molecules are discussed.

1. *Introduction*

The structures of complexes of first-row transition metals are mostly tetrahedral, square-planar or octahedral [1], or distorted modifications of these, whereas the structures of Cu(II) complexes are generally distorted variations of the base-geometries. The spectral and magnetic properties of Co(III), Ni(II), Co(II), Cr(III), etc. complexes are sensitive indicators of changes in the stereochemistry of the molecules [2—6], but in the case of Cu(II) complexes these properties do not give definite information on the structures of the molecules (see *e.g.* [7—10]).

The present paper gives a survey of the spectral, magnetic and *e.s.r.* properties of mononuclear Cu(II) complexes.

2. *Stereochemistry of compounds*

As a result of X-ray, electron- and neutron-diffraction structure investigations, several different geometrical structures can be shown to occur in the stereochemistry of Cu(II) complexes (Table I).

$K_2PbCu(NO_2)_6$ has a regular octahedral structure with six equivalent Cu—N bonds (2.11 Å) [11]. In $Cu(en)_3SO_4$ [12] there are also six equal Cu—N bonds (2.17 Å), but the presence of ethylene bridges lowers the symmetry to trigonal D_3. A flattened tetrahedron (D_{2d}) occurs, for instance, in the Cs_2CuCl_4 molecule [13]. Tetragonally-distorted six-coordination (D_{4h}) is also quite frequent, *e.g.* in $Cu(NH_3)_4(SCN)_2$ there are four shorter (2.08 Å) in-plane bonds (r_p) and two longer (3.00 Å) axial ones (r_a) [14]. Many rhombically-distorted (elongated) octahedral [15], tetragonally-distorted (compressed) [16] and rhombically-distorted (compressed) octahedral compounds [17] are known.

The Cu(II) chelates of aromatic Schiff bases are mainly square-planar, but the same coordination is found in $CaCuSi_4O_{10}$ [18], too. Moreover, Cu(II) complexes

Table I.

Stereochemistry of Cu(II) complexes

Coord. number	Stereochemistry	Symmetry group	Example*
4	square-planar	D_{4h}	$CaCuSi_4O_{10}$
		D_{2h}	$Cu(3\text{-}CH_3\text{-acac})_2$
	compressed tetrahedral	D_{2d}	Cs_2CuCl_4
5	trigonal-bipyramidal	D_{3h}	$Cu(NH_3)_2.Ag(SCN)_3$, $Cr(NH_3)_6.CuCl_5$
	square-pyramidal	C_{4v}	$Cu(NH_3)_4H_2O.SO_4$
6	octahedral	O_h	$K_2BaCu(NO_2)_6$, $K_2PbCu(NO_2)_6$
	elongated tetragonal	D_{4h}	$Cu(NH_3)_4(SCN)_2$, $Cu(H_2O)_4(COOH)_2$
	compressed tetragonal	D_{4h}	Ba_2CuF_6, K_2CuF_4
	elongated rhombic	D_{2h}	$CsCuCl_3$, $Ba_2Cu(COOH)_6.4\,H_2O$
	compressed rhombic	D_2	$Cu(dien)_2(NO_3)_2$
	trigonal	D_3	$Cu(en)_3SO_4$, $Cu(dip)_3Cl_2$
	cis-octahedral		$Cu(dip)_2ONO.NO_3$, $Cu(dip)_2I.I$
8	distorted dodecahedral	D_{2d}	$CaCu(CH_3COO)_4.6\,H_2O$

* Acac: acetylacetone, pdm: propylenediamine, dien: diethylene-triamine, en: ethylene-diamine, dip: α, α'-dipyridyl

involving five (trigonal-bipyramidal [19], square-pyramidal [20]) and eight-coordination [21] are also known.

The structure of a complex is influenced or determined by several factors: the JAHN—TELLER effect [22—26], semicoordination [27—32], the variation in tetragonal distortion [24, 33], π-bonding [27, 34, 35], and steric effects [31, 36—41].

3. *Electronic properties of complexes*

The Cu(II) ion has $3d^9$ outer electron configuration; being the total orbital angular moment $L=2$ and the spin multiplicity $r=2$, the spectroscopic ground state is ^2D.

Due to the effects of ligand fields, the ground-state splits (see *e.g.* Fig. 1). In an octahedral (O_h) field the energies of the x^2-y^2 and z^2 orbitals increase, while those of the xy, xz and yz orbitals decrease, the difference in energy being $10\,Dq$. In the case of a distorted octahedron or other lower symmetries, these levels split further and new energy levels with a maximum number of $(2L+1)$ may arise.

A summary of splitting schemes occurring for different symmetries is given in Figs. 1 and 2; the ground-states can be seen in Table II.

As regards a discussion of the d^9 electronic system on the basis of the ligand field theory, we refer to the literature [7—10, 42, 43].

Table II.

One electron orbitals playing roles in the longest wavelength transitions of Cu(II) complexes with various stereochemical arrangements

x^2-y^2	elongated tetragonal elongated rhombic square-planar [$CaCuSi_4O_{10}$-type] square-pyramidal	xy	compressed tetrahedral square-planar [$Cu(acac)_2$-type]
z^2	compressed tetragonal compressed rhombic trigonal-bipyramidal cis-octahedral	z^2, x^2-y^2	octahedral[a]
		xy, xz, yz	tetrahedral[b]
		xz, yz	elongated tetrahedral[c]

[a, b, c] Orbitally-degenerate states; with the exception of case a, the degeneracy is removed by spin-orbital coupling.

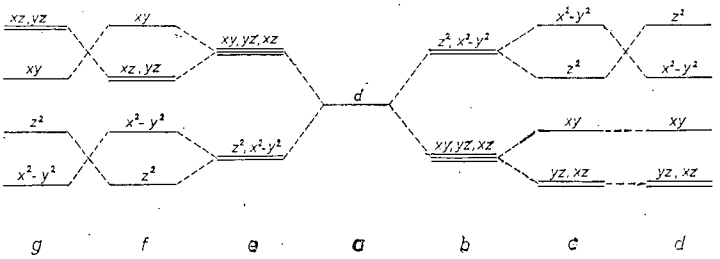

Fig. 1. The splitting of the ground-state of the Cu(II) ion in fields of different symmetries. *a)* free metal ion; *b)* in octahedral (O_h) field; *c)* in elongated tetragonal (D_{4h}) field; *d)* in compressed tetragonal field (D_{4h}); *e)* in tetrahedral (T_d) field; *f)* in compressed tetrahedral (D_{2d}) field; *g)* in elongated tetrahedral (D_{2d}) field.

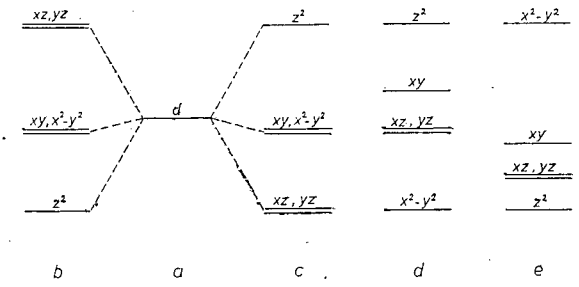

Fig. 2. The splitting of the ground-state of the Cu(II) ion in fields of different symmetries. *a)* free metal ion; *b)* in trigonal (D_3) field; *c)* in trigonal-bipyramidal (D_{3h}) field; *d)* in cis-octahedral (C_{2v}) field; *e)* in square-planar (D_{4h}) field.

4. *Magnetic properties*

When the individual Cu(II) ions in the complex are well separated from each other (~5 Å), the effective magnetic moment is in good accordance with the spin-only value (1.73 B.M.) [44]. In practice, the experimental values are somewhat higher; they lie in the range 1.80—2.10 B.M. (Table III) and are practically indepen-

Table III.

Magnetic moments of complexes of different stereochemistry [44]

Compound	Symmetry group	μ_{eff}	Compound	Symmetry group	μ_{eff}
$Cu(NH_3)_4(SCN)_2$	D_{4h}	1.81	$Cu(NH_3)_2.Ag(SCN)_3$	D_{3h}	1.83
$Cu(NH_3)_4H_2O.SO_4$	C_{4v}	1.87	$Cu(acac)_2$	D_{2h}	1.91
$Cu(dip)_2ONO.NO_3$	C_{2v}	1.89	$Cu(en)_2(BF_4)_2$	D_{2h}	1.88
Cs_2CuCl_4	D_{2d}	1.92	$CaCu(CH_3COO)_4.4\,H_2O$	D_{2d}	1.94
$K_2CuCl_4.2\,H_2O$		1.88	$Cu(NH_3)_4(NO_2)_2$	D_{4h}	1.89
$Cu(dip)_2NH_3.(ClO_4)_2$		1.92			

dent of the stereochemistry. The increase in the moment is a result of the spin-orbit coupling [44]. In simple Cu(II) complexes the electronic ground-state is orbitally nondegenerate, and therefore there is no inherent orbital moment contribution to the magnetic moment of the ground-state. The investigation of magnetic anisotropy offers much more information on stereochemistry [45]. If antiferromagnetic interaction occurs between the Cu(II) ions, then the observed magnetic moment is below the spin-only value [46]; this case, however, is primarily related to multinuclear complexes.

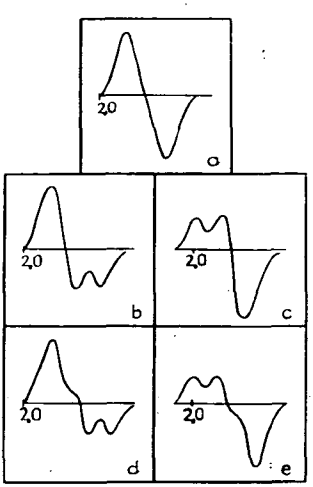

Fig. 3. Schematic structure of the *e.s.r.* spectra of Cu(II) complexes of different symmetries. *a)* isotropic spectrum; *b)* elongated tetragonal, $g>2.04$; *c)* compressed tetragonal, $g<2.03$; *d)* elongated rhombic, $g>2.04$; *e)* compressed rhombic, $g<2.03$ (derivative curves).

5. *Electron spin resonance spectrum*

Investigation of the *e.s.r.* spectrum [45—50] yields the following informations:

a) the electronic ground-state of the complex,
b) the symmetry of the effective ligand field around the central ion,
c) the orientation of the Cu(II) chromophores in the unit cell.

The spectra can be arranged in three general classes.

I. Isotropic spectra are observed for compounds with regular octahedral and tetrahedral structures [26, 51—53]; octahedral compounds undergoing JAHN—TELLER distortion; CuL_3X_2-type compounds; and CuL-type compounds with free rotational possibilities (Fig. 3/a).

II. Axial spectra occur [19, 27, 30, 53] when
a) $g > 2.04$; this is the case for tetragonally-distorted (elongated) octahedral, square-planar, square-pyramidal and trigonal-bipyramidal structures (Fig. 3/b).
b) $g < 2.03$; in the case of compressed tetragonal, trigonal-bipyramidal, and some compressed rhombic symmetries (Fig. 3/c).

III. Two types of rhombic spectra can be distinguished again [34, 54]:
a) $g > 2.04$; in the case of elongated rhombic, elongated axial, and distorted square-pyramidal symmetries (Fig. 3/d).
b) $g < 2.03$; in the case of compressed rhombic, compressed axial, distorted trigonal-bipyramidal and *cis*-octahedral structures (Fig. 3/e).

Table IV illustrates the relations between g values and spectrum types and stereochemistry, for a number of Cu(II) complexes, while the schematic *e.s.r.* spectra for five types mentioned can be seen in Fig. 3.

Table IV.

g values of Cu(II) complexes of different stereochemistry [71]

Spectrum type	Stereochemistry	Example	g values
Isotropic	octahedral	$K_2PbCu(NO_2)_6$	$g = 2.10$
	trigonal	$Cu(en)_3SO_4$	$g = 2.13$
Axial	elongated tetragonal	$Cu(NH_3)_4(SCN)_2$	$g_\perp = 2.056$, $g_\parallel = 2.237$
	square-planar	$CaCuSi_4O_{10}$	$= 2.054$, $= 2.326$
	trigonal-bipyramidal	$Cu(NH_3)_2 . Ag(SCN)_3$	$= 2.207$, $= 2.004$
Rhombic	elongated rhombic	$Cu(dien)_2Br_2 . H_2O$	$g_1 = 2.045$, $g_2 = 2.097$, $g_3 = 2.213$
	elongated rhombic	$Ba_2Cu(COOH)_6 . 4\,H_2O$	$g_1 = 2.078$, $g_2 = 2.109$, $g_3 = 2.383$
	compressed rhombic	$Cu(dien)_2(NO_3)_2$	$g_1 = 2.03$, $g_2 = 2.13$, $g_3 = 2.16$
	cis-octahedral	$Cu(dip)_2ONO . NO_3$	$g_1 = 2.029$, $g_2 = 2.170$, $g_3 = 2.205$

6. *Spectra*

Four types of transitions have to be taken into account in the spectra of Cu(II) complexes: those below 20 kK: (*i*) $d-d$ transitions, (*ii*) the possible vibrational overtones of the ligand; and those above 20 kK: (*iii*) charge-transfer transitions, (*iv*) intraligand transitions. In the following we deal only with $d-d$ transitions. These transitions are controlled by spin multiplicities (forbidding of intercombinations), and the LAPORTE rule [2, 4, 55, 56]; nevertheless, these selection rules are lifted in these multi-electron systems [2, 55, 56]. The reflection spectra, and especially the polarized single-crystal spectra, give good information on stereochemistry [57, 58]. Similarly to the term-splitting schemes (Figs. 1 and 2), the spectra are also discussed on the basis of one-electron energy levels; *i.e.* the electron-electron interactions are neglected.

I. *Four-coordination*

1. *Compressed tetrahedral structure*

In Cs_2CuCl_4 the Cu—Cl bond-length is 2.22 Å, and the Cl—Cu—Cl angles are 120° and 103° [13, 59]; the molecule is of D_{2d} symmetry. The complex is magnetically anisotropic: $g_1=2.083$, $g_2=2.103$, $g_3=2.384$ [60]. The bonds formed with the strongly polarizable Cl^- ions are predominantly covalent, as proved by the low value of the coupling constant λ [60, 61].

The characteristic maximum appears at 9.50 kK [62] in the fused-salt spectrum, at 7.00 kK [59] in the crystal spectrum, and at 12.40 kK for $CsCd_{1-x}Cu_xCl_3$ compounds. The fused-salt spectrum gives a band lying between the bands of the octahedral and the tetrahedral forms. With increasing temperature this band shifts towards the band of the tetrahedral form [62]. In the spectrum of the $CuCl_4^{2-}$ ion three transitions can be expected (see Fig. 1/f):

$$\begin{aligned}(z^2)^2(x^2-y^2)^2(xz,\,yz)^4(xy)^1 &\rightarrow (z^2)^2(x^2-y^2)^2(xz,\,yz)^3(xy)^2, \quad (\nu_1)\\ &\rightarrow (z^2)^2(x^2-y^2)^1(xz,\,yz)^4(xy)^2, \quad (\nu_2)\\ &\rightarrow (z^2)^1(x^2-y^2)^2(xz,\,yz)^4(xy)^2. \quad (\nu_3)\end{aligned} \tag{I}$$

The bands due to the above transitions appear at 4.28, 7.78 and 8.50 kK. The polarized crystal spectra also give bands between 5 and 9 kK [60]. The reflection spectrum (Fig. 4/1) yields a broad band at around 11.20 kK, which can be divided into two components, at 10.50 and 12.00 kK.

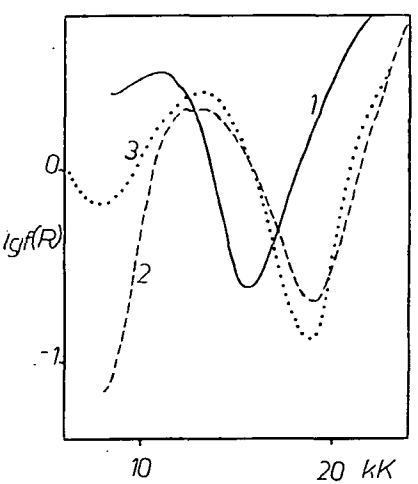

Fig. 4. Reflection spectra. *1:* Cs_2CuCl_4; *2:* $Cu(NH_3)_2.Ag(SCN)_3$; *3:* $K_2PbCu(NO_2)_6$.

These bands can be assigned to the transitions ν_2 and ν_3. The data indicate a strong distortion of the molecule. In aqueous solution the experimental band is broadened ($\nu_{max}=12.60$ kK). This is very likely due to the presence of $Cu(H_2O)_{6-x}Cl_x$-type species [64]. In pyridine the band shifts even further: ($\nu_{max}=14.12$ kK).

2. *Square-planar arrangement*

In the case of square-planar chelates π-bonds are formed with the xz and yz orbitals of the Cu(II) ion. In these complexes the in-plane bonds are shorter than those in the tetragonally-distorted octahedral molecules. Regular square-planar coordination (D_{4h}) occurs in $CaCuSi_4O_{10}$ [18], where all the Cu—O bond-lengths are roughly the same (1.91 Å).

The band of highest energy in the spectrum is assigned to the transition (see Fig. 2/e):

$$(z^2)^2(xz,\,yz)^4(xy)^2(x^2-y^2)^1 \rightarrow (z^2)^1(xz,\,yz)^4(xy)^2(x^2-y^2)^2.$$

The stereochemistry of $Cu(acac)_2$, with ligands capable of π-bonding, is rhombically-distorted square-planar (D_{2h} symmetry) [33, 57]. In the single-crystal spectrum the three bands at 14.50, 15.60 and 18.00 kK are then assigned to the transitions:

$$\begin{aligned}(xz, yz)^4(x^2-y^2)^2(z^2)^2(xy)^1 &\rightarrow (xz, yz)^4(x^2-y^2)^2(z^2)^1(xy)^2, \quad (\nu_1)\\ &\rightarrow (xz, yz)^4(x^2-y^2)^1(z^2)^2(xy)^2, \quad (\nu_2)\\ &\rightarrow (xz, yz)^3(x^2-y^2)^2(z^2)^2(xy)^2. \quad (\nu_3)\end{aligned} \qquad \text{(II)}$$

The interpretation of the spectrum becomes possible by the assumption of π-bonding [65]. The band measured in chloroform solution can be divided into three GAUSS bands, at 15.00, 15.20 and 18.80 kK [66]. There is only a slight difference between the spectrum of the crystal and that of the chloroform solution. This fact can be interpreted by the weak intramolecular interaction in the crystalline state [66].

II. *Five-coordination*

Trigonal-bipyramidal structure

In $Cu(NH_3)_2.Ag(SCN)_3$ the bond-lengths are: Cu—N(H)$_3$: 2.00 Å, Cu—N(CS): 1.92 Å [19]. The CuN_2N_3' chromophore has D_{3h} symmetry, and the compound is paramagnetic, with 1.83 B.M. [44]. The *e.s.r.* spectrum is of axial type, $g_{\parallel}=2.004$, $g_{\perp}=2.207$ [20], and the ground orbital is z^2.

According to the term-scheme there are two possible transitions (Fig. 2/c):

$$\begin{aligned}(xz, yz)^4(xy, x^2-y^2)^4(z^2)^1 &\rightarrow (xz, yz)^4(xy, x^2-y^2)^3(z^2)^2, \quad (\nu_1)\\ &\rightarrow (xz, yz)^3(xy, x^2-y^2)^4(z^2)^2. \quad (\nu_2)\end{aligned} \qquad \text{(III)}$$

On the other hand, in the single-crystal spectrum there are three bands [65], at 10.50, 13.30 and 14.60 kK. This fact is interpreted by spin-orbit coupling and by π-bonding, and it is proved by the low values of the coupling constant [67]. NH_3 and NCS^- lie near to each other in the spectrochemical series, and thus the spectrum of the complex is very similar to that of the complex $Cu(NH_3)_5^{2+}$. The reflection spectrum between 10 and 16 kK contains a wide complex band, the three components of which are at 11.20, 13.00 and 14.60 kK. In pyridine the maximum is at 14.60 kK.

III. *Six-coordination*

Regular octahedral Cu(II) complexes are hardly known, but several complexes of distorted octahedral structure can be prepared.

1. *Octahedral structure*

The complex $K_2PbCu(NO_2)_6$, containing the CuN_6 chromophore, is of octahedral structure [24, 51], but due to the dynamic JAHN—TELLER effect, this is distorted [24, 51]. The *e.s.r.* spectrum is isotropic, $g=2.11$, and assuming octahedral geometry (O_h) the ground-state is degenerate (z^2, x^2-y^2). The reflection spectrum

(Fig. 4/3) contains two bands, at 16.50 and 7.00 kK. Due to the JAHN—TELLER effect, the appearance of these bands can be interpreted by distortion of the octahedral symmetry (D_{4h}). Accordingly, the following three transitions have to be taken into account (Fig. 1/c):

$$\begin{aligned}(xz, yz)^4(xy)^2(z^2)^2(x^2-y^2)^1 &\rightarrow (xz, yz)^4(xy)^2(z^2)^1(x^2-y^2)^2, \quad (\nu_1)\\ &\rightarrow (xz, yz)^4(xy)^1(z^2)^2(x^2-y^2)^2, \quad (\nu_2)\\ &\rightarrow (xz, yz)^3(xy)^2(z^2)^2(x^2-y^2)^2. \quad (\nu_3)\end{aligned} \qquad \text{(IV)}$$

The ν_1 band merges into a wide band at around 16.50 kK. In aqueous solution ($\nu_{max}=13.10$ kK) this band indicates the presence of mixed aqua-nitro species. In pyridine the shift appears on a smaller scale ($\nu_{max}=15.30$ kK). The observed change, in comparison with the reflection spectrum, can be interpreted by interaction between the atomic orbitals of copper and the solvent molecules.

2. *Tetragonal structure*

The complexes $Cu(H_2O)_4(COOH)_2$, $Cu(NH_3)_4(NO_2)_2$, $Cu(NH_3)_4(SCN)_2$, *etc.* are tetragonally-distorted octahedral ones. $Cu(NH_3)_4(SCN)_2$ is of D_{4h} symmetry and is paramagnetic, with 1.81 B.M. [68]; $g_\perp=2.056$ and $g_\parallel=2.237$; the ground-state is: x^2-y^2 [34]. For this compound the measure of tetragonal distortion ($T=r_p/r_a$) is $T\sim0.70$.

The low-temperature single-crystal spectrum [34] contains three bands, at 17.90, 15.70 and 14.00 kK; these may be assigned to the transitions (IV). If π-bonding is also formed, then the z^2 and xy orbitals interchange. ν_1 is a measure of the tetragonal distortion, and a relationship can be found between ν_1 and the in-plane Cu-N bond-lengths. By the use of the spectrum and the *e.s.r.* data, the spin-orbit reduction factor can be calculated, $k_\parallel=0.74$ and $k_\perp=0.76$. These values indicate the predominant covalent character of the bonds [69]. The broad band appearing at 10—20 kK in the reflection spectrum (Fig. 5/1) can be resolved into three Gaussian curves at 14.00, 16.00 and 17.00 kK. The calculated [70] value of 10 Dq is 12.20 kK. In pyridine, only one, nearly symmetric band is obtained, at 14.50 kK.

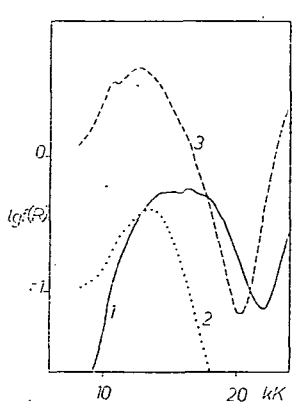

Fig. 5. Reflection spectra. *1:* $Cu(NH_3)_4(SCN)_2$; *2:* $Ba_2Cu(COOH)_6\cdot4\,H_2O$; *3:* $Cu(dip)_3Br_2$.

Examples of compressed tetragonal symmetry are less known and no polarized single-crystal spectrum for this type is available. Sometimes even the ground-states and the one-electron orbital sequences are contraversial in the different references.

3. *Rhombic structure*

$Ba_2Cu(COOH)_6\cdot4\,H_2O$ is of elongated rhombic structure [15] and is paramagnetic, with 1.88 B.M. The *e.s.r.* spectrum is of rhombic-type [15], $g_1=2.087$, $g_2=2.109$, $g_3=2.383$.

The polarized single-crystal spectrum is similar to those of the tetragonal complexes [34, 69], but spectra polarized in the x and y directions are different. The spectrum can be interpreted by D_{2h} symmetry; the ground-state is x^2-y^2 [71]. Four bands can be distinguished, at 8.40, 10.60, 13.10 and 14.50 kK [71], which can be assigned to the following transitions:

$$\begin{aligned}(xz)^2(yz)^2(xy)^2(z^2)^2(x^2-y^2)^1 &\rightarrow (xz)^2(yz)^2(xy)^2(z^2)^1(x^2-y^2)^2, \quad (\nu_1)\\ &\rightarrow (xz)^2(yz)^2(xy)^1(z^2)^2(x^2-y^2),^2 \quad (\nu_2)\\ &\rightarrow (xz)^2(yz)^1(xy)^2(z^2)^2(x^2-y^2)^2, \quad (\nu_3)\\ &\rightarrow (xz)^1(yz)^2(xy)^2(z^2)^2(x^2-y^2)^2. \quad (\nu_4)\end{aligned} \tag{V}$$

The reflection spectrum (Fig. 5/2) contains a wide band $\nu_{max}=13.40$ kK, the spectrum of the aqueous solution ($\nu_{max}=13.10$) is only slightly different, and in pyridine the band is shifted to 15.15 kK. The decrease in the coupling constants (0.78—0.86) indicates mainly ionic bonding [69].

Though the elongated rhombic form is more frequent, there are examples (*e.g.* Ba_2CuF_6, $Cu(dien)_2(NO_3)_2$) of the compressed version, too. The spectrum of the dien complex has been investigated by STEPHENS [17]. From the rhombic-type (symmetry: C_2) *e.s.r.* spectrum, $g_1=2.0266$, $g_2=2.1440$ and $g_3=2.1570$ [52]; the ground orbital is z^2.

In the single-crystal spectrum the presence of three bands can be detected, at 8.00, 12.00 and 16.00 kK; these are assigned to the $x^2-y^2\rightarrow z^2$, $xy\rightarrow z^2$ and $xz,yz\rightarrow z^2$ transitions [7]. The one-electron orbital sequence is $z^2>x^2-y^2>xy>xz, yz$. The broad band observed in the reflection spectrum can be resolved into three Gaussian curves, at 12.10, 14.00 and 16.00 kK (Fig. 6/3). In water or in pyridine, only one, nearly symmetric band is measurable, at 16.20 and 17.05 kK, respectively.

4. *Trigonal structure*

$Cu(dip)_3Br_2$ and $Cu(en)_3SO_4$ have trigonally-distorted structures. The en complex has an isotropic *e.s.r.* spectrum, $g=2.13$ [24]; the symmetry is D_3; the ground orbital is xy (see Fig. 2/b).

The single-crystal spectrum of $Cu/Zn(dip)_3Br_2\cdot 6\ H_2O$ shows three bands, at 6.40, 14.40 and 14.70 kK; in xy- and z-polarization the spectra are similar. The reflection spectrum of $Cu(en)_3SO_4$ yields only one band, at 15.60 kK. In aqueous solution this band is shifted considerably ($\nu_{max}=18.20$ kK). The spectrum of $Cu(dip)_3Br_2$ (Fig. 5/3) also contains a single wide band, the maximum being at 12.70 kK. The spectral character of the aqueous solution is similar, but the band is shifted to 14.00 kK. The structures of the spectra of aqueous and pyridine solutions are of the same character.

When interpreting the properties of these compounds, the JAHN—TELLER theorem has to be taken into account. According to this theorem, with a lower than octahedral symmetry a more stable structure is formed and consequently the degeneracy of the ground-state is removed. Hence, in the spectra there are more bands than is to be expected from the simple term-scheme.

5. *Cis-octahedral structure*

In the $Cu(dip)_2ONO.NO_3$ molecule (CuN_4O_2 chromophore) the lengths of the four Cu—N bonds are between 1.98 and 2.10 Å, and those of the two Cu—O bonds are 2.27 and 2.35 Å [36]. The symmetry of the molecule is C_{2v}. The complex is paramagnetic, with 1.89 B.M. [68]. From the rhombic-type *e.s.r.* spectrum, $g_1=2.029$, $g_2=2.170$ and $g_3=2.205$ [36]; the ground orbital is z^2.

The crystal spectrum changes with the direction of the polarization; the bands lie between 9.5 and 15.00 kK. These bands, according to the C_{2v} symmetry, are assigned to the transitions (see Fig. 2/d) [72]:

$$(x^2-y^2)^2(xz, yz)^4(xy)^2(z^2)^1 \rightarrow (x^2-y^2)^2(xz, yz)^4(xy)^1(z^2)^2, \quad (\nu_1)$$

$$\rightarrow (x^2-y^2)^2(xz, yz)^3(xy)^2(z^2)^2, \quad (\nu_2) \qquad \text{(VI)}$$

$$\rightarrow (x^2-y^2)^1(xz, yz)^4(xy)^2(z^2)^2. \quad (\nu_3)$$

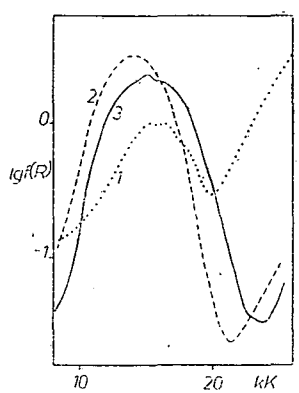

Fig. 6. Reflection spectra.
1: $Cu(dip)_2ONO \cdot NO_3$;
2: $CaCu(CH_3COO)_4 . 6\,H_2O$;
3: $Cu(dien)_2(NO_3)_2$.

The reflection spectrum is also strongly complex (Fig. 6/1), and the aqueous spectrum is only slightly changed in comparison with the reflection spectrum.

IV. *Eight-coordination*

Distorted dodecahedral structure

According to the structure investigations [21] on $CaCu(CH_3COO)_4 \cdot 6\,H_2O$, there are four shorter (1.97 Å) and four longer (2.79 Å) Cu—O bonds. The symmetry is D_{2d}. From the rhombic-type *e.s.r.* spectrum, $g_1=2.079$, $g_2=2.109$ and $g_3=2.383$ can be calculated [71].

The single-crystal spectrum was investigated by BILLING *et al.* [73], and by GLIEMANN and MORYS [74]. The results are similar, but as regards the ground-states, the assignments and the one-electron orbital sequences the opinions are divided. The reflection (Fig.6/2) and the absorption spectra of the aqueous solution are very similar; the band is at around 14 kK.

7. *Conclusions*

It can be stated that by the sole use of magnetic moments, the reflection or the absorption spectrum, structure determinations of Cu(II) complexes are quite impossible. Success can only be expected if multiple investigations of single-crystal polarization spectra, *e.s.r.* spectra and quantum-chemical calculations are carried out.

The maximum in the reflection spectrum can be taken as a measure of the in-plane field [75]; this increases with decrease of the axial field.

As expected for complexes with D_{4h} symmetry, 10 Dq varies inversely with the ratio r_p/r_a. Due to extremely complicated solvation equilibria, the spectra of solutions are even more difficult to interpret.

In most cases the ligand field calculations do not give exact orbital sequences. For the square-planar arrangement, for instance, it cannot be decided whether the z^2 orbital lies above or below the xy, xz and yz orbitals. It can be determined, however, which orbital has the highest energy and which will contain the odd electron. The following example [76] illustrates how the relation between the axial and in-plane fields affects the orbital sequences. In the case of elongated geometries:

$$r_p/r_a = 1.0-0.79: \quad (xz, yz) < xy < z^2 < x^2-y^2,$$

$$= 0.75 \quad : \quad (xz, yz) < z^2 < xy < x^2-y^2.$$

For compressed geometries:

$$r_p/r_a = 0.82 \quad : \quad xy < x^2-y^2 < (xz, yz) < z^2.$$

The real one-electron orbital sequence can only be given by quantum-chemical calculations.

The investigation of *e.s.r.* spectra is very important, as it allows determination of the molecular symmetry and of the ground orbitals on which the unpaired electron dwells. In the knowledge of the optical and *e.s.r.* spectra, the spin-orbit coupling constant λ can be calculated, and by using this conclusions can be drawn on the character of the bonds.

It is important to mention that a relationship was found between the degree of tetragonal distortion and the square of the frequency of the Cu—L stretching vibration [77].

Acknowledgement. The authors wish to express their thanks to Dr. M. I. BÁN for reading the manuscript and for valuable discussions.

References

[1] *Cotton, F. A., G. Wilkins:* Advanced Inorganic Chemistry, Intersci., London, 2nd ed., 1966.
[2] *Ballhausen, C. J.:* Introduction to Ligand Field Theory, McGraw-Hill, N. Y., 1962.
[3] *Császár J., Bán M.:* Optical Spectra, Ligand Field Theory and Structure of Complex Molecules, (in Hungarian), Akadémiai Kiadó, Budapest, 1972.
[4] *Jörgensen, C. K.:* Absorption Spectra and Chemical Bonding in Complexes, Pergamon Press Ltd., Oxford, 1962.
[5] *Orgel, L. E.:* An Introduction to Transition Metal Chemistry., Methuen and Co., London, 1960.
[6] *Schläfer, H. L., G. Gliemann:* Einführung in die Ligandenfeldtheorie., Akad. Vlg., Frankfurt/Main, 1967.
[7] *Ballhausen, C. J.:* Dan. Mat. Fys. Medd. **29,** No. 4. (1954).
[8] *Ballhausen, C. J., C. K. Jörgensen:* ibid, **29,** No. 14. (1955).
[9] *Day, P.:* Proc. Chem. Soc., *1964,* 84.
[10] *Hatfield, W. E., T. S. Piper:* Inorg. Chem. **3,** 841 (1964).
[11] *Isaacs, N. W., C. H. L. Kennard, D. A. Wheeler:* Chem. Comm. *1967,* 587.
[12] *Cola, M., G. Guiseppetti, F. Mazzi:* Atti Accad. Sci. Torino, **96,** 381 (1962).
[13] *Morosin, B., E. C. Lingafelter:* J. Phys. Chem., **65,** 50 (1961).
[14] *Porai-Koshitz, M. A.:* Zhur. strukt. Khim. **4,** 584 (1963).
[15] *Sundara Rao, R. V. G. et al.:* Z. Krist. **110,** 231 (1958).
[16] *Von Schnering, H. G.:* Z. anorg. allg. Chem. **353,** 13 (1967).
[17] *Stephens, F. S.:* J. Chem. Soc. *A, 1969,* 883.

[18] *Pabst, A.:* Acta Cryst., **12,** 733 (1959).
[19] *Huang Jin-Ling et al.:* Acta Chimica Sinica, **32,** 162 (1966).
[20] *Mazzi, F.:* Acta Cryst., **8,** 137 (1955).
[21] *Langs, D. A., C. R. Hare:* Chem. Comm., *1970*, 890.
[22] *Pryce, M. H. L., K. P. Sinha, Y. Tanabe:* Mol. Phys. **9,** 33 (1965).
Abragam, A., M. H. L. Pryce: Proc. Roy. Soc. *A*, **206,** 164 (1951).
[23] *Longuet-Higgins, H. C.:* Adv. Spectrosc., **2,** 429 (1969).
[24] *Hathaway, B. J. et al.:* J. Chem. Soc. *A*, *1968*, 85, *1969*, 2312.
Elliott, H. et al.: Inorg. Chem., **5,** 669, 885 (1966).
[25] *Palmer, R. A., T. S. Piper:* Inorg. Chem. **5,** 864 (1966).
[26] *Joesten, M. D., J. F. Forbes:* J. Am. Chem. Soc. **88,** 5465 (1966).
[27] *Hathaway, B. J., A. A. G. Tomlinson:* Coord. Chem. Rev. **5,** 1 (1970).
[28] *Brown, D. S. et al.:* Chem. Comm. *1968*, 852.
[29] *Brown, D. S. et al.:* Chem. Comm. *1967*, 369.
[30] *Procter, J. M., B. J. Hathaway, P. Nicholls:* J. Chem. Soc. *A*, *1968*, 1678.
[31] *Barclay, G. A., B. F. Hoskins, C. H. L. Kennard:* J. Chem. Soc. *A*, *1963*, 5691.
[32] *Akhtar, F. et al.:* Chem. Comm. *1968*, 1389.
[33] *Hathaway, B. J., D. E. Billing, R. J. Dudley:* J. Chem. Soc. *A*, *1970*, 1420.
[34] *Tomlinson, A. A. G. et al.:* J. Chem. Soc. *A*, *1969*, 65.
[35] *Hathaway, B. J., F. S. Stephens:* J. Chem. Soc. *A*, *1970*, 884.
[36] *Procter, J. M., F. S. Stephens:* J. Chem. Soc. *A*, *1969*, 1248.
[37] *Dori, Z.:* Chem. Comm., 714 (1968).
[38] *Stephens, F. S.:* J. Chem. Soc. *A*, *1969*, 2233.
[39] *Stephens, F. S.:* J. Chem. Soc. *A*, *1969*, 1723.
[40] *Veidis, M. V. et al.:* J. Am. Chem. Soc., **91,** 1859 (1969).
[41] *Stephens, F. S.:* J. Chem. Soc. *A*, *1969*, 2081.
[42] *Allen, G. C., N. S. Hush:* Inorg. Chem., **6,** 4 (1967).
[43] *Companion, A. L., M. A. Komarynski:* J. Chem. Educ. **41,** 257 (1964).
[44] *Figgis, B. N., L. Lewis:* Progr. Inorg. Chem., **6,** 37 (1964).
[45] *Figgis, B. N., M. Gerloch, J. Lewis, R. C. Slade:* J. Chem. Soc. *A*, *1968*, 2028.
[46] *Van Nierkerk, J. A., F. R. L. Schoening:* Acta Cryst. **6,** 227 (1953).
[47] *McGarvey, B. R.:* Transition Metal Chemistry, **3,** 89 (1966).
[48] *Sands, R. H.:* Phys. Rev., **99,** 1222 (1955).
[49] *Kneubühl, F. K.:* J. Chem. Phys., **33,** 1074 (1960).
[50] *Billing, D. E., B. J. Hathaway:* J. Chem. Phys., **50,** 2258 (1969).
[51] *Elliott, H., B. J. Hathaway, R. C. Slade:* Inorg. Chem., **5,** 669 (1966).
[52] *Hathaway, B. J., M. J. Bew, D. E. Billing:* J. Chem. Soc. *A*, *1969*, 1090.
[53] *Tomlinson, A. A. G., B. J. Hathaway:* J. Chem. Soc. *A*, *1968*, 2758.
[54] *Robertson, I., M. R. Truter:* J. Chem. Soc. *A*, *1967*, 309.
[55] *Dunn, T. M., J. Lewis, R. G. Wilkins:* Modern Coordination Chemistry., Intersci., N. Y., 1960., p. 229.
[56] *McClure, D. S.:* Solid State Physics, 9 (1959).
[57] *Hush, N. S., R. J. M. Hobbs:* Progr. Inorg. Chem. **10,** 259 (1968).
[58] *Hathaway, B. J., P. Nicholls, D. Bernard:* Spectrovision, **22,** 4 (1969).
[59] *Helmholz, L., R. F. Kruh:* J. Am. Chem. Soc. **74,** 1176 (1952).
[60] *Hathaway, B. J., D. E. Billing:* Coord. Chem. Rev. **5,** 143 (1970).
[61] *Sharnoff, M.:* J. Chem. Phys. **42,** 3383 (1965).
[62] *Gruen, D. M., R. L. McBeth:* Seventh Internatl. Conf. on Coord. Chemistry, 1962., p. 23.
[63] *Day, P.:* Proc. Chem. Soc. *A*, *1964*, 18.
[64] *Császár J.:* Magyar Kémiai Folyóirat, **73,** 337 (1967).
[65] *Ferguson, J.:* J. Chem. Phys. **34,** 1609 (1961).
[66] *Belford, R. L., M. Calvin, G. Belford:* J. Chem. Phys. **26,** 1165 (1957).
[67] *Hathaway, B. J. et al.:* J. Chem. Soc. *A*, *1970*, 806.
[68] *Landolt-Börnstein:* New Ser., Group II. Vol. 2., Springer Vlg., Berlin, 1966., p. 362.
[69] *Billing, D. E. et al.:* J. Chem. Soc. *A*, *1969*, 312, 316.
[70] *Owen, J.:* Proc. Roy. Soc. *A 227*, 183 (1955).
[71] *Hathaway, B. J.:* Essays in Chemistry., Vol. 2., Acad Press, 1971., p. 61.
[72] *Procter, I. M. et al.:* J. Chem. Soc. *A*, *1969*, 1192.
[73] *Billing, D. E. et al.:* J. Chem. Soc. *A*, *1970*, 1877.

[74] *Gliemann, G., P. Morys:* Z. physik. Chem. **243,** 281 (1970).
[75] *Lever, A. B. P., E. Mantovani:* Inorg. Chem., **10,** 817 (1971).
[76] *Fereday, R. J.:* Inorg. Phys. Theoret. 3035 (1971).
[77] *Dudley, R. J. et al.:* J. Inorg. Nucl. Chem. **36,** 1947 (1974).

СПЕКТРЫ, СТЕРЕОХИМИЯ И ЭЛЕКТРОННАЯ СТРУКТУРА КОМПЛЕКСОВ МЕДИ (II)

Й. Часар и Я. Балог

Обсуждаются зависимость между спектральными свойствами и стерической структурой медных (II) комплексов.

MOLAR HEAT CAPACITIES DESCRIBED MORE ACCURATELY

By

L. SERES, L. ZALOTAI and F. MÁRTA

Institute of General and Physical Chemistry,
Attila József University and Reaction Kinetics Research Group
of the Hungarian Academy of Sciences.
Szeged, Hungary

(Received 15 September 1977)

The heat capacity of chemicals is very important for research work and engineering design in the chemical industries. Curve fitting experimental C_p^0 values for gases using a polynomial form:

$$C_p^0 = a + bT + cT^2 + dT^3$$

has been shown to describe heat capacity data for more than 700 compounds over the range from 273 to 1000 K usually within an average percentage error of 0.1%. All data are given both in calories and joules as energy units.

The equilibrium constant of a chemical reaction can be calculated for any temperature from the standard enthalpies of formation ($\Delta H_{f,298}^0$) the standard entropies (S_{298}^0) and the molar heat capacities (C_p^0) of the compounds. The basic equation used in the calculation is

$$\ln K_p = \frac{\Delta S_T^0}{R} - \frac{\Delta H_T^0}{RT}$$

where the reaction enthalpy and reaction entropy are calculated from the standard state reaction enthalpy and reaction entropy by the equations

$$\Delta H_T^0 = \Delta H_{298}^0 + \int_{298}^{T} \Delta C_p^0 \, dT \tag{1}$$

and

$$\Delta S_T^0 = \Delta S_{298}^0 + \int_{298}^{T} \frac{\Delta C_p}{T} \, dT \tag{2}$$

ΔC_p^0 can be approximated by an average value, easily calculable from the known C_p^0 data taken from detailed tables, but the error committed is not always negligible.

Alternatively, empirical molar heat capacity functions may be used. They are generally given [1—7] in one of the forms:

$$C_p^0 = a + bT + cT^2$$

$$C_p^0 = a + bT + cT^{-2}$$

$$C_p^0 = a + bT + cT^2 + dT^3 \tag{3}$$

$$C_p^0 = a + be^{-c/T^n} \tag{4}$$

The last two formulae are known to describe the molar heat capacities of ideal gases to a precision of 0.5 per cent on the average in the temperature range of 298—1500 K. The polynomial forms have the advantage of giving a concise form of representation compared to the rather extensive tabular one and a simple way of calculation of the integrals in eqs. (1) and (2), which can be performed by a desk computer or even by hand; this is a considerable advantage in engineering and educational usage where single problems are to be solved rapidly [8, 9].

Equation (3) has been shown [3, 4, 7] to be less adequate than eq. (4) for describeing the C_p^0 values at both high and very low temperatures. On the other hand, it should be emphasized that our descriptions are aimed at calculating the enthalpy, entropy and Gibbs energy functions of compounds or reactions, and the exponential form has no specific advantage in this respect [5]. The unquestionable advantage of eq. (4) permitting extrapolations to very high and low temperatures can be useful in specific applications; however, most chemical reactions are studied between room temperature and 1000 K. Furthermore, the thermal instability of many of the compounds has been emphasized [5].

Considering all these facts, it was decided to make an extended collection of high—precision data of correlation coefficients calculated for a great number of compounds and radicals. Equation (3) was chosen for the calculation of correlation constants, but the error of approximation was decreased by calculating them for the temperature range of 298—1000 K instead of 298—1500 K. The restriction in the temperature range decreased the relative error of calculation in eq. (3). The computations were mostly based on the detailed and critical C_p^0 values published in the excellent book by STULL, WESTRUM and SINKE [10]; C_p^0 values of the radicals are taken from ref. [11].

The correlation constants of eq. (3), together with the $\Delta H_{f,298}^0$ and S_{298}^0 data, are collected in Table I for a great number of inorganic and organic compounds and some radicals.

As it may be desirable to have the results in SI units, too, all data are given using both calories and joules as energy units (symbols *C* and *J* in Table I). In order to avoid clerical errors the C_p^0 values were recalculated from eq. (3) and compared with the experimental data. The average and maximum errors are given in the last two columns of Table I.

In order to demonstrate the capability of the present choice of deriving correlation constants of high precision, C_p^0 correlation constants of eq. (3) have been computed from detailed C_p^0 tables [12] for both the temperature ranges of 298—1000 K and 298—1500 K (Table II). (No molar heat capacities for temperatures higher than 1000 K are to be found in ref [10]).

Table I.

Thermodynamic data of various species in the gas phase

INORGANIC COMPOUNDS

No.	Compound		ΔH_f^0 298 K	S° 298 K	$a \cdot 10$	$b \cdot 10^2$	$c \cdot 10^6$	$d \cdot 10^9$	Av. err. %	Max. rel. err. %
1	Carbon	C	0.00	1.36	−11.4860	1.32689	−8.91844	1.93701	0.08	0.198
		J	0.00	5.69	−48.0575	5.55169	−37.3148	8.10446	at 400 K	
2	Hydrogen	C	0.00	31.21	64.5042	0.23951	−3.60627	1.98299	0.09	0.225
		J	0.00	130.58	269.885	1.00210	−15.0886	8.29686	at 400 K	
3	Bromine [a]	C	0.00	36.38	80.8679	0.26881	−2.84643	1.08333	0.01	0.027
		J	0.00	152.21	338.351	1.12470	−11.9095	4.53266	at 500 K	
4	Chlorine	C	0.00	53.29	64.3097	0.80670	−9.19273	3.65709	0.08	0.190
		J	0.00	222.97	269.071	3.37525	−38.4624	15.3013	at 400 K	
5	Fluorine	C	0.00	48.45	55.4518	0.87342	−8.26923	2.87644	0.02	0.037
		J	0.00	202.71	232.010	3.65437	−34.5984	12.0350	at 900 K	
6	Iodine [b]	C	0.00	27.76	86.1816	0.10480	−0.94762	0.34259	0.01	0.005
		J	0.00	116.15	360.584	0.43848	−3.96484	1.43341	at 900 K	
7	Nitrogen	C	0.00	45.77	73.5693	−0.28143	5.70963	−2.43682	0.02	0.032
		J	0.00	191.50	307.814	−1.17751	23.8891	−10.1956	at 400 K	
8	Oxygen	C	0.00	49.00	67.1136	−0.00088	4.16903	−2.54445	0.11	0.250
		J	0.00	205.02	280.803	−0.00368	17.4432	−10.6460	at 400 K	
9	Hydrogen bromide	C	−8.66	47.44	72.8295	−0.20953	3.87271	−1.37929	0.03	0.085
		J	−36.23	198.49	304.718	−0.87669	16.2034	−5.77096	at 298 K	
10	Cyanogen bromide	C	43.35	59.07	78.6815	1.47942	−14.5492	5.54065	0.13	0.317
		J	181.38	247.15	329.203	6.18989	−60.8738	23.1821	at 400 K	
11	Cyanogen chloride	C	31.60	56.28	69.4893	1.70429	−16.7541	6.33739	0.16	0.426
		J	132.21	235.48	290.743	7.13074	−70.0991	26.5156	at 400 K	
12	Phosgene	C	−52.80	67.82	67.0860	3.24979	−32.8057	12.1067	0.12	0.304
		J	−220.92	283.76	280.688	13.5971	−137.259	50.6546	at 400 K	
13	Carbonyl fluoride	C	−153.00	61.84	32.3268	3.53198	−30.7328	9.97596	0.04	0.063
		J	−640.15	258.74	135.255	14.7778	−128.586	41.7394	at 400 K	
14	Hydrogen cyanide	C	31.20	48.21	52.2084	1.44760	−11.8432	4.33510	0.10	0.279
		J	130.54	201.71	218.440	6.05677	−49.5521	18.1381	at 400 K	
15	Cyanogen iodide	C	53.80	61.33	89.3035	1.18558	−11.4784	4.42436	0.10	0.253
		J	225.10	256.60	373.645	4.96046	−48.0255	18.5115	at 400 K	
16	Carbon monoxide	C	−26.42	47.30	73.7126	−0.30674	6.66606	−3.03653	0.05	0.100
		J	−110.54	197.90	308.413	−1.28339	27.8908	−12.7048	at 600 K	
17	Carbonyl sulfide	C	−33.08	55.32	52.6321	2.08053	−19.3731	6.93582	0.11	0.279
		J	−138.41	231.46	220.213	8.70493	−81.0572	29.0195	at 400 K	
18	Carbon dioxide	C	−94.05	51.07	47.2691	1.75324	−13.3815	4.09619	0.04	0.091
		J	−393.51	213.68	197.774	7.33555	−55.9880	17.1385	at 400 K	
19	Carbon disulfide	C	27.98	56.83	65.5346	1.94088	−18.3063	6.38265	0.08	0.199
		J	117.07	237.78	274.196	8.12064	−76.5935	26.7050	at 400 K	
20	Cyanogen	C	73.84	57.90	84.9890	2.24759	−20.0032	7.29535	0.13	0.300
		J	308.95	242.25	355.594	9.40392	−83.6932	30.5237	at 400 K	
21	Carbon suboxide	C	−22.38	66.05	83.1497	3.29189	−26.0099	8.17586	0.25	0.425
		J	−93.64	276.35	347.898	13.7733	−108.826	34.2078	at 400 K	
22	Acetylene-dicarbonitrile	C	127.50	69.31	114.537	3.99329	−35.3041	12.5643	0.13	0.344
		J	533.46	289.99	479.223	16.7079	−147.712	52.5688	at 400 K	
23	Perchloryl fluoride	C	−6.49	66.65	29.4200	5.71878	−56.1227	19.8932	0.10	0.217
		J	−27.15	278.86	123.093	23.9273	−234.818	83.2332	at 400 K	

[a] Ideal gas state from 332.62 K [b] Ideal gas state from 458.39 K.

Table I. (cont.)

No.	Compound		ΔH_f^0 298 K	S° 298 K	$a \cdot 10$	$b \cdot 10^2$	$c \cdot 10^6$	$d \cdot 10^9$	Av. err. %	Max. rel. err. %
24	Hydrogen chloride	C	−22.06	44.64	72.3371	−0.17173	2.97529	−0.93086	0.03	0.097
		J	−92.30	186.77	302.658	−0.71851	12.4486	−3.89472		at 400 K
25	Nitrosyl chloride	C	12.57	62.53	81.3383	1.07282	−8.04210	2.45402	0.05	0.129
		J	52.59	261.63	340.319	4.48866	−33.6481	10.2676		at 400 K
26	Nitryl chloride	C	3.12	65.01	57.7747	3.05042	−26.8917	8.81780	0.05	0.135
		J	13.05	272.00	241.729	12.7629	−112.515	36.8937		at 400 K
27	Thionyl chloride	C	−50.60	73.23	102.323	2.63976	−27.9930	10.5586	0.10	0.246
		J	−211.71	306.39	428.121	11.0448	−117.123	44.1772		at 400 K
28	Sulfuryl chloride	C	−85.40	74.37	96.3610	4.12216	−45.3315	17.5003	0.14	0.341
		J	−357.31	311.16	403.174	17.2471	−189.667	73.2212		at 400 K
29	Sulfur monochloride	C	−4.66	76.35	122.678	2.51616	−30.0199	12.2213	0.13	0.320
		J	−19.50	319.45	513.286	10.5276	−125.603	51.1339		at 400 K
30	Hydrogen fluoride	C	−64.80	41.51	69.4116	0.01579	−0.48543	0.59797	0.03	0.073
		J	−271.12	173.68	290.418	0.06606	−2.03103	2.50189		at 400 K
31	Nitrosyl fluoride	C	−15.70	59.27	65.6311	1.43947	−12.0657	3.89199	0.04	0.098
		J	−65.69	247.99	274.600	6.02273	−50.4828	16.2841		at 400 K
32	Nitryl fluoride	C	−19.00	62.24	42.3348	3.39036	−30.1014	9.95429	0.07	0.178
		J	−79.50	260.41	177.128	14.1852	−125.944	41.6487		at 400 K
33	Sulfur tetrafluoride	C	−174.10	69.58	29.5760	6.76422	−74.8376	28.9088	0.21	0.500
		J	−728.43	291.12	123.746	28.3015	−313.121	120.954		at 400 K
34	Hydrogen iodide	C	6.30	49.35	73.7285	−0.29777	6.27655	−2.75178	0.01	0.017
		J	26.36	206.48	308.480	−1.24588	26.2611	−11.5134		at 800 K
35	Hydrogen nitrate	C	−32.02	63.68	24.3115	4.47573	−36.5813	11.3499	0.03	0.099
		J	−133.97	266.44	101.720	18.7264	−153.056	47.4880		at 700 K
36	Water	C	−57.80	45.11	79.1209	−0.08050	4.52165	−1.78026	0.04	0.117
		J	−241.84	188.74	331.042	−0.33683	18.9186	−7.44860		at 400 K
37	Hydrogen peroxide	C	−32.53	55.66	43.7848	2.63807	−24.3565	8.62144	0.05	0.086
		J	−136.11	232.88	183.196	11.0377	−101.908	36.0721		at 900 K
38	Sulfuric acid	C	−194.45	37.49	87.3176	12.9904	−190.725	101.733	0.04	0.055
		J	−813.58	156.86	365.337	54.3518	−797.995	425.650		at 298 K
39	Hydrogen sulfide	C	−4.82	49.18	76.2736	0.03430	5.80808	−2.80972	0.02	0.047
		J	−20.17	205.77	319.129	0.14351	24.3010	−11.7559		at 400 K
40	Ammonia	C	−10.92	46.03	65.2275	0.56910	4.07713	−2.82965	0.11	0.328
		J	−45.69	192.59	272.912	2.38113	17.0587	−11.8393		at 400 K
41	Hydrazine	C	22.75	57.41	17.1396	4.80640	−43.4577	16.0157	0.26	0.591
		J	95.19	240.20	71.7120	20.1099	−181.827	67.0094		at 400 K
42	Nitric oxide	C	21.60	50.35	76.5366	−0.39187	8.41319	−4.03457	0.10	0.196
		J	90.37	210.66	320.229	−1.63958	35.2008	−16.8806		at 400 K
43	Nitrogen dioxide	C	8.09	57.35	60.4622	1.04283	−3.21450	−0.63769	0.08	0.232
		J	33.85	239.95	252.974	4.36319	−13.4495	−2.66808		at 400 K
44	Nitrous oxide	C	19.49	52.56	51.6269	1.73826	−13.8008	4.36984	0.05	0.125
		J	81.55	219.91	216.007	7.27287	−57.7428	18.2834		at 400 K
45	Sulfur dioxide	C	−70.95	59.30	59.1923	1.49703	−10.3565	2.48316	0.06	0.185
		J	−296.85	248.11	247.660	6.26356	−43.3316	10.3895		at 400 K
46	Ozone	C	34.00	57.05	43.9309	2.20263	−19.8425	6.46368	0.05	0.120
		J	142.26	238.70	183.806	9.21580	−83.0212	27.0440		at 400 K
47	Sulfur trioxide	C	−94.47	61.19	33.4938	3.77767	−31.3285	9.95898	0.06	0.177
		J	−395.26	256.02	140.138	15.8058	−131.078	41.6683		at 400 K

Table I. (cont.)

HYDROCARBONS

No.	Compound		ΔH_f^0 298 K	S° 298 K	$a \cdot 10$	$b \cdot 10^2$	$c \cdot 10^6$	$d \cdot 10^9$	Av. err. %	Max. rel. err. %
101	Methane	C	−17.89	44.52	60.6064	0.40338	17.0402	−9.75829	0.23	0.676
		J	−74.85	186.27	253.576	0.16877	71.2959	−40.8286		at 400 K
102	Ethane	C	−20.24	54.85	19.5639	3.85853	−9.56761	−1.66412	0.15	0.465
		J	−84.68	229.49	81.8553	16.1441	−40.0309	−6.96267		at 400 K
103	Propane	C	−24.82	64.51	−12.7422	7.41401	−39.3353	8.28374	0.10	0.346
		J	−103.85	269.91	−53.3136	31.0202	−164.579	34.6591		at 400 K
104	Butane	C	−30.15	74.12	−4.24611	9.24822	−46.1826	8.32206	0.11	0.376
		J	−126.15	310.12	−17.7657	38.6945	−193.228	34.8195		at 400 K
105	2-Methylpropane	C	−32.15	70.42	−25.9145	10.2886	−60.1083	14.1979	0.08	0.282
		J	−134.52	294.64	−108.426	43.0473	−251.493	59.4037		at 400 K
106	Pentane	C	−35.00	83.40	−8.09997	11.5888	−60.1667	11.6097	0.11	0.359
		J	−146.44	348.95	−33.8903	48.4876	−251.737	48.5748		at 400 K
107	2-Methylbutane	C	−36.92	82.12	−26.9545	12.3338	−68.8008	15.2498	0.10	0.322
		J	−154.47	343.59	−112.778	51.6047	−287.8622	63.8052		at 400 K
108	2,2-Dimethyl-propane	C	−39.67	73.23	−48.2254	13.7538	−87.0097	22.0712	0.10	0.355
		J	−165.98	306.39	−201.775	57.5459	−364.049	92.3459		at 400 K
109	Hexane	C	−39.96	92.83	−2.87839	13.4878	−68.2091	12.4964	0.13	0.329
		J	−167.19	388.40	−12.0432	56.4332	−285.387	52.2847		at 600 K
110	2-Methylpentane	C	−41.66	90.95	−30.4564	15.0698	−90.4900	22.0076	0.11	0.371
		J	−174.31	380.53	−127.429	63.0522	−378.610	92.0796		at 400 K
111	3-Methylpentane	C	−41.02	90.77	−11.3403	13.9165	−74.1050	14.9306	0.11	0.369
		J	−171.63	379.78	−47.4477	58.2267	−310.055	62.4697		at 400 K
112	2,2-Dimethyl-butane	C	−44.35	85.62	−50.4135	15.6393	−93.5182	21.7576	0.20	0.559
		J	−185.56	358.23	−210.930	65.4349	−391.280	91.0338		at 400 K
113	2,3-Dimethyl-butane	C	−42.49	87.42	−39.2145	14.9389	−84.9397	18.5425	0.09	0.301
		J	−177.78	365.76	−164.074	62.5044	−355.388	77.5820		at 400 K
114	Heptane	C	−44.88	102.27	−13.3980	16.1774	−86.9557	17.6888	0.10	0.334
		J	−187.7	427.90	−56.0573	67.6862	−363.822	74.0097		at 400 K
115	2-Methylhexane	C	−46.59	100.38	−13.3980	16.1774	−86.9557	17.6888	0.10	0.334
		J	−194.93	419.99	−56.0573	67.6862	−363.822	74.0097		at 400 K
116	3-Methylhexane	C	−45.96	101.37	−13.3980	16.1774	−86.9557	17.6888	0.10	0.334
		J	−192.30	424.13	−56.0573	67.6862	−363.822	74.0097		at 400 K
117	3-Ethylpentane	C	−45.33	98.35	−13.3980	16.1774	−86.9557	17.6888	0.10	0.334
		J	−189.66	411.50	−56.0573	67.6862	−363.822	74.0097		at 400 K
118	2,2-Dimethyl-pentane	C	−49.27	93.90	−13.3980	16.1774	−86.9557	17.6888	0.10	0.334
		J	−206.15	392.88	−56.0573	67.6862	−363.822	74.0097		at 400 K
119	2,3-Dimethyl-pentane	C	−47.62	98.96	−13.3980	16.1774	−86.9557	17.6888	0.10	0.334
		J	−199.24	414.05	−56.0573	67.6862	−363.822	74.0097		at 400 K
120	2,4-Dimethyl-pentane	C	−48.28	94.80	−13.3980	16.1774	−86.9557	17.6888	0.10	0.334
		J	−202.00	396.64	−56.0573	67.6862	−363.822	74.0097		at 400 K
121	3,3-Dimethyl-pentane	C	−48.17	95.53	−13.3980	16.1774	−86.9557	17.6888	0.10	0.334
		J	−201.54	399.70	−56.0573	67.6862	−363.822	74.0097		at 400 K
122	2,2,3-Trimethyl-butane	C	−48.95	91.61	−62.8126	18.3781	−111.747	26.5196	0.13	0.429
		J	−204.81	383.30	−262.808	76.8941	−467.550	110.958		at 400 K
123	Octane	C	−49.82	111.55	−17.8137	18.5783	−102.349	21.9041	0.10	0.344
		J	−208.45	466.73	−74.5327	77.7318	−428.230	91.6466		at 400 K
124	2-Methylheptane	C	−51.50	108.81	−17.8137	18.5783	−102.349	21.9041	0.10	0.344
		J	−215.48	455.26	−74.5327	77.7318	−428.230	91.6467		at 400 K

Table I. (1. cont.)

No.	Compound		ΔH_f^0 298 K	S° 298 K	$a \cdot 10$	$b \cdot 10^2$	$c \cdot 10^6$	$d \cdot 10^9$	Av. err. %	Max. rel. err. %
125	3-Methylheptane	C	−50.82	110.32	−17.8137	18.5783	−102.349	21.9041	0.10	0.344
		J	−212.63	461.58	−74.5327	77.7318	−428.230	91.6466	at 400 K	
126	4-Methylheptane	C	−50.69	108.35	−17.8137	18.5783	−102.349	21.9041	0.10	0.344
		J	−212.09	453.34	−74.5327	77.7318	−428.230	91.6466	at 400 K	
127	3-Ethylhexane	C	−50.40	109.51	−17.8137	18.5783	−102.349	21.9041	0.10	0.344
		J	−210.87	458.19	−74.5327	77.7318	−428.230	91.6466	at 400 K	
128	2,2-Dimethyl-hexane	C	−53.71	103.06	−17.8137	18.5783	−102.349	21.9041	0.10	0.344
		J	−224.72	431.20	−74.5327	77.7318	−428.230	91.6466	at 400 K	
129	2,3-Dimethyl-hexane	C	−51.13	106.11	−17.8137	18.5783	−102.349	21.9041	0.10	0.344
		J	−213.93	443.96	−74.5327	77.7318	−428.230	91.6466	at 400 K	
130	2,4-Dimethyl-hexane	C	−52.44	106.51	−17.8137	18.5783	−102.349	21.9041	0.10	0.344
		J	−219.41	445.64	−74.5327	77.7318	−428.230	91.6466	at 400 K	
131	2,5-Dimethyl-hexane	C	−53.21	104.93	−17.8137	18.5783	−102.349	21.9041	0.10	0.344
		J	−222.63	439.03	−74.5327	77.7318	−428.230	91.6466	at 400 K	
132	3,3-Dimethyl-hexane	C	−52.61	104.70	−17.8137	18.5783	−102.349	21.9041	0.10	0.344
		J	−220.12	438.06	−74.5327	77.7318	−428.230	91.6466	at 400 K	
133	3,4-Dimethyl-hexane	C	−50.91	107.15	−17.8137	18.5783	−102.349	21.9041	0.10	0.344
		J	−213.01	448.32	−74.5327	77.7318	−428.230	91.6466	at 400 K	
134	3-Ethyl-2--methylpentane	C	−50.48	105.43	−17.8137	18.5783	−102.349	21.9041	0.10	0.344
		J	−211.21	441.12	−74.5327	77.7318	−428.230	91.6466	at 400 K	
135	3-Ethyl-3--methylpentane	C	−51.38	103.48	−17.8137	18.5783	−102.349	21.9041	0.10	0.344
		J	−214.97	432.96	−74.5327	77.7318	−428.230	91.6466	at 400 K	
136	2,2,3-Trimethyl-pentane	C	−52.61	101.62	−17.8137	18.5783	−102.349	21.9041	0.10	0.344
		J	−220.12	425.18	−74.5327	77.7318	−428.230	91.6466	at 400 K	
137	2,2,4-Trimethyl-pentane	C	−53.57	101.15	−17.8137	18.5783	−102.349	21.9041	0.10	0.344
		J	−224.14	423.21	−74.5327	77.7318	−428.230	91.6466	at 400 K	
138	2,3,3-Trimethyl-pentane	C	−51.73	103.14	−17.8137	18.5783	−102.349	21.9041	0.10	0.344
		J	−216.44	431.54	−74.5327	77.7318	−428.230	91.6466	at 400 K	
139	2,3,4-Trimethyl-pentane	C	−51.97	102.31	−17.8137	18.5783	−102.349	21.9041	0.10	0.344
		J	−217.44	428.07	−74.5327	77.7318	−428.230	91.6466	at 400 K	
140	2,2,3,3-Tetra-methylbutane	C	−53.99	93.06	−106.691	23.3942	−160.159	43.4570	0.09	0.305
		J	−225.89	389.36	−446.394	97.8813	−670.106	181.824	at 400 K	
141	Nonane	C	−54.74	120.86	−19.9958	20.8426	−115.192	24.6206	0.10	0.335
		J	−229.03	505.68	−83.6626	87.2055	−481.963	103.013	at 400 K	
142	2-Methyloctane	C	−56.45	118.52	8.65972	20.0906	−106.837	21.0212	0.12	0.335
		J	−236.19	495.89	36.2323	84.0590	−447.008	87.9526	at 400 K	
143	3-Methyloctane	C	−55.77	119.90	−28.2415	21.3603	−121.689	26.8737	0.11	0.303
		J	−233.34	501.66	−118.162	89.3715	−509.147	112.440	at 400 K	
144	4-Methyloctane	C	−55.77	119.90	−28.2415	21.3603	−121.689	26.8737	0.11	0.303
		J	−233.34	501.66	−118.162	89.3715	−509.147	112.440	at 400 K	
145	3-Ethylheptane	C	−55.08	118.52	−65.1427	22.6300	−136.541	32.7263	0.10	0.271
		J	−230.45	495.89	−272.557	94.6841	−571.286	136.927	at 400 K	
146	4-Ethylheptane	C	−55.08	118.52	−65.1427	22.6300	−136.541	32.7263	0.10	0.271
		J	−230.45	495.89	−272.557	94.6841	−571.286	136.927	at 400 K	
147	2,2-Dimethyl-heptane	C	−59.00	113.07	−44.3373	22.8410	−142.561	35.8395	0.12	0.383
		J	−246.86	473.08	−185.507	95.5666	−596.476	149.952	at 400 K	
148	2,3-Dimethyl-heptane	C	−56.32	116.79	−50.8233	22.2259	−132.231	31.0871	0.08	0.192
		J	−235.64	488.64	−212.645	92.9931	−553.254	130.069	at 400 K	
149	2,4-Dimethyl-heptane	C	−57.48	116.79	−85.9365	23.3957	−145.193	35.9011	0.08	0.149
		J	−240.50	488.65	−359.558	97.8874	−607.489	150.210	at 400 K	

Table 1. (2. cont.)

No.	Compound		ΔH_f° 298 K	S° 298 K	$a \cdot 10$	$b \cdot 10^2$	$c \cdot 10^6$	$d \cdot 10^9$	Av. err. %	Max. rel. err. %
150	2,5-Dimethyl-heptane	C	−57.48	116.79	−85.9365	23.3957	−145.193	35.9011	0.08	0.149
		J	−240.50	488.65	−359.558	97.8874	−607.489	150.210		at 400 K
151	2,6-Dimethyl-heptane	C	−58.17	114.03	−49.0353	22.1259	−130.342	30.0486	0.08	0.183
		J	−243.38	477.10	−205.164	92.5749	−545.350	125.723		at 400 K
152	3,3-Dimethyl-heptane	C	−57.74	115.25	−81.2385	24.1107	−157.413	41.6920	0.11	0.351
		J	−241.58	482.21	−339.902	100.879	−658.615	174.439		at 400 K
153	3,4-Dimethyl-heptane	C	−55.63	117.48	−87.7245	23.4956	−147.082	36.9397	0.08	0.158
		J	−232.76	491.54	−367.039	98.3057	−615.393	154.556		at 400 K
154	3,5-Dimethyl-heptane	C	−56.79	116.10	−122.838	24.6654	−160.045	41.7537	0.07	0.143
		J	−237.61	485.76	−513.953	103.200	−669.628	174.697		at 298 K
155	4,4-Dimethyl-heptane	C	−57.74	113.87	−81.2385	24.1107	−157.413	41.6920	0.11	0.351
		J	−241.58	476.43	−339.902	100.879	−658.615	174.439		at 400 K
156	3-Ethyl-2-methyl-hexane	C	−55.63	116.79	−87.7245	23.4956	−147.082	36.9397	0.08	0.158
		J	−232.76	488.65	−367.039	98.3057	−615.393	154.556		at 400 K
157	4-Ethyl-2-methyl-hexane	C	−56.79	115.41	−122.838	24.6654	−160.045	41.7537	0.07	0.143
		J	−237.61	482.88	−513.953	103.200	−669.628	174.697		at 298 K
158	3-Ethyl-3-methyl-hexane	C	−56.48	115.25	−118.140	25.3804	−172.264	47.5446	0.10	0.319
		J	−236.31	482.21	−49.4296	106.192	−720.754	198.926		at 400 K
159	3-Ethyl-4-methyl-hexane	C	−54.94	116.79	−124.626	24.7653	−161.934	42.7922	0.08	0.145
		J	−229.87	488.65	−521.434	103.618	−677.532	179.043		at 298 K
160	2,2,3-Trimethyl-hexane	C	−57.65	111.34	−103.820	24.9763	−167.955	45.9054	0.08	0.241
		J	−241.21	465.85	−434.384	104.501	−702.722	192.068		at 400 K
161	2,2,4-Trimethyl-hexane	C	−58.13	111.34	−138.934	26.1460	−180.9170	50.7194	0.08	0.200
		J	−243.22	465.85	−581.298	109.395	−756.957	212.210		at 400 K
162	2,2,5-Trimethyl-hexane	C	−60.71	109.96	−102.032	24.8763	−166.065	44.8669	0.08	0.233
		J	−254.01	460.07	−426.903	104.082	−694.818	187.723		at 400 K
163	2,3,3-Trimethyl-hexane	C	−57.08	112.14	−103.820	24.9762	−167.954	45.9053	0.08	0.241
		J	−238.82	469.19	−434.382	104.500	−702.719	192.068		at 400 K
164	2,3,4-Trimethyl-hexane	C	−56.18	114.37	−110.306	24.3612	−157.624	41.1531	0.07	0.129
		J	−235.06	478.52	−461.522	101.927	−659.499	172.185		at 298 K
165	2,3,5-Trimethyl-hexane	C	−58.03	112.30	−108.518	24.2612	−155.734	40.1145	0.07	0.127
		J	−242.80	469.86	−454.039	101.509	−651.593	167.839		at 298 K
166	2,4,4-Trimethyl-hexane	C	−57.56	112.14	−138.934	26.1460	−180.917	50.7195	0.08	0.200
		J	−240.83	469.19	−581.298	109.395	−756.957	212.210		at 400 K
167	3,3,4-Trimethyl-hexane	C	−56.39	113.52	−140.722	26.2460	−182.806	51.7580	0.08	0.208
		J	−235.94	474.97	−588.779	109.813	−764.861	216.555		at 400 K
168	3,3-Diethyl-pentane	C	−55.44	110.31	−155.041	26.6502	−187.116	53.3971	0.09	0.287
		J	−231.96	461.54	−648.691	111.504	−782.893	223.413		at 400 K
169	3-Ethyl-2,2-dimethylpentane	C	−56.96	109.96	−130.886	25.8408	−178.232	50.0362	0.07	0.169
		J	−238.32	460.07	−547.628	108.118	−745.725	209.352		at 400 K
170	3-Ethyl-2,3--dimethylpentane	C	−55.82	112.14	−140.722	26.2460	−182.806	51.7580	0.08	0.208
		J	−233.55	469.19	−588.779	109.813	−764.861	216.555		at 400 K
171	3-Ethyl-2,4--dimethylpentane	C	−56.18	112.30	−110.306	24.3612	−157.624	41.1531	0.07	0.129
		J	−235.06	469.86	−461.522	101.927	−659.499	172.185		at 298 K
172	2,2,3,3-Tetra-methylpentane	C	−56.70	106.69	−146.982	27.3214	−199.105	59.0020	0.08	0.251
		J	−237.23	446.39	−614.973	114.313	−833.054	246.864		at 400 K
173	2,2,3,4-Tetra-methylpentane	C	−56.64	108.23	−125.697	25.8011	−177.801	49.7683	0.06	0.150
		J	−236.98	452.83	−525.915	107.952	−743.921	208.230		at 298 K
174	2,2,4,4-Tetra-methylpentane	C	−57.83	103.13	−155.029	27.6267	−201.789	59.6852	0.09	0.282
		J	−241.96	431.50	−648.643	115.590	−844.286	249.723		at 400 K

Table I. (3. cont.)

No.	Compound		ΔH_f° 298 K	S° 298 K	$a \cdot 10$	$b \cdot 10^2$	$c \cdot 10^6$	$d \cdot 10^9$	Av. err. %	Max. rel. err. %
175	2,3,3,4-Tetra-methylpentane	C	−56.46	107.65	−126.402	25.8418	−178.496	50.1188	0.07	0.153
		J	−236.23	450.41	−528.867	108.122	−746.829	209.697	at 298 K	
176	Decane	C	−59.67	130.17	−22.1694	23.1021	−127.845	27.1954	0.10	0.331
		J	−249.66	544.63	−92.7568	96.6592	−534.902	113.786	at 400 K	
177	2-Methylnonane	C	−61.38	127.74	21.2178	21.9020	−114.783	21.9437	0.12	0.356
		J	−256.81	534.46	88.7752	91.6379	−480.253	91.8125	at 400 K	
178	3-Methylnonane	C	−60.70	129.12	−15.6834	23.1717	−129.635	27.7963	0.11	0.327
		J	−253.97	540.24	−65.6194	96.9504	−542.392	116.300	at 400 K	
179	4-Methylnonane	C	−60.70	129.12	−15.6834	23.1717	−129.635	27.7963	0.11	0.327
		J	−253.97	540.24	−65.6194	96.9504	−542.392	116.300	at 400 K	
180	5-Methylnonane	C	−60.70	127.74	−15.6834	23.1717	−129.635	27.7963	0.11	0.327
		J	−253.97	534.46	−65.6194	96.9504	−542.392	116.300	at 400 K	
181	3-Ethyloctane	C	−60.01	127.74	−52.5846	24.4414	−144.486	33.6489	0.10	0.298
		J	−251.08	534.46	−220.014	102.263	−604.531	140.787	at 400 K	
182	4-Ethyloctane	C	−60.01	129.12	−52.5846	24.4414	−144.486	33.6489	0.10	0.298
		J	−251.08	540.24	−220.014	102.263	−604.531	140.787	at 400 K	
183	2,2-Dimethyl-octane	C	−63.93	122.29	−31.7792	24.6524	−150.507	36.7619	0.13	0.398
		J	−267.48	511.66	−132.964	103.145	−629.721	153.812	at 400 K	
184	2,3-Dimethyl-octane	C	−62.41	126.01	−73.3785	25.2071	−153.139	36.8236	0.0.8	0.189
		J	−261.12	527.23	−307.016	105.466	−640.734	154.070	at 400 K	
185	2,4-Dimethyl-octane	C	−61.25	126.01	−38.2652	24.0373	−140.177	32.0096	0.09	0.227
		J	−256.27	527.23	−160.102	100.572	−586.499	133.928	at 400 K	
186	2,5-Dimethyl-octane	C	−62.41	126.01	−73.3785	25.2071	−153.139	36.8236	0.08	0.189
		J	−261.12	527.23	−307.016	105.466	−640.734	154,070	at 400 K	
187	2,6-Dimethyl-octane	C	−62.41	126.01	−73.3781	25.2070	−153.138	36.8235	0.08	0.189
		J	−261.12	527.23	−307.014	105.466	−640.731	154.069	at 400 K	
188	2,7-Dimethyl-octane	C	−63.10	123.25	−36.4773	23.9373	−138.287	30.9710	0.09	0.219
		J	−264.01	515.68	−152.621	100.154	−578.595	129.583	at 400 K	
189	3,3-Dimethyl-octane	C	−62.67	124.47	−68.6801	25.9220	−165.358	42.6144	0.12	0.370
		J	−262.21	520.78	−287.358	108.458	−691.858	178.298	at 400 K	
190	3,4-Dimethyl-octane	C	−60.56	126.70	−75.1664	25.3070	−155.028	37.8621	0.08	0.196
		J	−253.38	530.11	−314.496	105.885	−648.638	158.415	at 400 K	
191	3,5-Dimethyl-octane	C	−61.72	126.70	−110.280	26.4768	−167.991	42.6761	0.08	0.158
		J	−258.24	530.11	−461.410	110.779	−702.873	178.557	at 400 K	
192	3,6-Dimethyl-octane	C	−61.72	125.32	−110.280	26.4768	−167.991	42.6761	0.08	0.158
		J	−258.24	524.34	−461.410	110.779	−702.873	178.557	at 400 K	
193	4,4-Dimethyl-octane	C	−62.67	124.47	−68.6801	25.9220	−165.358	42.6144	0.12	0.370
		J	−262.21	520.78	−287.358	108.458	−691.858	178.298	at 400 K	
194	4,5-Dimethyl-octane	C	−60.56	125.32	−75.1664	25.3070	−155.028	37.8623	0.08	0.196
		J	−253.38	524.34	−314.496	105.885	−648.638	158.416	at 400 K	
195	4-Propylheptane	C	−60.01	125.56	−52.5844	24.4414	−144.486	33.6486	0.10	0.298
		J	−251.08	525.34	−220.013	102.263	−604.529	140.786	at 400 K	
196	4-Isopropyl-heptane	C	−60.02	124.63	−75.1661	25.3070	−155.028	37.8620	0.08	0.196
		J	−251.12	521.45	−314.495	105.884	−648.635	158.415	at 400 K	
197	3-Ethyl-2-methyl-heptane	C	− 60.56	126.01	−64.7389	24.7217	−145.648	33.2774	0.11	0.226
		J	−253.38	527.23	−270.868	103.435	−609.392	139.232	at 500 K	
198	4-Ethyl-2-methyl-heptane	C	−61.72	126.01	−71.6600	24.3089	−133.252	25.6957	0.24	0.745
		J	−258.24	527.23	−299.825	101.708	−557.525	107.511	at 500 K	
199	5-Ethyl-2-methyl-heptane	C	−61.72	124.63	−110.279	26.4767	−167.990	42.6760	0.08	0.158
		J	−258.24	521.45	−461.408	110.778	−702.870	178.556	at 400 K	

Table I. (4. cont.)

No.	Compound		ΔH_f° 298 K	S° 298 K	$a \cdot 10$	$b \cdot 10^2$	$c \cdot 10^6$	$d \cdot 10^9$	Av. err. %	Max. rel. err. %
200	3-Ethyl-3-methyl-heptane	C	−61.41	124.47	−105.582	27.1918	−180.210	48.4670	0.11	0.341
		J	−256.94	520.78	−441.754	113.771	−753.999	202.786		at 400 K
201	4-Ethyl-3-methyl-heptane	C	−59.87	126.70	−112.067	26.5767	−169.879	43.7146	0.08	0.166
		J	−250.50	530.11	−468.889	111.197	−710.774	182.902		at 400 K
202	3-Ethyl-5-methyl-heptane	C	−61.04	126.01	−147.180	27.7464	−182.841	48.5286	0.07	0.144
		J	−255.39	527.23	−615.802	116.091	−765.008	203.043		at 298 K
203	3-Ethyl-4-methyl-heptane	C	−59.87	126.01	−112.067	26.5767	−169.879	43.7146	0.08	0.166
		J	−250.50	527.23	−468.889	111.197	−710.774	182.902		at 400 K
204	4-Ethyl-4-methyl-heptane	C	−61.41	124.47	−105.581	27.1918	−180.209	48.4669	0.11	0.341
		J	−256.94	520.70	−441.752	113.770	−753.996	202.785		at 400 K
205	2,2,3-Trimethyl-heptane	C	−62.58	120.56	−91.2622	26.7877	−175.900	46.8279	0.09	0.271
		J	−261.83	504.42	−381.841	112.080	−735.967	195.928		at 400 K
206	2,2,4-Trimethyl-heptane	C	−63.06	120.56	−126.375	27.9574	−188.862	51.6417	0.08	0.234
		J	−263.84	504.42	−528.753	116.973	−790.198	216.069		at 400 K
207	2,2,5-Trimethyl-heptane	C	−64.95	120.56	−126.375	27.9574	−188.862	51.6417	0.08	0.234
		J	−271.75	504.42	−528.753	116.973	−790.198	216.069		at 400 K
208	2,2,6-Trimethyl-heptane	C	−65.64	119.18	−89.4739	26.6876	−174.011	45.7892	0.09	0.263
		J	−274.64	498.65	−374.359	111.661	−728.060	191.582		at 400 K
209	2,3,3-Trimethyl-heptane	C	−62.01	121.36	−91.2619	26.7876	−175.900	46.8277	0.09	0.271
		J	−259.45	507.77	−381.840	112.079	−735.964	195.927		at 400 K
210	2,3,4-Trimethyl-heptane	C	−61.11	123.59	−97.7479	26.1725	−165.569	42.0754	0.07	0.129
		J	−255.68	517.10	−408.977	109.506	−692.742	176.043		at 298 K
211	2,3,5-Trimethyl-heptane	C	−62.27	123.59	−132.861	27.3423	−178.532	46.8894	0.07	0.130
		J	−260.54	517.10	−555.890	114.400	−746.976	196.185		at 298 K
212	2,3,6-Trimethyl-heptane	C	−62.96	122.90	−95.9599	26.0726	−163.680	41.0369	0.07	0.127
		J	−263.42	514.21	−401.496	109.087	−684.838	171.698		at 298 K
213	2,4,4-Trimethyl-heptane	C	−62.49	121.36	−126.375	27.9574	−188.862	51.6417	0.08	0.234
		J	−261.46	507.77	−528.753	116.973	−790.198	216.069		at 400 K
214	2,4,5-Trimethyl-heptane	C	−62.27	123.59	−132.861	27.3423	−178.532	46.8894	0.07	0.130
		J	−260.54	517.10	−555.890	114.400	−746.976	196.185		at 298 K
215	2,4,6-Trimethyl-heptane	C	−60.52	121.52	−131.073	27.2423	−176.642	45.8509	0.06	0.128
		J	−253.22	508.44	−548.409	113.982	−739.072	191.840		at 298 K
216	2,5,5-Trimethyl-heptane	C	−64.38	121.36	−126.375	27.9574	−188.862	51.6417	0.08	0.234
		J	−269.37	507.77	−528.753	116.973	−790.198	216.069		at 400 K
217	3,3,4-Trimethyl-heptane	C	−61.32	122.74	−128.163	28.0573	−190.751	52.6803	0.08	0.241
		J	−256.56	513.54	−536.234	117.392	−798.103	220.414		at 400 K
218	3,3,5-Trimethyl-heptane	C	−61.80	122.74	−163.276	29.2271	−203.713	57.4943	0.08	0.204
		J	−258.57	513.54	−683.147	122.286	−852.337	240.556		at 400 K
219	3,4,4-Trimethyl-heptane	C	−61.32	122.74	−128.163	28.0573	−190.751	52.6803	0.08	0.241
		J	−256.56	513.54	−536.234	117.392	−798.103	220.414		at 400 K
220	3,4,5-Trimethyl-heptane	C	−60.43	123.59	−134.649	27.4423	−180.421	47.9280	0.07	0.132
		J	−252.84	517.10	−563.371	114.818	−754.881	200.530		at 298 K
221	3-Isopropyl-2-methylhexane	C	−61.11	121.52	−97.7479	26.1725	−165.569	42.0754	0.07	0.129
		J	−255.68	508.44	−408.977	109.506	−692.742	176.043		at 298 K
222	3,3-Diethylhexane	C	−60.15	122.29	−142.482	28.4651	−195.061	54.3194	0.10	0.312
		J	−251.67	511.66	−596.146	119.083	−816.135	227.272		at 400 K
223	3,4-Diethylhexane	C	−59.17	123.25	−148.969	27.8465	−184.731	49.5672	0.08	0.146
		J	−247.57	515.68	−623.286	116.510	−772.916	207.389		at 298 K
224	3-Ethyl-2,2-dimethylhexane	C	−61.83	120.56	−128.163	28.0573	−190.751	52.6803	0.08	0.241
		J	−258.95	504.42	−536.234	117.392	−798.103	220.414		at 400 K

Table I. (5. cont.)

No.	Compound		ΔH_f° 298 K	S° 298 K	$a \cdot 10$	$b \cdot 10^2$	$c \cdot 10^6$	$d \cdot 10^9$	Av. err. %	Max. rel. err. %
225	4-Ethyl-2,2-dimethylhexane	C	−62.37	119.18	−162.540	29.1814	−202.846	56.9831	0.07	0.200
		J	−260.96	498.65	−680.068	122.095	−848.708	238.417	at 400 K	
226	3-Ethyl-2,3-dimethylhexane	C	−60.75	122.74	−128.163	28.0573	−190.751	52.6803	0.08	0.241
		J	−254.18	513.54	−536.234	117.392	−798.103	220.414	at 400 K	
227	4-Ethyl-2,3-dimethylhexane	C	−60.43	122.90	−134.649	27.4423	−180.421	47.9280	0.07	0.132
		J	−252.84	514.21	−563.371	114.818	−754.881	200.530	at 298 K	
228	3-Ethyl-2,4-dimethylhexane	C	−60.43	123.59	−134.649	27.4423	−180.421	47.9280	0.07	0.132
		J	−252.84	517.10	−563.371	114.818	−754.881	200.530	at 298 K	
229	4-Ethyl-2,4-dimethylhexane	C	−61.23	121.36	−163.276	29.2271	−203.713	57.4943	0.08	0.204
		J	−256.19	507.77	−683.147	122.286	−852.337	240.556	at 400 K	
230	3-Ethyl-2,5-dimethylhexane	C	−62.27	122.90	−132.861	27.3423	−178.532	46.8894	0.07	0.130
		J	−260.54	514.21	−555.890	114.400	−746.976	196.185	at 298 K	
231	4-Ethyl-3,3-dimethylhexane	C	−60.63	121.36	−165.064	29.3270	−205.603	58.5328	0.08	0.211
		J	−253.68	507.77	−690.628	122.704	−860.241	244.901	at 400 K	
232	3-Ethyl-3,4-dimethylhexane	C	−60.06	122.74	−165.064	29.3270	−205.603	58.5328	0.08	0.211
		J	−251.29	513.54	−690.628	122.704	−860.241	244.901	at 400 K	
233	2,2,3,3-Tetramethylhexane	C	−61.63	115.91	−134.423	29.1327	−207.050	59.9242	0.09	0.279
		J	−257.86	484.97	−562.428	121.891	−866.295	250.723	at 400 K	
234	2,2,3,4-Tetramethylhexane	C	−60.55	118.14	−150.745	28.9229	−201.293	56.8937	0.07	0.154
		J	−253.34	494.30	−630.716	121.013	−842.209	238.043	at 298 K	
235	2,2,3,5-Tetramethylhexane	C	−64.29	117.45	−148.957	28.8229	−199.404	55.8551	0.07	0.152
		J	−268.99	491.41	−623.235	120.595	−834.305	233.698	at 298 K	
236	2,2,4,4-Tetramethylhexane	C	−61.50	115.91	−179.372	30.7077	−224.586	66.4600	0.09	0.278
		J	−257.32	484.97	−750.495	128.481	−939.670	278.069	at 400 K	
237	2,2,4,5-Tetramethylhexane	C	−63.61	117.45	−148.957	28.8229	−199.404	55.8551	0.07	0.152
		J	−266.14	491.41	−623.237	120.595	−834.309	233.699	at 298 K	
238	2,2,5,5-Tetramethylhexane	C	−68.18	112.35	−142.471	29.4381	−209.735	60.6079	0.09	0.307
		J	−285.27	470.07	−596.100	123.169	−877.531	253.582	at 400 K	
239	2,3,3,4-Tetramethylhexane	C	−60.66	119.63	−150.745	28.9230	−201.294	56.8941	0.07	0.154
		J	−253.80	500.53	−630.718	121.014	−842.213	238.044	at 298 K	
240	2,3,3,5-Tetramethylhexane	C	−61.83	118.25	−148.957	28.8230	−199.405	55.8555	0.07	0.151
		J	−258.70	494.76	−623.237	120.595	−834.309	233.699	at 298 K	
241	2,3,4,4-Tetramethylhexane	C	−59.98	119.63	−150.745	28.9230	−201.294	56.8941	0.07	0.154
		J	−250.96	500.53	−630.718	121.014	−842.213	238.044	at 298 K	
242	2,3,4,5-Tetramethylhexane	C	−61.67	119.10	−120.330	27.0382	−176.112	46.2892	0.06	0.118
		J	−258.03	498.31	−503.461	113.128	−736.151	193.673	at 298 K	
243	3,3,4,4-Tetramethylhexane	C	−60.37	116.71	−171.325	30.4026	−221.902	65.7772	0.08	0.250
		J	−252.59	488.31	−716.825	127.204	−928.438	275.211	at 400 K	
244	2,4-Dimethyl-3-isopropylpentane	C	−61.67	116.23	−150.745	28.9230	−201.294	56.8941	0.07	0.154
		J	−258.03	486.31	−630.718	121.014	−842.213	238.044	at 298 K	
245	3,3-Diethyl-2-methylpentane	C	−59.49	119.18	−165.065	29.3271	−205.604	58.5332	0.08	0.212
		J	−248.91	498.65	−690.631	122.705	−860.245	244.902	at 400 K	
246	3-Ethyl-2,2,3-trimethylpentane	C	−60.37	117.29	−171.325	30.4026	−221.902	65.7772	0.08	0.250
		J	−252.59	490.74	−716.825	127.204	−928.438	275.211	at 400 K	
247	3-Ethyl-2,2,4-trimethylpentane	C	−60.55	115.91	−150.745	28.9230	−201.294	56.8938	0.07	0.154
		J	−253.34	484.97	−630.718	121.014	−842.213	238.044	at 298 K	
248	3-Ethyl-2,3,4-trimethylpentane	C	−60.09	118.25	−148.783	28.8012	−198.981	55.5308	0.06	0.149
		J	−251.42	494.76	−622.509	120.504	−832.536	232.341	at 298 K	
249	2,2,3,3,4-Pentamethylpentane	C	−59.08	112.80	−137.335	29.1879	−208.445	60.6943	0.06	0.138
		J	−247.19	471.96	−574.611	122.122	−872.133	253,945	at 298 K	

Table I. (6. cont.)

No.	Compound		ΔH_f° 298 K	S° 298 K	$a \cdot 10$	$b \cdot 10^2$	$c \cdot 10^6$	$d \cdot 10^9$	Av. err. %	Max. rel. err. %
250	2,2,3,4,4-Penta-methylpentane	C	−59.04	110.62	−166.841	30.4036	−222.166	65.8599	0.08	0.216
		J	−247.02	462.83	−698.063	127.209	−929.542	275.556		at 400 K
251	Undecane	C	−64.60	139.48	−26.8042	25.5186	−143.578	31.6159	0.10	0.338
		J	−270.29	583.58	−112.149	106.770	−600.731	132.280		at 400 K
252	Dodecane	C	−69.52	148.78	−29.0415	27.7842	−156.370	34.2766	0.10	0.325
		J	−290.87	622.50	−121.510	116.249	−654.255	143.413		at 400 K
253	Tridecane	C	−74.45	158.09	−31.3571	30.0557	−169.314	37.0385	0.10	0.322
		J	−311.50	661.45	−131.198	125.753	−708.408	154.969		at 400 K
254	Tetradecane	C	−79.38	167.40	−35.6392	32.4494	−184.606	41.2082	0.10	0.326
		J	−332.13	700.40	−149.114	135.768	−772.392	172.415		at 400 K
255	Pentadecane	C	−84.31	176.71	−38.0935	34.7260	−197.572	43.9535	0.10	0.326
		J	−352.75	739.35	−159.383	145.293	−826.639	183.900		at 400 K
256	Hexadecane	C	−89.23	186.02	−39.9948	36.9731	−210.101	46.4996	0.10	0.320
		J	−373.34	778.31	−167.338	154,695	−879.063	194.554		at 400 K
257	Heptadecane	C	−94.15	195.33	−44.6911	39.3911	−225.808	50.8851	0.10	0.327
		J	−393.92	817.26	−186.988	164.812	−944.778	212.903		at 400 K
258	Octadecane	C	−99.08	204.64	−46.6541	41.6399	−238.310	53.3966	0.10	0.324
		J	−414.55	856.21	−195.201	174.221	−997.088	223.411		at 400 K
259	Nonadecane	C	−104.00	213.95	−48.8362	43.9042	−251.152	56.1132	0.10	0.320
		J	−435.14	895.17	−204.331	183.695	−1050.82	234.777		at 400 K
260	Eicosane	C	−108.93	223.26	−53.4624	46.3158	−266.696	60.3917	0.10	0.326
		J	−455.76	934.12	−223.687	193.785	−1115.86	252.679		at 400 K
261	Ethylene	C	12.50	52.45	9.09005	3.73965	−19.9360	4.19088	0.11	0.356
		J	52.30	219.45	38.0327	15.6467	−83.4124	17.5346		at 400 K
262	Propene	C	4.88	63.80	12.1642	5.39215	−23.8708	3.17470	0.11	0.360
		J	20.42	266.94	50.8950	22.5607	−99.8733	13.2829		at 400 K
263	1-Butene	C	−0.03	73.04	−9.58677	8.54739	−49.1797	11.4753	0.06	0.217
		J	−0.13	305.60	−40.1110	35.7622	−205.768	48.0124		at 400 K
264	2-Butene, cis	C	−1.67	71.90	−12.4250	7.69408	−33.3051	3.72688	0.15	0.464
		J	−6.99	300.83	−51.9863	32.1920	−139.348	15.5933		at 400 K
265	2-Butene, trans	C	−2.67	70.86	28.4367	6.87311	−27.3093	2.28571	0.11	0.356
		J	−11.17	293.59	118.979	28.7570	−114.262	9.56338		at 400 K
266	2-Methylpropene	C	−4.04	70.17	15.0138	7.78551	−41.0994	8.58453	0.05	0.176
		J	−16.90	293.59	62.8179	32.5746	−171.960	35.9177		at 400 K
267	1-Pentene	C	−5.00	82.65	9.37615	9.89924	−49.0280	8.28006	0.23	0.713
		J	−20.92	345.81	39.2297	41.4183	−205.133	34.6437		at 298 K
268	2-Pentene, cis	C	−6.71	82.76	−37.2040	11.1466	−62.8738	13.8833	0.12	0.393
		J	−28.07	346.27	−155.661	46.6372	−263.064	58.0874		at 400 K
269	2-Pentene, trans	C	−7.59	81.36	5.39978	9.92839	−50.5928	9.55564	0.09	0.306
		J	−31.76	340.41	22.5927	41.5404	−211.680	39.9808		at 400 K
270	2-Methyl-1-butene	C	−8.68	81.15	−0.67429	10.3890	−55.6257	11.2103	0.10	0.318
		J	−36.32	339.53	−2.82125	43.4676	−232.738	46.9037		at 400 K
271	3-Methyl-1-butene	C	−6.92	79.70	15.3871	10.9250	−70.5366	19.5920	0.05	0.151
		J	−28.95	333.46	64.3793	45.7103	−295.126	81.9730		at 400 K
272	2-Methyl-2-butene	C	−10.17	80.92	−3.15847	9.89337	−48.7067	8.60660	0.08	0.269
		J	−42.55	338.57	−13.2151	41.3939	−203.789	36.0519		at 400 K
273	1-Hexene	C	−9.96	91.93	−4.17211	12.6789	−69.3163	14.4616	0.08	0.333
		J	−41.67	384.64	−17.4562	53.0483	−290.020	60.5073		at 400 K
274	2-Hexene, cis	C	−12.51	92.37	−29.8244	13.0524	−71.1780	14.8058	0.14	0.481
		J	−52.34	386.48	−124.786	54.6115	−297.810	61.9475		at 400 K

Table I. (7. cont.)

No.	Compound		ΔH_f° 298 K	S° 298 K	$a \cdot 10$	$b \cdot 10^2$	$c \cdot 10^6$	$d \cdot 10^9$	Av. err. %	Max. rel. err. %
275	2-Hexene, trans	C	−12.88	90.97	12.5935	11.8369	−58.7363	10.2574	0.13	0.415
		J	−53.89	380.62	52.6912	49.5255	−245.752	42.9169		at 400 K
276	3-Hexene, cis	C	−11.38	90.73	−58.2666	14.2453	−86.5308	21.0675	0.13	0.408
		J	−47.61	379.61	−243.787	59.6022	−362.045	88.1462		at 400 K
277	3-Hexene, trans	C	−13.01	89.59	−13.3671	13.3325	−81.4189	20.7995	0.09	0.242
		J	−54.43	374.84	−55.9278	55.7832	−340.657	87.0251		at 400 K
278	2-Methyl-1-pentene	C	−12.49	91.34	4.47136	12.7050	−71.3569	15.6520	0.04	0.126
		J	−52.26	382.17	18.7082	53.1575	−298.557	65.4879		at 400 K
279	3-Methyl-1-pentene	C	−10.76	90.06	7.87744	13.5864	−88.8683	24.5363	0.05	0.104
		J	−45.02	376.81	32.9591	56.8456	−371.826	102.660		at 700 K
280	4-Methyl-1-pentene	C	−10.54	87.89	−31.5229	13.3763	−78.5756	18.6291	0.07	0.187
		J	−44.10	367.73	−131.893	55.9664	−328.761	77.9442		at 400 K
281	2-Methyl-2-pentene	C	−14.28	90.45	−38.4962	13.7258	−83.0584	20.7328	0.08	0.233
		J	−59.75	378.44	−161.069	57.4289	−347.518	86.7462		at 400 K
282	3-Methyl-2-pentene, cis	C	−13.80	90.45	−38.4962	13.7258	−83.0584	20.7328	0.08	0.233
		J	−57.74	378.44	−161.069	57.4289	−347.518	86.7462		at 400 K
283	3-Methyl-2-pentene, trans	C	−14.02	91.26	−38.4962	13.7258	−83.0584	20.7328	0.08	0.233
		J	−58.66	381.83	−161.069	57.4289	−347.518	86.7462		at 400 K
284	4-Methyl-2-pentene, cis	C	−12.03	89.23	−4.00491	12.8434	−72.7146	16.1337	0.22	0.802
		J	−50.33	373.34	−16.7566	53.7369	−304.238	67.5034		at 400 K
285	4-Methyl-2-pentene, trans	C	−12.99	88.02	30.1614	12.3110	−71.8228	17.4999	0.02	0.051
		J	−54.35	368.28	126.195	51.5091	−300.508	73.2199		at 300 K
286	2-Ethyl-1-butene	C	−12.32	90.01	−31.7052	14.3860	−95.9739	27.1871	0.05	0.141
		J	−51.55	376.60	−132.655	60.1911	−401.556	113.751		at 400 K
287	2,3-Dimethyl-1-butene	C	−13.32	87.39	19.6228	13.1893	−85.7122	24.0734	0.06	0.127
		J	−55.73	365.64	82.1017	55.1839	−358.621	100.723		at 400 K
288	3,3-Dimethyl-1-butene	C	−10.31	82.16	−40.1920	13.6833	−79.5127	17.5833	0.21	0.555
		J	−43.14	343.76	−168.164	57.2508	−332.683	73.5688		at 400 K
289	2,3-Dimethyl-2-butene	C	−14.15	87.15	16.5298	10.2879	−31.1702	2.27860	0.16	0.141
		J	−59.20	364.64	69.1606	43.0447	−130.416	−9.53369		at 400 K
290	1-Heptene	C	−14.89	101.24	−7.88735	15.0360	−83.8660	18.1656	0.09	0.274
		J	−62.30	423.59	−33.0008	62.9107	−350.896	76.0050		at 400 K
291	1-Octene	C	−19.82	110.55	−9.78879	17.2832	−96.3957	20.7119	0.08	0.270
		J	−82.93	462.54	−40.9565	72.3128	−403.320	86.6587		at 400 K
292	1-Nonene	C	−24.74	119.86	−11.9623	19.5427	−109.048	23.2867	0.08	0.274
		J	−103.51	501.49	−50.0506	81.7665	−456.260	97.4315		at 400 K
293	1-Decene	C	−29.67	129.17	−16.5971	21.9591	−124.782	27.7077	0.09	0.287
		J	−124.14	540.45	−69.4423	91.8768	−522.087	115.926		at 400 K
294	1-Undecene	C	−34.60	138.48	−19.1151	24.2419	−137.887	30.5380	0.08	0.278
		J	−144.77	579.40	−79.9776	101.428	−576.920	127.771		at 400 K
295	1-Dodecene	C	−39.52	147.78	−21.0781	26.4906	−150.390	33.0495	0.08	0.278
		J	−165.35	618.31	−88.1906	110.837	−629.230	138.279		at 400 K
296	1-Tridecene	C	−44.45	157.09	−22.9795	28.7378	−162.919	35.5957	0.08	0.275
		J	−185.98	657.26	−96.1462	120.239	−681.653	148.932		at 400 K
297	1-Tetradecene	C	−49.36	166.40	−27.8864	31.1666	−178.776	40.0446	0.09	0.288
		J	−206.52	696.22	−116.677	130.401	−747.998	167.546		at 400 K
298	1-Pentadecene	C	−54.31	175.71	−30.0686	33.4309	−191.619	42.7612	0.09	0.286
		J	−227.23	735.17	−125.807	139.875	−801.732	178.913		at 400 K
299	1-Hexadecene	C	−59.23	185.02	−32.0315	35.6796	−204.021	45.2726	0.08	0.300
		J	−247.82	774.12	−134.020	149.283	−854.040	189.420		at 400 K

Table I. (8. cont.)

No.	Compound		$H\dot{a}_T^\circ$ 298 K	S° 298 K	$a \cdot 10$	$b \cdot 10^2$	$c \cdot 10^6$	$d \cdot 10^9$	Av. err. %	Max. rel. err. %
300	1-Heptadecene	C	−64.15	194.33	−36.4471	38.0805	−219.514	49.4879	0.08	0.294
		J	−268.40	813.08	−152.495	159.329	−918.448	207.057	at 400 K	
301	1-Octadecene	C	−69.08	203.64	−38.6292	40.3447	−232.356	52.2045	0.09	0.291
		J	−289.03	852.03	−61.625	168.802	−972.179	218.423	at 400 K	
302	1-Nonadecene	C	−74.00	212.95	−41.0836	42.6214	−245.323	54.9496	0.09	0.293
		J	−309.62	890.98	−171.894	178.328	−1026.43	229.909	at 400 K	
303	1-Eicosene	C	−78.93	222.26	−45.4377	45.0208	−260.743	59.1997	0.09	0.297
		J	−330.24	929.94	−190.111	188.367	−1090.95	247.692	at 400 K	
304	Allene	C	45.92	58.30	15.7092	5.17981	−35.9228	10.5582	0.03	0.055
		J	192.13	243.93	65.7272	21.6723	−150.301	44.1754	at 500 K	
305	1,2-Butadiene	C	38.77	70.03	23.4488	6.69210	−38.1442	8.89410	0.05	0.167
		J	162.21	293.01	98.1095	27.9997	−159.595	37.2128	at 400 K	
306	1,3-Butadiene	C	26.33	66.62	−38.9642	9.88036	−81.8327	27.4669	0.06	0.138
		J	110.16	278.74	−163.026	41.3394	−342.388	114.922	at 500 K	
307	1,2-Pentadiene	C	34.80	79.70	5.95325	10.1418	−69.3111	20.1094	0.06	0.128
		J	145.60	333.46	24.9084	42.4333	−289.997	84.1373	at 400 K	
308	1,3-Pentadiene, cis	C	18.70	77.50	−64.1532	12.2066	−91.6435	28.2011	0.09	0.193
		J	78.24	324.26	−268.417	51.0725	−383.437	117.993	at 500 K	
309	1,3-Pentadiene, trans	C	18.60	76.40	−19.6331	11.1821	−82.0453	24.7939	0.08	0.177
		J	77.82	319.66	−82.1448	46.7860	−343.277	103.277	at 500 K	
310	1,4-Pentadiene	C	25.20	73.70	−1.01453	10.4662	−74.2881	22.4402	0.06	0.130
		J	105.44	333.46	−4.2448	43.7905	−310.821	93.8898	at 700 K	
311	2,3-Pentadiene	C	33.10	77.60	29.8861	8.28752	−41.8414	7.97643	0.06	0.182
		J	138.49	324.68	125.043	34.6749	−175.065	33.3733	at 400 K	
312	3-Methyl-1,2-butadiene	C	31.00	76.40	29.5424	8.91161	−52.5366	12.8699	0.03	0.060
		J	129.70	319.66	123.605	37.2862	−219.813	53.8477	at 400 K	
313	2-Methyl-1,3-butadiene	C	18.10	75.44	−36.0800	12.2833	−99.4281	33.1289	0.09	0.173
		J	75.73	315.64	−150.959	51.3932	−416.007	138.611	at 298 K	
314	Acetylene	C	54.19	48.00	37.8032	3.06220	−30.5447	12.0855	0.19	0.458
		J	226.73	200.83	158.169	12.8122	−127.799	50.5659	at 400 K	
315	Propyne	C	44.32	59.30	35.1251	4.45231	−28.0207	7.69991	0.03	0.044
		J	185.43	248.11	146.963	18.6284	−117.239	32.2164	at 500 K	
316	Butadiyne	C	113.00	59.76	58.2603	5.38236	−54.0162	21.0166	0.21	0.559
		J	472.79	250.04	243.761	22.5198	−226.004	87.9334	at 400 K	
317	1-Buten-3-yne	C	72.80	66.77	16.1386	6.78355	−54.0850	17.8117	0.07	0.120
		J	304.60	279.37	67.5238	28.3824	−226.292	74.5240	at 400 K	
318	1-Butyne	C	39.48	69.51	21.9537	7.01411	−44.6876	12.1932	0.03	0.051
		J	165.18	290.83	91.8541	29.3470	−186.973	51.0162	at 400 K	
319	2-Butyne	C	34.97	67.71	45.2148	5.26277	−18.0461	0.16668	0.11	0.334
		J	146.31	283.30	189.179	22.0194	−75.5049	0.69738	at 400 K	
320	1-Pentyne	C	34.56	78.82	38.6149	8.62586	−49.2686	11.3206	0.11	0.341
		J	144.35	329.78	161.565	36.0906	−206.140	47.3652	at 400 K	
321	2-Pentyne	C	30.80	79.30	29.1619	7.99315	−37.4954	6.04213	0.09	0.260
		J	128.87	331.79	122.013	33.4433	−156.881	25.2803	at 400 K	
322	3-Methyl-1-butyne	C	32.60	76.23	11.1498	9.74372	−62.8681	16.7256	0.04	0.119
		J	136.40	318.95	46.6506	40.7677	−263.040	69.9798	at 700 K	
323	1-Hexyne	C	29.55	88.13	28.2428	11.1164	−64.5223	15.0847	0.05	0.163
		J	123.64	368.74	118.168	46.5111	−269.961	63.1145	at 400 K	
324	1-Heptyne	C	24.62	97.44	25.3603	13.4245	−78.2087	18.3126	0.05	0.184
		J	103.01	407.69	106.107	56.1681	−327.225	76.6199	at 400 K	

Table I. (9. cont.)

No.	Compound		ΔH_f° 298 K	S° 298 K	$a \cdot 10$	$b \cdot 10^2$	$c \cdot 10^6$	$d \cdot 10^9$	Av. err. %	Max. rel. err. %
325	1-Octyne	C	19.70	106.75	23.1867	15.6840	−90.8615	20.8874	0.06	0.200
		J	82.42	446.64	97.0132	65.6218	−380.165	87.3927		at 400 K
326	1-Nonyne	C	14.77	116.06	18.5519	18.1004	−106.595	25.3077	0.07	0.223
		J	61.80	485.60	77.6212	75.7323	−445.993	105.888		at 400 K
327	1-Decyne	C	9.85	125.36	16.0339	20.3832	−119.700	28.1387	0.07	0.221
		J	41.21	524.51	67.0859	85.2834	−500.826	117.732		at 400 K
328	1-Undecyne	C	4.92	134.67	14.0709	22.6320	−132.203	30.6502	0.07	0.226
		J	20.59	563.46	58.8728	94.6921	−553.136	128.240		at 400 K
329	1-Dodecyne	C	−0.01	143.98	9.71681	25.0313	−147.624	34.9002	0.07	0.239
		J	0.04	602.41	40.6551	104.731	−617.657	146.023		at 400 K
330	1-Tridecyne	C	−4.93	153.29	8.48471	27.2532	−159.810	37.2898	0.07	0.252
		J	−20.63	641.37	35.5000	114.027	−668.644	156.021		at 400 K
331	1-Tetradecyne	C	−9.86	162.60	5.08047	29.5722	−173.431	40.3619	0.07	0.247
		J	−41.25	680.32	21.2567	123.730	−725.637	168.874		at 400 K
332	1-Pentadecyne	C	−14.78	171.91	0.66481	31.9731	−188.825	44.5772	0.08	0.258
		J	−61.84	719.27	2.78156	133.775	−790.044	186.511		at 400 K
333	1-Hexadecyne	C	−19.71	181.22	−1.29817	34.2218	−201.328	47.0886	0.08	0.259
		J	−82.47	758.22	−5.43154	143.184	−842.355	197.019		at 400 K
334	1-Heptadecyne	C	−24.64	190.53	−3.48028	36.4861	−214.170	49.8052	0.08	0.259
		J	−103.09	797.18	−14.5615	152.658	−896.087	208.385		at 400 K
335	1-Octadecyne	C	29.56	199.84	−8.38719	38.9149	−230.027	54.2541	0.08	0.271
		J	−123.68	836.13	−35.0920	162.820	−962.431	226.999		at 400 K
336	1-Nonadecyne	C	−34.49	209.15	−10.2886	41.1621	−242.556	56.8004	0.08	0.269
		J	−144.31	875.08	−43.0476	172.222	−1014.86	237.653		at 400 K
337	1-Eicosyne	C	−39.41	218.46	−12.2516	43.4108	−255.059	59.3119	0.08	0.269
		J	−164.89	914.04	−51.2607	181.631	−1067.17	248.161		at 400 K
338	Cyclopropene	C	12.74	56.75	−72.3129	8.53656	−60.0680	17.3163	0.16	0.556
		J	53.30	237.44	−302.557	35.7170	−251.324	72.4514		at 400 K
339	Cyclobutane	C	6.37	63.43	−90.4082	10.5769	−63.6895	14.9042	0.16	0.584
		J	26.65	265.39	−378.268	44.2537	−266.477	62.3594		at 400 K
340	Cyclopentane	C	−18.46	70.00	−133.049	13.1352	−72.3998	14.1392	0.21	0.620
		J	−77.24	292.88	−556.676	54.9577	−302.921	59.1582		at 400 K
341	Cyclohexane	C	−29.43	71.28	−132.165	14.7597	−62.4665	3.80884	0.22	0.697
		J	−123.14	298.24	−552.976	61.7546	−261.360	15.9362		at 400 K
342	Cycloheptane	C	−28.52	81.82	−181.970	18.7875	−100.394	18.0576	0.17	0.537
		J	−119.33	342.33	−761.361	78.6068	−420.050	75.5530		at 400 K
343	Cyclooctane	C	−30.06	87.66	−231.792	22.8188	−138.446	32.4059	0.12	0.414
		J	−125.77	366.77	−969.817	95.4737	−579.257	135.586		at 400 K
344	Cyclobutene	C	31.00	62.98	−66.1323	9.31935	−63.0929	17.0345	0.09	0.321
		J	129.70	263.51	−276.697	38.9922	−263.981	71.2722		at 400 K
345	Cyclopentene	C	7.87	69.23	−93.1607	10.6645	−53.9373	8.50310	0.21	0.698
		J	32.93	289.66	−389.784	44.6203	−225.674	35.5769		at 400 K
346	Cyclohexene	C	−1.28	74.27	−140.313	16.1870	−112.148	30.9151	0.09	0.322
		J	−5.36	310.75	−587.071	67.7265	−469.225	129.349		at 400 K
347	Methylcyclo-pentane	C	−25.50	81.24	−121.012	15.2734	−86.7055	18.4687	0.16	0.528
		J	−106.69	339.91	−506.313	63.9038	−362.776	77.2731		at 400 K
348	Ethylcyclo-pentane	C	−30.37	90.42	−151.133	19.1145	−126.155	35.3326	0.29	0.575
		J	−127.07	378.32	−632.342	79.9750	−527.833	147.831		at 500 K
349	1,1-Dimethyl-cyclopentane	C	−33.05	85.87	−140.026	18.3665	−107.169	23.2781	0.18	0.585
		J	−138.28	359.38	−585.870	76.8453	−448.395	97.3955		at 400 K

Table I. (10 cont.)

No.	Compound		ΔH_f° 298 K	S° 298 K	$a \cdot 10$	$b \cdot 10^2$	$c \cdot 10^6$	$d \cdot 10^9$	Av. err. %	Max. rel. err. %
350	1,2-Dimethyl-cyclopentane, cis	C	−30.96	87.51	−136.896	18.3715	−109.072	24.5622	0.17	0.562
		J	−129.54	366.14	−572.772	76.8665	−456.358	102.768		at 400 K
351	1,2-Dimethyl-cyclopentane, trans	C	−32.67	87.67	−135.635	18.3870	−110.249	25.3078	0.18	0.579
		J	−136.69	366.81	−567.496	76.9313	−461.280	105.888		at 400 K
352	1,3-Dimethyl-cyclopentane, cis	C	−32.47	87.67	−135.635	18.3870	−110.249	25.3078	0.18	0.579
		J	−135.85	366.81	−567.496	76.9313	−461.280	105.888		at 400 K
353	1,3-Dimethyl-cyclopentane, trans	C	−31.93	87.67	−135.635	18.3870	−110.249	25.3078	0.18	0.579
		J	−133.60	366.81	−567.496	76.9313	−461.280	105.888		at 400 K
354	Propylcyclo-pentane	C	−35.39	99.73	−154.357	21.4411	−140.126	38.6958	0.24	0.875
		J	−148.07	417.27	−645.831	89.7097	−586.288	161.903		at 400 K
355	Butylcyclopentane	C	−40.22	109.04	−278.892	31.2972	−297.213	126.432	0.47	0.824
		J	−168.28	456.22	−1166.89	130.947	−1243.54	528.990		at 500 K
356	1-Cyclopentyl-pentane	C	−45.15	118.35	−160.885	26.1000	−168.100	45.5206	0.16	0.589
		J	−188.91	495.18	−673.143	109.202	−703.747	190.458		at 400 K
357	1-Cyclopentyl-hexane	C	−50.07	127.66	−163.068	28.3643	−181.043	48.2373	0.14	0.532
		J	−209.49	534.13	−682.276	118.676	−757.483	201.825		at 400 K
358	1-Cyclopentyl-heptane	C	−55.00	136.96	−165.586	30.6471	−194.148	51.0682	0.12	0.467
		J	−230.12	573.04	−692.811	128.227	−812.316	213.669		at 400 K
359	1-Cyclopentyl-octane	C	−59.92	146.27	−142.566	31.3539	−180.526	40.3667	0.12	0.796
		J	−250.71	611.99	−596.498	131.185	−755.321	168.894		at 400 K
360	1-Cyclopentyl-nonane	C	−64.85	155.58	−171.903	35.2952	−222.071	57.8298	0.09	0.347
		J	−271.33	650.95	−719.242	147.675	−929.146	241.960		at 400 K
361	1-Cyclopentyl-decane	C	−69.78	164.89	−174.357	37.5718	−235.037	60.5749	0.08	0.300
		J	−291.96	689.90	−729.510	157.200	−983.394	253.445		at 400 K
362	1-Cyclopentyl-undecane	C	−74.70	174.20	−178.992	39.9882	−250.770	64.9952	0.07	0.254
		J	−312.54	728.85	−748.902	167.311	−1049.22	271.940		at 400 K
363	1-Cyclopentyl-dodecane	C	−80.28	183.51	−180.955	42.2370	−263.273	67.5067	0.06	0.222
		J	−335.89	767.81	−757.115	176.720	−1101.53	282.448		at 400 K
364	1-Cyclopentyl-tridecane	C	−84.55	192.89	−182.918	44.4857	−275.775	70.0182	0.05	0.190
		J	−353.76	807.05	−765.328	186.128	−1153.84	292.956		at 400 K
365	1-Cyclopentyl-tetradecane	C	−89.48	202.13	−187.553	46.9022	−291.509	74.4386	0.05	0.161
		J	−374.38	845.71	−784.720	196.239	−1219.67	311.451		at 400 K
366	1-Cyclopentyl-pentadecane	C	−94.41	211.44	−190.007	49.1788	−304.474	77.1836	0.04	0.136
		J	−395.01	884.66	−794.989	205.764	−1273.92	322.936		at 400 K
367	1-Cyclopentylhexa-decane	C	−99.33	220.75	−191.908	51.4259	−317.004	79.7299	0.04	0.117
		J	−415.60	923.62	−802.944	215.166	−1326.34	333.590		at 400 K
368	1-Methylcyclo-pentene	C	−1.30	78.00	−70.4254	11.8711	−48.6942	1.14169	0.49	0.684
		J	−5.44	326.35	−294.660	49.6686	−203.736	4.77683		at 400 K
369	3-Methylcyclo-pentene	C	2.07	79.00	−103.268	13.6111	−78.4507	16.6087	0.21	0.087
		J	8.66	330.54	−432.073	57.1582	−328.238	69.4907		at 400 K
370	4-Methylcyclo-pentene	C	3.53	78.60	−98.3732	13.4115	−74.9855	15.0786	0.16	0.537
		J	14.77	328.86	−411.594	56.1137	−313.739	63.0887		at 400 K
371	Methylcyclohexane	C	−36.99	82.06	−138.731	18.1448	−94.6485	15.8052	0.16	0.502
		J	−154.77	343.34	−580.450	75.9177	−396.009	66.1289		at 400 K
372	Ethylcyclohexane	C	−41.05	91.44	−143.558	20.6637	−110.873	19.8402	0.13	0.442
		J	−171.75	382.58	−600.648	86.4571	−463.892	83.0112		at 400 K
373	1,1-Dimethyl-cyclohexane	C	−43.26	87.24	−148.827	20.048	−93.357	9.86533	0.19	0.601
		J	−181.00	365.01	−622.691	83.8838	−390.608	41.2765		at 400 K
374	1,2-Dimethylcyclo-hexane, cis	C	−41.15	89.51	−150.540	20.6199	−107.111	17.3019	0.18	0.574
		J	−172.17	374.51	−629.859	86.2735	−448.153	72.3913		at 400 K

Table I. (11. cont.)

No.	Compound		ΔH_f° 298 K	S° 298 K	$a \cdot 10$	$b \cdot 10^2$	$c \cdot 10^6$	$d \cdot 10^9$	Av. err. %	Max. rel. err. %
375	1,2-Dimethylcyclo-	C	−43.02	88.65	−159.917	21.5245	−122.195	24.5849	0.14	0.439
	hexane, trans	J	−180.00	370.91	−669.095	90.0586	−511.262	102.863	at 400 K	
376	1,3-Dimethylcyclo-	C	−44.16	88.54	−140.710	20.1726	−100.137	14.3830	0.20	0.618
	hexane, cis	J	−184.77	370.45	−588.73	84.4023	−418.973	60.1784	at 400 K	
377	1,3-Dimethylcyclo-	C	−42.20	89.92	−139.711	20.2181	−103.205	16.0051	0.18	0.608
	hexane, trans	J	−176.56	376.23	−584.550	84.5925	−431.811	66.9652	at 400 K	
378	1,4-Dimethylcyclo-	C	−42.22	88.54	−142.518	20.3892	−106.333	17.7079	0.19	0.632
	hexane, cis	J	−176.65	370.45	−596.294	85.3083	−444.895	74.0900	at 400 K	
379	1,4-Dimethylcyclo-	C	−44.12	87.19	−160.219	21.2938	−116.714	21.6413	0.16	0.509
	hexane, trans	J	−184.60	364.80	−670.357	89.0933	−488.333	90.5472	at 400 K	
380	Propylcyclo-	C	−46.20	100.27	−148.184	23.4670	−133.789	27.2734	0.14	0.486
	hexane	J	−193.30	419.53	−620.001	98.1859	−559.772	114.112	at 400 K	
381	1,3,5-Trimethylcyc-	C	−51.48	93.30	−142.688	22.2005	−105.625	12.9607	0.23	0.706
	lohexane, cis, cis	J	−215.39	390.37	−597.007	92.8867	−441.934	54.2278	at 400 K	
382	1,3,5-Trimethylcyc-	C	−49.37	95.60	−146.304	22.6335	−118.016	19.6106	0.22	0.731
	lohexane, cis, trans	J	−206.56	400.00	−612.134	94.6986	−493.780	82.0509	at 400 K	
383	Butylcyclohexane	C	−50.95	109.58	−144.115	25.3661	−140.441	26.8306	0.13	0.452
		J	−213.17	458.48	−602.975	106.102	−587.605	112.259	at 400 K	
384	Pentylcyclohexane	C	−55.88	118.89	−156.385	28.2191	−163.322	34.7931	0.14	0.454
		J	−233.80	497.44	−654.315	118.069	−683.338	145.574	at 400 K	
385	1-Cyclohexyl-	C	−60.80	128.20	−159.248	30.5267	−177.040	38.0185	0.14	0.484
	hexane	J	−254.39	536.39	−666.294	127.724	−740.735	159.069	at 400 K	
386	1-Cyclohexyl-	C	−65.73	137.51	−162.853	32.8748	−191.239	41.4107	0.12	0.420
	heptane	J	−275.01	575.34	−681.375	137.548	−800.145	173.262	at 400 K	
387	1-Cyclohexyl-	C	−70.65	146.82	−158.783	34.7740	−197.891	40.9679	0.12	0.400
	octane	J	−295.60	614.29	−664.349	145.494	−827.977	171.410	at 400 K	
388	1-Cyclohexyl-	C	−75.58	156.12	−163.380	37.1779	−213.225	45.0955	0.13	0.439
	nonane	J	−316.23	653.21	−683.582	155.552	−892.134	188.680	at 400 K	
389	1-Cyclohexyl-	C	−80.51	165.43	−173.198	39.8787	−233.215	51.3542	0.13	0.432
	decane	J	−336.85	692.16	−724.660	166.853	−975.771	214.866	at 400 K	
390	1-Cyclohexyl-	C	−85.43	174.74	−169.848	41.8336	−241.143	51.7131	0.12	0.414
	undecane	J	−357.44	731.11	−710.643	175.032	−1008.94	216.368	at 400 K	
391	1-Cyclohexyl-	C	−90.36	184.05	−175.905	44.3340	−258.233	56.8091	0.11	0.380
	dodecane	J	−378.07	770.07	−735.985	185.493	−1080.45	237.689	at 400 K	
392	1-Cyclohexyl-	C	−95.28	193.36	−178.049	46.5857	−270.676	59.2328	0.12	0.404
	tridecane	J	−398.65	809.02	−744.956	194.915	−1132.51	247.830	at 400 K	
393	1-Cyclohexyltetra-	C	−100.21	202.67	−180.193	48.8375	−283.118	61.6566	0.12	0.425
	decane	J	−419.28	847.97	−753.927	204.336	−1184.57	257.971	at 400 K	
394	1-Cyclohexylpenta-	C	−105.14	211.98	−186.250	51.3378	−300.208	66.7526	0.12	0.395
	decane	J	−439.91	886.92	−779.270	214.798	−1256.07	279.293	at 400 K	
395	1-Cyclohexyl-	C	−110.06	221.29	−182.900	53.2928	−308.106	67.1115	0.11	0.383
	hexadecane	J	−460.49	925.88	−765.253	222.976	−1289.24	280.794	at 400 K	
396	Benzene	C	19.82	64.34	−104.593	12.5040	−89.8842	25.4575	0.07	0.241
		J	82.93	269.20	−437.617	52.3169	−376.076	106.514	at 400 K	
397	Toluene	C	11.95	76.64	−104.292	14.4239	−95.4442	24.9345	0.10	0.331
		J	50.00	320.66	−436.357	60.3494	−399.338	104.326	at 400 K	
398	Ethylbenzene	C	7.12	86.15	−102.917	16.8889	−114.909	31.0676	0.07	0.261
		J	29.79	360.45	−430.603	70.6631	−480.780	129.986	at 400 K	
399	m-Xylene	C	4.12	85.49	−69.6458	15.0393	−89.4786	20.2488	0.11	0.353
		J	17.24	357.69	−291.398	62.9243	−374.379	84.7210	at 400 K	

Table I. (12. cont.)

No.	Compound		ΔH_f° 298 K	S° 298 K	$a \cdot 10$	$b \cdot 10^2$	$c \cdot 10^6$	$d \cdot 10^9$	Av. err. %	Max. rel. err. %
400	o-Xylene	C	4.54	84.31	−37.8568	14.2358	−82.2281	17.9778	0.09	0.295
		J	19.00	352.75	−158.393	59.5624	−344.042	75.2192		at 400 K
401	p-Xylene	C	4.29	84.23	−59.9201	14.4245	−80.5613	16.2887	0.12	0.398
		J	17.95	352.42	−250.706	60.3520	−337.068	68.1517		at 400 K
402	Propylbenzene	C	1.87	95.76	−93.6484	18.6798	−121.062	30.7663	0.08	0.278
		J	7.82	400.66	−391.825	78.1563	−506.524	128.726		at 400 K
403	Cumene	C	0.94	92.87	−113.201	19.5946	−132.744	35.4031	0.06	0.177
		J	3.93	388.57	−473.633	81.9839	−555.399	148.127		at 400 K
404	m-Ethyltoluene	C	−0.46	96.60	−78.1101	17.8991	−111.701	27.3003	0.10	0.337
		J	−1.92	404.17	−326.813	74.8899	−467.358	114.225		at 400 K
405	o-Ethyltoluene	C	0.29	95.42	−44.6124	16.9832	−102.249	23.7389	0.09	0.269
		J	1.21	399.24	−186.658	71.0576	−427.812	99.3236		at 400 K
406	p-Ethyltoluene	C	−0.78	95.34	−70.1543	17.3898	−104.487	24.1627	0.10	0.364
		J	−3.26	398.90	−293.526	72.7591	−437.173	101.097		at 400 K
407	1,2,3-Trimethyl-benzene	C	−2.29	91.98	−4.04318	14.3649	−65.5605	8.15073	0.13	0.398
		J	−9.58	384.84	−16.9167	60.1028	−274.305	34.1027		a 400 K
408	1,2,4-Trimethyl-benzene	C	−3.33	94.59	−11.3147	14.6736	−68.5618	9.00028	0.14	0.443
		J	−13.93	395.76	−47.3408	61.3943	−286.863	37.6572		at 400 K
409	Mesitylene	C	−3.84	92.09	−39.0839	15.5762	−78.8874	13.0492	0.13	0.428
		J	−16.07	385.30	−163.527	65.1710	−330.065	54.5979		at 400 K
410	Butylbenzene	C	−3.30	105.04	−97.5023	21.0204	−135.046	34.0540	0.08	0.280
		J	−13.81	439.49	−407.949	87.9494	−565.034	142.482		at 400 K
411	m-Diethylbenzene	C	−5.22	104.99	−83.7001	20.6034	−131.066	32.7307	0.09	0.286
		J	−21.84	439.28	−350.201	86.2048	−548.379	136.945		at 400 K
412	o-Diethylbenzene	C	−4.53	103.81	−51.9110	19.7999	−123.815	30.4597	0.08	0.245
		J	−18.95	434.34	−217.196	82.8429	−518.043	127.443		at 400 K
413	p-Diethylbenzene	C	−5.32	103.73	−73.9744	19.9886	−122.148	28.7705	0.10	0.318
		J	−22.26	434.01	−309.509	83.6324	−511.069	120.376		at 400 K
414	1,2,3,4-Tetra-methylbenzene	C	−10.02	99.55	11.6203	17.5132	−97.2955	20.4366	0.08	0.256
		J	−41.92	416.52	48.6592	73.2753	−407.084	85.5067		at 400 K
415	1,2,3,5-Tetra-methylbenzene	C	−10.71	100.99	13.7972	16.8311	−85.7482	15.0165	0.11	0.331
		J	−44.81	422.54	57.7276	70.4213	−358.770	62.8291		at 400 K
416	1,2,4,5-Tetra-methylbenzene	C	−10.82	100.03	43.9827	15.3638	−65.8206	6.42756	0.13	0.419
		J	−45.27	418.53	184.023	64.2823	−275.393	26.8929		at 400 K
417	Pentylbenzene	C	−8.23	114.47	−100.704	23.3498	−149.101	37.4718	0.09	0.292
		J	−34.43	478.94	−421.345	97.6955	−623.838	156.782		at 400 K
418	Pentamethyl-benzene	C	−17.80	106.09	−0.85140	20.9306	−128.591	31.6843	0.04	0.139
		J	−74.48	443.88	−3.56227	87.5734	−538.023	132.567		at 400 K
419	Hexylbenzene	C	−13.15	123.78	−104.384	25.7050	−163.627	41.1760	0.09	0.300
		J	−55.02	517.90	−436.742	107.550	−684.617	172.280		at 400 K
420	1,2,3-Triethyl-benzene	C	−16.25	121.23	−25.1242	22.7111	−127.941	26.8735	0.10	0.304
		J	−67.99	507.23	−105.120	95.0233	−535.304	112.439		at 400 K
421	1,2,4-Triethyl-benzene	C	−16.99	123.84	−32.3958	23.0198	−130.942	27.7230	0.11	0.338
		J	−71.09	518.15	−135.544	96.3148	−547.861	115.993		at 400 K
422	1,3,5-Triethyl-benzene	C	−17.86	121.34	−60.1650	23.9224	−141.268	31.7720	0.10	0.324
		J	−74.73	507.69	−251.730	100.091	−591.063	132.934		at 400 K
423	Hexamethyl-benzene	C	−25.26	108.12	8.17885	23.9982	−158.367	43.1246	0.03	0.070
		J	−105.69	452.37	34.2203	100.408	−662.606	180.433		at 400 K
424	1-Phenylheptane	C	−18.08	133.09	−106.566	27.9693	−176.470	43.8926	0.09	0.296
		J	−75.65	556.85	−445.872	117.024	−738.349	183.646		at 400 K

Table I. (13. cont.)

No.	Compound		ΔH_f° 298 K	S° 298 K	$a \cdot 10$	$b \cdot 10^2$	$c \cdot 10^6$	$d \cdot 10^9$	Av. err. %	Max. rel. err. %
425	1-Phenyloctane	C	−23.00	142.40	−109.020	30.2459	−189.435	46.6376	0.09	0.298
		J	−96.23	595.80	−456.140	126.549	−792.597	195.132		at 400 K
426	1,2,3,4-Tetra-ethylbenzene	C	−29.46	138.55	−16.4878	28.6415	−180.469	45.4003	0.07	0.204
		J	−123.26	579.69	−68.9849	119.836	−755.082	189.955		at 400 K
427	1,2,3,5-Tetraethyl-benzene	C	−29.36	139.99	−14.3108	27.9593	−168.922	39.9802	0.08	0.253
		J	−122.84	585.72	−59.8765	116.982	−706.768	167.277		at 400 K
428	1,2,4,5-Tetraethyl-benzene	C	−29.46	139.03	47.2557	25.0790	−128.789	22.1476	0.14	0.457
		J	−123.26	581.70	197.718	104.930	−538.854	92.6656		at 400 K
429	1-Phenylnonane	C	−27.93	151.71	−113.374	32.6453	−204.856	50.8877	0.09	0.305
		J	−116.86	634.75	−474.358	136.588	−857.117	212.914		at 400 K
430	1-Phenyldecane	C	−32.86	161.02	−115.612	34.9109	−217.649	53.5483	0.09	0.296
		J	−137.49	673.71	−483.719	146.067	−910.642	224.046		at 400 K
431	Pentaethyl-benzene	C	−41.87	154.84	−35.9865	34.8409	−232.558	62.8889	0.06	0.127
		J	−175.18	647.85	−150.567	145.774	−973.021	263.127		at 400 K
432	1-Phenylundecane	C	−37.78	170.32	−117.855	37.1768	−230.464	56.2301	0.09	0.295
		J	−158.07	712.62	−493.106	115.548	−964.260	235.267		at 400 K
433	1-Phenyldodecane	C	−42.71	179.63	−122.490	39.5932	−246.197	60.6505	0.09	0.302
		J	−178.70	751.57	−512.498	165.658	−1030.09	253.762		at 400 K
434	Hexaethyl-benzene	C	−53.60	166.62	−33.9832	40.6906	−283.127	80.5701	0.05	0.129
		J	−224.26	697.14	−142.186	170.249	−1184.60	337.105		at 300 K
435	1-Phenyltridecane	C	−47.63	188.94	−124.664	41.8527	−258.850	63.2253	0.09	0.302
		J	−199.28	790.52	−521.592	175.112	−1083.03	264.534		at 400 K
436	1-Phenyltetra-decane	C	−52.56	198.25	−126.565	44.0999	−271.380	65.7716	0.09	0.299
		J	−219.91	829.48	−529.548	184.514	−909.517	275.188		at 400 K
437	1-Phenylpenta-decane	C	−57.99	207.56	−131.261	46.5179	−287.086	70.1571	0.09	0.306
		J	−240.54	868.43	−549.197	194.631	−1201.17	293.537		at 400 K
438	1-Phenylhexa-decane	C	−62.41	216.87	−133.505	48.7838	−299.901	72.8389	0.09	0.305
		J	−261.12	907.38	−558.585	204.111	−1254.79	304.758		at 400 K
439	Styrene	C	35.22	82.48	−88.1869	15.8975	−115.890	33.6517	0.05	0.164
		J	147.36	345.10	−368.974	66.5153	−484.883	140.799		at 400 K
440	α-Methylstyrene	C	27.00	91.70	−58.1114	16.5570	−108.180	28.1957	0.08	0.251
		J	112.97	383.67	−243.138	69.2746	−452.624	117.971		at 400 K
441	Propenylbenzene, cis	C	29.00	91.70	−58.1111	16.5570	−108.180	28.1957	0.08	0.251
		J	121.34	383.67	−243.137	69.2744	−452.622	117.970		at 400 K
442	Propenylbenzene, trans	C	28.00	90.90	−70.098	17.2792	−117.791	31.9939	0.06	0.233
		J	117.15	380.33	−293.292	72.2963	−492.836	133.862		at 400 K
443	m-Methylstyrene	C	27.60	93.10	−58.1111	16.5570	−108.179	28.1956	0.08	0.251
		J	115.48	389.53	−243.137	69.2744	−452.622	117.970		at 400 K
444	p-Methylstyrene	C	28.30	91.70	−58.1111	16.5570	−108.179	28.1956	0.08	0.251
		J	118.41	383.67	−243.137	69.2744	−452.622	117.970		at 400 K
445	p-Methylstyrene	C	27.40	91.70	−58.1111	16.5570	−108.179	28.1956	0.08	0.251
		J	114.64	383.67	−243.137	69.2744	−452.622	117.970		at 400 K
446	Naphthalene	C	36.08	80.22	−148.490	19.4731	−141.927	40.4168	0.06	0.214
		J	150.96	335.64	−621.280	81.4754	−593.822	169.104		at 400 K
447	1-Methyl-naphthalene	C	27.93	90.21	−142.641	21.8966	−158.609	45.1022	0.05	0.180
		J	116.86	377.44	−596.812	91.6152	−663.618	188.708		at 400 K
448	2-Methyl-naphthalene	C	27.75	90.83	−124.240	21.0150	−147.874	40.997	0.05	0.198
		J	116.11	380.03	−519.819	87.9270	−618.705	171.531		at 400 K
449	1-Ethyl-naphthalene	C	23.10	99.94	−152.422	24.8302	−181.922	52.6424	0.04	0.155
		J	96.65	418.15	−637.733	103.890	−761-161	220.256		at 400 K
450	2-Ethyl-naphthalene	C	22.92	100.56	−134.020	23.9487	−171.187	48.5367	0.05	0.171
		J	95.90	420.74	−560.740	100.201	−716.251	203.078		at 400 K

Table I. (14. cont.)

No.	Compound		ΔH_f° 298 K	S° 298 K	$a \cdot 10$	$b \cdot 10^2$	$c \cdot 10^6$	$d \cdot 10^9$	Av. err. %	Max. rel. err. %
451	1,2-Dimethyl-naphthalene	C	19.97	97.23	−142.030	24.3566	−175.012	49.4535	0.05	0.182
		J	83.55	406.81	−594.255	101.908	−732.254	206.914		at 400 K
452	1,3-Dimethyl-naphthalene	C	19.55	97.86	−123.628	23.4750	−164.278	45.3483	0.05	0.198
		J	81.80	409.45	−517.262	98.2198	−687.340	189.738		at 400 K
453	1,4-Dimethyl-naphthalene	C	19.72	95.86	−142.030	24.3566	−175.012	49.4535	0.05	0.182
		J	82.51	401.08	−594.255	101.908	−732.254	206.914		at 400 K
454	1,5-Dimethyl-naphthalene	C	19.55	95.86	−142.030	24.3566	−175.012	49.4535	0.05	0.182
		J	81.80	401.08	−594.255	101.908	−732.254	206.914		at 400 K
455	1,6-Dimethyl-naphthalene	C	19.72	97.86	−123.628	23.4750	−164.278	45.3483	0.05	0.198
		J	82.51	409.45	−517.262	98.2198	−687.340	189.738		at 400 K
456	1,7-Dimethyl-naphthalene	C	19.55	97.86	−123.628	23.4750	−164.278	45.3483	0.05	0.198
		J	81.80	409.45	−517.262	98.2198	−687.340	189.738		at 400 K
457	2,3-Dimethyl-naphthalene	C	19.97	98.22	−76.5168	21.1683	−134.549	33.2712	0.07	0.231
		J	83.55	410.95	−320.148	88.5683	−562.955	139.207		at 400 K
458	2,6-Dimethyl-naphthalene	C	19.72	97.68	−95.7439	22.3642	−152.158	41.2287	0.07	0.182
		J	82.51	408.69	−400.594	93.5720	−636.630	172.501		at 400 K
459	2,7-Dimethyl-naphthalene	C	19.72	97.68	−93.9111	22.2821	−150.989	40.6956	0.06	0.195
		J	82.51	408.69	−392.924	93.2285	−631.738	170.270		at 400 K
460	1-Propyl-naphthalene	C	17.85	109.55	−143.861	26.6555	−188.511	52.5299	0.06	0.208
		J	74.68	458.36	−601.917	111.527	−788.735	219.786		at 400 K
461	2-Propyl-naphthalene	C	17.65	110.18	−126.963	25.8372	−178.477	48.5915	0.06	0.163
		J	73.85	460.99	−531.215	108.103	−746.752	203.307		at 400 K
462	2-Ethyl-3-methyl-naphthalene	C	15.72	109.33	−82.9244	23.8972	−154.215	38.7991	0.06	0.162
		J	65.77	457.44	−346.956	99.9859	−654.235	162.335		at 400 K
463	2-Ethyl-6-methyl-naphthalene	C	14.65	108.79	−188.816	30.3922	−268.639	99.4777	0.64	0.713
		J	61.30	455.18	−790.006	127.161	−1123.98	416.214		at 400 K
464	2-Ethyl-7-methyl-naphthalene	C	14.65	108.79	−188.816	30.3922	−268.639	99.4777	0.64	0.713
		J	61.30	455.18	−790.006	127.161	−1123.98	416.214		at 400 K
465	1-Butyl-naphthalene	C	12.68	118.83	−146.530	28.9328	−201.627	55.4257	0.07	0.228
		J	53.05	497.18	−613.083	121.055	−843.609	231.901		at 400 K
466	2-Butyl-naphthalene	C	12.50	119.46	−125.298	27.8751	−187.492	49.3400	0.06	0.180
		J	52.30	499.82	−524.247	116.629	−784.466	206.438		at 400 K
467	1-Pentyl-naphthalene	C	7.75	128.26	−153.320	31.4642	−218.854	60.4203	0.06	0.220
		J	32.43	536.64	−641.489	131.646	−915.686	252.798		at 400 K
468	2-Pentyl-naphthalene	C	7.57	128.89	−132.806	30.4623	−205.994	55.1363	0.05	0.174
		J	31.67	539.28	−555.661	127.454	−861.880	230.690		at 400 K
469	Spiropentane	C	44.27	67.45	−99.1311	12.8757	−91.4187	26.0775	0.08	0.286
		J	185.23	282.21	−414.764	53.8720	−382.496	109.108		at 400 K
470	1,3,5-Cycloheptatriene	C	43.47	75.44	−102.024	16.3974	−130.799	41.6292	0.04	0.074
		J	181.88	315.64	−426.869	68.6066	−547.263	174.176		at 900 K
471	Ethynylbenzene	C	78.22	76.88	−91.5779	15.7443	−128.254	41.1621	0.04	0.081
		J	327.27	321.67	−383.162	65.8740	−536.615	172.222		at 900 K
472	1,3,5,7-Cyclooctatetraene	C	71.23	78.10	−99.5823	16.3613	−119.421	34.6178	0.11	0.376
		J	298.03	326.77	−416.652	68.4558	−499.658	144.841		at 400 K
473	Azulene	C	66.90	80.75	−173.684	20.1827	−149.130	42.9011	0.06	0.231
		J	279.91	337.86	−726.696	84.4446	−623.959	179.498		at 400 K
474	Decahydro-naphthalene, cis	C	−40.38	90.28	−262.199	26.4227	−153.598	32.4075	0.18	0.578
		J	−168.95	377.73	−1097.04	110.553	−642.652	135.593		at 400 K
475	Decahydro-naphthalene, trans	C	−43.57	89.52	−233.276	24.9481	−130.801	21.4460	0.20	0.355
		J	−182.30	374.55	−976.025	104.383	−547.272	89.7301		at 500 K
476	Biphenyl	C	43.52	93.85	−210.472	25.3666	−195.274	58.6573	0.06	0.188
		J	182.09	392.67	−880.613	106.134	−817.025	245.422		at 400 K

Table I. (cont.)

CARBON, HYDROGEN AND OXYGEN COMPOUNDS

No.	Compound		ΔH_f° 298 K	S° 298 K	$a \cdot 10$	$b \cdot 10^2$	$c \cdot 10^6$	$d \cdot 10^9$	Av. err. %	Max. rel. err. %
501	Methyl ether	C	−43.99	63.83	47.9702	3.85380	−5.16360	−4.40920	0.15	0.439
		J	−184.05	267.06	200.707	16.1243	−21.6045	−18.4481		at 400 K
502	Ethyl methyl ether	C	−51.73	74.24	57.2387	5.64464	−11.3160	−4.71049	0.14	0.422
		J	−216.44	310.62	239.487	23.6172	−47.3462	−19.7087		at 400 K
503	Ethyl ether	C	−60.28	81.90	53.3849	7.98526	−25.3001	−1.42287	0.13	0.394
		J	−252.21	342.67	223.362	33.4103	−105.856	−5.95328		at 400 K
504	Methyl propyl ether	C	−56.82	83.52	53.3849	7.98526	−25.3001	−1.4228	0.13	0.394
		J	−237.73	349.45	223.362	33.4103	−105.856	−5.95328		at 400 K
505	Methyl isopropyl ether	C	−60.24	80.86	34.5303	8.73028	−33.9344	2.21729	0.12	0.352
		J	−252.04	338.32	144.474	36.5275	−141.981	9.27712		at 400 K
506	Methyl tert-butyl ether	C	−70.00	84.36	10.6850	12.0574	−58.9993	8.89489	0.23	0.613
		J	−292.88	352.96	44.7057	50.4482	−246.853	37.2162		at 400 K
507	Propyl ether	C	−70.00	100.98	47.8415	12.5891	−52.3784	4.82663	0.12	0.359
		J	−292.88	422.50	200.169	52.6727	−219.151	20.1946		at 400 K
508	Isopropyl ether	C	−76.20	93.27	47.8415	12.5891	−52.3784	4.82663	0.12	0.359
		J	−318.82	390.24	200.169	52.6727	−219.151	20.1946		at 400 K
509	Isopropyl tert-butyl ether	C	−85.60	99.89	49.7011	14.7090	−63.7379	7.17517	0.15	0.421
		J	−358.15	417.94	207.950	61.5426	−266.679	30.0209		at 400 K
510	Butyl ether	C	−79.80	119.60	41.4890	17.2390	−80.3252	11.5881	0.11	0.352
		J	−333.88	500.41	173.590	72.1282	−336.081	48.4848		at 400 K
511	sec-Butyl ether	C	−86.20	110.57	41.4890	17.2390	−80.3252	11.5881	0.11	0.352
		J	−360.66	462.62	173.590	72.1282	−336.081	48.4848		at 400 K
512	tert-Butyl ether	C	−87.20	102.12	41.4890	17.2390	−80.3252	11.5881	0.11	0.352
		J	−364.84	427.27	173.590	72.1282	−336.081	48.4848		at 400 K
513	Ethylene oxide	C	−12.58	57.94	−17.9619	5.30677	−30.0067	6.18902	0.15	0.505
		J	−52.63	242.42	−75.1526	22.2035	−125.548	25.8949		at 400 K
514	Propylene oxide	C	−22.17	68.53	−18.7772	7.71386	−46.5739	11.0891	0.10	0.340
		J	−92.76	286.73	−78.5638	32.2748	−194.865	46.3966		at 400 K
515	Furan	C	−8.29	63.86	−84.8425	10.3213	−82.4936	25.6554	0.07	0.207
		J	−34.69	267.19	−354.981	43.1843	−345.153	107.342		at 400 K
516	p-Dioxone	C	−75.30	71.65	−86.4367	12.3653	−69.0906	12.0565	0.31	0.997
		J	−315.06	299.78	−361.651	51.7362	−289.075	50.4442		at 400 K
517	Methanol	C	−48.08	57.29	50.5146	1.69268	6.17571	−6.80664	0.24	0.684
		J	−201.17	239.70	211.353	7.08219	25.8392	−28.4790		at 400 K
518	Ethyl alcohol	C	−56.12	67.54	13.5801	5.62403	−30.0661	6.33049	0.15	0.456
		J	−234.81	282.59	56.8192	23.5309	−125.797	26.4868		at 400 K
519	Propyl alcohol	C	−61.55	77.63	21.3401	7.19721	−32.8382	4.63536	0.13	0.406
		J	−257.53	324.80	89.2869	30.1131	−137.395	19.3943		at 400 K
520	Isopropyl alcohol	C	−65.15	74.07	−17.3480	9.41971	−63.4070	17.7604	0.16	0.578
		J	−272.59	309.91	−72.5842	39.4121	−265.295	74.3094		at 400 K
521	Butyl alcohol	C	−65.59	86.80	18.9468	9.47791	−46.0132	7.56913	0.12	0.391
		J	−274.43	363.17	79.2735	39.6556	−192.519	31.6692		at 400 K
522	sec-Butyl alcohol	C	−69.86	85.81	13.9114	10.2096	−57.5167	12.6306	0.12	0.399
		J	−292.29	359.03	58.2054	42.7169	−240.650	52.8465		at 400 K
523	tert-Butyl alcohol	C	−77.87	77.98	−10.9726	11.5006	−74.6090	19.8468	0.07	0.227
		J	−325.81	326.27	−45.9092	48.1184	−312.164	83.0391		at 400 K

Table 1. (1. cont.)

No.	Compound		ΔH_f° 298 K	S° 298 K	$a \cdot 10$	$b \cdot 10^2$	$c \cdot 10^6$	$d \cdot 10^9$	Av. err. %	Max. rel. err. %
524	Pentyl alcohol	C	−72.27	96.21	16.5536	11.7586	−59.1879	10.5028	0.12	0.381
		J	−302.38	402.54	69.2601	49.1979	−247.642	43.9438		at 400 K
525	tert-Pentyl alcohol	C	−78.65	87.68	−22.5584	13.4797	−78.4851	17.2329	0.21	0.593
		J	−329.07	366.85	−94.3843	56.3991	−328.382	72.1025		at 400 K
526	Hexyl alcohol	C	−76.39	105.52	14.1604	14.0393	−72.3629	13.4366	0.11	0.374
		J	−319.62	441.50	59.2468	58.7403	−302.766	56.2186		at 400 K
527	Heptyl alcohol	C	−80.03	114.83	11.7671	16.3200	−85.5379	16.3704	0.11	0.369
		J	−334.85	480.45	49.2335	68.2827	−357.890	68.4934		at 400 K
528	Octyl alcohol	C	−85.34	124.14	9.37388	18.6007	−98.7129	19.3041	0.11	0.365
		J	−357.06	519.40	39.2202	77.8251	−413.014	80.7682		at 400 K
529	Nonyl alcohol	C	−92.47	133.45	6.98062	20.8814	−111.888	22.2379	0.11	0.361
		J	−386.89	558.35	29.2069	87.3675	−468.138	93.0430		at 400 K
530	Decyl alcohol	C	−96.38	142.76	4.58736	23.1621	−125.063	25.1716	0.11	0.359
		J	−403.25	597.31	19.1935	96.9100	−523.262	105.318		at 400 K
531	Undecyl alcohol	C	−100.91	152.07	2.19410	25.4428	−138.238	28.1054	0.11	0.357
		J	−422.21	636.26	9.18012	106.453	−578.387	117.593		at 400 K
532	Dodecyl alcohol	C	−105.84	161.38	−0.19916	27.7235	−151.413	31.0392	0.10	0.355
		J	−442.83	675.21	−0.83327	115.995	−633.512	129.868		at 400 K
533	1-Tridecanol	C	−110.77	170.37	−7.59032	30.2809	−169.436	36.6154	0.10	0.343
		J	−463.46	712.83	−31.7579	126.695	−708.918	153.198		at 400 K
534	1-Tetradecanol	C	−115.70	179.68	−10.0445	32.5575	−182.401	39.3604	0.10	0.342
		J	−484.09	751.78	−42.0263	136.220	−763.166	164.684		at 400 K
535	1-Pentadecanol	C	−120.62	188.99	−11.9460	34.8046	−194.931	41.9067	0.10	0.335
		J	−504.67	790.73	−49.9819	145.622	−815.589	175.337		at 400 K
536	1-Hexadecanol	C	−125.54	198.30	−16.6423	37.2226	−210.637	46.2922	0.10	0.341
		J	−525.26	829.69	−69.6313	155.739	−881.304	193.686		at 400 K
537	1-Heptadecanol	C	−130.47	207.61	−18.6052	39.4714	−223.139	48.8037	0.10	0.337
		J	−545.89	868.64	−77.8444	165.148	−933.614	204.194		at 400 K
538	1-Octadecanol	C	−135.39	216.92	−20.7873	41.7356	−235.982	51.5203	0.10	0.333
		J	−566.47	907.59	−86.9743	174.622	−987.347	215.561		at 400 K
539	1-Nonadecanol	C	−140.32	226.23	−25.4136	44.1473	−251.526	55.7988	0.10	0.338
		J	−587.10	946.55	−106.330	184.712	−1052.38	233.462		at 400 K
540	1-Eicosanol	C	−145.25	235.54	−30.0398	46.5590	−267.070	60.0774	0.10	0.343
		J	−607.73	985.50	−125.687	194.802	−1117.42	251.363		at 400 K
541	Allyl alcohol	C	−31.55	73.51	−2.63664	7.51386	−48.5174	12.7086	0.06	0.142
		J	−132.01	307.57	−11.0317	31.4380	−202.997	53.1726		at 400 K
542	Ethylene glycol	C	−93.05	77.33	69.8659	6.87960	−53.6543	17.6408	0.26	0.499
		J	−389.32	323.55	292.318	28.7842	−224.490	73.8092		at 800 K
543	Cyclohexanol	C	−70.40	78.32	−100.671	15.7112	−74.9334	8.95188	0.17	0.535
		J	−294.55	327.69	−421.207	65.7354	−313.521	37.4546		at 400 K
544	Formaldehyde	C	−27.70	52.29	63.0609	0.44175	11.4453	−7.37248	0.19	0.557
		J	−115.90	218.78	263.847	1.84827	47.8872	−30.8465		at 400 K
545	Acetaldehyde	C	−39.76	63.15	36.9463	3.45322	−10.3300	−0.95573	0.13	0.402
		J	−166.36	264.22	154.583	14.4483	−43.2209	−3.99877		at 400 K
546	Propionaldehyde	C	−45.90	72.83	27.9909	6.24296	−31.0390	5.07665	0.06	0.171
		J	−192.05	304.72	117.114	26.1205	−129.867	21.2407		at 400 K
547	Butyraldehyde	C	−49.00	82.44	33.6254	8.25556	−41.1432	6.89389	0.08	0.142
		J	−205.02	344.93	140.689	34.5413	−172.143	28.8440		at 400 K

Table I. (2. cont.)

No.	Compound		ΔH_f° 298 K	S° 298 K	$a \cdot 10$	$b \cdot 10^2$	$c \cdot 10^6$	$d \cdot 10^9$	Av. err. %	Max. rel. err. %
548	Valeraldehyde	C	−54.45	91.53	34.0083	10.3335	−50.3183	7.55102	0.09	0.181
		J	−227.82	382.96	142.291	43.2354	−210.532	31.5934		at 400 K
549	Hexanal	C	−59.37	101.07	28.2373	12.8285	−67.7382	13.0146	0.09	0.300
		J	−248.40	422.88	118.144	53.6743	−283.417	54.4529		at 400 K
550	Heptanal	C	−63.10	110.34	25.088	15.1414	−81.1268	15.8724	0.08	0.215
		J	−264.01	461.66	104.968	63.3516	−339.435	66.4100		at 400 K
551	Octanal	C	−69.23	119.66	25.2955	17.2573	−91.2527	17.1276	0.08	0.266
		J	−289.66	500.66	105.836	72.2045	−381.801	71.6620		at 400 K
552	Nonanal	C	−74.16	128.97	19.6305	19.7241	−107.758	21.9005	0.11	0.338
		J	−310.29	539.61	82.1336	82.5255	−450.860	91.6314		at 400 K
553	Decanal	C	−79.09	138.28	16.3753	22.0652	−122.061	25.4490	0.08	0.274
		J	−330.91	578.56	68.5139	92.3208	−510.704	106.479		at 400 K
554	Acetone	C	−52.00	70.49	33.3866	5.41177	−17.8317	−0.50376	0.15	0.454
		J	−217.57	294.93	139.689	22.6328	−74.6080	−2.10772		at 400 K
555	2-Butanone	C	−56.97	80.81	57.4339	7.08230	−26.1433	0.87469	0.14	0.453
		J	−238.36	338.11	240.303	29.6323	−109.384	3.65968		at 400 K
556	2-Pentanone	C	−61.82	89.91	2.73937	11.4727	−67.2992	15.9102	0.01	0.017
		J	−258.65	376.18	11.4615	48.0020	−281.580	66.5681		at 300 K
557	Ketene	C	−14.60	57.79	47.4912	3.23379	−25.0958	8.26863	0.07	0.154
		J	−61.09	241.79	198.703	13.5301	−105.001	34.5959		at 400 K
558	Cyclohexanone	C	−55.00	77.00	−90.2797	13.2282	−46.6438	−3.66316	0.17	0.518
		J	−230.12	322.17	−377.730	55.3466	−195.158	−15.3267		at 400 K
559	Formic acid	C	−90.49	59.45	27.9756	3.24215	−20.0869	4.81604	0.09	0.246
		J	−378.61	248.74	117.050	13.5652	−84.0437	20.1503		at 600 K
560	Acetic acid	C	−103.93	67.52	11.5623	6.08567	−41.8646	11.8218	0.09	0.194
		J	−434.84	282.50	48.3767	25.4624	−175.161	49.4624		at 700 K
561	Methyl formate	C	−83.60	72.00	12.6503	6.01761	−40.4770	11.0023	0.15	0.324
		J	−349.78	301.25	52.9287	25.1777	−169.356	46.0334		at 400 K
562	Acetic anhydride	C	−137.60	93.20	−55.7638	12.2429	−88.1118	25.3328	0.09	0.223
		J	−575.72	389.95	−233.316	51.2241	−368.660	105.992		at 700 K
563	Ethyl acetate	C	−105.86	86.70	58.9779	7.84435	−23.5139	−4.87477	0.35	0.470
		J	−442.92	362.75	246.763	32.8207	−98.3821	−20.3960		at 600 K
564	Acrylic acid	C	−80.36	75.29	4.16262	7.61929	−56.1674	16.6606	0.07	0.176
		J	−336.23	315.01	17.4164	31.8790	−235.004	69.708		at 700 K
565	Phenol	C	−23.03	75.43	−85.5920	14.2846	−115.250	36.4646	0.04	0.080
		J	−96.36	315.60	−358.117	59.7665	−482.206	152.568		at 500 K
566	m-Cresol	C	−31.63	85.27	−110.277	17.5199	−147.196	51.5023	0.21	0.793
		J	−132.34	356.77	−461.400	73.3031	−615.869	215.486		at 300 K
567	o-Cresol	C	−30.47	85.47	−62.1508	16.0015	−130.116	45.1051	0.10	0.298
		J	−127.49	357.61	−260.039	66.9501	−544.405	188.719		at 400 K
568	p-Cresol	C	−29.97	83.09	−88.9770	16.5306	−133.584	45.5479	0.10	0.300
		J	−125.39	347.65	−372.280	69.1641	−558.916	190.572		at 400 K
569	Benzoic acid	C	−69.36	88.19	−91.7748	13.6212	−81.1634	16.3601	0.30	0.901
		J	−290.20	368.99	−383.985	56.9908	−339.588	68.4504		at 400 K

Table I. (cont.)

NITROGEN COMPOUNDS

No.	Compound		ΔH_f° 298 K	S° 298 K	$a \cdot 10$	$b \cdot 10^2$	$c \cdot 10^6$	$d \cdot 10^9$	Av. err. %	Max. rel. err. %
601	Methylamine	C	−5.50	57.98	38.4542	2.90161	−5.44728	−2.17126	0.14	0.425
		J	−23.01	242.59	160.892	12.1403	−22.7914	−9.08454		at 400 K
602	Ethylamine	C	−11.00	68.08	8.81493	6.57066	−37.8077	9.09415	0.06	0.216
		J	−46.02	284.85	36.8817	27.4916	−158.187	38.0493		at 400 K
603	Propylamine	C	−17.30	77.48	15.9821	8.35408	−43.5086	8.56400	0.09	0.319
		J	−72.38	324.18	66.8690	34.9535	−182.040	35.8318		at 400 K
604	Butylamine	C	−22.00	86.76	12.1282	10.6947	−57.4927	11.8516	0.09	0.313
		J	−92.05	363.00	50.7444	44.7466	−240.549	49.5872		at 400 K
605	sec-Butylamine	C	−24.90	83.90	7.25383	10.5723	−49.6477	5.78014	0.09	0.192
		J	−104.18	351.04	30.3500	44.2346	−207.723	24.1841		at 900 K
606	tert-Butylamine	C	−28.65	80.76	−27.9974	12.8597	−84.3362	22.3132	0.09	0.310
		J	−119.87	337.90	−117.141	53.8051	−352.863	93.3585		at 400 K
607	Dimethylamine	C	−4.50	65.24	−0.40548	6.43768	−31.7522	5.58751	0.15	0.464
		J	−18.83	272.96	−1.69654	26.9352	−132.851	23.3781		at 400 K
608	Diethylamine	C	−17.30	84.18	4.86855	10.5802	−52.1327	8.72360	0.13	0.414
		J	−72.38	352.21	20.3700	44.2677	−218.123	36.4995		at 400 K
609	Trimethylamine	C	−5.70	69.02	−19.5966	9.48592	−52.9888	11.0384	0.15	0.469
		J	−23.85	288.78	−81.9922	39.6891	−221.705	46.1848		at 400 K
610	Triethylamine	C	−23.80	96.90	−9.42204	15.5034	−81.9402	15.5895	0.16	0.529
		J	−99.58	405.43	−39.4218	64.8663	−342.837	65.2263		at 400 K
611	Ethyleneimine	C	29.50	59.90	−49.6036	7.21785	−49.2621	13.4848	0.11	0.368
		J	123.43	250.62	−207.541	30.1994	−206.113	56.4204		at 400 K
612	Pyrrolidine	C	−0.86	73.97	−120.084	12.6165	−75.4361	17.0866	0.16	0.551
		J	−3.60	309.49	−502.430	52.7875	−315.624	71.4903		at 400 K
613	Pyridine	C	33.50	67.59	−95.0238	11.7649	−84.9656	23.9807	0.09	0.304
		J	140.16	282.80	−397.579	49.2244	−355.496	100.335		at 400 K
614	2-Picoline	C	23.65	77.68	−84.6290	13.2476	−87.1791	22.4875	0.09	0.306
		J	98.95	325.01	−354.088	55.4278	−364.757	94.0876		at 400 K
615	3-Picoline	C	25.37	77.67	−86.2232	13.2691	−87.2808	22.4247	0.09	0.326
		J	106.15	324.97	−360.758	55.5176	−365.183	93.8248		at 400 K
616	Aniline	C	20.76	76.28	−96.7496	15.2444	−122.579	39.0063	0.04	0.079
		J	86.86	319.16	−404.800	63.7824	−512.871	163.202		at 500 K
617	Acetonitrile	C	21.00	58.19	48.9068	2.85671	−10.7318	0.76457	0.07	0.200
		J	87.86	243.47	204.626	11.9525	−44.9020	3.19895		at 400 K
618	Acrylonitrile	C	44.20	65.47	25.5381	5.27235	−37.3852	10.99308	0.03	0.049
		J	184.93	273.93	106.851	22.0595	−156.420	45.9950		at 700 K
619	Propionitrile	C	12.10	68.50	36.7805	5.36207	−26.2715	4.66598	0.06	0.170
		J	50.63	286.60	153.889	22.4349	−109.920	19.5225		at 400 K
620	Butyronitrile	C	8.14	77.78	36.3251	7.65734	−39.1219	7.12405	0.07	0.240
		J	34.06	325.43	151.9838	32.0383	−163.686	29.8070		at 400 K
621	Isobutyronitrile	C	6.07	74.88	14.6566	8.69771	−53.0477	12.9999	0.05	0.143
		J	25.40	313.30	61.3231	36.3911	−221.952	54.3913		at 400 K
622	Benzonitrile	C	52.30	76.73	−61.1978	13.6477	−105.189	31.9209	0.05	0.100
		J	218.82	321.04	−256.052	57.1017	−440.109	133.557		at 400 K
623	Nitromethane	C	−17.86	65.73	17.7249	4.72298	−25.8257	4.97929	0.10	0.303
		J	−74.73	275.01	74.1606	19.7609	−108.550	20.8333		at 400 K

Table I. (1. cont.)

No.	Compound		ΔH_f° 298 K	S° 298 K	$a \cdot 10$	$b \cdot 10^2$	$c \cdot 10^6$	$d \cdot 10^9$	Av. err. %	Max. rel. err. %
624	Nitroethane	C	−24.20	75.39	−14.5813	8.27846	−55.5934	14.9272	0.07	0.237
		J	−101.25	315.43	−61.0082	34.6370	−232.603	62.4551		at 400 K
625	1-Nitropropane	C	−29.80	85.00	−6.08516	10.1127	−62.4407	14.9655	0.09	0.290
		J	−124.68	355.64	−25.4603	42.3114	−261.252	62.6155		at 400 K
626	2-Nitropropane	C	−33.50	83.10	−27.7536	11.1530	−76.3664	20.8413	0.06	0.200
		J	−140.16	347.69	−116.121	46.6642	−319.517	87.1997		at 400 K
627	1-Nitrobutane	C	−34.40	94.28	−9.93902	12.4533	−76.4245	18.2531	0.09	0.290
		J	−143.93	394.47	−41.5849	52.1045	−319.761	76.3708		at 400 K
628	2-Nitrobutane	C	−39.10	91.62	−28.7935	13.1983	−85.0590	21.8932	0.08	0.253
		J	−163.59	383.34	−120.472	55.2216	−355.887	91.6021		at 400 K
629	Methyl nitrite	C	−15.30	67.95	30.1091	4.81232	−26.9874	5.36383	0.08	0.249
		J	−64.02	284.30	125.976	20.1347	−112.915	22.4422		at 400 K
630	Methyl nitrate	C	−28.80	72.15	40.7654	5.75272	−35.7540	8.33428	0.05	0.138
		J	−120.50	301.88	170.562	24.0694	−149.595	34.8706		at 400 K
631	Ethyl nitrate	C	−36.80	83.25	8.45928	9.30821	−65.5217	18.2821	0.04	0.123
		J	−153.97	348.32	35.3935	38.9454	−274.142	76.4923		at 400 K
632	Propyl nitrate	C	−41.60	92.10	16.9555	11.1424	−72.3688	18.3204	0.06	0.191
		J	−174.05	385.35	70.9414	46.6197	−302.791	76.6526		at 400 K
633	Isopropyl nitrate	C	−45.65	89.20	−4.71306	12.1828	−86.2949	24.1963	0.05	0.114
		J	−191.00	373.21	−19.7194	50.9727	−361.058	101.237		at 400 K

Table I. (cont.)

HALOGEN COMPOUNDS

No.	Compound		ΔH_f° 298 K	S° 298 K	$a \cdot 10$	$b \cdot 10^2$	$c \cdot 10^6$	$d \cdot 10^9$	Av. err. %	Max. rel. err. %
701	Fluoromethane	C	−55.90	53.25	40.4618	1.55846	4.52688	−5.74336	0.24	0.240
		J	−233.89	222.80	169.292	6.52060	18.9405	−24.0302		at 900 K
702	Difluoromethane	C	−108.24	58.94	29.4025	2.76205	−10.8355	0.18488	0.18	0.381
		J	−452.88	246.60	123.020	11.5773	−45.3358	0.77353		at 400 K
703	Trifluoromethane	C	−166.71	62.04	9.19947	4.96457	−43.8303	14.9999	0.33	0.661
		J	−697.51	259.58	38.4904	20.7717	−183.386	62.7593		at 500 K
704	Carbon tetrafluoride	C	−223.00	62.50	19.5162	5.68660	−52.8349	17.9365	0.07	0.141
		J	−933.03	261.50	81.6554	23.7927	−221.061	75.0464		at 700 K
705	Fluoroethane	C	−62.50	63.32	11.0978	5.06102	−24.9140	4.15875	0.12	0.362
		J	−261.50	264.51	46.4332	21.1753	−104.240	17.4002		at 400 K
706	1,1-Difluoro-ethane	C	−118.00	67.52	12.9397	6.17654	−42.6513	12.1713	0.15	0.451
		J	−493.71	282.50	54.1394	25.8426	−178.453	50.9248		at 700 K
707	1,1,1-Trifluoro-ethane	C	−178.20	68.66	13.6960	7.50280	−62.0435	20.1072	0.04	0.067
		J	−745.59	287.27	57.3038	31.3916	−259.590	84.1282		at 900 K
708	Hexafluoroethane	C	−321.00	79.73	34.1448	10.0138	−98.2938	34.5525	0.09	0.154
		J	−1343.06	332.08	142.861	41.8978	−411.261	144.567		at 900 K
709	1-Fluoropropane	C	−67.20	72.71	17.7695	6.94365	−32.3577	4.48312	0.14	0.452
		J	−281.16	304.22	74.3475	29.0522	−135.385	18.7699		at 400 K
710	2-Fluoropropane	C	−69.00	69.82	−3.89897	7.98402	−46.2837	10.3619	0.11	0.339
		J	−288.70	292.13	−16.3133	33.4051	−193.651	43.3543		at 400 K
711	Octafluorocyclo-butane	C	−365.20	95.69	21.6050	15.8904	−153.745	54.2171	0.11	0.293
		J	−1528.00	400.37	90.3948	66.4854	−643.268	226.845		at 500 K

Table I. (1. cont.)

No.	Compound		ΔH_f° 298 K	S° 298 K	$a \cdot 10$	$b \cdot 10^2$	$c \cdot 10^6$	$d \cdot 10^9$	Av. err. %	Max. rel. err. %
712	1,1-Difluoro-ethylene	C	−82.50	63.38	7.78281	5.81931	−49.8528	16.6371	0.09	0.131
		J	−345.18	265.18	32.5632	24.3480	−208.584	69.6093		at 300 K
713	Trifluoroethylene	C	−118.50	69.94	39.5965	5.47749	−46.6213	15.1265	0.04	0.060
		J	−495.80	292.63	165.671	22.9178	−195.063	63.2893		at 400 K
714	Tetrafluoro-ethylene	C	−157.40	71.69	69.0914	5.44769	−48.7591	16.2463	0.06	0.145
		J	−658.56	299.95	289.078	22.7931	−204.008	76.9743		at 400 K
715	Fluorobenzene	C	−27.86	72.33	−91.7233	13.5038	−105.424	32.1433	0.05	0.141
		J	−116.57	302.63	−383.770	56.4999	−441.095	134.488		at 400 K
716	m-Difluoro-benzene	C	−74.09	76.57	−63.8750	13.6615	−110.911	34.6320	0.04	0.076
		J	−309.99	320.37	−267.253	57.1598	−464.051	144.900		at 700 K
717	o-Difluorobenzene	C	−70.39	76.94	−58.5159	13.3627	−105.668	32.6198	0.03	0.071
		J	−294.51	321.92	−244.831	55.9095	−442.114	136.481		at 500 K
718	p-Difluorobenzene	C	−73.43	75.43	−61.7201	13.6544	−111.511	35.1409	0.03	0.065
		J	−307.23	315.60	−258.237	57.1299	−466.562	147.029		at 500 K
719	Hexafluorobenzene	C	−228.64	91.59	86.3911	12.5954	−108.795	34.8520	0.04	0.082
		J	−956.63	383.21	361.460	52.6990	−455.197	145.821		at 400 K
720	α, α, α-Trifluoro-toluene	C	−143.42	89.05	−96.5126	17.4773	−139.927	43.2606	0.05	0.119
		J	−600.07	372.59	−403.809	73.1248	−585.454	181.002		at 400 K
721	p-Fluorotoluene	C	−35.38	81.15	−80.2709	14.8859	−105.648	29.6467	0.06	0.220
		J	−148.03	339.53	−335.853	62.2827	−442.030	124.042		at 400 K
722	Chloromethane	C	−20.63	56.04	32.8153	2.44468	−9.69892	0.82007	0.11	0.354
		J	−86.32	234.47	137.299	10.2285	−40.5803	3.43118		at 400 K
723	Dichloromethane	C	−22.80	64.59	28.3856	4.11642	−35.6563	12.4875	0.54	1.229
		J	−95.40	270.24	118.765	17.2231	−149.186	52.2478		at 500 K
724	Chloroform	C	−24.20	70.66	57.3149	4.52075	−43.9598	15.8973	0.09	0.178
		J	−101.25	295.64	239 805	18.9148	−183.928	66.5143		at 400 K
725	Carbon tetrachloride	C	−24.00	74.12	97.2297	4.89180	−54.2024	21.1128	0.15	0.323
		J	−100.42	310.12	406.808	20.4673	−226.783	88.3358		at 400 K
726	Chloroethane	C	−26.70	65.93	8.99416	5.69633	−35.3404	8.95101	0.07	0,232
		J	−111.71	275.85	37.6316	23.8334	−147.864	37.4510		at 400 K
727	1,1-Dichloroethane	C	−31.05	72.89	29.7873	6.43770	−48.9499	15.0472	0.03	0.049
		J	−129.91	304.97	124.630	26.9353	−204.803	62.9576		at 400 K
728	1,2-Dichloroethane	C	−31.00	73.66	62.7788	5.17082	−34.7157	9.73220	0.12	0.327
		J	−129.70	308.19	262.666	21.6347	−145.250	40.7194		at 298 K
729	1,1,2-Trichloro-ethane	C	−33.10	80.57	44.2199	7.39755	−65.1156	22.1554	0.06	0.094
		J	−138.49	337.10	185.0158	30.9513	−272.444	92.6981		at 900 K
730	1,1,2,2-Tetra-chloroethane	C	−36.50	86.69	66.0162	7.76878	−71.0736	24.5654	0.06	0.111
		J	−152.72	362.71	276.211	32.5045	−297.372	102.782		at 900 K
731	Pentachloroethane	C	−34.00	90.95	104.268	8.09057	−80.6001	29.1697	0.07	0.129
		J	−142.26	380.53	436.256	33.8509	−337.231	122.046		at 500 K
732	Hexachloroethane	C	−33.80	94.77	146.253	8.50508	−93.4743	35.9598	0.15	0.330
		J	−141.42	396.52	611.923	35.5852	−391.096	150.456		at 400 K
733	1-Chloropropane	C	−31.10	76.20	0.28311	8.23190	−52.9932	14.2338	0.03	0.110
		J	−130.12	318.82	1.18452	34.4423	−221.724	59.5540		at 400 K
734	2-Chloropropane	C	−35.00	72.70	3.15597	8.37577	−54.0667	14.1414	0.09	0.319
		J	−146.44	304.18	13.2046	35.0442	−226.215	59.1675		at 400 K
735	1,2-Dichloro-propane	C	−39.60	84.80	24.7773	8.73757	−62.3097	18.5407	0.06	0.157
		J	−165.69	354.80	103.668	36.5579	−260.704	77.5740		at 400 K
736	1,3-Dichloro-propane	C	−38.60	87.76	42.5054	8.06204	−54.8370	15.4760	0.05	0.104
		J	−161.50	367.19	177.842	33.7315	−229.438	64.7513		at 500 K

Table I. (2. cont.)

No.	Compound		ΔH_f° 298 K	S° 298 K	$a \cdot 10$	$b \cdot 10^2$	$c \cdot 10^6$	$d \cdot 10^9$	Av. err. %	Max. rel. err. %
737	2,2-Dichloro-propane	C	−42.00	77.92	25.6438	9.79145	−80.5031	26.6027	0.05	0.083
		J	−175.73	326.02	107.293	40.9674	−336.825	111.306		at 500 K
738	1,2,3-Trichloro-propane	C	−44.40	91.52	64.1998	8.64914	−66.5441	20.9856	0.06	0.104
		J	−185.77	382.92	268.611	36.1879	−278.421	87.8036		at 500 K
739	1-Chlorobutane	C	−35.20	85.58	−2.11013	10.5126	−66.1682	17.1675	0.05	0.158
		J	−147.28	358.07	−8.82879	43.9847	−276.847	71.8288		at 400 K
740	Chlorobutane	C	−38.60	85.94	−0.40281	10.4934	−64.8301	16.5223	0.09	0.300
		J	−161.50	359.57	−1.68537	43.9043	−271.249	69.1295		at 400 K
741	1-Chloro-2-methylpropane	C	−38.10	84.56	−0.40281	10.4934	−64.8301	16.5223	0.09	0.300
		J	−159.41	353.80	−1.68537	43.9043	−271.249	69.1295		at 400 K
742	2-Chloro-2-methylpropane	C	−43.80	77.00	1.26241	11.2880	−80.1812	24.2105	0.08	0.134
		J	−183.26	322.17	5.28191	47.2289	−335.478	101.297		at 500 K
743	1-Chloropentane	C	−41.80	94.89	−4.50339	12.7933	−79.3432	20.1013	0.05	0.189
		J	−174.89	397.02	−18.8422	53.5272	−331.972	84.1037		at 400 K
744	1-Chloro-3-methylbutane	C	−43.10	95.56	−5.94292	13.3651	−89.1059	24.7528	0.08	0.232
		J	−180.33	399.82	−24.8652	55.9197	−372.819	103.566		at 400 K
745	2-Chloro-2-methylbutane	C	−48.40	88.06	−25.9002	13.9346	−92.1343	24.5029	0.16	0.438
		J	−202.51	368.44	−108.366	58.3023	−385.490	102.520		at 400 K
746	Chloroethylene	C	8.40	63.08	14.2107	4.82204	−36.6808	11.3950	0.04	0.082
		J	35.15	263.93	59.4575	20.1754	−153.472	47.6768		at 500 K
747	1,1-Dichloro-ethylene	C	0.30	68.85	35.3759	5.53156	−50.2098	17.6675	0.10	0.208
		J	1.26	288.07	148.013	23.1441	−210.078	73.9206		at 400 K
748	1,2-Dichloro-ethylene, cis	C	0.45	69.20	27.3389	5.6513	−50.4024	17.4122	0.07	0.113
		J	1.88	289.53	114.386	23.6401	−210.884	72.8525		at 400 K
749	1,2-Dichloro-ethylene, trans	C	1.00	69.29	43.4243	5.02632	−42.2929	13.9360	0.03	0.073
		J	4.18	289.91	181.687	21.0301	−176.953	58.3081		at 900 K
750	Trichloroethylene	C	−1.40	77.63	70.4336	5.46372	−52.0644	18.5548	0.09	0.205
		J	−5.86	324.80	294.694	22.8602	−217.837	77.6334		at 400 K
751	Tetrachloro-ethylene	C	−3.40	81.46	109.956	5.37880	−54.6679	19.9793	0.11	0.229
		J	−14.23	340.83	460.055	22.5049	−228.731	83.5934		at 400 K
752	3-Chloro-1-propene	C	−0.15	73.29	15.5932	6.79160	−46.6596	13.4936	0.03	0.068
		J	−0.63	306.65	65.2421	28.4161	−195.224	56.4572		at 900 K
753	Chlorobenzene	C	12.39	74.92	−74.1263	13.1307	−102.865	31.4567	0.06	0.147
		J	51.84	313.47	−310.144	54.9390	−430.386	131.615		at 400 K
754	o-Dichlorobenzene	C	7.16	81.61	−34.1551	13.1549	−107.839	34.1363	0.03	0.060
		J	29.96	341.46	−142.905	55.0402	−451.199	142,826		at 500 K
755	m-Dichloro-benzene	C	6.32	82.09	−32.4643	13.1181	−107.578	34.0768	0.04	0.078
		J	26.44	343.46	−135.831	54.8860	−450.107	142.577		at 500 K
756	p-Dichlorobenzene	C	5.50	80.47	−34.2623	13.2197	−108.874	34.5773	0.03	0.061
		J	23.01	336.69	−143.3533	55.3111	−455.531	144.671		at 500 K
757	Hexachloro-benzene	C	−8.10	105.45	130.031	12.9950	−123.172	42.5960	0.07	0.163
		J	−33.89	441.20	544.051	54.3711	−515.350	178.222		at 400 K
758	Acetyl chloride	C	−58.30	70.47	59.7472	4.08573	−23.5366	5.29938	0.05	0.164
		J	−243.93	294.85	249.982	17.0947	−98.4773	22.1726		at 400 K
759	Bromomethane	C	−9.00	58.75	34.4592	2.60621	−12.9015	2.38893	0.07	0.246
		J	−37.66	245.81	144.177	10.9044	−53.9797	9.99527		at 400 K
760	Bromoethane	C	−15.30	68.71	15.8969	5.60794	−35.1707	9.08486	0.09	0.240
		J	−64.02	287.48	66.5125	23.4636	−147.154	38.0110		at 400 K
761	1,2-Dibromo-ethane	C	−9.30	78.81	61.0916	5.94983	−42.8776	13.0744	0.09	0.230
		J	−38.91	329.74	255.607	24.8941	−179.400	54.7033		at 400 K

Table I. (3. cont.)

No.	Compound		ΔH_f° 298 K	S° 298 K	$a \cdot 10$	$b \cdot 10^2$	$c \cdot 10^6$	$d \cdot 10^9$	Av. err. %	Max. rel. err. %
762	1-Bromopropane	C	−21.00	79.08	7.83709	8.07521	−51.4658	13.6377	0.06	0.105
		J	−87.86	330.87	32.7904	33.7867	−215.333	57.0602		at 298 K
763	2-Bromopropane	C	−23.20	75.53	7.36662	8.38822	−55.2212	14.8531	0.09	0.245
		J	−97.07	316.02	30.8220	35.0963	−231.045	62.1455		at 400 K
764	1,2-Dibromo-propane	C	−17.40	89.90	31.5415	8.99470	−65.9457	19.5643	0.14	0.358
		J	−72.80	376.14	131.969	37.6338	−275.917	81.8570		at 300 K
765	1-Bromobutane	C	−25.65	88.39	5.44384	10.3559	−64.6408	16.5715	0.06	0.141
		J	−107.32	369.82	22.7770	43.3291	−270.457	69.3350		at 400 K
766	2-Bromobutane	C	−28.70	88.50	−0.07602	10.7588	−68.5968	17.9228	0.10	0.329
		J	−120.08	370.28	−0.31808	45.0148	−287.009	74.9890		at 400 K
767	2-Bromo-2-methyl-propane	C	−32.00	79.34	−21.0886	12.6448	−95.9709	29.3752	0.06	0.185
		J	−133.89	331.96	−88.2347	52.9057	−401.542	122.906		at 400 K
768	1,2-Dibromo-butane	C	−23.70	97.70	41.6592	10.8303	−75.0020	21.0276	0.08	0.170
		J	−99.17	408.78	174.302	45.3139	−313.808	87.9794		at 400 K
769	2,3-Dibromo-butane	C	−24.40	94.40	14.5573	11.8093	−85.1419	24.2999	0.07	0.136
		J	−102.09	394.97	60.9079	49.4103	−356.234	101.671		at 298 K
770	2,3-Dibromo-2-methylbutane	C	−33.20	98.60	−14.2313	15.5207	−115.964	34.0417	0.13	0.416
		J	−138.91	412.54	−59.5439	64.9386	−485.193	142.431		at 400 K
771	1-Bromopentane	C	−30.87	97.70	3.05060	12.6366	−77.8158	19.5052	0.06	0.175
		J	−129.16	408.78	12.7637	52.8716	−325.581	81.6099		at 400 K
772	Bromoethylene	C	18.73	65.83	21.5809	4.69485	−35.9252	11.2837	0.03	0.047
		J	78.37	275.43	90.2946	19.6433	−150.311	47.2109		at 500 K
773	3-Bromo-1-propene	C	11.80	75.80	15.9200	7.05702	−50.4262	14.8941	0.04	0.119
		J	49.37	317.15	66.6094	29.5266	−210.983	62.3168		at 298 K
774	Bromobenzene	C	25.10	77.53	−67.6393	12.7269	−96.7009	28.5929	0.06	0.201
		J	105.02	324.39	−283.003	53.2492	−404.596	119.633		at 400 K
775	Iodomethane	C	3.34	60.71	35.6318	2.79720	−16.5183	4.18004	0.04	0.134
		J	13.97	254.01	149.084	11.7035	−69.1126	17.4893		at 400 K
776	Diiodomethane	C	28.20	73.88	52.1573	4.78441	−33.5023	11.7548	0.08	0.117
		J	117.99	309.11	218.226	15.8341	−140.174	49.1822		at 700 K
777	Triiodomethane	C	50.40	85.00	99.3206	3.66242	−37.1390	13.9420	0.10	0.196
		J	210.87	355.64	415.557	15.3235	−155.390	58.3334		at 400 K
778	Iodoethane	C	−2.00	70.82	24.7596	5.35305	−32.6132	8.25378	0.03	0.095
		J	−8.37	296.31	103.594	22.3972	−136.453	34.5338		at 400 K
779	1,2-Diiodoethane	C	15.90	83.30	61.9069	5.61342	−40.2204	11.7395	0.05	0.116
		J	66.53	348.53	259.019	23.4866	−168.282	49.1170		at 500 K
780	1-Iodopropane	C	−7.30	80.32	28.8304	7.43082	−43.2015	10.0308	0.07	0.251
		J	−30.54	336.06	120.626	31.0906	−180.755	41.9687		at 400 K
781	2-Iodopropane	C	−10.00	77.55	11.6745	8.33443	−55.1031	14.9258	0.06	0.202
		J	−41.84	324.47	48.8461	34.8712	−230.551	62.4497		at 400 K
782	1,2-Diiodopropane	C	8.60	94.60	39.9343	8.65342	−61.9715	18.1561	0.04	0.097
		J	35.98	395.81	167.085	36.2059	−259.289	75.9652		at 500 K
783	2-Iodo-2-methyl-propane	C	−17.60	81.79	−12.6736	12.4545	−94.1225	28.7639	0.07	0.175
		J	−73.64	342.21	−53.0264	52.1095	−393.809	120.348		at 400 K
784	1,2-Diidobutane	C	2.85	101.80	55.2548	10.2662	−68.0983	18.4151	0.06	0.171
		J	11.92	425.93	231.186	42.9537	−284.923	77.0488		at 400 K
785	3-Iodo-1-propene	C	22.90	76.46	25.6768	7.25380	−54.9574	17.0669	0.07	0.214
		J	95.81	319.91	107.432	30.3499	−229.942	71.4079		at 700 K
786	Iodobenzene	C	38.85	79.84	−59.1881	12.7438	−98.9369	30.0247	0.06	0.155
		J	162.55	334.05	−247.643	53.3202	−413.952	125.624		at 400 K

Table I. (cont.)

ORGANIC SULFUR COMPOUNDS

No.	Compound		ΔH_f° 298 K	S° 298 K	$a \cdot 10$	$b \cdot 10^2$	$c \cdot 10^6$	$d \cdot 10^9$	Av. err. %	Max. rel. err. %
800	Methyl sulfide	C	−8.97	68.32	54.3197	4.67884	−19.7073	2.64836	0.06	0.206
		J	−37.53	285.85	227.273	19.5763	−82.4553	11.0808		at 400 K
801	Ethyl methyl sulfide	C	−14.25	79.62	38.9456	7.31702	−35.6300	6.49051	0.07	0.241
		J	−59.62	333.13	162.948	30.6144	149.076	27.1563		at 400 K
802	Ethyl sulfide	C	−19.95	87.96	34.7078	9.43872	−43.3958	7.30327	0.09	0.287
		J	−83.47	368.02	145.217	39.4916	−181.568	30.5569		at 400 K
803	Isopropyl methyl sulfide	C	−21.61	85.87	32.5837	9.67742	−50.0188	12.2840	0.07	0.176
		J	−90.42	359.28	136.329	40.4903	−209.279	51.3965		at 400 K
804	Methyl propyl sulfide	C	−19.54	88.84	38.2843	9.36640	−44.1946	7.82698	0.07	0.241
		J	−81.76	371.71	160.182	39.1890	−184.910	32.7481		at 400 K
805	Butyl methyl sulfide	C	−24.42	98.43	44.2465	11.1682	−48.3067	7.26253	0.07	0.247
		J	−102.17	411.83	185.127	46.7277	−202.115	30.3864		at 400 K
806	Ethyl propyl sulfide	C	−25.00	98.97	37.5699	11.2405	−47.5080	6.73882	0.09	0.287
		J	−104.60	414.09	157.193	47.0303	−198.773	28.1952		at 400 K
807	Butyl ethyl sulfide	C	−29.92	108.27	34.3465	13.5641	−61.4125	10.0554	0.09	0.286
		J	−125.19	453.00	143.706	56.7523	−256.950	42.0718		at 400 K
808	Isopropyl sulfide	C	−33.76	99.30	−12.0193	17.3336	−123.815	36.9295	0.04	0.090
		J	−141.25	415.47	−50.2888	72.5238	−518.041	154.513		at 400 K
809	Methyl pentyl sulfide	C	−29.34	107.73	41.0230	13.4918	−62.2113	10.5791	0.08	0.252
		J	−122.76	450.74	171.640	56.4498	−260.292	44.2630		at 400 K
810	Propyl sulfide	C	−29.96	107.16	38.2280	13.1612	−53.4486	7.02146	0.10	0.321
		J	−125.35	448.36	159.946	55.0665	−223.629	29.3778		at 400 K
811	Butyl propyl sulfide	C	−34.88	117.90	37.2086	15.3659	−65.5247	9.49096	0.09	0.286
		J	−145.94	493.29	155.681	64.2911	−274.155	39.7102		at 400 K
812	Ethyl pentyl sulfide	C	−34.85	117.58	31.9532	15.8448	−74.5875	12.9892	0.09	0.292
		J	−145.81	491.95	133.692	66.2948	−312.074	54.3467		at 400 K
813	Hexyl methyl sulfide	C	−34.27	117.04	38.6298	15.7725	−75.3862	13.5129	0.08	0.262
		J	−143.39	489.70	161.627	65.9922	−315.416	56.5379		at 400 K
814	Butyl sulfide	C	−39.99	125.84	34.8154	17.6466	−78.6996	12.4247	0.09	0.291
		J	−167.32	526.51	145.667	73.8335	−329.279	51.9850		at 400 K
815	Ethyl hexyl sulfide	C	−39.77	126.89	28.7298	18.1685	−88.4920	16.3058	0.09	0.291
		J	−166.40	530.91	120.205	76.0168	−370.251	68.2233		at 400 K
816	Heptyl methyl sulfide	C	−39.19	126.35	35.4063	18.0961	−89.2912	16.8295	0.08	0.264
		J	−163.97	528.65	148.140	75.7142	−373.594	70.4145		at 400 K
817	Pentyl propyl sulfide	C	−39.81	127.21	34.8154	17.6466	−78.6993	12.4247	0.09	0.291
		J	−166.57	532.25	145.668	73.8334	−329.278	51.9849		at 400 K
818	Butyl pentyl sulfide	C	−44.92	136.52	31.5919	19.9703	−92.6042	15.7413	0.09	0.290
		J	−187.95	571.20	132.181	83.5555	−387.456	65.8616		at 400 K
819	Ethyl heptyl sulfide	C	−44.70	136.20	26.0912	20.4644	−101.956	19.4099	0.09	0.297
		J	−187.02	569.86	109.166	85.6229	−426.584	81.2110		at 400 K
820	Hexyl propyl sulfide	C	−44.73	136.52	31.5919	19.9703	−92.6042	15.7413	0.09	0.290
		J	−187.15	571.20	132.181	83.5555	−387.456	65.8616		at 400 K
821	Methyl octyl sulfide	C	−44.12	135.66	32.7678	20.3921	−102.755	19.9336	0.08	0.273
		J	−184.60	567.60	137.101	85.3204	−429.926	83.4022		at 400 K
822	Butyl hexyl sulfide	C	−49.84	145.83	28.9534	22.2662	−106.068	18.8454	0.09	0.296
		J	−208.53	610.15	121.141	93.1617	−443.790	78.8493		at 400 K

Table I. (1. cont.)

No.	Compound		ΔH_f° 298 K	S° 298 K	$a \cdot 10$	$b \cdot 10^2$	$c \cdot 10^6$	$d \cdot 10^9$	Av. err. %	Max. rel. err. %
823	Ethyl octyl sulfide	C	−49.63	145.51	22.9012	22.7866	−115.789	22.6661	0.09	0.303
		J	−207.65	608.81	95.8187	95.3393	−484.461	94.8349		at 400 K
824	Heptyl propyl sulfide	C	−49.66	145.83	28.9534	22,2661	−106.068	18.8454	0.09	0.295
		J	−207.78	610.15	121.141	93.1613	−443.788	78.8491		at 400 K
825	Methyl nonyl sulfide	C	−49.05	144.97	29.5778	22.7143	−116.587	23.1897	0.08	0.281
		J	−205.23	606.55	123.753	95.0363	−487.801	97.0257		at 400 K
826	Pentyl sulfide	C	−49.84	144.45	28.9534	22.2661	−106.068	18.8454	0.09	0.295
		J	−208.53	604.38	121.141	93.1613	−443.788	78.8491		at 400 K
827	Butyl heptyl sulfide	C	−54.77	155.14	25.7634	24.5884	−119.901	22.1016	0.09	0.301
		J	−229.16	649.11	107.794	102.878	−501.664	92.4729		at 400 K
828	Decyl methyl sulfide	C	−53.97	154.28	26.9406	25.0071	−129.984	26.2472	0.08	0.281
		J	−225.81	645.51	112.719	104.629	−543.854	109.818		at 400 K
829	Ethyl nonyl sulfide	C	−54.55	154.82	20.2640	25.0794	−129.185	25.7235	0.09	0.301
		J	−228.24	647.77	84.7843	104.932	−540.512	107.627		at 400 K
830	Octyl propyl sulfide	C	−54.56	155.14	25.7634	24.5884	−119.901	22.1016	0.09	0.301
		J	−228.28	649.11	107.794	102.878	−501.664	92.4729		at 400 K
831	Butyl octyl sulfide	C	−59.69	164.45	23.1262	26.8812	−133.298	25.1590	0.09	0.300
		J	−249.74	688.06	96.7595	112.471	−557.717	105.265		at 400 K
832	Decyl ethyl sulfide	C	−59.84	164.13	17.0393	27.4061	−143.157	29.0867	0.09	0.304
		J	−250.37	686.72	71.2921	114.667	−598.969	121.699		at 400 K
833	Hexyl sulfide	C	−59.69	163.07	23.1262	26.8812	−133.298	25.1590	0.09	0.300
		J	−249.74	682.28	96.7595	112.471	−557.717	105.265		at 400 K
834	Methyl undecyl sulfide	C	−58.90	163.59	23.7159	27.3338	−143.956	29.6104	0.09	0.286
		J	−246.44	684.46	99.2268	114.364	−602.311	123.890		at 400 K
835	Nonyl propyl sulfide	C	−59.51	164.45	23.1262	26.8812	−133.298	25.1590	0.09	0.300
		J	−248.99	688.06	96.7595	112.471	−557.717	105.265		at 400 K
836	Butyl nonyl sulfide	C	−64.62	173.76	19.9015	29.2079	−147.269	28.5223	0.09	0.300
		J	−270.37	727.01	83.2673	122.206	−616.174	119.337		at 400 K
837	Decyl propyl sulfide	C	−64.44	173.76	19.9015	29.2079	−147.269	28.5223	0.09	0.303
		J	−269.62	727.01	83.2673	122.206	−616.174	119.337		at 400 K
838	Dodecyl methyl sulfide	C	−63.82	172.90	22.2372	29.5616	−156.311	32.1585	0.08	0.275
		J	−267.02	723.41	93.0401	123.685	−654.003	134.551		at 400 K
839	Ethyl undecyl sulfide	C	−64.40	173.44	14.4021	29.6989	−156.554	32.1442	0.09	0.303
		J	−269.45	725.67	60.2579	124.260	−655.022	134.491		at 400 K
840	Butyl decyl sulfide	C	−69.55	183.07	17.2642	31.5007	−160.666	31.5797	0.09	0.302
		J	−291.00	765.96	72.2331	131.799	−672.227	132.129		at 400 K
841	Dodecyl ethyl sulfide	C	−69.33	182.75	11.4226	32.0104	−170.237	35.3371	0.09	0.305
		J	−290.08	764.63	47.7920	133.931	−712.269	147.850		at 400 K
842	Heptyl sulfide	C	−69.54	181.69	15.7926	31.5920	−162.401	32.6020	0.09	0.307
		J	−290.96	760.19	66.0759	132.181	−679.485	136.407		at 400 K
843	Methyl tridecyl sulfide	C	−68.75	182.21	18.0992	31.9381	−171.035	35.8608	0.09	0.289
		J	−287.65	762.37	75.7267	133.629	−715.611	150.041		at 400 K
844	Propyl undecyl sulfide	C	−69.36	183.07	17.2642	31.5007	−160.666	31.5797	0.09	0.302
		J	−290.20	765.96	72.2331	131.799	−672.227	132.129		at 400 K
845	Butyl undecyl sulfide	C	−74.47	192.38	14.2848	33.8122	−174.349	34.7726	0.09	0.304
		J	−311.58	804.92	59.7671	141.470	−729.474	145.488		at 400 K
846	Dodecyl propyl sulfide	C	−74.29	192.38	14.2848	33.8122	−174.349	34.7726	0.09	0.304
		J	−310.83	804.92	59.7671	141.470	−729.474	145.488		at 400 K

Table I. (2. cont.)

No.	Compound		ΔH_f° 298 K	S° 298 K	$a \cdot 10$	$b \cdot 10^2$	$c \cdot 10^6$	$d \cdot 10^9$	Av. err. %	Max. rel. err. %
847	Ethyl tridecyl sulfide	C	−74.26	192.06	8.29914	34.3341	−184.141	38.6537	0.09	0.304
		J	−310.71	803.58	34.7235	143.653	−770.446	161.727		at 400 K
848	Methyl tetradecyl sulfide	C	−73.68	191.52	14.9757	34.2617	−184.940	39.1774	0.09	0.288
		J	−308.28	801.32	62.6582	143.351	−773.788	163.918		at 400 K
849	Butyl dodecyl sulfide	C	−79.40	201.69	11.1613	36.1359	−188.253	38.0892	0.09	0.302
		J	−332.21	843.87	46.6987	151.192	−787.651	159.365		at 400 K
850	Ethyl tetradecyl sulfide	C	−79.18	201.36	5.07568	36.6577	−198.046	41.9703	0.09	0.302
		J	−331.29	842.49	21.2366	153.375	−828.623	175.603		at 400 K
851	Methyl pentadecyl sulfide	C	−78.60	200.82	11.7523	36.5854	−198.845	42.4940	0.09	0.288
		J	−328.86	840.23	49.1713	153.073	−831.964	177.794		at 400 K
852	Octyl sulfide	C	−79.39	200.31	11.1613	36.1359	−188.253	38.0892	0.09	0.302
		J	−332.17	838.10	46.6987	151.192	−787.651	159.365		at 400 K
853	Propyl tridecyl sulfide	C	−79.22	201.69	11.1613	36.1359	−188.253	38.0892	0.09	0.302
		J	−331.46	843.87	46.6987	151.192	−787.651	159.365		at 400 K
854	Butyl tridecyl sulfide	C	−84.32	210.99	7.93783	38.4595	−202.158	41.4058	0.09	0.301
		J	−352.79	882.78	33.2118	160.914	−845.827	173.241		at 400 K
855	Ethyl pentadecyl sulfide	C	−84.11	210.67	2.68242	38.9384	−211.221	44.9041	0.09	0.304
		J	−351.92	881.44	11.2232	162.918	−883.748	187.878		at 400 K
856	Hexadecyl methyl sulfide	C	−83.53	210.13	9.35898	38.8661	−212.020	45.4280	0.09	0.291
		J	−349.49	879.18	39.1580	162.616	−887.092	190.071		at 400 K
857	Propyl tetradecyl sulfide	C	−84.14	210.99	7.93783	38.4595	−202.158	41.4058	0.09	0.301
		J	−352.04	882.78	33.2118	160.914	−845.827	173.241		at 400 K
858	Butyl tetradecyl sulfide	C	−89.25	220.30	5.54458	40.7402	−215.333	44.3396	0.09	0.303
		J	−373.42	921.74	23.1985	170.456	−900.951	185.516		at 400 K
859	Ethyl hexadecyl sulfide	C	−89.03	219.98	−0.54104	41.2620	−225.126	48.2207	0.09	0.303
		J	−372.50	920.40	−2.26372	172.640	−941.926	201.755		at 400 K
860	Heptadecyl methyl sulfide	C	−88.45	219.44	6.13553	41.1897	−225.925	48.7446	0.09	0.290
		J	−370.07	918.14	25.6711	172.338	−945.268	203.947		at 400 K
861	Nonyl sulfide	C	−89.25	218.92	5.54455	40.7402	−215.333	44.3398	0.09	0.303
		J	−373.42	915.96	23.1984	170.457	−900.955	185.518		at 400 K
862	Pentadecyl propyl sulfide	C	−89.07	220.30	5.54455	40.7402	−215.333	44.3398	0.09	0.303
		J	−372.67	921.74	23.1984	170.457	−900.955	185.518		at 400 K
863	Butyl pentadecyl sulfide	C	−94.18	229.61	−39.7951	45.2155	−259.299	60.3121	0.29	0.843
		J	−394.05	960.69	−166.503	189.181	−1084.91	252.345		at 600 K
864	Ethyl heptadecyl sulfide	C	−93.96	229.29	−3.17955	43.5580	−238.590	51.3248	0.09	0.305
		J	−393.13	959.35	−13.3032	182.246	−998.259	214.743		at 400 K
865	Hexadecyl propyl sulfide	C	−93.99	229.61	2.32110	43.0638	−229.238	47.6564	0.09	0.302
		J	−393.25	960.69	9.71149	180.179	−959.131	199.394		at 400 K
866	Methyl octadecyl sulfide	C	−93.38	228.75	3.49701	43.4856	−239.389	51.8487	0.09	0.293
		J	−390.70	957.09	14.6315	181.944	−1001.60	216.935		at 400 K
867	Butyl hexadecyl sulfide	C	−99.10	238.92	−0.31741	45.3598	−242.702	50.7606	0.09	0.304
		J	−414.63	999.64	−1.32806	189.785	−1015.47	212.382		at 400 K
868	Decyl sulfide	C	−99.10	237.54	−0.31741	45.3598	−242.702	50.7606	0.09	0.304
		J	−414.63	993.87	−1.32806	189.785	−1015.47	212.382		at 400 K
869	Ethyl octadecyl sulfide	C	−98.89	238.60	−6.36962	45.8802	−252.424	54.5810	0.09	0.308
		J	−413.76	998.30	−26.6505	191.963	−1056.14	228.367		at 400 K
870	Heptadecyl propyl sulfide	C	−98.92	238.92	−0.31741	45.3598	−242.702	50.7604	0.09	0.304
		J	−413.88	999.64	−1.32806	189.785	−1015.47	212.382		at 400 K

Table I. (3. cont.)

No.	Compound		ΔH_f° 298 K	S° 298 K	$a \cdot 10$	$b \cdot 10^2$	$c \cdot 10^6$	$d \cdot 10^9$	Av. err. %	Max. rel. err. %
871	Methyl nonadecyl sulfide	C	−98.31	238.06	0.30698	45.8079	−253.221	55.1047	0.09	0.296
		J	−411.33	996.04	1.28440	191.660	−1059.48	230.558		at 400 K
872	Methyl disulfide	C	−5.77	80.46	83.5808	5.50682	−26.6308	4.49777	0.07	0.198
		J	−24.14	336.64	349.702	23.0405	−111.423	18.8187		at 700 K
873	Ethyl disulfide	C	−17.84	99.07	53.8044	11.5500	−73.7162	18.7899	0.07	0.215
		J	−74.64	414.51	225.118	48.3250	−308.428	78.6168		at 400 K
874	Propyl disulfide	C	−28.01	118.30	54.3904	15.4122	−85.7186	19.3354	0.07	0.202
		J	−117.19	494.97	227.569	64.4847	−358.647	80.8993		at 400 K
875	Butyl disulfide	C	−37.86	136.91	48.7737	20.0165	−112.798	25.5858	0.07	0.224
		J	−158.41	572.83	204.069	83.7492	−471.947	107.051		at 400 K
876	Pentyl disulfide	C	−47.71	155.53	42.9118	24.6360	−140.166	32.0064	0.08	0.239
		J	−199.62	650.74	179.543	103.077	−586.455	133.915		at 400 K
877	Hexyl disulfide	C	−57.56	174.15	37.0845	29.2511	−167.396	38.3200	0.08	0.251
		J	−240.83	728.64	155.162	122.387	−700.384	160.331		at 400 K
878	Heptyl disulfide	C	−67.41	192.77	31.2226	33.8706	−194.764	44.7407	0.08	0.259
		J	−282.04	806.55	130.635	141.715	−814.894	187.195		at 400 K
879	Octyl disulfide	C	−77.27	211.39	25.1197	38.5057	−222.351	51.2502	0.08	0.264
		J	−323.30	884.46	105.101	161.108	−930.318	214.431		at 400 K
880	Nonyl disulfide	C	−87.12	230.00	19.5029	43.1101	−249.432	57.5007	0.08	0.269
		J	−364.51	962.32	−81.6003	180.373	−1043.62	240.583		at 400 K
881	Decyl disulfide	C	−96.97	248.62	13.6410	47.7297	−276.800	63.9214	0.08	0.273
		J	−405.72	1040.23	57.0738	199.701	−1158.13	267.447		at 400 K
882	Thiacyclopropane	C	−19.65	61.01	−28.4667	6.65125	−51.5224	16.0774	0.06	0.109
		J	−82.22	255.27	−119.105	27.8288	−215.570	67.2679		at 500 K
883	Thiacyclobutane	C	14.61	68.17	−46.6570	8.60408	−53.8486	13.1260	0.12	0.386
		J	61.13	285.22	−195.213	35.9995	−225.303	54.9193		at 400 K
884	Thiacyclopentane	C	−8.08	73.94	−79.4323	12.3147	−86.8658	24.7955	0.05	0.107
		J	−33.81	309.36	−332.345	51.5248	−363.446	103.745		at 298 K
885	Thiacyclohexane	C	−15.12	77.26	−124.354	15.1059	−80.9204	14.5664	0.23	0.732
		J	−63.26	323.26	−520.298	63.2033	−338.571	60.9459		at 400 K
886	Thiacycloheptane	C	−14.66	86.50	−168.546	17.3952	−57.6233	−11.7768	0.74	0.764
		J	−61.34	361.92	−705.195	72.7815	−241.096	−49.2743		at 298 K
887	Thiophene	C	27.66	66.65	−71.0359	10.6014	−88.3326	28.9751	0.05	0.102
		J	115.73	278.86	−297.214	44.3562	−369.584	121.232		at 500 K
888	2-Methylthiophene	C	20.00	76.62	−45.6756	11.3896	−81.1596	23.1272	0.05	0.188
		J	83.68	320.58	−191.107	47.6539	−339.572	96.7642		at 400 K
889	3-Methylthiophene	C	19.79	76.79	−55.2854	11.9006	−90.0250	27.1458	0.05	0.093
		J	82.80	321.29	−231.314	49.7922	−376.665	113.578		at 400 K
890	Methanethiol	C	−5.49	60.96	47.0575	2.77850	−11.5313	1.51163	0.07	0.224
		J	−22.97	255.06	196.888	11.6253	−48.2470	6.32465		at 400 K
891	Ethanethiol	C	−11.02	70.77	33.7507	5.52522	−29.9366	6.68050	0.05	0.159
		J	−46.11	296.10	141.213	23.1175	−125.255	27.9512		at 400 K
892	1-Propanethiol	C	−16.22	80.40	36.6129	7.32701	−34.0487	6.11605	0.06	0.190
		J	−67.86	336.39	153.188	30.6562	−142.460	25.5896		at 400 K
893	2-Propanethiol	C	−18.22	77.51	15.8720	8.65177	−54.3025	14.1078	0.06	0.207
		J	−76.23	324.30	66.4085	36.1990	−227.201	59.0268		at 400 K
894	1-Butanethiol	C	−21.05	89.68	42.5750	9.12881	−38.1608	5.55161	0.06	0.206
		J	−88.07	375.22	178.134	38.1949	−159.665	23.2279		at 400 K

Table 1. (4. cont.)

No.	Compound		ΔH_f° 298 K	S° 298 K	$a \cdot 10$	$b \cdot 10^2$	$c \cdot 10^6$	$d \cdot 10^9$	Av. err. %	Max. rel. err. %
895	2-Butanethiol	C	−23.00	87.65	15.5563	10.8667	−66.1510	15.9335	0.07	0.220
		J	−96.23	366.73	65.0876	45.4662	−276.776	66.6660		at 400 K
896	2-Methyl-1-propanethiol	C	−23.24	86.73	−3.25494	11.7934	−80.4798	22.0317	0.06	0.201
		J	−97.24	362.88	−13.6187	49.3434	−336.727	92.1805		at 400 K
897	2-Methyl-2-propanethiol	C	−26.17	80.79	−1.15918	11.8434	−76.8318	19.7358	0.08	0.270
		J	−109.50	338.03	−4.85002	49.5529	−321.464	82.5746		at 400 K
898	2-Methyl-2-butanethiol	C	−30.36	92.48	8.34674	13.4673	−81.1805	18.9417	0.10	0.320
		J	−127.03	386.94	34.9228	56.3473	−339.659	79.2521		at 400 K
899	1-Pentanethiol	C	−25.91	99.28	40.3011	11.4266	−51.6485	8.65565	0.07	0.230
		J	−108.41	415.39	168.620	47.8090	−216.097	36.2152		at 400 K
900	1-Hexanethiol	C	−30.83	108.58	37.0776	13.7502	−65.5531	11.9722	0.07	0.238
		J	−128.99	454.30	155.133	57.5310	−274.274	50.0918		at 400 K
901	1-Heptanethiol	C	−35.76	117.89	34.6844	16.0309	−78.7281	14.9060	0.07	0.250
		J	−149.62	493.25	145.119	67.0735	−329.398	62.3667		at 400 K
902	1-Octanethiol	C	−40.68	127.20	31.4609	18.3546	−92.6326	18.2226	0.08	0.253
		J	−170.21	532.20	131.633	76.7955	−387.575	76.2433		at 400 K
903	1-Nonanethiol	C	−45.61	136.51	28.8224	20.6505	−106.097	21.3267	0.08	0.263
		J	−190.83	571.16	120.593	86.4016	−443.909	89.2310		at 400 K
904	1-Decanethiol	C	−50.54	145.82	25.6324	22.9727	−119.930	24.5829	0.08	0.272
		J	−211.46	610.11	107.2459	96.1179	−501.785	102.855		at 400 K
905	1-Undecanethiol	C	−55.46	155.13	22.9951	25.2656	−133.327	27.6403	0.08	0.273
		J	−232.04	649.06	96.2117	105.711	−557.838	115.647		at 400 K
906	1-Dodecanethiol	C	−60.39	164.44	19.7704	27.5923	−147.298	31.0036	0.08	0.278
		J	−252.67	688.02	82.7194	115.446	−616.296	129.719		at 400 K
907	1-Tridecanethiol	C	−65.31	173.75	17.1332	29.8851	−160.695	34.0611	0.08	0.279
		J	−273.26	726.97	71.6852	125.039	−672.348	142.512		at 400 K
908	1-Tetradecanethiol	C	−70.24	183.06	14.1537	32.1966	−174.378	37.2540	0.08	0.282
		J	−293.88	765.92	59.2192	13.4711	−729.596	155.871		at 400 K
909	1-Pentadecanethiol	C	−75.17	192.37	11.0303	34.5202	−188.282	40.5706	0.08	0.282
		J	−314.51	804.88	46.1507	144.433	−787.773	169.747		at 400 K
910	1-Hexadecanethiol	C	−80.09	201.67	7.80682	36.8438	−202.187	43.8872	0.08	0.282
		J	−335.10	843.79	32.6637	154.155	−845.950	183.624		at 400 K
911	1-Heptadecanethiol	C	−85.02	210.98	5.41357	39.1245	−215.362	46.8209	0.08	0.285
		J	−355.72	882.74	22.6504	163.697	−901.074	195.899		at 400 K
912	1-Octadecanethiol	C	−89.94	220.29	2.19012	41.4481	−229.266	50.1375	0.08	0.285
		J	−376.31	921.69	9.16348	173.419	−959.250	209.775		at 400 K
913	1-Nonadecanethiol	C	−94.87	229.60	2.78306	43.5977	−240.629	52.2770	0.09	0.297
		J	−396.94	960.65	11.6443	182.413	−1006.79	218.727		at 400 K
914	Eicosanethiol	C	−99.80	238.91	−3.63843	46.0663	−256.563	56.4978	0.09	0.292
		J	−417.56	999.60	−15.2232	192.741	−1073.46	236.387		at 400 K
915	Cyclopentanethiol	C	−11.45	86.38	−86.9286	13.9016	−84.7170	20.2109	0.10	0.354
		J	−47.91	361.41	−363.709	58.1645	−354.456	84.5624		at 400 K
916	Benzenethiol	C	26.66	80.51	−74.9482	13.7858	−105.622	32.0540	0.05	0.123
		J	111.55	336.85	−313.583	57.6799	−441.927	134.114		at 400 K
917	Isothiocyanic acid	C	30.50	59.28	35.3143	3.46105	−34.9145	13.3656	0.20	0.516
		J	127.61	248.03	147.755	14.4810	−146.082	55.9215		at 400 K
918	Thioacetic acid	C	−43.49	74.86	91.9370	3.89759	−16.7405	1.14629	0.23	0.537
		J	−181.96	313.21	384.665	16.3075	−70.0424	4.79610		at 700 K

Table I. (cont.)

FREE RADICALS

No.	Radical		ΔH_f° 298 K	S° 298 K	$a \cdot 10$	$b \cdot 10^2$	$c \cdot 10^6$	$d \cdot 10^9$	Av. err. %	Max. rel. err. %
1001	$CH_3^\bullet$	C	34.0	46.4	60.3536	0.61738	5.54378	−3.75381	0.26	0.608
		J	142.3	194.1	252.520	2.58313	23.1952	−15.7059		at 500 K
1002	$C_2H_5^\bullet$	C	25.7	59.5	−0.03838	4.67829	−29.3463	8.47246	0.13	0.301
		J	107.5	248.9	−0.16057	19.5740	−122.785	35.4488		at 400 K
1003	$n-C_3H_7^\bullet$	C	20.7	68.1	17.4997	6.24272	−33.4701	7.58098	0.19	0.366
		J	86.6	284.9	73.2189	26.1196	−140.039	31.7188		at 600 K
1004	$i-C_3H_7^\bullet$	C	17.6	67.0	36.5238	5.19485	−19.9818	2.17358	0.17	0.413
		J	73.6	280.3	152.816	21.7353	−83.6038	9.09427		at 500 K
1005	$CH_3\dot{C}HCH_2CH_3$	C	2.3	77.6	37.0702	7.27014	−27.6785	1.55819	0.14	0.265
		J	9.6	324.7	155.102	30.4183	−115.807	6.51945		at 600 K
1006	$(CH_3)_3C^\bullet$	C	8.9	72.2	0.55392	6.96961	−17.0626	−3.79718	0.37	0.870
		J	37.2	302.1	2.31760	29.1608	−71.3899	−15.8874		at 500 K
1007	$\text{Ø}^\bullet$	C	80.0	69.1	−89.1977	11.6246	−84.9627	24.3985	0.02	0.055
		J	334.7	289.1	−373.203	48.6372	−355.484	102.083		at 400 K
1008	$\text{ØCH}_2^\bullet$	C	45.0	75.4	−79.2028	13.7134	−95.7835	26.4695	0.15	0.367
		J	188.3	315.5	−331.384	57.3770	−400.758	110.748		at 400 K
1009	$\text{ØC}\dot{\text{H}}\text{CH}_3$	C	36.6	85.1	−85.9307	15.9819	−107.707	28.2797	0.12	0.260
		J	153.1	356.1	−359.534	66.8683	−450.644	118.322		at 500 K
1010	$\text{ØO}^\bullet$	C	19.5	73.7	−99.0662	13.8135	−111.034	35.1033	0.04	0.095
		J	81.6	308.4	−414.493	57.7955	−464.567	146.872		at 400 K
1011	$\text{ØS}^\bullet$	C	49.5	76.5	−70.8897	12.9128	−98.2763	28.5316	0.09	0.208
		J	207.1	320.1	−296.603	54.0270	−411.188	119.376		at 400 K
1012	$\text{ØC}(\text{CH}_3)_2^\bullet$	C	26.3	90.6	−45.7918	16.0172	−89.2669	17.3478	0.21	0.469
		J	110.0	379.1	−191.593	67.0159	−373.493	72.5833		at 400 K
1013	$CH_3S^\bullet$	C	28.0	57.6	41.1623	2.04837	−4.24743	−1.55349	0.99	2.274
		J	117.2	241.0	172.223	8.57036	−17.7712	−6.49980		at 500 K
1014	$CH_3CH_2S^\bullet$	C	22.3[a]	67.2	22.1283	4.99504	−24.2188	4.24309	0.39	1.02
		J	93.4	281.2	92.5847	20.8993	−101.332	17.7531		at 400 K
1015	$(CH_3)_2CHS^\bullet$	C	15.3	74.2	8.35534	8.04106	−49.4003	12.2476	0.29	0.694
		J	64.2	310.5	34.9587	33.6438	−206.691	51.2439		at 400 K
1016	$(CH_3)_3CS^\bullet$	C	7.3[a]	77.2	−17.7325	11.7623	−82.6916	23.4183	0.31	0.728
		J	30.4	323.0	−74.1929	49.2135	−345.981	97.9823		at 400 K
1017	$CH_3O^\bullet$	C	3.9	54.3	32.3550	2.00044	−1.17211	−3.17925	0.56	1.321
		J	16.3	227.2	135.248	8.36983	−4.90410	−13.3020		at 400 K
1018	$CH_3CH_2O^\bullet$	C	4.9	64.6	33.8226	3.69938	−1.63848	−7.54882	0.67	1.588
		J	20.5	270.3	141.514	15.4782	−6.85540	−31.5843		at 500 K
1019	$(CH_3)_2CHO^\bullet$	C	−6.69	71.1	14.5989	7.13127	−31.3451	2.56060	0.28	0.676
		J	−28.0	297.5	61.0817	29.8372	−131.148	10.7136		at 500 K
1020	$(CH_3)_3CO^\bullet$	C	−21.5	75.0	11.0459	9.54936	−45.0195	5.01243	0.36	0.845
		J	−90.0	313.8	46.2161	39.9545	−188.362	20.9720		at 500 K
1021	$CH_2=CHCH_2^\bullet$	C	39.6	62.1	−13.2380	6.56231	−45.5646	13.1745	0.18	0.378
		J	165.7	259.8	−55.3878	27.4567	−190.642	55.1220		at 600 K
1022	$CH_2=C(CH_3)CH_2^\bullet$	C	29.6	68.8	−11.0347	9.10765	−66.1467	20.5824	0.11	0.221
		J	123.8	287.9	−46.1691	38.1064	−276.758	86.1166		at 600 K
1023	$CH_2=CH\dot{C}HCH_3$	C	30.4	70.8	−15.4190	8.74819	−56.5500	14.9133	0.07	0.168
		J	127.2	296.2	−64.5129	36.6024	−236.605	62.3974		at 400 K

Table I. (1. cont.)

No.	Radical		ΔH_f° 298 K	S° 298 K	$a \cdot 10$	$b \cdot 10^2$	$c \cdot 10^6$	$d \cdot 10^9$	Av. err. %	Max. rel. err. %
024	$CH_3CO\dot{2}$	C	−49.7	66.6	62.7632	2.23532	−2.44894	−2.88438	0.12	0.281
		J	−207.9	278.7	262.601	9.35260	−10.2464	−12.0682		at 400 K
1025	$CH_3CH_2CO\dot{2}$	C	−55.0	76.2	66.3594	4.75244	−23.1130	4.46461	0.18	0.339
		J	−230.1	318.8	277.648	19.8842	−96.7050	18.6799		at 600 K
1026	$NH\dot{2}$	C	41.0	48.4	50.1229	1.45866	−17.4743	9.46511	0.44	0.862
		J	171.5	202.5	209.714	6.10305	−73.1125	39.6020		at 600 K
1027	$\dot{C}H_2C{\equiv}N$	C	51.1	58.5	16.8955	3.82508	−30.3805	10.2424	0.06	0.121
		J	213.8	244.8	70.6907	16.0041	−127.112	42.8542		at 400 K
1028	$CH_3\dot{C}HC{\equiv}N$	C	42.72[a]	68.8	−0.81586	6.30949	−42.7553	11.6441	0.08	0.206
		J	178.7	287.9	−3.41355	26.3989	−178.888	48.7190		at 400 K
1029	$(CH_3)_2\dot{C}{-}C{\equiv}N$	C	33.8	75.8	64.1754	5.44520	−16.1227	−1.24778	0.53	1.212
		J	141.4	317.1	268.510	22.7827	−67.4573	−5.22070		at 500 K
1030	$CH_3\dot{N}H$	C	34.9	59.0	39.1535	2.81741	−12.6148	2.22128	0.11	0.249
		J	146.0	246.9	163.818	11.7880	−52.7803	9.29385		at 600 K
1031	$(CH_3)_2\dot{N}$	C	31.9	66.2	21.7546	5.12302	−21.9637	2.84355	0.30	0.700
		J	133.5	277.0	91.0212	21.4347	−91.8961	11.8974		at 400 K
1032	$\O\dot{N}H$	C	47.3	75.3	−112.809	15.5828	−131.384	43.1410	0.04	0.081
		J	197.9	315.1	−471.994	65.1983	−549.711	180.502		at 600 K
1033	$\O\dot{N}CH_3$	C	48.6	83.3	−85.7191	16.1242	−116.862	33.1859	0.06	0.130
		J	203.3	348.5	−358.649	67.4637	−488.949	138.850		at 400 K
1034	$\dot{C}OOH$	C	−53.3	60.7	42.4427	2.49971	−18.0493	5.12770	0.59	1.100
		J	−223.0	254.0	177.580	10.4588	−75.5183	21.4543		at 600 K
1035	$(CH_3)_3C\dot{C}H_2$	C	7.1[a]	78.8	61.6004	6.62492	34.4757	−42.9253	0.54	1.048
		J	29.7	329.7	257.736	27.7187	144.246	−179.599		at 400 K
1036	$CH_3\dot{C}HCH(CH_3)_2$	C	5.3[a]	84.7	14.9877	10.3417	−52.7143	10.2847	0.13	0.255
		J	22.2	354.4	62.7086	43.2695	−220.557	43.0311		at 400 K

[a]) Calculated from the group additivity values of ref. [11].

[b]) Calculated from data in ref [12]. Since the C_p^0 values in ref. [10] and ref. [12] are slightly different, the correlation cofficients are also different.

The enthalpy increments between 298 and 800 K were calculated from both sets of correlation constants and compared with the experimental data for a number of compounds (Table III). The improvement in the calculated values is marked in most cases. For this reason, the correlation constants compiled in Table I should be preferred when the calculation of thermodynamic functions is to be performed in the temperature range of 298—1000 K.

Since the data collected in Table I are based on C_p^0 values between 298 and 1000 K, they are not applicable at considerably higher temperatures. However, as can be judged from the data of Table IV, extrapolations up to 1100 K are allowed without an important increase in the error of calculation.

Table II.

The improvement of heat capacity prediction by decreasing the temperature range of calculation of correlation constans of eq. (3).[a])

Compound	Temp. range K	a	$b \cdot 10^3$	$c \cdot 10^6$	$d \cdot 10^9$	Max. rel. err. %
Carbon dioxide	298—1000	19.7352	73.7457	−56.8008	17.7092	0.15 at 400 K
	298—1500	21.5238	63.8891	−40.7492	9.75347	0.38 at 400 K
Methane	298—1000	24.9065	19.7660	67.1427	−39.9065	0.64 at 400 K
	298—1500	17.8571	58.8245	3.07692	−7.89514	1.53 at 400 K
Acetylene	298—1000	15.8398	128.050	−127.788	50.6153	0.49 at 400 K
	298—1500	23.4733	85.7216	−58.2873	15.8497	1.31 at 400 K
Propene	298—1000	5.09112	225.513	−99.6863	13.2019	0.35 at 400 K
	298—1500	3.25367	236.086	−117.883	22.7792	0.47 at 400 K
1,3-Butadiene	298—1000	−16.1192	412.161	−340.122	113.673	0.13 at 500 K
	298—1500	−2.89908	339.772	−223.279	56.3757	0.92 at 500 K
c-Hexane	298—1000	−55.3308	617.495	−261.029	15.6487	0.67 at 400 K
	298—1500	−67.6047	687.584	−380.544	77.952	1.08 at 400 K
Benzene	298—1000	−43.7404	522.853	−375.335	106.086	0.21 at 400 K
	298—1500	−35.8988	480.836	−309.542	74.9846	0.51 at 500 K

[a]) C_p^0 in J mol^{-1} K^{-1}

Table III

The improvement of enthalpy calculation by decreasing the temperature range of calculation of correlation constants

Compound	A kJ mol^{-1}	B kJ mol^{-1}	Rel. err. of B %	C kJ mol^{-1}	Rel. err. of C %
Carbon dioxide	22.97	22.79	0.78	22.81	0.70
Methane	24.74	24.88	0.57	24.80	0.24
Acetylene	27.65	27.56	0.33	27.64	0.04
Propene	49.84	49.90	0.12	49.89	0.10
1,3-Butadiene	61.85	61.70	0.24	61.86	0.02
c-Hexane	101.63	101.8	0.17	101.7	0.07
Benzene	72.01	71.92	0.12	72.04	0.04

A: experimental value of $\int_{298}^{800} Cp\, dT$ [12]

B: calculated value of the above integral (constants derived for the temperature range 298—1500 K)

C: calculated value of the above integral (constants derived for the temperature range 298—1000 K).

Acknowledgements

The authors gratefully acknowledge the kind permission of the McGraw Hill Co. to reproduce ΔH_{298}^0 and S_{298}^0 values from ref. [10]. The authors are also indebted to Mrs. R. Czeglédi and Miss V. Albert for technical assistance.

Table IV

Extrapolations to higher temperatures

Compound	C_p^0 at 1100 K J mol^{-1} K^{-1} exp.	calc.	C_p^0 at 1200 K J mol^{-1} K^{-1} exp.	calc.	Rel. err. at 1100 K %	Rel. err. at 1200 K %
Carbon dioxide	55.48	55.70	56.44	57.04	0.40	1.06
Methane	75.70	74.75	79.0	76.35	1.25	3.35
Acetylene	68.42	69.44	70.06	72.95	1.01	1.04
Propene	150.6	150.11	156.1	154.97	0.33	0.72
1,3-Butadiene	175.8	175.72	181.3	180.72	0.05	0.32
c-Hexane	331.8	328.90	343.9	336.87	0.87	2.04
Benzene	218.2	218.44	225.4	226.52	0.11	0.50

References

[1] *Kobe, A. A., C. W. Arnold:* Petroleum Refiner **43,** 123 (1974).
[2] *Spencer, H. M.:* Ind. Eng. Chem. **40,** 2152 (1948).
[3] *Yuan, S. C., Y. I. Mok:* Hydrocarbon Processing **47,** No. 3., 133 (1968).
[4] *Yuan, S. C., Y. I. Mok:* Hydrocarbon Processing **47,** No. 7., 153 (1968).
[5] *Thinh, T. P., J. L. Duran, R. S. Ramalho, S. Kaliaguine:* Hydrocarbon Processing **50,** No. 1., 98 (1971).
[6] *Yaws, C. L., et al.:* Chem. Eng., June 1974—August 1976.
[7] *Duran, J. L.:* Hydrocarbon Processing **55,** No. 8., 153 (1976).
[8] *Karapetyanc, M. H.:* Chemical Thermodynamics (in Hungarian), Akadémiai Kiadó, Budapest, 1951.
[9] *Zalotai, L., L. Seres, P. Fejes:* Computer Programs in Physical Chemistry (in Hungarian), Műszaki Könyvkiadó, Budapest (in press).
[10] *Stull, D. R., E. F. Westrum, G. C. Sinke:* The Chemical Thermodynamics of Organic Compounds, John Wiley and Sons, New York, 1969.
[11] *Benson, S. W., H. E. O'Neal:* Kinetic Data on Gas Phase Unimolecular Reactions NRSD—NBS 21, Washington, D. C., 1970.
[12] *Landolt-Börnstein:* Zahlenwerte und Funktionen II. Band, 4. Teil, Springer Verlag, 1961.

БОЛЕЕ ТОЧНОЕ ОПРЕДЕЛЕНИЕ МОЛЯРНЫХ ТЕПЛОЕМКОСТЕЙ

Л. Шереш, Л. Залотаи и Ф. Марта

Сведения о теплоемкостях химических соединений весьма важны как при научных экспериментах, так и при проектировании промышленных производств. В работе приведены теплоемкости более чем 700 соединений с относительной ошибкой не превышающей 0,1% для интервала температур от 273 до 1000 К, на основании кривых рассчитанных с использованием полинома:

$$C_p^0 = a + bT + cT^2 + dT^3.$$

Полученные кривые хорошо удовлетворяют экспериментальным значениям C_p^0. Представленные данные выражены как в единицах калории, так и в джоулях.

OXIDATION POTENTIAL OF PEROXO-MONOPHOSPHORIC ACID

By

J. SCHNEIDER

Institute of Inorganic and Analytical Chemistry, Attila József University, Szeged*

(Received 15 August, 1977)

The oxidation potential of peroxo-monophosphoric acid was determined as a function of the peroxo acid, hydrogen peroxide and phosphate ion concentrations and the pH. In the absence of hydrogen peroxide the potential can be described by the formula:

$$E = E^0 + \frac{RT}{F} \ln [H_3PO_5]^{0.95} [H^+]^{1.05}. \quad E^0 = 1.19 \pm 0.01 \text{ V}.$$

In the presence of hydrogen peroxide the empirical formula

$$E = E^0 + \frac{RT}{F} \ln \frac{[H_3PO_5]^{1.73} [H^+]^{0.96}}{[H_2O_2]^{1.73}}$$

is valid, with a value of $E^0 = 0.88 \pm 0.01$ *V*. The oxidation potential is regarded as a mixed potential brought about by a local cell mechanism at the surface of the Pt electrode.

Peroxo-monophosphoric acid (in the following HOOA) is frequently used as a reagent of high oxidizing power and at the same time of high reactivity. However, reference can not be found in the literature with regard to the oxidation potential of HOOA. In the present paper we report the results of experiments made to determine the oxidation potential, and these are compared with earlier findings relating to peroxo-monosulphuric acid [1] and peroxo-acetic acid [2].

Experimental

Materials: The chemicals used were Merck and Reanal products of p.a. purity. With the exceptions of sodium hydroxide and sodium perchlorate, from solutions of which heavy metal ion trace impurities were removed by the method of D'ANS and MATTNER [3], these chemicals were used without further purification.

A phosphate-free HOOA solution was prepared by perchloric acid hydrolysis of sodium peroxo-diphosphate (1,0 M perchloric acid, 298 K, ca. 4 hr). After neutralization with sodium hydrogen carbonate, barium perchlorate was used to precipitate the phosphate ions from the resulting solution. For the more complete removal of

* Present address: VITUKI, 1095 Budapest IX., Kvassai u. 1.

barium phosphate, barium carbonate too was added to the solution, which was filtered after a standing period of 30 min. If the presence of phosphate ions was not disturbing, the hydrolysis was performed with 2 M phosphoric acid. During 90 min at 333 K the hydrolysis is quantitative; under these conditions there is practically no formation of hydrogen peroxide. Peroxo-diphosphate ($K_4P_2O_8$) was prepared as described by FICHTER and GUTZWILLER [4], and was converted according to INDELLI and BONORA [5] to $Na_4P_2O_8$, which is more easily purifiable by recrystallization.

Analysis: After attainment of the equilibrium potential, the HOOA and possible hydrogen peroxide contents of the solutions were determined as described earlier [6], with the modification that the sulphuric acid concentration of the solution was raised to 1 M in order to avoid precipitation of cerium(IV) phosphate during the cerimetric titration in the case of higher phosphate ion contents. After flushing-out of the dissolved oxygen with CO_2, the total oxidizing capacity of the solutions was determined iodometrically, as described by CHULSKY [7].

Potential measurement: The pH of the HOOA solutions was adjusted with acetate and phosphate buffer, and by the addition of perchloric acid or sodium hydroxide, while the ionic strength was adjusted by the addition of sodium perchlorate. The potential was determined as described previously [2]. Prior to the measurements, the electrodes (in the present case 1.0 · 0.6 cm Pt sheets 0.15 mm thick) were left to stand for about 30 min in chromic acid cleaning mixture. They were then washed, immersed for 10 min in 3% hydrogen peroxide solution acidified nitric acid, re-washed, and left to stand for several hours in distilled water short-circuited to one another. By this means it was generally possible to achieve equalization of the initially different potentials of the individual electrodes. The potential data given in the Figures and Tables are the means of the potentials of three Pt electrodes immersed in a given solution in each case.

Results

a) Oxidation potential in the absence of hydrogen peroxide

In H_2O_2-free solution ($[H_2O_2] < 10^{-6}$ M) in the range $pH_3PO_5 = 2.0—5.0$, the E *vs.* pH_3PO_5 data determine a straight line, the slope of which (established by the GAUSS least squares method) is

$$\Delta E/\Delta pH_3PO_5 = -56 \text{ mV}.$$

The potential is independent of the phosphate ion concentration, and is not affected by changes in the ionic strength either. It is further independent of the quantity of dissolved O_2 in the solution.

The potential of the HOOA depends on the pH of the solution. In the interval pH = 2.0—6.2, the E *vs.* pH data determine a straight line, the slope of which is

$$\Delta E/\Delta pH = -62 \text{ mV}.$$

The rest potential and the potential measured in the intensively-stirred solution virtually do not differ from each other.

On the above basis, in the absence of hydrogen peroxide the potential of HOOA can be described by the empirical formula

$$E = E^0 + \frac{RT}{F} \ln \{[H_3PO_5]^{0.95}[H^+]^{1.05}\}. \quad (1)$$

The apparent oxidation normal potential calculated via formula (1) (see Table 1) is $E^\circ = 1.19 \pm 0.01$ V (referred to a hydrogen electrode).

Table I

Oxidation potential of peroxo-monophosphoric acid in the absence of hydrogen peroxide

H_3PO_5 $M \cdot 10^4$	pH	$E_{obs.}$ (V) *vs.* SCE	E° (V)
53.5	3.50	0.564	1.148
43.4	4.09	0.560	1.186
30.3	3.55	0.570	1.171
27.3	2.55	0.640	1.182
26.0	3.91	0.584	1.211
24.8	3.90	0.566	1.194
18.5	2.55	0.629	1.180
17.4	3.86	0.573	1.206
14.4	2.45	0.636	1.187
12.5	2.60	0.635	1.199
11.7	2.40	0.642	1.195
11.5	3.00	0.603	1.194
9.6	2.70	0.616	1.192
8.6	2.40	0.636	1.196
6.5	4.50	0.506	1.203
6.0	3.40	0.576	1.207
5.5	4.50	0.490	1.192
3.8	2.90	0.572	1.183
3.5	2.45	0.614	1.199
2.5	2.80	0.580	1.195
2.4	2.71	0.586	1.197
2.1	4.50	0.480	1.205
1.8	2.60	0.574	1.185

b) Oxidation potential in the presence of hydrogen peroxide

If hydrogen peroxide is added to an HOOA solution, the peroxo acid and the hydrogen ion concentrations being maintained constant ($pH_3PO_5 = 2.9$; pH = 3.9), up to a hydrogen peroxide concentration of about $2.5 \cdot 10^{-5}$ M the potential exhibits no, or scarcely any change. On further increase of the hydrogen peroxide concentration, the potential begins to fall significantly, (Fig. 1) the rate of the linear decrease being

$$\Delta E / \Delta (pH_2O_2)_{pH_3PO_5 = \text{const.}} = -97 \text{ mV}.$$

If the concentration ratio $[H_3PO_5]/[H_2O_2]$ falls below 0.25, a stage is again observed in which the potential changes only slightly on further increase of the hydrogen peroxide concentration (Fig. 1). The slope of this stage is

$$\Delta E / \Delta pH_2O_2 = -10 \text{ mV}.$$

A similar result is found if the HOOA concentration of the solution is varied while the hydrogen peroxide concentration and the pH are maintained constant. The slope of the steeper section of the curve is

$$\Delta E/\Delta(pH_3PO_5)_{pH_2O_2=\text{const.}} = -101 \text{ mV}.$$

On the above basis, the potential varies according to the function

$$E = f\{\log([H_3PO_5]^x/[H_2O_2]^y)\}.$$

For a further checking of the exponents x and y, the potentials were measured in solutions with constant pH, but different concentration ratios $[H_3PO_5]/[H_2O_2]$. The resulting E *vs.* p ($[H_3PO_5]/[H_2O_2]$) data determined a straight line (Fig. 2) which is possible only if $x=y$. The slope of the steep stage is

$$\Delta E/\Delta p([H_3PO_5]/[H_2O_2]) = -102 \text{ mV},$$

while that of the less steep stage is -8 mV.

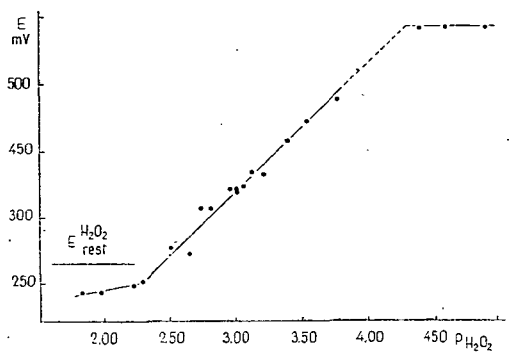

Fig. 1. Dependence of oxidation potential of H_3PO_5 on hydrogen peroxide concentration.

$pH_3PO_5 = 2.9$, pH = 3.9

The potential of HOOA does not depend on the phosphate ion concentration in the presence of hydrogen peroxide either, nor on the ionic strength of the solution. The potential again depends on the pH of the solution

$$\Delta E/\Delta \text{pH} = -57 \text{ mV}.$$

It is noteworthy that in the presence of hydrogen peroxide, and predominantly in the range $p([H_3PO_5]/[H_2O_2]) = -0.8 - +1.2$, the potential depends strongly on the state of motion of the solution. The rest potential is about 80—100 mV more positive than the potential measured in the vigorously-stirred solution.

In the presence of hydrogen peroxide, therefore, the oxidation potential of peroxo-monophosphoric acid can be described by the empirical formula

$$E = E^0 + \frac{RT}{F}\ln\frac{[H_3PO_5]^{1.73}[H^+]^{0.96}}{[H_2O_2]^{1.73}} \qquad (2)$$

The apparent standard oxidation potential, calculated on the basis of formula (2) is $E^0 = 0.88 \pm 0.01$ V (Table 2).

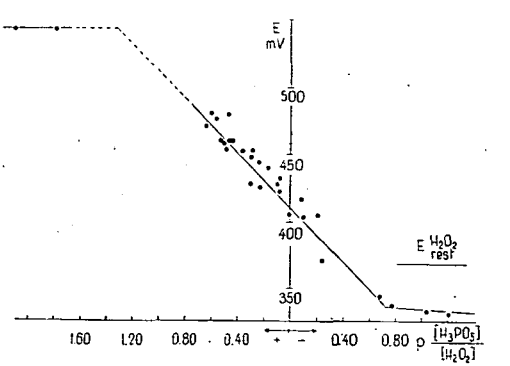

Fig. 2. Oxidation potential of peroxo-monophosphoric acid as a function of

$p([H_3PO_5]/[H_2O_2])$. pH = 3.9

Table II

Dependence of the oxidation potential on the H_3PO_5/H_2O_2 concentration ratio and pH

H_3PO_5 $M \cdot 10^3$	H_2O_2 $M \cdot 10^3$	pH	$p\frac{[H_3PO_5]}{[H_2O_2]}$	$E_{obs.}$ (V) vs. SCE	E^0 (V)
4.72	0.98	2.84	−0.683	0.562	0.894
1.25	0.28	3.20	−0.650	0.515	0.871
3.99	0.98	3.03	−0.609	0.536	0.865
3.92	1.06	3.19	−0.568	0.522	0.886
3.20	0.94	5.10	−0.532	0.386	0.862
3.07	0.95	3.90	−0.509	0.458	0.868
1.19	0.39	3.06	−0.484	0.507	0.872
3.04	0.98	2.77	−0.492	0.551	0.899
3.07	1.06	3.87	−0.462	0.462	0.875
3.08	1.07	3.87	−0.459	0.462	0.876
2.46	1.06	3.90	−0.366	0.458	0.883
1.98	0.98	2.77	−0.305	0.518	0.884
1.19	0.59	3.00	−0.305	0.485	0.865
2.08	1.06	3.96	−0.293	0.450	0.886
3.00	1.75	5.10	−0.234	0.369	0.876
1.24	0.73	3.33	−0.229	0.461	0.867
1.58	1.06	4.05	−0.173	0.431	0.884
1.35	1.06	2.98	−0.105	0.487	0.884
3.57	2.97	3.90	−0.080	0.422	0.876
1.29	1.06	4.03	−0.085	0.424	0.885
0.84	0.84	3.00	+0.000	0.462	0.873
0.87	1.06	3.90	0.086	0.416	0.887
1.19	1.55	3.00	0.104	0.460	0.881
0.64	1.06	3.08	0.219	0.456	0.894
1.22	2.16	2.45	0.248	0.462	0.867
1.06	5.00	2.25	0.676	0.447	0.884
0.96	5.78	2.25	0.779	0.440	0.888
0.93	10.25	2.25	1.042	0.434	0.909
0.89	14.57	2.25	1.214	0.432	0.924

Discussion

For a qualitative explanation of the oxidation potential measured in HOOA solutions, we may set out from the finding that the potential in either the absence or the presence of hydrogen peroxide is not so „stable" and well-reproducible as the potential to be measured in the solution of a well-poised redox system (*e.g.* iron(II)/iron(III)). Even after a waiting period of 20—60 min, the potentials measured at the individual electrodes exhibit differences of *ca.* ±10 mV. From this behaviour it is concluded that in the absence of hydrogen peroxide the potential is not determined by the process

$$HOOA + 2e + 2H^+ \rightleftharpoons HOA + H_2O$$

for then the potential would be „more stable" (better poised), and should also depend on the concentration of phosphate ions, which was not supported by the measurements. It is probable, therefore, that the potential observed is a mixed potential, brought about by a local cell mechanism. The HOOA is reduced on the cathodic sites of the electrode, and oxidized on the anodic sites, and the potential is determined

by the $i_c = i_a$ state. As regards the cathode reaction, we may consider the voltammetric findings of SECCO and VENTURINI [8], who suggested that, on the 1-electron reduction of HOOA on a platinized Pt electrode:

$$HOOA + H^+ + e \rightleftharpoons OH + HOA, \tag{3}$$

a phosphate species corresponding to the pH of the medium is formed, and an OH radical is transferred to the Pt electrode. The above authors state that the more acidic the leaving group, the easier it is for the reduction to occur. The OH radical next participates in a further electrode reaction, or is stabilized by disproportionation. Only assumptions are possible with regard to the anode reaction. It may be assumed that the HOOA is oxidized to a peroxo-phosphate radical:

$$HOOA \rightleftharpoons OOA + H^+ + e \tag{4}$$

which is either oxidized to oxygen and phosphate ions, or undergoes dismutation to oxygen and HOOA.

In the presence of hydrogen peroxide, the potential-dependence changes. While the concentration ratio $[HOOA]/[H_2O_2]$ is larger than 20, the potential decreases only slightly on the addition of hydrogen peroxide, but even this decrease disappears after a short waiting period, the potential being restored to the original value. The high potential gradient observed in the presence of somewhat more hydrogen peroxide is in all probability connected with the fact that the hydrogen peroxide interacts with the products of electrode reactions (3) and (4) on the surface of the electrode, and these Pt-surface reactions alter the concentration ratio $[HOOA]/[H_2O_2)$ on the surface of the electrode. We consider it probable that the dependence of the potential on the state of motion of the solution can also be attributed to this. If the increase in the flux of reacting substances on the surface is enhanced not only by diffusion, but also by convection, the potential will become more negative. Under the conditions of potential measurement the ratio solution volume:surface is generally high, and therefore a change in the composition of the solution as a consequence of the surface reactions can not be observed, even after a longer time. However, if the ratio solution volume:surface is strongly decreased (*e.g.* to a value of about 1), by the use of a special vessel, a well-measurable concentration change can be observed even in a short time. The very slow reaction $HOOA + H_2O_2$ with a stoichiometry of 1:1 under the homogeneous conditions is accelerated 20—25-fold on the effect of surface catalysis, but in addition the ratio $[HOOA]/[H_2O_2]$ is increased because of the faster decomposition of the hydrogen peroxide. This is why we state that the concentration ratio $[HOOA]/[H_2O_2]$ is larger on the surface of the electrode than in the bulk of the solution. The potential-dependence (eqn. (2)) observed in the presence of hydrogen peroxide does not only originate from the shift in the concentration ratio; a mixed potential arising as a result of several simultaneous electrode reactions (a multicouple system) is also involved. In other words, the hydrogen peroxide too participates in the local cell mechanism.

In the event of a larger excess of hydrogen peroxide, the role of the peroxomonophosphoric acid is forced into the background, and the potential gradient is then only 8—10 mV. This is probably related with the fact that primarily the

hydrogen peroxide predominantly occupying the active sites takes part in the local cell mechanism:

$$H_2O_2 + e + H^+ \rightleftharpoons H_2O + OH$$

$$H_2O_2 \rightleftharpoons HO_2 + H^+ + e.$$

The effect of the HOOA can be observed even then, however, for the potential is more negative than the rest H_2O_2 potential measured under similar conditions in the absence of HOOA ($E_{rest}^{H_2O_2}$ is indicated on the left-hand side of Fig. 2).

We have already pointed out that oxidation potential of peroxo-monophosphoric acid is analogous with the potentials determined in the cases of peroxo-monosulphuric acid [1] and peroxo-acetic acid [2]. In all probability, the cause of this is that the peroxo acids give rise to analogous electrochemical and chemical reactions. Our findings show that the powers of the peroxo acid and the hydrogen peroxide in the potential dependence observed in the presence of hydrogen peroxide are functions of the rate of the reaction $HOOA + H_2O_2$ on the Pt surface. The rate of this surface reaction is the highest for Caro's acid (power: 2.25), lower for peroxo-phosphoric acid, and the lowest for peroxo-acetic acid (power: 1.66). On the basis of these observations, we are of the opinion that, besides detailed electrode-kinetic investigations, a study of the Pt-catalyzed $HOOA + H_2O_2$ reactions is necessary for a quantitative clarification of the oxidation potentials measured in solutions of the peroxo acids. Such measurements are now in progress.

References

[1] *Csányi, L. J.:* Acta. Chim. Hung. **14,** 275 (1958).
[2] *Schneider, J., L. J. Csányi:* Acta Chim. Hung. **46,** 181 (1965).
[3] *D'Ans, J., J. Mattner:* Angew. Chem. **64,** 448 (1952).
[4] *Fichter, F., E. Gutzwiller:* Helv. Chim. Acta **11,** 323 (1928).
[5] *Indelli, A., P. L. Bonora:* J. Amer. Chem. Soc. **88,** 924 (1966).
[6] *Csányi, L. J., F. Solymosi:* Acta Chim. Hung. **13,** 275 (1958).
[7] *Chulski, T.:* Ph. D. Thesis, Michigan State University, (1953).
[8] *Secco, F., M. Venturini:* J. C. S. Dalton Trans. 634 (1977).

ОКИСЛИТЕЛЬНЫЙ ПОТЕНЦИАЛ ПЕРОКСО-МОНОФОСФОРНОЙ КИСЛОТЫ

Й. Шнейдер

Окислительный потенциал пероксо-монофосфорной кислоты определен как функция концентрации пероксо-кислоты, перекиси водорода, ионов фосфата и pH. В отсутствие перекиси водорода потенциал может быть выражен формулой:

$$E = E^0 + \frac{RT}{F} \ln [H_3PO_5]^{0.95} [H^+]^{1.05}. \quad E^0 = 1.19 \pm 0.01 \ V.$$

В присутствии перекиси водорода эмпирическая формула

$$E = E^0 + \frac{RT}{F} \ln \frac{[H_3PO_5]^{1.73} [H^+]^{0.96}}{[H_2O_2]^{1.73}}$$

действительна при значении $E^0 = 0.88 \pm 0{,}01$. Окислительный потенциал рассматривается как смешанный потенциал, возникающий по клеточному механизму на поверхности платинового электрода.

ВЛИЯНИЕ ДОЛИ ЛИПОФИЛЬНЫХ ЗВЕНЬЕВ НА СТАБИЛИЗИРУЮЩЕЕ ДЕЙСТВИЕ СТАТИСТИЧЕСКОГО СОПОЛИМЕРА МЕТАКРИЛОВОЙ КИСЛОТЫ И МЕТИЛМЕТАКРИЛАТА ПРИ СУСПЕНЗИОННОЙ ПОЛИМЕРИЗАЦИИ

И. А. АНДОР

Институт общей и физической химии университета им. Аттилы Йожефа, Сегед

(Поступило в редакцию 15 сентября 1977 г.)

Синтезированы статистические сополимеры метакриловой кислоты и метилметакрилата с долей липофильных звеньев 0.05, 0.10, 0.15, 0.20 и 0.25 в цепях макромолекул. Изучены вязкостные характеристики растворов синтезированных сополимеров и сопоставлены с экспериментальными данными полученными по выходу полимера и эффективности стабилизации полимеризующихся эмульсий метилметакрилата. На основании экспериментальных данных обсуждается влияние внутри- и межмолекулярных гидрофобных взаимодействий на стабилизирующее действие растворов изученных сополимеров при суспензионной полимеризации.

Изучение полимеризационных процессов, проводимых в эмульсиях, несмотря на долгую предысторию вопроса, остается в центре внимания многих исследователей вследствие большого практического значения и еще далеко не исчерпанных возможностей этого способа в экономичном получении полимеров с необходимыми свойствами [1]. Однако, относительно мало имеется публикаций по одному из разновидностей эмульсионной полимеризации, по, так называемой, суспензионной полимеризации [2, 3]. Основным затруднением этого способа получения полимеров является обеспечение стабильности полимеризующейся эмульсии мономера в течение процесса. В качестве стабилизаторов применяются вещества, обладающие определенной гидрофильно-липофильной структурой, но не имеющих свойства мыл. Такими могут быть твердые порошки [4], или водорастворимые синтетические и естественные полимеры [5].

У полимерных стабилизаторов синтетического и естественного происхождения дифильный баланс макромолекул определяется структурой элементарных звеньев. Однако, в синтетических сополимерных стабилизаторах, или модифицированных естественных полимерах, за счет изменения структуры некоторых элементарных звеньев, представляется возможность изменить липофильный баланс макромолекул стабилизаторов, в зависимости от количества и порядка расположения в цепях звеньев с измененной структурой. Увеличение липофильной части макромолекул до определенного предела, как это было показано рядом авторов [5—7] улучшает стабилизирующие свойства дифильных полимеров. В литературе практически отсутствуют данные относительно влия-

ния дифильного баланса на стабилизирующие свойства полиэлектролитных стабилизаторов при суспензионной полимеризации.

Задача данной работы заключалась в определении влияния доли метилметакрилатных звеньев в статистических сополимерах метакриловой кислоты и метилметакрилата (МКМ) на вязкостные свойства растворов и стабилизирующее действие при суспензионной полимеризации метилметакрилата инициированной перекисью бензоила.

Методика исследования

Метилметакрилат (ММА) и метакриловая кислота (МАК) использовались фирмы *Флука* марки «purum» после многократной вакуум перегонки в токе азота высокой чистоты. Другие реактивы применялись фирмы *Рэанал* аналитической степени чистоты.

Синтез сополимеров МКМ проводили в массе мономеров с перекисью бензоила в качестве инициатора. Полученные сополимеры растворяли в этаноле и переосаждали в избытке бензола, затем сушили в вакууме при температуре 323 К. Состав полученных сополимеров контролировали потенциометрическим титрованием [8, 9]. Полученные образцы МКМ соответствовали, в пределах ошибки анализа, исходным соотношениям смеси мономеров в которых доля ММА звеньев составляла: 0.05, 0.10, 0.15, 0.20 и 0.25 от общего числа звеньев сополимеров.

Растворы МКМ разного гидрофильно-липофильного баланса готовили при постоянном перемешивании и нагревании до температуры полимеризационных опытов с добавлением *NaOH* по расчету достижения степени нейтрализации 0,2. Вязкость растворов сополимеров определяли в вискозиметрах *Уббелоде* при 313 К. Характеристическую вязкость находили графическим методом при изоионном разбавлении растворами *NaCl* [10].

Во всех опытах все условия проведения суспензионной полимеризации ММА соблюдались строго постоянными: температура поддерживалась 348 К; соотношение фаз мономер:вода была 1:2; в качестве инициатора применяли перекись бензоила с концетрацией 0.05 $mol \cdot dm^{-3}$ мономера; скорость перемешивания составляла 12.14 $rad \cdot s^{-1}$.

Оценку стабилизирующего действия растворов МКМ проводили по предложенному нами ранее методу [11, 12] по величине поверхности полимерных гранул, образовавшихся из единицы объема мономера.

Экспериментальные данные и их обсуждение

Многие авторы [5, 7, 13] считают наиболее важным свойством поверхностную активность не только для обычных эмульгаторов, но и для полимерных стабилизаторов при суспензионной полимеризации. Мы, в согласии с авторами, которые придерживаются другого мнения [14—16], указывали ранее [17, 18], что поверхностная активность стабилизаторов не является однозначной характеристикой их стабилизирующего качества. Проведенные измерения поверхностной активности полученных нами сополимеров, снова показали наличие

ряда принципиальных экспериментальных и теоретических трудностей, не позволяющих провести корректную оценку результатов. Поэтому, вопросы влияни доли липофильных звеньев в сополимере на поверхностную активность и ее связи со стабилизирующим действием в данной работе не обсуждаются.

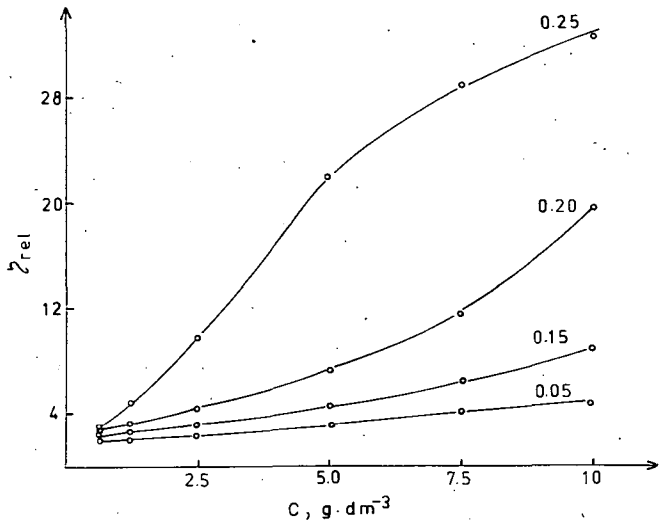

Рис. 1. Зависимость относительной вязкости (η_{rel}) растворов МКМ от концентрации (цифры на кривых соответствуют доле ММА звеньев в сополимере)

На рис. 1 представлена зависимость относительной вязкости растворов МКМ от их концентрации. Из рисунка видно, что увеличение доли ММА звеньев в сополимере приводит ко все более резкому возрастанию вязкости растворов от концентрации. Однако, необходимо отметить, что при высших концентрациях (7.5 и 10 g·dm^{-3}) образца МКМ—0.25, относительный рост вязкости несколько уменьшается. Явление столь резкого возрастания вязкости растворов сополимеров с увеличением доли липофильных звеньев в МКМ объясняется, вероятно, возникновением межмолекулярных гидрофобных взаимодействий, приводящих к образованию надмолекулярных образований. Однако, при высоком содержании липофильных звеньев в цепи сополимера увеличивается вероятность возникновения внутримолекулярных гидрофобных взаимодействий [9], что приводит к образованию более свернутых конформаций макромолекул, и вязкости растворов сополимеров с разным содержанием липофильных звеньев, в результате вышеупомянутых двух противодействующих влияний, при малых концетрациях относительно меньше отличаются.

Непосредственным доказательством изложенных представлений может служить изучение зависимости приведенной вязкости растворов МКМ от концентрации и определение характеристической вязкости, как меры эффективного объема макромолекулярных клубков в растворах. Данные рис. 2 отчетливо показывают, что, в отличие от растворов аполярных полимеров, наклон пря-

Таблица

Характеристическая вязкость [η], тангенс угла возрастания приведенной вязкости с концентрацией (tg α) и относительные увеличения этих параметров для растворов МКМ

	ПМАК	МКМ—0.05	МКМ—0.10	МКМ—0.15	МКМ—0.20	МКМ—0.25
[η], $cm^3 \cdot g^{-1}$	9.5	10.0	11.1	14.3	12.5	10.3
Относительное увеличение [η]	—	1.05	1.17	1.50	1.32	1.08
tg α	32	32	72	108	80	64
Относительное увеличение tg α	—	1.00	2.25	3.37	2.50	2.00

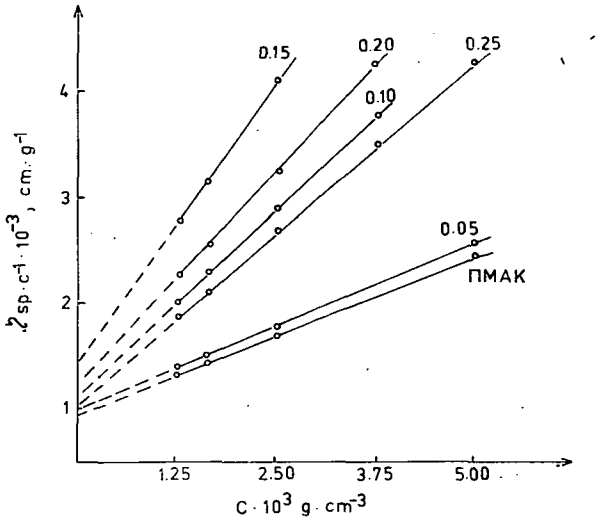

Рис. 2. Зависимость приведенной вязкости ($\eta_{sp} \cdot C^{-1}$) растворов МКМ от концетрации при изоионном разбавлении (цифры на прямых соответствуют доле ММА звеньев в сополимере)

мых зависимости $\eta_{sp} \cdot C^{-1}$ от C, довольно значительный, что свидетельствует о резком нарастании межмолекулярных взаимодействий с ростом концентрации. В таблице представлены полученные экспериментальные данные по характеристической вязкости растворов МКМ и тангенсы углов наклона прямых зависимости приведенной вязкости от концентрации при изоионном разбавлении растворами *NaCl*. С увеличением доли ММА звеньев в сополимере до 0.15 увеличивается тангенс угла наклона, а также возрастает характеристическая вязкость, т.е. удельный объем макромолекулярных клубков, но при при отно-

сительно высоких содержаниях липофильных звеньев (0.20 и 0.25) снова наблюдается некоторое уменьшение рассматриваемых величин. Происходящие изменения количественно наиболее ярко отражаются представленными в таблице относительными (по отношению к полиметакриловой кислоте) увеличениями значений характеристической вязкости и тангенса угла наклона зависимости $\eta_{sp} \cdot C^{-1}$ от C.

Физический смысл наблюдаемых явлений сводится, по-видимому, в основном к тому, что с увеличением доли ММА звеньев до 0.15 в сополимере преобладающую роль играют межмолекулярные взаимодействия при исследуемых концентрациях, а при более высоких содержаниях ММА начинают играть все большую роль внутримолекулярные взаимодействия.

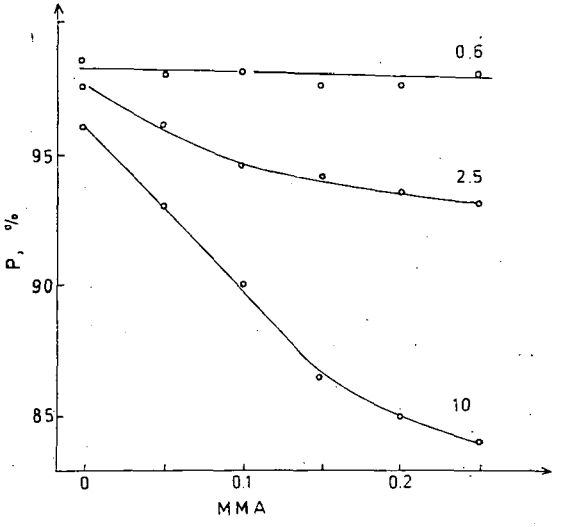

Рис. 3. Зависимость выхода ПММА в гранулах от доли ММА звеньев в МКМ как стабилизатора (цифры на кривых соответствуют концентрациям, $g \cdot dm^{-3}$).

Для выяснения роли липофильных звеньев на стабилизирующее действие растворов МКМ, нами были проведены суспензионные полиимеризации в присутствии растворов всех полученных образцов в широком интервале концентраций. На рис. 3 представлены данные по выходу гранульного полиметилметакрилата (ПММА) в зависимости от доли липофильных звеньев в цепи стабилизатора. В результате относительно трудной воспроизводимости данных, получаемых при суспензионной полимеризации, нами в дальнейшем представляются средние величины, рассчитанные на основании не менее чем пяти опытов. Как видно из данных рис. 3, с увеличением доли липофильных звеньев в цепи стабилизатора уменьшается выход полимера в гранулах. При этом, уменьшение выхода, т. е. возрастание доли полимерных частиц, обладающих коллоидными размерами [7, 19], тем значительнее, чем выше концентрация раствора применяемого стабилизатора. Несомненно, что возникающие липо-

фильные группировки в макромолекулах и в надмолекулярных образованиях МКМ создают благоприятные условия для прохождения реакции полимеризации по механизму аналогичному с мицеллярным, имеющему место при применении мылоподобных эмульгаторов.

Полная картина эффективности стабилизации полимеризующейся эмульсии ММА растворами МКМ представлена на рис. 4. Полученная сложная зависимость эффективности стабилизации от доли липофильных звеньев при разных концентрациях растворов МКМ, нетрудно объяснить с точки зрения развитых нами представлений [20—23] о роли конформационных состояний и гибкости цепей макромолекул полиэлектролитных стабилизаторов в растворах.

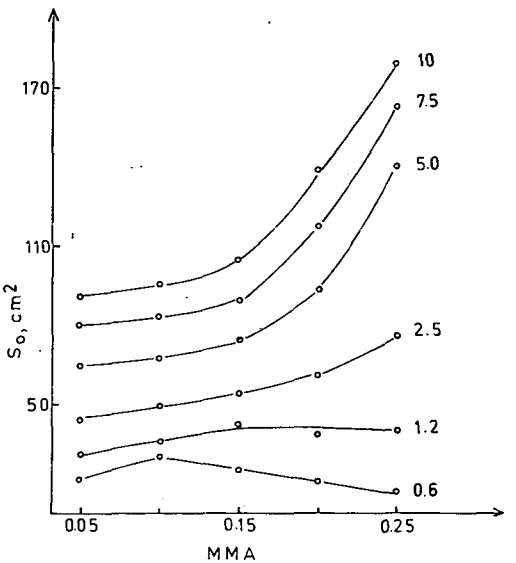

Рис. 4. Зависимость эффективности стабилизации (S_0) от доли ММА звеньев в МКМ как стабилизатора (цифры на кривых соответствуют концентрациям, $g \cdot dm^{-3}$).

При весьма низкой концентрации ($0.6\ g \cdot dm^{-3}$) и прменяемой степени нейтрализации растворов МКМ равной 0.2, степень ионизации карбоксильных групп довольно значительна. Увеличение доли липофильных участков цепей способствует адсорбции макромолекул стабилизатора на каплях мономера и мономерно-полимерных частиц. Относительно меньшее значение внутримолекулярных гидрофобных взаимодействий при невысокой доли липофильных звеньев (0.05 и 0.10) сначала не снижает в значительной мере гибкость цепей, но с возрастанием доли липофильных участков (0.15—0.25), гидрофобные связи начинают тормозить свободное вращение звеньев и, несмотря на возрастающую адсорбционную способность макромолекул, эффективность стабилизации снижается.

С увеличением концентрации растворов МКМ, над внутримолекулярными взаимодействиями начинают преобладать межмолекулярные, образуется больше надмолекулярных образований и больших размеров, что значительно улучшает стабилизацию полимеризующейся эмульсии. Однако, необходимо обратить внимание на то обстоятельство, что при весьма высоких вязкостях дисперсионной среды (при концентрациях превышающих $10 g \cdot dm^{-3}$, липофильной доли 0.15 и выше) появляются затруднения гидродинамического характера. По этой причине может происходить некоторое замедление роста величины эффективности стабилизации уже при концентрациях превышающих $5.0\ g \cdot dm^{-3}$ (рис. 4).

Дифференциальные кривые распределения гранул ПММА, полученных при концентрации $10\ g \cdot dm^{-3}$ стабилизаторов с различной долей липофиль-

ных звеньев, представлены на рис. 5. Гранулометрическое распределение частиц по размеру показывает смещение максимума распределения в сторону уменьшения диаметров с увеличением липофильной доли, однако, как это уже отмечалось нами ранее [12], достаточно обоснованных количественных выводов относительно стабилизирующего действия на их основании сделать трудно.

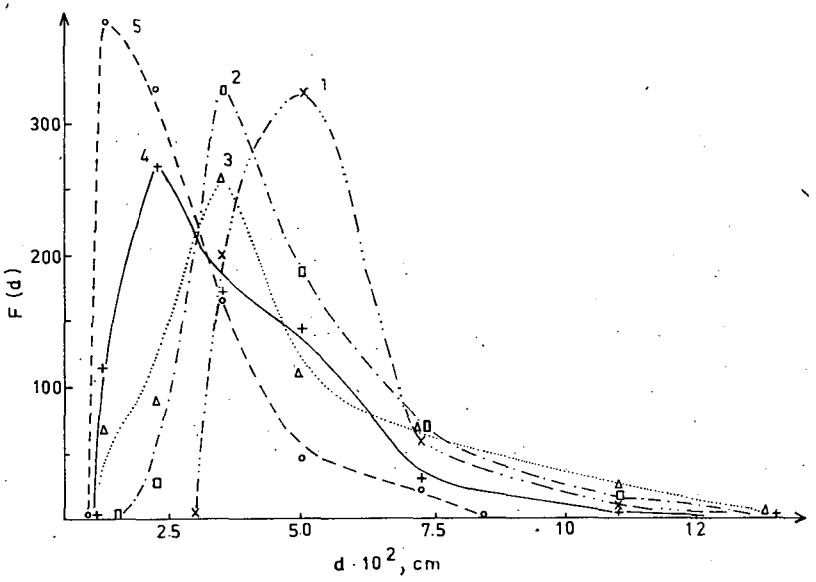

Рис. 5. Дифференциальные кривые распределения гранул суспензионного ПММА, полученных в присутствии МКМ (концентрации 10 g·dm^{-3}) с разной долей ММА звеньев:

1 – 0.05, 2 – 0.10, 3 – 0.15, 4 – 0.20, 5 – 0.25.

Из приведенных данных работы следует, что увеличение доли ММА звеньев в сополимере МКМ, по-видимому, вследствие повышения адсорбционной способности и конформационных изменений макромолекул, улучшает стабилизирующее действие сополимеров в исследованной области гидрофильно-липофильного баланса и концентраций растворов стабилизаторов. Для достижения требуемого распределения молимерных частиц по размеру, необходимо соответственно подобрать концентрацию и гидрофильно-липофильный баланс применяемого стабилизатора.

* * *

Автор выражает благодарность С. Н. Колточихиной за участие в выполнении экспериментальной части работы.

Литература

[1] *Елисеева, В. И., С. С. Иванчев, С. И. Кучанов, А. В. Лебедев:* Эмульсионная полимеризация и ее применение в промышленности, «Химия», Москва, 1976.
[2] *Trommsdorf, E., C. E. Schildknecht:* High Polymers, vol. 10, Inersci. Publ., New York—London, 1956.
[3] *Houwink, R., A. J. Staverman:* Chemie und Technologie der Kunststoffe B. 2. Akad. Verl. Leipzig 1963.
[4] *Wenning, H.:* Kolloid-Z. und Z. Polymere **182,** 60 (1962).
[5] *Gerspacher, P.:* Diss. Dokt. ETH, Juris Verl. Zürich, 1963.
[6] *Winslow, F. H., W. Matreyek:* Ind. Eng. Chem. **43,** 1108 (1951).
[7] *Hopff, H., E. Lutz:* Kunst. Plast. **5,** 341 (1958).
[8] *Leyte, J. C., M. Mandel:* J. Polymer Sci. **A2,** 1879 (1964).
[9] *Моравец, Г.:* Макромолекулы в растворе, «Мир», Москва, 1967.
[10] *Цветков, В. Н., В. Е. Эскин, С. Я. Френкель:* Структура макромолекул в растворах, «Наука», Москва, 1964. ст. 194.
[11] *Юрженко, А. И., И. А. Андор, Н. Н. Заяц:* Коллоидн. ж. **30,** 455 (1968).
[12] *Andor, J.:* Acta Phys. et Chem. Szeged **19,** 115 (1973).
[13] *Wenning, H.:* Kunst. Plast. **5,** 328 (1958).
[14] *Hohenstein, W. P., H. Mark:* High Molecular Weight Organic Compounds, vol. 6, Intersci. Publ. New York, 1949.
[15] *Trommsdorf, E.:* Makromol. Chem. **13,** 76 (1954).
[16] *Karásek, B.:* Chemicke listy **55,** 673 (1961).
[17] *Юрженко, А. И., И. А. Андор:* Коллоидн. ж. **32,** 130 (1970).
[18] *Andor, J., A. E. Shamrakova:* Acta Phys. et Chem. Szeged **19,** 305 (1973).
[19] *Andor, J., A. E. Shamrakova, A. I. Jurzhenko:* Acta Phys. et Chem. Szeged **18,** 245 (1972).
[20] *Юрженко, А. И., И. А. Андор:* Докл. АН СССР **181,** 658 (1968).
[21] *Андор, И. А., А. И. Юрженко:* В сборн. Поверхностные явления в полимерах, «Наукова думка», Киев, 1970. ст. 30.
[22] *Андор, И. А., А. И. Юрженко, А. Э. Шамракова:* Коллоидн. ж. **32,** 644 (1970).
[23] *Андор, И. А., А. И. Юрженко:* Коллоинд. ж. **33,** 492 (1971).

THE INFLUENCE OF THE RATIO OF THE LIPOPHILIC PARTS ON THE STABILIZATION EFFECTS OF METHACRYLIC ACID—METHYL METHACRYLATE STATISTICAL COPOLYMERS IN SUSPENSION POLYMERIZATION

J. A. Andor

The statistical copolymers of methacrylic acid and methyl methacrylate with lipophilic part ratios of 0.05, 0.1, 0.15, 0.2 and 0.25 were synthetized. The viscosity properties of solutions of the synthetized copolymers were investigated and were correlated to the yield of polymer and to the stabilization effects for polymerized emulsions of methyl methacrylate. On the basis of the experimental data the influences of inter- and intramolecular hydrophobic interactions on the stabilization effects of the copolymer solutions in suspension polymerization were discussed.

SOME CORRELATIONS OF THE EQUILIBRIUM THERMODYNAMICS OF THE ADSORPTION OF LIQUID MIXTURES AT SOLID-LIQUID INTERFACES

By

I. DÉKÁNY[1] and L. G. NAGY[2]

Department of Colloid Chemistry, József Attila University, Szeged, Hungary.
Department of Applied Chemistry, Budapest Technical University, Budapest; Central Chemical Research Institute of the Hungarian Academy of Sciences, Budapest, Hungary.

(Received September 26, 1977)

In the thermodynamic treatment of the adsorption of liquid mixtures on a solid-liquid interface, the most important regularities determining the adsorption equilibria for the mixtures were analyzed primarily on the basis of the work of SCHAY and NAGY. A study was made of how the shapes of the excess isotherms are influenced by modification of the surface of the adsorbent and by systematic variation of the mosaic structure of the surface, and a new model isotherm equation relating to this was introduced. The specific free enthalpy of immersion wetting was calculated by integration of the excess isotherms, and the influence of the surface modification on the shapes of these functions was analyzed. It was demonstrated that the energy of interaction on the solid-liquid interface (for a given binary liquid mixture) depends to a decisive extent on the proportions of the hydrophilic and hydrophobic surface parts, that is on the surface heterogeneity.

Introduction

Liquid phase adsorption differs from gas adsorption in a number of respects. In the case of liquid adsorption the surface of the adsorbent can always be regarded as completely covered, and it is not the surface coverage which changes as a consequence of the surface forces (as in the case of gas adsorption), but the proportions of the liquid components in the interfacial phase. This means that the composition of the interfacial phase in general differs from that of the liquid phase in equilibrium with it.

The immersion method may be used for the quantitative determination of the adsorption of liquid mixtures; a known mass m of adsorbent is submerged in a quantity N° of the liquid mixture in question, in which the mole franctions of the components are x_i^0 initially and x_i after the adsorption equilibrium has been established. The specific excess adsorption of the liquid mixture (n_i^σ) can therefore be calculated by measurement of the change in concentration of the mixture, in accordance with the following relation:

$$n_i^\sigma = \frac{N^0}{m}(x_i^0 - x_i) = n_0 \Delta x_i \quad (i = 1, 2, \ldots) \tag{1}$$

The physical content of the adsorption excess isotherm for the mixture, $n_i^\sigma = f(x_i)$, is illustrated by the following mass balance for binary mixtures:

$$n^0 x_1^0 = n_1^s + (n^0 - n^s)x_1 \qquad (2)$$

The OSTWALD-de IZAGUIRRE equation is obtained free from all assumptions from the mass balance:

$$n^0(x_1^0 - x_1) = n_1^\sigma = n_1^s - n^s x_1 = n^s(x_1^s - x_1) \qquad (3)$$

where $n^s = n_1^s + n_2^s$ is the mass content of the interfacial phase (*e.g.* mmole/g), and $x_1^s = n_1^s/n^s$ is the mole fraction of the interfacial phase. According to eqn. (3), therefore, the excess isotherm arises from a combination of the "individual" isotherms $n_1^s = f(x_1)$ and $n_2^s = f(x_1)$. The excess isotherms found experimentally for the adsorption of binary liquid mixtures can be classified into five basic types [1, 2]. The magnitudes of the adsorption capacities can be determined from the excess isotherms by means of the analysis procedure of SCHAY and NAGY [1—3].

In the case of the purely physical adsorption of binary liquid mixtures which mix in all proportions, it is possible to describe the selective adsorption of the liquid mixtures on a solid adsorbent on the basis of the thermodynamics of ideal and regular mixtures [1]. SCHAY and NAGY primarily studied the roles of the differences between the properties of the components of the liquid mixture (differences between the sizes of the molecules, and the strengths of their interactions) in the development of the characters of the isotherms. It may be stated that a difference between the components of the mixture, as a factor affecting the adsorption equilibrium, appears as an activity coefficient in the thermodynamic treatment of a liquid mixture. Investigations were made to establish the extents to which the selective adsorption is influenced by the magnitudes of the activity coefficients, their ratio, and variations in them, *i.e.* to determine what types of excess isotherms are obtained for the various mixtures [4, 6].

The sum of the present work is to present the thermodynamics of the adsorption equilibria of liquid mixtures and to establish the correlations, and on this basis to study how modifications of the surface of the adsorbent and surface heterogeneities of the adsorbent can be characterized with the functions introduced. Further, we should like to demonstrate that changes in the composition of the interfacial phase and also the extent of selective liquid sorption are influenced significantly not only by the properties of the liquid phase, but by the mosaic structure of the surface of the adsorbent too.

Equilibrium constant for adsorption of a liquid mixture

It follows from the displacement nature of the adsorption of a liquid mixture that enrichment of one the components on the surface is possible only by the expulsion of the other component. Accordingly, the adsorption of binary mixtures can be described by the following exchange reaction scheme leading to equilibrium:

$$\beta(1) + (2)^s \rightleftharpoons \beta(1)^s + (2) \qquad (4)$$

where $\beta = a_{m,2}/a_{m,1}$ is the exchange constant characteristic of the exchange cross-sectional areas of components (2) and (1). The cross-sectional areas of the components of the mixture can be calculated from the molar volumes of the pure liquids at the temperature of the isotherm.

(The upper index s always refers to the interfacial phase.) The equilibrium constant of the exchange process is

$$K = \frac{a_2 (a_1^s)^\beta}{a_2^s (a_1)^\beta} \tag{5}$$

or, introducing the activity coefficients:

$$K = \frac{x_2 f_2}{x_2^s f_2^s} \left(\frac{x_1^s f_1^s}{x_1 f_1} \right)^\beta . \tag{6}$$

For ideal mixtures consisting of molecules of the same dimensions, it holds that $f_2/f_1 = 1$ and $\beta = 1$, and if it is further assumed that the interfacial phase too behaves ideally, *i.e.* $f_1^s/f_2^s = 1$, then eqn. (6) simplifies to the following form:

$$K_{\text{ideal}} = \frac{x_1^s x_2}{x_2^s x_1} = S \tag{7}$$

where S is the separation factor for the adsorption of the liquid mixture; this may be determined in the knowledge of the compositions of the interfacial phase and the homogeneous liquid phase. In the above special case, therefore, $K_{\text{ideal}} = S$, but in general the separation factor is not constant, but is a function of the composition x_1 [7].

If the cross-sectional areas of the components of the mixture are approximately the same ($\beta \approx 1$) and the activity coefficients of the interfacial phase compensate one another ($f_1^s/f_2^s \approx 1$), then eqn. (6) can be written in the following form:

$$x_1^s = \frac{x_1}{\frac{1}{K'} \frac{f_2}{f_1} (1 - x_1) + x_1} = \frac{a_1}{\frac{1}{K'} a_2 + a_1} . \tag{8}$$

According to this equation, the equilibrium diagram $x_1^s = f(x_1)$ describing the adsorption of the mixture is determined by the change in the activity of the homogeneous liquid phase and by the value of K'.

By taking into account eqn. (8) and $x_2^s = 1 - x_1^s$, we obtain for the separation factor S defined in eqn. (7):

$$S = K' \frac{f_1}{f_2} . \tag{9}$$

The activity coefficients are generally calculated from liquid-vapour equilibrium data, or in the case of regular mixtures on the basis of the HILDEBRAND equations [6].

Thermodynamics of a monomolecular adsorption layer

In the thermodynamic discussion of a monomolecular adsorption layer, our considerations are based on the generally used conception that the field of the adsorbent acts as an external field on the interfacial layer of the liquid [1]. In general, if some external force acts on the molecules of a homogeneous phase, its potential must be included in the more strictly taken chemical potential in order for us to be able to describe equilibrium distributions.

In accordance with the above train of thought, if an adsorbent is wetted by some pure liquid, and the potential of the field of the adsorbent referred to one mole of the surface layer is η_i, then the condition of equilibrium is

$$\mu_i^s + \eta_i = \mu_i^l \tag{10}$$

As regards the potentials η_i introduced in the above, it must be noted that they refer to the total surface of the adsorbent, and if this surface is energetically heterogeneous, then they are average values. Since the wetting is an exothermic process, η_i is negative, and thus $\mu_i^s > \mu_i$; this can be interpreted in that the liquid behaves as if it is under compression in the field of the adsorbent, and hence its chemical potential is in itself increased [1].

For the chemical potential we may write

$$\mu_i^s = \mu_i^0 + RT \ln a_i^s \quad \text{and} \quad \mu_i = \mu_i^0 + RT \ln a_i \tag{11}$$

It must be added that these equations refer to the same standard state; that is, a_i^s does not become unity if a pure liquid is in contact with the adsorbent [1].

For binary mixtures the equilibrium conditions given by eqn. (10) are

$$\mu_1^s + \eta_1 = \mu_1^l \quad \text{and} \quad \mu_2^s + \eta_2 = \mu_2^l. \tag{12}$$

According to the above:

$$\ln \frac{a_1^s a_2}{a_2^s a_1} = \frac{\eta_2 - \eta_1}{RT} \tag{13}$$

or if the activities are expressed as products of the activity coefficients and the mole fractions:

$$\ln \frac{x_1^s x_2}{x_2^s x_1} = \ln S = \ln \frac{f_1 f_2^s}{f_2 f_1^s} + \frac{\eta_2 - \eta_1}{RT}. \tag{14}$$

The above relation indicates that the extent of selective liquid adsorption is influenced not only by the activity coefficients, but also by the difference in the molar adsorption potentials.

If the condition $f_1^s / f_2^s \approx 1$ is accepted (calculations [5, 6] show this to be permitted), then from eqn. (14) we obtain a correlation formally identical to eqn. (8):

$$x_1^s = \frac{x_1}{\frac{f_2}{f_1}(1 - x_1) e^{-(\eta_2 - \eta_1)/RT} + x_1} \tag{15}$$

where K' in eqn. (8) is given by $K' = e^{(\eta_2 - \eta_1)/RT}$.

After the experimental determination of the excess isotherm for adsorption of the mixture according to eqn. (1), the equilibrium diagram $x_1^s = f(x_1)$ can be determined on the basis of eqn. (3), and the value of K' can be calculated from eqns. (8) and (15) in the knowledge of the activities. In most cases it may be stated that the value of K' varies with the equilibrium composition x_1. This means that the η_i values are not constant either, since it is much more probable that the potential energy of a molecule in the field of the adsorbent is also influenced by what liquid molecules are in its immediate environment, and thus η_i depends on the composition.

The effect of surface modification on selective liquid sorption

Our investigation on the adsorptions of mixtures on various natural silicate adsorbents (primarily montmorillonite and kaolinite) indicate that excess isotherms of type II are obtained in the case of a binary polar-apolar liquid mixture (*e.g.* alcohol-benzene); that is, the alcohols are preferentially adsorbed on the silicate surface. It can be seen in Fig. 1 that compared to the isotherm observed for the

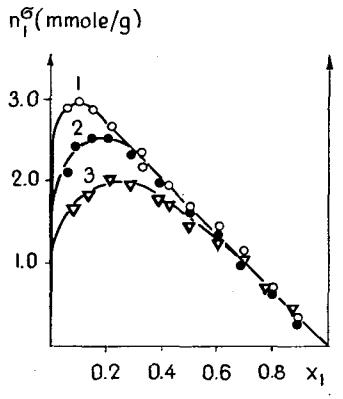

Fig. 1. Excess isotherms for adsorption of a liquid mixture on montmorillonites; 1. original, 2. sample treated with 1 : 1 water-isopropanol mixture, 3. sample treated with methanol. Mixture: methanol(1)-benzene(2)

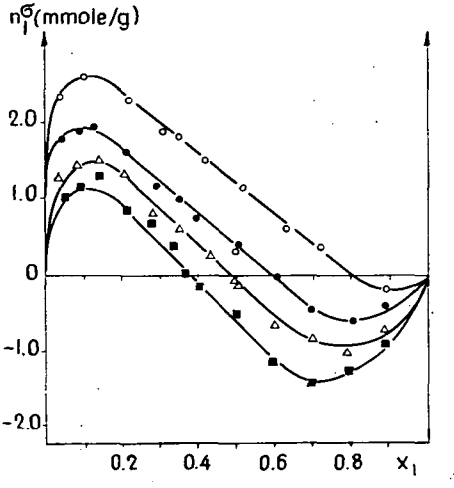

Fig. 2. Excess isotherms for adsorption of a liquid mixture on HDP-montmorillonites. Mixture: methanol(1)-benzene(2)

initially pure montmorillonite, the shapes of the isotherms are altered by pretreatment with alcohol; this may be explained by the chemisorption of the alcohols. This effect is essentially due to a slight surface modification. If the surface of the adsorbent is modified by some apolar compound (*e.g.* with hexadecylpyridinium cations by means of ion-exchange adsorption), the excess isotherms obtained for a polar-apolar mixture are of type IV; thus the apolar component is enriched in the interfacial

phase in a comparatively wide equilibrium concentration range [8—10] (Fig. 2). From analysis of the excess isotherms it can be stated that the adsorption capacity of the apolar component increases in proportion to the extent of the surface modification, and hence the components of the mixture are adsorbed *preferentially* on the surface parts of appropriate polarity. On the basis of concrete experimental data, this means that the magnitude of the surface part calculated from the adsorption capacity of the apolar component agrees well with the size of the modified surface part [11, 12].

Let us examine next how the value of K' can be correlated with the surface modification. Setting out from eqn. (6), let us assume that $\beta \approx 1$ and $f_1^s/f_2^s \approx 1$. For K' we then obtain:

$$K' = \frac{x_1^s x_2 f_2}{x_2^s x_1 f_1} = \frac{x_1^s a_2}{(1-x_1^s) a_1}. \tag{16}$$

Let us calculate the value of K' for the equilibrium composition x_1 where $a_2/a_1 = 1$. For the example of the methanol-benzene binary liquid mixture featuring in Table I, this composition is $x_1 = 0.68$. (For definitely regular mixtures the calculation must be carried out at a mole fraction $x_1 = 0.5$. (Since $x_1^s = n_1^s/n^s$ and $1 - x_1^s = n_2^s/n^s$, eqn. (16) can be written in the following form:

$$K'_{x_1=0.68} = \frac{x_1^s}{1-x_1^s} = \frac{n_1^s}{n_2^s} = K^*. \tag{17}$$

After WILLIAMS, the following equation may be written for a monomolecular layer completely covering the adsorbent:

$$n_1^s a_{m,1} + n_2^s a_{m,2} = a_{\text{equ.}}^s \tag{18}$$

where $a_{\text{equ.}}^s$ is the equivalent specific surface area. If eqn. (18) is divided by $a_{\text{equ.}}^s$:

$$\frac{n_1^s a_{m,1}}{a_{\text{equ.}}^s} = \theta_1 \quad \text{and} \quad \frac{n_2^s a_{m,2}}{a_{\text{equ.}}^s} = \theta_2 \tag{19}$$

i.e.

$$\theta_1 + \theta_2 = 1 \tag{20}$$

where θ_1 and θ_2 are the polar and apolar surface proportions, respectively. Hence, from eqns. (17) and (19), we obtain

$$K^* = \frac{\theta_1 \beta}{1-\theta_1} = \frac{(1-\theta_2)\beta}{\theta_2}. \tag{21}$$

If the value of K^* is substituted into eqn. (8), the equilibrium diagram can be calculated with the equation

$$x_1^s = \frac{x_1}{\frac{\theta_2}{(1-\theta_2)\beta}\frac{f_2}{f_1}(1-x_1) + x_1}. \tag{22}$$

The model isotherms calculated in accordance with the above equation and to be seen in Fig. 3 well illustrate the shapes of the functions that can be ascribed to the varius θ_2 values in the case of the binary methanol-benzene liquid mixtures.

If calculations are made with the apolar surface proportion $\theta_2 = a^s_{HDP}/a^s_{equ.}$ for hexadecylpyridinium-montmorillonites (HDP-montmorillonites) with surfaces modified to various extents, the model isotherms to be seen in Fig. 4 are obtained. (The characteristics of the adsorbents may be found in Table I).

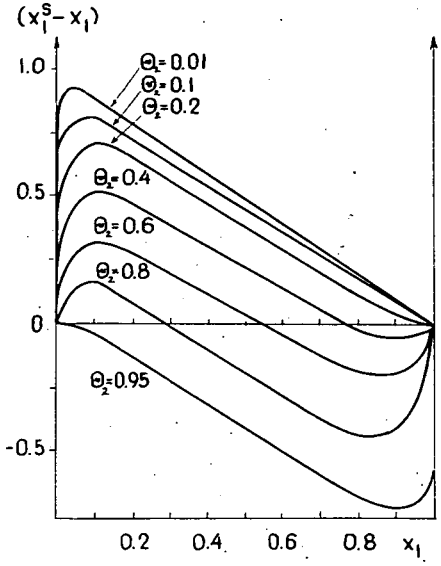

Fig. 3. Effect of surface modification on the shapes of the model isotherms on the basis of eqn. (22)

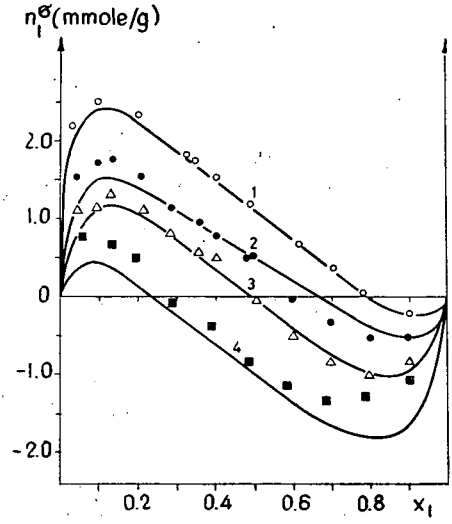

Fig. 4. Comparison of model excess isotherms and experimental data;
1. $\theta_2 = 0.326$, 2. $\theta_2 = 0.536$, 3. $\theta_2 = 0.635$,
4. $\theta_2 = 0.842$

Table I

Parameters characteristic of selective liquid sorption
Mixture: methanol(1)-benzene(2)

Adsorbent	HDP cation mequ./g	θ_2	$a^s_{equ.}$ (m^2/g)	$\varepsilon'_{2,0} - \varepsilon'_{1,0}$ (J/g)	$\Delta G^\sigma_{2,1}$ (mJ/m^2)	K (35) eqn.	K* (21) eqn.	x_1^a (24) eqn.	x_1^a exp.
montmorillonite	0.0	0.0	323	33.30	101.80	50.10	—	0.99	1.00
montm. (treated with methanol)	0.0	0.0	323	17.80	55.41	8.28	—	0.94	0.98
HDP-montm. I.	0.200	0.326	448	13.11	29.80	3.88	3.85	0.78	0.80
HDP-montm. II.	0.397	0.536	541	5.46	10.12	1.72	1.66	0.62	0.58
HDP-montm. III.	0.555	0.635	636	1.56	2.45	1.14	1.09	0.51	0.49
HDP-montm. IV.	0.683	0.678	733	0.59	0.80	1.06	0.99	0.47	0.43
HDP-montm. V.	0.812	0.773	764	−1.60	−2.10	0.88	0.59	0.36	0.37
HDP-montm. VI.	0.900	0.842	778	−2.85	−3.66	0.79	0.47	0.26	0.27

$$a_{m\,HDP} = 728\ m^2/mmol\ .\ \theta_2 = \frac{a^s_{HDP}}{a^s_{equ.}} \quad \beta = 1.8947$$

It can be seen that in the event of minor or moderate surface modifications the agreement with the experimental data is very good. The differences observed in the initial and final sections of the isotherm for the sample with $\theta_2=0.842$ can be explained by the appreciable desaggregation of the adsorbent (see the values of $a^s_{equ.}$ in Table I).

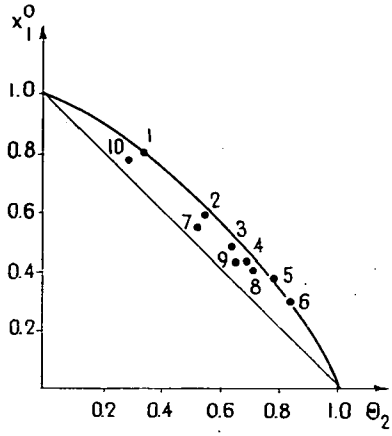

Fig. 5. Variation of the adsorption azeotrope composition with the surface modification according to eqn. (24)

The adsorption azeotrope composition (x^a_1) may also be correlated with the surface modification, for at the azeotrope composition the specific excess adsorption of the liquid mixture is

$$n^a_1 = n^s(x^s_1 - x_1) = 0, \quad \text{and so} \quad x^s_1 = x^a_1. \tag{23}$$

Hence, on the basis of eqns. (17) and (21), we may write

$$x^a_1 = \frac{K^*}{1+K^*} = \frac{\theta_1\beta}{\theta_2+\theta_1\beta}. \tag{24}$$

According to eqn. (24), the value of x^a_1 is determined to a first approximation by the magnitude of the polar-apolar surface ratio (*i.e.* by the mosaic structure of the surface), and also by β.

It can be seen in Fig. 5 and in Table I that the experimental x^a_1 values obtained for the adsorbent with its surface modified to various extents approximate very well to the function calculated with eqn. (24). Equation (24) provides a possibility for us to be able to characterize the mosaic structure of the surface of the adsorbent in the knowledge of the adsorption azeotrope composition.

Free enthalpy of immersion wetting

The thermodynamic laws regarding the interfacial interaction of a solid and a liquid can be expressed by the generalized equation of GIBBS—DUHEM type [1, 13]:

$$S^\sigma dT - V^\sigma dp + ZdF + \Sigma n^\sigma_i d\mu_i = 0. \tag{25}$$

In this equation, the notation σ means the corresponding excess of the extensive variables; the expression ZdF denotes the interfacial energy, written in general form, so that F is the corresponding intensity factor, and Z is the related extensive variable (*e.g.* it can be identified with the extent of the interface).

According to SCHAY [1], the generalized GIBBS—DUHEM equation can be written in the following concrete form for the adsorption of binary liquid mixtures on a solid surface:

$$S^{\sigma(2)}dT - V^{\sigma(2)}dp + m^a d\varepsilon' + n^{\sigma(2)}_1 d\mu_1 = 0 \tag{26}$$

where the index $\sigma(2)$ means the relative excess relating to component 2. In this equation the extensive variable Z is identified with m^a, the mass of the adsorbent, and the connected intensity factor will be denoted by ε'. An excess energy ε^a compared

to its compact state is characteristic of all extensively dispersed solid bodies (adsorbents) even in themselves, *i.e.* in vacuum, and the adsorption and wetting decrease this excess (exothermic adsorption and wetting heat). The notations

$$\varepsilon' = \varepsilon - \varepsilon^a \quad \text{and} \quad \varepsilon' < 0 \tag{27}$$

are introduced into eqn. (26) in such a sense. It should be noted that the corresponding correlations are usually written in general for ε instead of ε' in the relevant literature, or for the very problematical surface tension even in the case of a solid-liquid interface [14—16].

Under the customary conditions of experimental determination of liquid adsorption isotherms, *i.e.* at constant temperature and pressure, the form of the equation of the GIBBS adsorption isotherm valid for this case follows from eqn. (26):

$$-d\varepsilon' = \frac{n_1^{\sigma(2)}}{m^a} d\mu_1. \tag{28}$$

Since the following relations hold between the reduced and relative excesses [1]:

$$n_1^{\sigma(n)} = -n_2^{\sigma(n)} = x_2 n_1^{\sigma(2)} = -x_2 n_2^{\sigma(1)} \tag{29}$$

and since $d\mu_1 = RT\, d \ln a_1$, after the substitutions we obtain from eqn. (28):

$$-d\varepsilon' = RT \frac{n_1^{\sigma(n)}}{m^a x_2} d \ln a_1. \tag{30}$$

Integrating eqn. (30) over the total composition interval:

$$\varepsilon'(a_2 = 1) - \varepsilon'(a_1 = 1) = RT \int_{a_1=1}^{a_2=1} \frac{n_1^{\sigma(n)}}{x_2 a_1} da_1 \tag{31}$$

where $\varepsilon'(a_2=1) - \varepsilon'(a_1=1) = \varepsilon'_{2,0} - \varepsilon'_{1,0}$ is the difference in the excess energy changes relating to the interfaces between the solid and pure component 2 and 1, respectively. (The dimensions are, for example, joule/g or erg/g.) Integration of the excess isotherm is performed graphically, and it is beneficial to reckon with the specific excess adsorption of the liquid mixture, *i.e.* $m^a = 1$ g. Numerous references are to be found in the literature with regard to the application of eqn. (31) [17—19].

The variation of ε' as a function of the composition is illustrated in the following two Figures. The function to be seen in Fig. 6/A is obtained by integration of excess isotherms of types I, II and III; the value of the integral, $\varepsilon' - \varepsilon'_{1,0} = \Delta\varepsilon'$, is always positive. The function in Fig. 6/B arises from isotherms of types IV and V; in a certain range of composition, $\varepsilon' < \varepsilon'_{1,0}$, the value of the integral may also be negative [20—22].

By integration of our adsorption excess isotherms determined for liquid mixtures on montmorillonites and their organophilic derivatives [10, 11, 23], we calculated the variation of $\Delta\varepsilon'$ with the equilibrium composition in accordance with eqn. (31). It can be seen in Fig. 7 what functions are characteristic for the adsorption of a benzene-n-heptane mixture on montmorillonite and two organophilic montmorillonites (isotherm of type I).

Figure 8 demonstrates very illustratively how the course of the $\Delta\varepsilon'$ function is influenced by surface modification (organophilization) for a methanol-benzene mixture (isotherm of type IV). On the above basis it may be stated that adsorbents with different surface heterogeneities can be characterized in an exact way in a thermodynamic sense with the excess energy change calculated from integration of the excess isotherm.

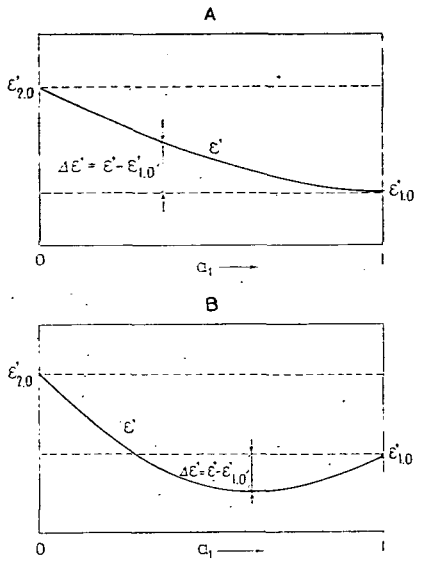

Fig. 6. Variation of ε' defined by eqn. (27) with the activity of the equilibrium homogeneous liquid phase

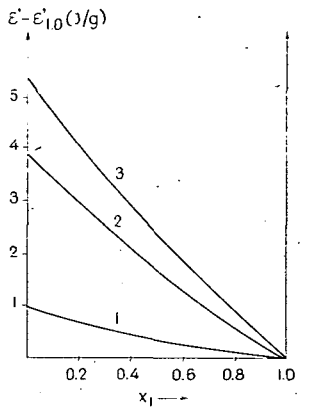

Fig. 7. Variation of $\Delta\varepsilon'$ with the equilibrium composition in the case of isotherms of type I; 1. montmorillonite, 2. $\theta_2 = 0.635$, 3. $\theta_2 = 0.842$

According to the thermodynamic laws of adsorption [1, 13], the excess free enthalpy can be given by the following equation:

$$G^\sigma = H^\sigma - TS^\sigma = FZ + \Sigma\mu_i n_i^\sigma. \tag{32}$$

In the case of the adsorption of binary liquid mixtures ($FZ = m^a\varepsilon'$):

$$G^{\sigma(2)} = m^a\varepsilon' + \Sigma\mu_1 n_1^{\sigma(2)}. \tag{33}$$

In the simplest case, when the adsorbent is immersed into a pure liquid, when adsorption does not occur in the sense of the GIBBS convention, since $n_1^{\sigma(2)} = 0$ and $m^a = 1$ g, eqn. (33) reduces to

$$G = \varepsilon' \tag{34}$$

where the ε' defined in eqn. (27) is equal to the specific free enthalpy of the immersion wetting, but ε' is not the same as the calorimetrically measured wetting enthalpy (immersion heat); the difference is given by eqn. (32). Hence, the value of $\varepsilon'_{2,0} - \varepsilon'_{1,0}$

obtained from integration of the excess isotherm is *the difference in the specific free enthalpies of immersion wetting in the pure components 1 and 2.* The notation $\Delta G^{\sigma}_{2,1}$ is used to indicate reference to unit surface area (see Table I).

The difference in the specific free enthalpies of immersion wetting in methanol(1) and in benzene (2) is depicted in Fig. 9 as a function of the surface modification.

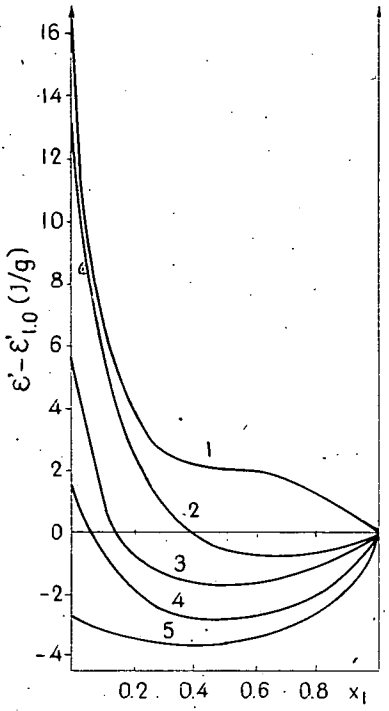

Fig. 8. Variation of $\Delta\varepsilon'$ with the equilibrium composition in the case of isotherms of type IV;
1. montmorillonite, 2. $\theta_2=0.326$, 3. $\theta_2=0.536$, 4. $\theta_2=0.678$, 5. $\theta_2=0.842$

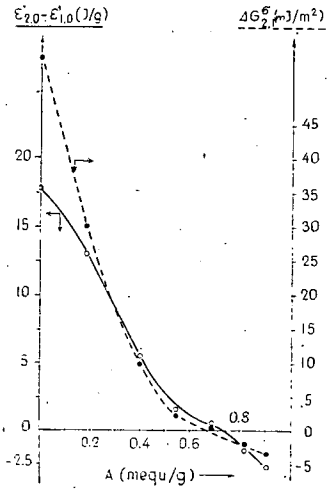

Fig. 9. Variation of the difference in specific free enthalpy of immersion wetting with the surface modification. A: HDP cation (mequiv./g)

The calculation show that the value of $\varepsilon'_{2,0}-\varepsilon'_{1,0}$, or $\Delta G^{\sigma}_{2,1}$, is considerable on the high-energy silicate surface; then, with increase of the apolar character of the surface, it decreases rapidly and changes in sign. The negative range (where $\varepsilon'_{2,0}<\varepsilon'_{1,0}$) is characteristic of organophilic montmorillonites of strongly hydrophobic character, with apolar surfaces.

Similar calculations were performed by PARFITT *et al.* [18] to characterize graphite surfaces with varius properties, with the essential difference that, instead of $\varepsilon'_{2,0}-\varepsilon'_{1,0}$, they calculate with the surface tension difference $\sigma^0_2-\sigma^0_1$, which is difficult to interpret in the case of a solid/liquid interface.

$\varepsilon'_{2,0}-\varepsilon'_{1,0}$ obtained by integration of the excess isotherms in accordance with eqn. (31) can be correlated with the equilibrium constant for adsorption of the liquid mixture [7, 16]:

$$\frac{\varepsilon'_{2,0}-\varepsilon'_{1,0}}{n^s RT} = \ln K \tag{35}$$

MYERS *et al.* [16, 17] state that the equilibrium constant K may be calculated in the following manner:

$$\frac{a^s_{\text{equ.}}(\sigma^0_2-\sigma^0_1)}{n^s RT} = \ln K. \tag{36}$$

According to eqn. (35), therefore, the constant K can be determined directly by integration of the excess isotherm over the total concentration interval. Strictly, however, the value of K is constant only if the adsorption capacity n^s too is constant; this is possible if the molecular dimensions of the components of the mixture are the same, *i.e.* if $\beta = a_{m,2}/a_{m,1} = 1$ [1, 7].

If the constant K determined in accordance with eqn. (35) is substituted in place of K' in eqn. (8) we may calculate the equilibrium diagram $x^s_1 = f(x_1)$ and, in the knowledge of n^s, the excess isotherm too. Our calculations confirmed that for the given system (by taking into consideration the activity coefficients) we do indeed obtain an isotherm approximating well to the experimental data; thus, our results can be regarded as thermodynamically consistent. In essence, the model isotherms to be seen in Fig. 3 confirm the applicability of the thermodynamic consistency test, with the difference that here calculations were made not with K, but with the K^* values defined in eqn. (21). On the other hand, it emerges from the data of Table I that the K values obtained by integration display an approximately good agreement with K^*, and therefore, on the basis of a comparison of eqns. (21) and (35), we may write:

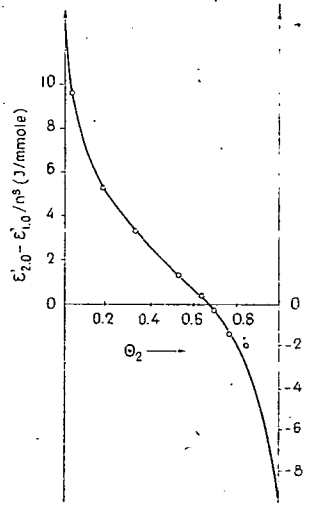

Fig. 10. Comparison of eqn. (37) with the experimental data

$$\varepsilon'_{2,0}-\varepsilon'_{1,0} \approx RTn^s \ln \frac{(1-\theta_2)\beta}{\theta_2}. \tag{37}$$

Thus, according to the above, the difference in specific free enthalpies of immersion wetting in liquids of different polarities is determined decisively by the apolar-polar surface ratio, and by the adsorption capacity. When the $(\varepsilon'_{2,0}-\varepsilon'_{1,0})/n^s$ values are calculated in accordance with eqn. (37) as a function of θ_2, the logarithmic function drawn as a continuous line in Fig. 10 is obtained. On the basis of eqn. (31), the integral values calculated with adsorbents of different organophilicities correspond to the course of the function.

The authors wish to express their thanks to Prof. Dr. GÉZA SCHAY, Academician, for his advice in connection with the interpretation of the results.

References

[1] *Schay, G., L. G. Nagy:* A kémia újabb eredményei **18,** Akadémiai Kiadó, Budapest, 1974.
[2] *Kipling, J. J.:* Adsorption from Solutions of Non-Electrolytes, Academic Press, London, 1965.
[3] *Schay, G.:* in "Proc. Int. Symp. Surface Area Determination", 273 p. Ed. D. H. Everett, London, Butterworths 1970.
[4] *Nagy, L. G., G. Schay:* Magy. Kémiai Folyóirat **66,** 31 (1960).
[5] *Schay, G., L. G. Nagy:* J. Chim. Phys. 149 (1961).
[6] *Nagy, L. G., G. Schay:* Magy. Kémiai Folyóirat **73,** 298 (1967).
[7] *Everett, D. H.:* Colloid Sci. Vol. 1. The Chemical Society London 1973.
[8] *Dékány, I., F. Szántó, L. G. Nagy, G. Fóti:* Magy. Kémiai Folyóirat **80,** 231 (1974).
[9] *Dékány, I., F. Szántó, L. G. Nagy, G. Fóti:* J. Colloid Interface Sci. **50,** 265 (1975).
[10] *Dékány, I., F. Szántó, L. G. Nagy:* Magy. Kémiai Folyóirat **82,** 491 (1976).
[11] *Dékány, I., F. Szántó, L. G. Nagy:* J. Colloid and Polymer Sci. *256,* 150 (1978).
[12] *Dékány, I., L. G. Nagy, G. Schay:* Magy. Kémiai Folyóirat 1978. (under press).
[13] *Schay, G.:* Int. Conference Colloid and Surface Sci. Budapest, 1975. (plenary lectures).
[14] *Larinov, O. G., A. L. Myers:* Chemical Eng. Sci. **26,** 1025 (1971).
[15] *Sircar, S., A. L. Myers:* Amer. Inst. Chem. Engineers J. **17,** 186 (1971).
[16] *Sircar, S., A. L. Myers:* J. Phys. Chem. **74,** 2828 (1970).
[17] *Myers, A. L., S. Sircar:* J. Phys. Chem. **76,** 3412 (1972).
[18] *Parfitt, G. D., P. C. Thompson:* Trans. Faraday Soc. **67,** 3372 (1971).
[19] *Nagy, L. G.:* Periodica Polytechnica **7,** 75 (1962).
[20] *Tóth, J.:* Acta Chim. Acad. Sci. Hung. **63,** 67 (1970).
[21] *Tóth, J.:* Acta Chim. Acad. Sci. Hung. **63,** 197 (1970).
[22] *Tóth, J.:* J. Colloid Interface Sci. **46,** 38 (1974).
[23] *Szántó, F., I. Dékány, L. G. Nagy:* Proc. Int. Conference Colloid and Surface Sci. Vol. 1. 99 p. (Ed. E. Wolfram), Akadémiai Kiadó, Budapest, 1975.

НЕКОТОРЫЕ ТЕРМОДИНАМИЧЕСКИЕ АСПЕКТЫ АДСОРБЦИИ ИЗ ЖИДКИХ СМЕСЕЙ НА ПОВЕРХНОСТИ ТВЕРДЫХ ТЕЛ

И. Декань и Л. Дь. Надь

Термодинамическое рассмотрение вопросов адсорбции из жидких смесей на границе раздела фаз жидкость-твердое тело проведено на основании изотерм адсорбции по работам Шай и Надя. Изучено влияние систематического изменения мозаичной структуры поверхности на вид кривых изотерм адсорбции и предложено новое уравнение изотермы адсорбции для таких случаев. Из уравнения изотермы рассчитана специфическая свободная энергия смачивания и проведен анализ влияния модификации поверхности на вид уравнений. Показано, что энергия взаимодействия на границе жидкость-твердое тело (для принятой бинарной смеси) зависит главным образом от соотношения гидрофильных и гидрофобных частей т. е. от мозаичности поверхности.

REFLECTIONS ON CONTROL OF PEPTIDE SYNTHESIS*)

By

K. BRUNFELDT

The Danish Institute of Protein Chemistry,
affiliated to The Danish Academy of Technical Sciences, 4 Venlighedsvej,
DK—2970 Hørsholm, Denmark

(Received 1 September 1977)

Three principal possibilities for the analytical control of the effectiveness of coupling and deprotection steps during the solid phase peptide synthesis are the following: 1. analysis on samples 2. determination on the whole batch of resin-bound peptide. 3. measurement on the liquid phase. These different methods are discussed in detail.

In the past few decades a dramatic and ever increasing broadening of our insight into living matter has taken place. The growing information about hormones, enzymes, and other susbstances of a protein nature in the normal and the pathologic organism has for various reasons augmented the demand for synthetic peptides for biochemical and biological studies or for use in the clinic.

To the young generation, peptide synthesis certainly appears to be a rather modern invention. The fact is, however, that it dates back to 1882 in Leipzig, when the 25-year-old THEODOR CURTIUS, assistant to professor HERMAN KOLBE, reported the first synthesis of a peptide [1]. The result was achieved inadvertently by benzoylation of silver glycinate in an attempt to clarify the structure of hippuric acid. He thus carried out the first mixed anhydride coupling resulting in the formation of benzoyl-glycylglycine. About 70 years later CURTIUS' experiment inspired THEODOR WIELAND to initiate his studies of mixed anhydrides. As is well known, EMIL FISCHER also contributed to the origin of peptide synthesis, and in 1907 he was able to report the synthesis of a leucine and glycine-containing peptide consisting of 18 amino acid residues [2].

Elemental analysis was the only method of control at hand for CURTIUS and FISCHER, and is today — almost 100 years after the first reported peptide synthesis — still a fundamental method for characterization of low molecular weight peptides.

The real challenge to peptide synthesis was launched in 1955, when SANGER reported the complete amino acid sequence of bovine insulin [3]. Peptide synthesis can in no way be said to have caught up with the rate with which larger and larger proteins are being sequenced.

Two main principles are applied in the attempts to synthesize larger peptides by organic chemical means, which involves the use of organic solvents. In one case,

* Based upon lectures given at the Universities of Szeged and Budapest, Hungary, and the Institute of Bioorganic Chemistry, USSR Academy of Sciences.

called synthesis in solution, larger chains are obtained by condensation of fragments. In another case, the synthesis is performed on a polymeric support, and the growing peptide is covalently bound to the polymer, which is generally insoluble. This method is termed solid-phase peptide synthesis. In this case, stepwise elongation is usually preferred.

In both synthesis in solution and in solid-phase synthesis, the chain elongation is carried out from the C-terminal amino acid in order to avoid racemization. The advantage of synthesis in solution — whether by stepwise chain elongation or by fragment condensation — is that in principle an intermediate purification is possible, especially if the intermediate products can crystallize. An advantage of fragment condensation compared to the stepwise approach is that the isolation is in principle facilitated by the pronounced difference in molecular size between the reactants and the product.

The yield of a single reaction in synthesis in solution is thus not crucial for obtaining the final product as long as isolation of the desired product is possible, whether this be an intermediate or the final product. Serious obstacles, however, fairly soon set a limit as to how large molecules can be built by synthesis in solution, restricting the considerations to the synthesis of molecules with a predetermined sequence and not considering polyamino acids.

One of the limitations to the use of synthesis in solution is the fact that the solubility of the protected peptides may be low and is decreased by increasing chain length. The coupling reaction in such a case is therefore carried out with the reactants partly dissolved, and the phrase 'synthesis in solution' is then not a very correct one.

The low solubility also restricts the use of an excess of the acylating fragment, and the coupling between large fragments is hampered significantly by the size of the molecule and proceeds slowly. If glycine is not the C-terminal amino acid in the activated fragment, there always exists a danger of racemization, due to the adjacent peptide bond. Finally an economic consideration is involved, as peptides are always expensive.

The fundamental advantage of fragment condensation is that the amino acid sequence in the final product is the desired one, as it corresponds to the fragments assembled.

The evidence demonstrates that it is possible to obtain reasonable quantities of products of high purity, containing 30—40 amino acid residues, but it should be stressed that the results have always required a very great effort. The synthesis of sheep insulin by ZAHN and coworkers [4] and later of ox insulin by a Chinese group [5], in amounts which were sufficient for crystallization, are certainly the most impressive achievements in classical peptide synthesis.

In the solid-phase technique, the isolation of the reaction product is carried out by simple filtration, and the procedure of chain elongation can be automated. Whether all solubility problems are circumvented, however, is open to discussion. Thus, it cannot be excluded that the use of certain solvents might result in a conformation of the polymer-bound peptide unfavorable to the process of chain elongation. The shortcomings of the solid-phase technique are inherent in the very principle. Thus, shorter peptides lacking one or more residues will be accumulated if the addition of an amino acid is not performed with a yield of 100%. Furthermore, damage which takes place to a slight degree in each step will be aggravated due to the repe-

titive procedure. Difficulties may also be encountered in the cleavage of the final product from the polymer. The application of the technique therefore easily results in a very complex mixture of peptides, from which it is often impossible to isolate the desired product.

In the synthesis of large peptides either in solution or by the solid-phase technique, mainly naturally-occurring substances have been prepared. In these cases a comparison of the synthesized product with the authentic substance is possible. When dealing with complex reaction mixtures one is lost, unless additional information can be obtained. In fact, with large molecules we must be content with an examination of biological or biochemical activity. However, such an activity may be due to the presence of shorter sequences or other byproducts. In the case of the synthesis of large molecules possessing only slight or no hormonal or enzymatic activity at all, no adequate proof of the achievement of the synthesis is at present obtainable.

The analytical problems to cope with in peptide chemistry when not considering rather small peptides are complex, and the complexity increases with increasing molecular size. The above-mentioned considerations only dealt with the process of chain elongation. For both the mentioned synthetic principles, however, common problems exist regarding protection and deprotection of functional side-chain groups, due to the fact that no procedure is at hand for a specific formation of the peptide bond between the α-amino and α-carboxyl groups.

Amino acid analysis is widely used in the control of the synthesis and is often considered a trivial matter of routine. In fact, however, even when we are dealing with small proteins, the shortcomings of the technique are evident. Several hydrolyses have to be performed with and without additives. In order to achieve usable results for some amino acids, it may even be necessary to correct the values through comparison with the values for these amino acids obtained by analysis of a closely-related protein with known sequence.

The introduction of the solid-phase technique by MERRIFIELD [6], LETSINGER and KORNET [7] was received with enthusiasm. The reasons were the facility of isolation of the resin-bound product, the relative ease of automation and the possibility of scaling up the synthetic procedure. The results, however, have not fulfilled the expectations. The ease with which the procedure is carried out has led many astray, tyring to synthesize much larger molecules than the technique allows. For the synthesis of chains of up to approximately 30 amino acids, the technique has turned out to be valuable in several cases, especially where a rigorous purification is possible, as in the case of cyclic peptides. By fragment condensation on the resin, using Pro-Pro-Gly SAKAKIBARA *et al.* prepared $(Pro\text{-}Pro\text{-}Gly)_{10}$. A sufficient purity for crystallization of the final product was obtained [8].

Calculations have been carried out by Bayer et al. of the required minimum yield of the single increment for a certain yield of the desired peptide. The calculations are based on the C-terminal polymer-bound amino acid [9]. Provided there is a yield of 99% for the addition of each amino acid, the total yields of the desired polymer-bound peptide chains for human growth hormone, consisting of 190 residues, and for the A-chain of insulin, consisting of 21 residues, are 15 and 82%, respectively. However, low yields in some steps of the synthesis, and damage occuring during the process of chain elongation or through the cleavage of the product from the resin or the deprotection, often result in a low total yield and lead to a mixture of closely-

related substances, from which it may be impossible to isolate the desired peptide. Cleavage of peptide from the resin during the synthesis leads to a reduction of the total yield, but it does not complicate the isolation procedure.

It is evident, therefore that unless at least the process of chain elongation is brought under control, the solid-phase technique is not to be expected to be generally applicable. The ideal solution for the monitoring of the process would be an automated non-destructive continuous procedure for determination of the number of free amino groups liberated by cleavage of the α-amino protection group, and the number of peptide bonds formed during each coupling. This would allow us to follow the time-course of the reaction and determine the final yields. No such method exists, however.

An excellent survey of the literature dealing with analytical procedures applied is solid-phase syntheses up to 1973 is given by HIRT *et al.* in Chemistry of Polypeptides, Essays in Honor of Leonidas Zervas [10].

The developed methods most suited for monitoring are based on determination of the number of free amino groups after the coupling and after the cleavage of the protection group. Indirect measurement has been carried out by UV monitoring of the liquid phase after deprotection or coupling.

Three principal possibilities exist for carrying out an analytical control: 1) analysis on samples; 2) determination on the whole batch of resin-bound peptide; 3) measurement on the liquid phase (Fig. 1).

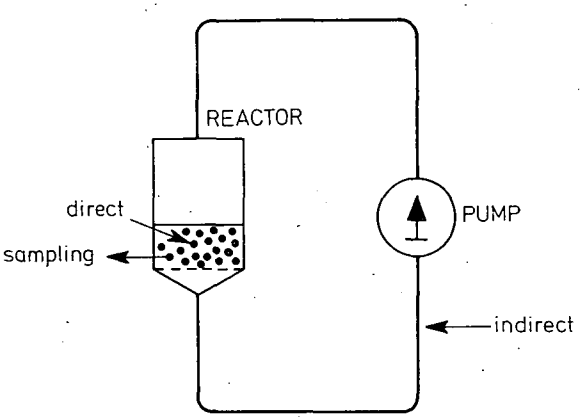

Fig. 1. Different principles for analytical control of solid-phase synthesis [10*a*]

1. Sampling

Several analytical procedures have been applied for analysis on samples, thus for example automatic Edman degradation, mass-spectrometry, amino acid analysis and Schiff base formation. For detection of residual amino groups after the coupling, ninhydrin was used by KAISER *et al.* [11]. As little as 5 μmole/g resin can be detected. It is difficult, however, to evaluate whether the test is positive or negative, especially if the resin is colored during the synthesis. The use of fluorescamine was introduced

by FELIX and JIMENEZ [12]. By this method as little as 0.6 μmole/g resin is claimed to be detected. The experience up to now is rather limited and interference from non-specific binding seems to reduce the value of the test. With ninhydrin N-terminal proline and β-benzyl aspartate only give rise to an unsatisfactory color development; with fluorescamine no reaction takes place with proline.

Quantitative analysis based on samples is complicated, because it must be known with great accuracy how much the sample amounts to of the total quantity of peptide resin. In synthesis on a minor scale this can be determined by drying the total mount of resin and carrying out the analysis on an aliquot. In principle this determination could be facilitated by the use of an internal standard, also making it possible to monitor a synthesis on a large scale, but up to now this appears not to have been achieved.

Quantitative measurements of free amino groups by titration with perchloric acid on samples have been carried out by SCHOU [13] (Fig. 4). The starting amount of resin was 25 g, and 1 g was withdrawn after each deblocking and coupling cycle. Regarding the perchloric acid titration, a closer description will be given in the following.

The development in high performance liquid chromatography, HPLC, has resulted in a highly efficient technique for analyzing peptide preparations. Coupling with a fluorescent compound may facilitate the detection of peptides with a free amino group [13*a*]. Characterization by HPLC is to be considered as a standard procedure in peptide synthesis for investigation of the homogeneity of the end product, even regarding chirality [13*b*].

The possibility of carrying out the separation on a small scale makes the method applicable for monitoring of peptide synthesis, however, by solid phase synthesis, taking into consideration artefacts deriving from the cleavage of the peptide from the resin. The fact that small scale preparative fractionation is easily performed allows a closer examination of the various fractions, for example by mass spectrometry [35].

2. *Determination on the whole batch of resin-bound peptide*

MERRIFIELD [14] introduced a procedure for the estimation of the amount of free amino groups, after cleavage of the Boc groups with N HCl/HOAc. The resin was treated with triethylamine in dimethyl formamide, the filtrates were collected and the chloride was determined by the Volhard procedure. BAYER *et al.* [15] used this procedure to monitor the synthesis of apoferredoxin, 55 residues, and demonstrated a significant decrease in free amino groups during the synthesis. DORMAN modified the procedure so that it could also be used for measurement of residual free amino groups after the coupling [16]. This was achieved by using pyridine hydrochloride for conversion of free amino groups into the hydrochloride. The hydrochloride is removed by triethylamine and the chloride is determined in the collected filtrates.

GISIN [17] used picric acid for protonation of the free amino groups. After displacement of the bound picric acid by diisopropyl-ethylamine, the amount was determined photometrically. This procedure has been automated [18]. However, adsorption of picric acid on the polymer seems to create complications.

In our institute we have investigated a procedure for the estimation of free amino groups based on a potentiometric end-point titration with perchloric acid in acetic acid, with the resin suspended in a mixture of methylene chloride and acetic acid [19]. By the applied procedure, the same end-point can be used irrespective of the N-terminal amino acid. This is because the acetic acid protonates the amino groups and is replaced by the perchlorate. It is thus in fact the acetate ions which are titrated and not the amino groups, a so-called levelling effect. As this takes place mainly inside the resin, the titration may proceed rather slowly, usually lasting from 5 min up to 1 hour. The accuracy of the determination, however, is rather high: up to $\pm 0.3\%$ per single determination.

The procedure can be carried out on the entire batch or as previously mentioned on withdrawn samples. The procedure has been included in systems for automated peptide synthesis, and in this case the titration is carried out on the entire amount of resin [20, 21].

It is to be stressed that the method is not specific for amino groups, as other groups may be sufficiently basic to allow a titration under the conditions applied. Thus, the imidazole group of Boc-benzyl histidine is titrated, leading to an equivalent increase in the titration value [22].

As a strong acid such as perchloric acid is used for the titration, the utmost care must be taken to reduce the danger of overtitration even locally in the liquid phase close to and in the resin. Otherwise, cleavage of acid-labile protection groups such as Boc may take place.

The titration must therefore be carried out as an automatic end-point titration with a slow addition of the titrant and adjustment of the titrator ensuring a proportional slowing down of the addition of titrant within the preset proportional band. The stirring must be highly effective.

As mentioned, one of the potential errors of the solid-phase technique is an accumulation of artefacts during the synthesis, such as blocking of α-amino groups leading to so-called truncated peptide chains. By the perchloric acid titration it has been possible to demonstrate blocking of amino groups by impurities present in methylene chloride [23], during coupling with histidine [22] and by residual acetic acid [24]. The last example is rather informative and will therefore be dealt with further in detail.

The experiment concerned the synthesis of a sequence of the cyclic decapeptide antamanide, and was carried out and controlled automatically by a punched-tape controlled synthesizer. Dicyclohexyl-carbodiimide (DCC) was used as coupling reagent and tertiary-butyloxy-carbonyl (Boc) for protection of the α-amino groups. The result was rather disappointing because it seemed completely inconsistent with what was to be expected [20]. However, we have been able to show that the titration reflected exactly what really occurred, and via the obtained information we have been able to improve the synthetic procedure.

In the first attempt, starting the synthesis with coupling of Boc-proline to a proline resin, the titration indicated a pronounced loss of the ester-bound proline due to formation of proline diketopiperazine. A new attempt was then made by coupling of Boc-alanine to a phenylalanine-resin.

As seen from Fig. 2, the total yield was low, approximately 20%, as calculated by subtraction of the value of the Boc-protected N-terminal phenylalanine from the value obtained after cleavage of the Boc-group and the difference compared with

the corresponding value for the C-terminal phenylalanine. It is seen that the decreases in certain positions are more pronounced than in others. In the titration values of the Boc-protected peptide chains an increase occurred, especially after the incorporation of Boc-valine.

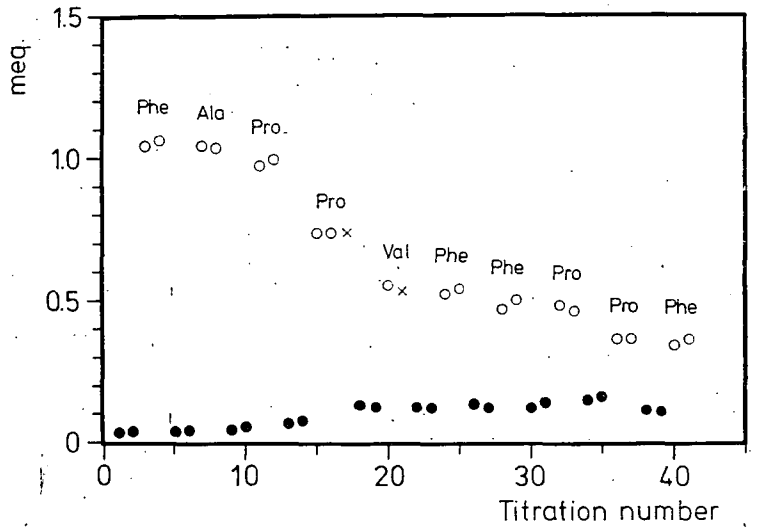

Fig. 2. Titration values determined during the synthesis of the sequence of antamanide: HPhe-Pro-Pro-Phe-Phe-Val-Pro-Pro-Ala-Phe-resin. x indicates that the procedure for cleavage of the Boc group was repeated before the titration. Filled circles before, and open circles after Boc group cleavage [20]

A repetition of the cleavage procedure at the tetra- and pentapeptide stage did not result in higher values, indicating irreversible blocking of the amino groups. If so, a number of shorter peptides should be present in the final product, and amino acid analysis of the total product should differ considerably from the theoretical.

Peptide expected: D_3CCO - Phe - Pro - Pro - Phe - Phe - Val - Pro - Pro - Ala - Phe - OMe

Identified : D_3CCO - Phe - Pro - Pro - Phe - Phe - Val - Pro - Pro -

Shorter peptides identified:
- Ac - Pro - Ala - Phe - OMe
- Ac - Pro - Pro - Ala - Phe - OMe
- Ac - Phe - Phe - Val *
- Ac - Pro - Phe - Phe - Val - Pro - Pro - Ala -

Failure sequences:
- Ac - Pro —— Phe —— Val - Pro *
- Ac - Pro - Phe - Phe - Val —— Pro —— Ala *
- D_3CCO - Phe —— Pro —— Phe - Phe - Val *

*) near detection limit.

Fig. 3. Peptides demonstrated by mass-spectrometry to be present in the product, cleaved from the resin in the experiment shown in Fig. 2 [24].

The presence of the predicted peptides was confirmed by mass-spectrometry, and the blocking shown to be due to acetylation (Fig. 3). The mass-spectrometric analysis was carried out on the entire mixture after deutero acetylation and permethylation, using a technique developed for mass-spectrometric sequence determination of peptide mixtures [25]. By the mass-spectrometry the presence of peptides lacking a proline or a phenylalanine residue due to incomplete coupling is also demonstrated. The reason why only missing proline or phenylalanine residues are demonstrated is probably that these are repeated, and absence of one of them thus leads to the same deleted sequence, and thus to a higher concentration of these sequences.

The reason for the acetylation was that a reactor chiefly made of teflon had been used. Due to the microporosity of teflon, acetic acid was absorbed during the deblocking and titration cycle, and this leaked out during the coupling cycle and was activated by the coupling reagent, DCC. The reason why the acetylation was more pronounced in the coupling of Boc-proline to proline and Boc-valine to proline is simply that these couplings proceed more slowly than the others, allowing more acetic acid to be washed out before the coupling of the derivative was terminated.

Let us return to the Figure illustrating the synthesis. As the blocking occurs during the coupling cycle, theoretically the amount of each amino acid incorporated can be calculated by subtracting the titration value after the coupling from the value after the cleavage of the Boc group. Thus, it is possible to calculate the amino acid composition of the final product — provided loss of peptide does not take place, or to only a slight degree, during the synthesis.

As seen from Table I, A, the amino acid analysis of the resin-bound product shows a fairly good agreement with the titration, thus proving the correctness of the

Table I

Amino acid content of synthetic decapeptide determined by titration and by amino acid analysis [26]

Boc-Phe-0-resin	Amino acid	Theo-retical	Titration	Amino acid analysis			
	Phe	4	4.00	4.00[1]	4.00[2]	4.00[3]	
2.2 g	Ala	1	1.97	1.74	1.88	1.92	
1.00 mequiv (A)	Pro	4	4.23	4.52[4]	4.55[4]	4.73[4]	
	Val	1	0.82	0.76	0.77	0.82	
	Phe	4	4.00	4.00[1]		4.00[3]	4.00[5]
2.9 g	Ala	1	1.20	1.13		1.09	1.01
1.32 mequiv (B)	Pro	4	4.02	3.92[4]		4.16[4]	3.97[4]
	Val	1	0.98	0.97		1.06	1.01
	Phe	4	4.00	4.00[1]		4.00[3]	4.00[5]
6.0 g	Ala	1	1.27	1.08		1.05	1.00
2.74 mequiv (C)	Pro	4	4.04	3.57[4]		3.59[4]	3.96[4]
	Val	1	0.98	0.96		0.92	0.98

[1] Resin-bound product.
[2] Cleaved crude product.
[3] Ether-precipitated product.
[4] Proline (amino acid analysis) corrected for concentration-dependency of calibration factor.
[5] Cyclized peptide (antamanide).

titration values. The experiment clearly demonstrates why amino acid analysis in the synthesis of even small peptides by the solid-phase method may be impossible to interpret. By manually carrying out the synthesis in an all-glass reactor, the total yield of resin-bound peptide calculated from the titration values could be increased to 64% (Table I, B and C). Still, a gradual decrease could be observed in the titration values after deblocking, and also an increase in the values of the Boc-protected peptides after the incorporation of valine. The accuracy was increased, and due to this it was possible to observe on titration of the proline nos. 4 and 9 from the resin that a slight decrease was observed in a second titration, and then constant values in further titrations. The phenomenon must evidently be due to the presence of two adjacent prolines, the N-terminal with a free amino group. It has not been possible to explain this phenomenon, which, however, does not prohibit the coupling reaction.

By reducing the number of treatments by carrying out the titration on withdrawn samples, a further increase to 89% in the total yield of the resin-bound peptide was achieved (Fig. 4) [13]. Here also the abnormality was observed on titration of the two above-mentioned proline residues. By reduction of the number of treatments by the automatically performed synthesis, and using an all-glass reactor, total yields of the same order were obtained by automatic synthesis of other peptides.

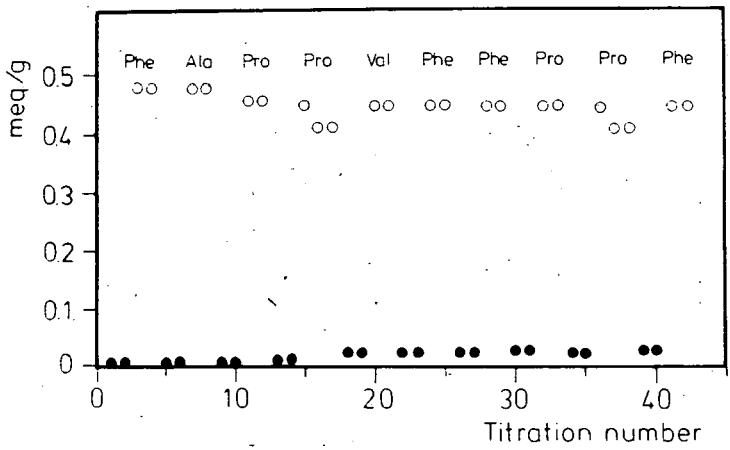

Fig. 4. Titration values on withdrawn samples obtained during the chain elongation in the synthesis of antamanide carried out from the C-terminal Phe (left) to the N-terminal Phe (right). The ordinate values are the numbers of meq calculated per g of Boc-Phe-O-resin. Filled circles before, and open circles after Boc group cleavage [13].

Acetic acid is only removed with difficulty from the resin, and thus could cause terminations by acetylation. Amino acid analysis of the final products, however, indicates that the gradual decrease must be due at least mainly to loss of peptide, resin-bound or cleaved from the resin (Fig. 5).

By replacing proline in position 4 from the resin with leucine, it was ascertained that the increase in the titration values of the Boc-protected peptides was due to proline in this position, as no increase occurred [26]. In a synthesis using ^{3}H-labelled

proline in the same position and ^{14}C-labelled phenylalanine as N-terminal, a binding by alkylation of the proline residue to residual chloromethyl groups on the resin could be demonstrated. As the resulting tertiary amine can be protonated, the apparent increase in the titrations of the Boc-protected peptides was explained and also why the coupling was inhibited to the same extent as the increase in the titration value [27].

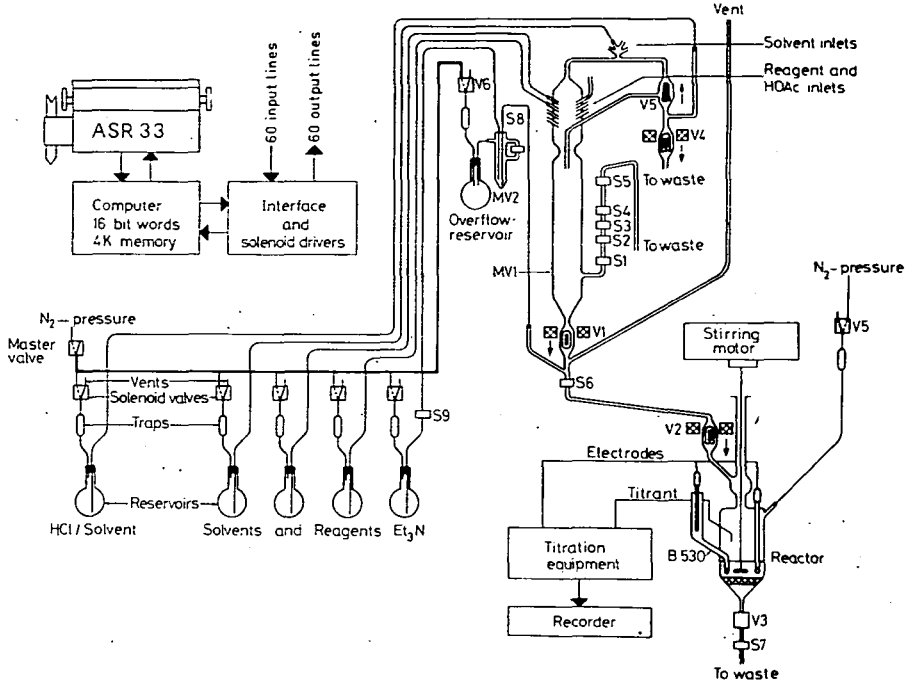

Fig. 5. Schematic drawing of the solid-phase peptide synthesizer. MV1 and MV2, metering vessels; S1 through S9, liquid detectors; V1 through V4, solenoid valves; V5 valve operated by fluid pressure in the line. → indicates flow direction for open valve [30].

The esterification of the first amino acid to the resin was carried out according to LOFFET [28], using the tetramethylammonium salt of Boc-Phe, which leaves some chloromethyl groups intact. If the later-published esterification procedure of GISIN [29], using the cesium salt of Boc-phenylalanine, had been used, no residual chloromethyl groups would have been present, and we would have missed an interesting experiment.

The cleavage of the Boc groups was originally assumed to proceed without difficulties. However, various authors have reported that difficulties may occur. In our laboratory we have experienced that the cleavage of the Boc group from resin-bound phenylalanine with N HCl/HOAc was incomplete after 30 min at 20°, but complete at 25° [30].

Observations like this stress the importance of a quantitative controlling of every step in a solid-phase synthesis. Perchloric acid titration has also been used to monitor

syntheses carried out by other means of coupling than by DCC: thus, by condensation with o-nitro-phenylsulfenyl-protected N-carboxyanhydrides or activated esters, provided, of course, that the protection group does not allow protonation and is stable under the conditions of the titration procedure [31].

None of the methods used for a quantitative analysis on the total amount of resin-bound peptides are specific for amino groups. Thus, as mentioned above, the imidazole group of Boc-benzyl-histidine is also titrated, leading to an equivalent increase in the titration value [22].

The discussion of monitoring solid-phase syntheses will not be ended without mentioning the possibility of achieving this through a color change of the resin due to coupling and deprotection. Using quite another synthetic procedure than in the solid-phase peptide synthesis, namely by forming an active ester on the resin and letting this react with a carboxyl-protected amino acid or peptide, GUARNERI *et al.* obtained a color shift from yellow to green [32]. A prerequisite is that the reaction proceeds uniformly throughout the resin beads if the color change is to be measured by light reflection. If so, the principle may be applied in solid-phase synthesis, provided the use of a suitable colored protection group is feasible.

As previously mentioned, one of the interesting aspects of the solid-phase synthesis is the possibility of automation, due to the fact that the isolation of the resin-bound product can be carried out by simple filtration. We succeeded some years ago in developing a system in which the coding for the process was performed on punched tape [33, 34]. The control unit was based on sequential logics, which means that a return signal must be received making sure that a function has been carried out properly, before the next code can be read. Electronically, this is achieved through the use of electronic gates, here as integrated circuits. An alarm system paralyses the equipment if errors should occur in the function of the system.

It is possible to code for an entire synthesis. The system can initiate the function of analytical units as a titrator, but is incapable of evaluating analytical data, and consequently no change of a predetermined sequence of operations can take place automatically. The first prototype was ready in 1967, and the equipment marketed by Schwarz Bioresearch in 1969.

The control unit used in the original system is today outdated by a computer. The diagram shows the construction of the system at present in use in our institute, in which a minicomputer with an 8 K 16-bit core memory is used as a control unit (Fig. 5) [30]. As in the original system, the liquid is transported by nitrogen pressure in individual tubings, excluding the possibility of contamination.

The use of a computer as control unit has several advantages: a higher reliability of the electronics and flexibility for attachments of accessories such as analytical units, and an automatic evaluation of the analytical data leading to automatic decisions for the course of the synthesis. As an advantage it must also be considered that a complete print-out of the entire synthesis is obtained (Fig. 6). The coding for the synthesis is read via the teletype into the computer and checked for valid input. A letter indicates the proper function, and numeral the additional parameter. Thus, for example, in X2, the X means stirring, and 2 means for two minutes.

In the now further-developed system [35, 36] the titration is controlled by the computer. Automatic calculations are carried out on analytical data, and comparison is made with preceeding results. It is made possible by the programming to take a progressive change of value, such as a decrease due to cleavage of peptide from the

resin, into consideration in the comparisons. If more than one titration of a coupling or deblocking cycle is desired, the computer makes a comparison between consecutive titration values, and if a preset deviation is exceeded, the titration will be repeated until the last two obtained values are within the preset limit for deviation. To limit the number of titrations, if stability is not obtained, for example by increasing values due to cleavage of a protection group, the procedure is brought to an end after a preset number of titrations after a coupling or deblocking.

If the value for titration is accepted, and the comparison with the value after a previous coupling or deblocking is accepted, the synthesis will be continued according to the information on the punched tape. If the result of the titration leads to a repeating of the coupling or the deblocking cycle, this will be performed according to information stored in the computer during the last performed cycle. Thus, a stepwise feed-back system for process control is obtained through the described system (Fig. 7).

```
VI  03568          START POTENTIAL (MV) :   +3.800000E+02
                   LAST POTENTIAL  (MV) :   +4.310000E+02
                   ADDED TITRANT   (ML) :   +1.300000E-01
                   MEQ                  :   +7.867600E-03
                   MEQ/G                :   +5.377606E-03
          00008    TERMINATED BY SHUT OFF TIME
YI  03576  00000
AI  03576  00001
X4  03577  00003
YI  03580  00000
AI  03580  00001
X4  03581  00003
YI  03584  00000
/2  03584  00000

#1  03584  00000
AI  03584  00001
X4  03585  00003
YI  03588  00000
AI  03588  00001
W0  03589  00001
AI  03590  00000
X4  03590  00003
X2  03593  00002
YI  03595  00000
AI  03595  00001
X4  03596  00003
YI  03599  00000
AI  03599  00001
X4  03600  00003
YI  03603  00000
BI  03603  00001
X4  03604  00003
YI  03607  00000
BI  03607  00001
X4  03608  00003
YI  03611  00000
BI  03611  00001
X4  03612  00003
YI  03615  00000
BI  03615  00001
AI  03616  00000
VI  03616          START POTENTIAL (MV) :   +3.260000E+02
                   LAST POTENTIAL  (MV) :   +4.450000E+02
                   ADDED TITRANT   (ML) :   +1.900000E-01
                   MEQ                  :   +1.149880E-02
                   MEQ/G                :   +7.859578E-03
          00008    TERMINATED BY SHUT OFF TIME
                   TITR. ACCEPTED (MEQ) :   +9.683200E-03
                   COUPLING ACCEPTED
```

Fig. 6. Print-out from two titration cycles after removal of the Boc group. The three columns indicate: The code, total elapsed time, and duration of the single functions, both in minutes

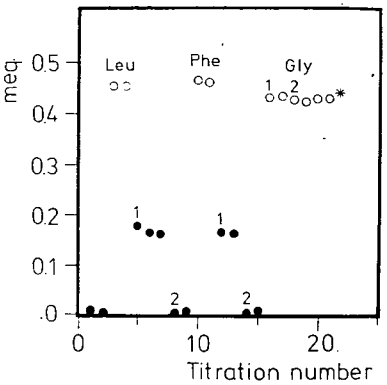

Fig. 7. Example of automatic decisions of the synthesizer. Preset value for deprotection: 0.470 (+0.015, −0.020) meq, allowing a slight decrease during the synthesis. Preset value for the coupling: 0.003±0.010. The last accepted mean value is used for comparison with the succeeding value for deprotection or coupling. Allowed deviation of titration values: 0.005 meq.

Only 75% of the theoretical amounts of Boc-amino acids and DCC are used leading to repetition of the coupling procedure for Boc-Leu and Boc-Phe. Too low value of deprotection of BocGly leads to a repetition of deprotection procedure. Finally, titration values are accepted, but too low mean value leads to interruption of the synthetic procedure. Two washings with methylene chloride, however, are performed to avoid damage until a new command is given to the synthesizer.

Filled circles before, and open circles after Boc-group cleavage. Paralysation.

3. Measurements on the liquid phase

However, it is desirable to have continuous information about the course of the single reactions. A principle for this, based on measurements of absorption in the ultraviolet region, was introduced by GUT and RUDINGER [37], and later used by BIRR [38], who developed an interesting reactor in which the liquid phase is circulated by centrifugation and monitoring is performed on the circulating fluid. The pathway of the flow cell is 0.5 mm.

Such a system provides the use of UV-absorbing protection groups and spectral stability of the dissolved components. The measurements must, if usable in practice, be performed at concentrations optimal for the synthesis. Such indirect measurements must always be considered with caution, as measurements on the liquid phase do not always exactly reflect what happens inside the resin. In spite of the mentioned reservations, such continuous non-destructive monitoring will certainly be of great value for optimizing solid-phase synthesis, as it will render information about the time-course of the single reactions and also about the distribution of the dissolved components between the interior of the resin and the sorrounding liquid, which may tell us about changes in the resin such as swelling.

To be able to operate at concentrations optimal for the synthesis, it is necessary in practice (due to the often high specific molar extinction of the amino acid derivatives) to use a flow cell with as small a light pathway as 0.03 mm. An experimental set-up with such a cell, using either a peristaltic pump or a reiprocating system, has been used for preliminary experiments. Further experiments must be performed to investigate whether the stepwise control by titration can be replaced by a continuous indirect method of monitoring on the circulating fluid. As mentioned above, however, we consider such a system as being of great interest.

Concluding remarks

The analytical methods at hand have proved valuable in the synthesis of shorter chains, especially by the solid-phase technique. It is to be expected that improvements of the analytical technique for both solid-phase synthesis and synthesis in solution will take place, hopefully also regarding control of racemization.

In the further investigation of the solid-phase technique, special attention has to be directed to a very important point, namely whether it is possible to improve the properties of the polymeric support.

The usually much longer coupling times in solid-phase synthesis of shorter peptides compared to synthesis in solution indicate that much could be gained through improvement. Hitherto, resins of the polystyrene type have been used almost exclusively, but other types of polymers have to be considered, such as polyacrylamide as proposed by ATHERTON and SHEPPARD [39].

In the synthetic reactions common to synthesis on a polymeric support and in solution, the fundamental problem has not been solved, namely the invention of a coupling reaction leading to 100% yield by a specific reaction between the α-amino group and the α-carboxyl group, thereby avoiding the use of covalently-bound protecting groups in the side-chains. As a matter of fact, the huge amount of work dedicated to invention of new protecting groups, purification and characterization procedures, has only been needed because no ideal coupling procedure is at hand. Will the problem be completely solved by imitation of nature, using components such as nucleic acids and enzymes? We do not know.

In Denmark we have a common phrase saying that it is difficult to prophesy — especially about the future — because it is no longer what is used to be. My personal opinion is that organic chemical synthesis of peptides in the forseeable future will be used for the synthesis of peptides of moderate chain length, and of course for the preparation of peptides with unusual structures, such as peptides labelled with isotopes in specific positions, or with a content of D-amino acids. However, for the synthesis of long peptide chains containing the usual protein-bound amino acids, quite another procedure may be the method of choice, namely genetic engineering, whereby genetic material is introduced into microorganisms, forcing them to synthesize special compounds. The increasing knowledge of the system for biosynthesis in the microorganism and the recent achievements in polynucleotide synthesis seem to justify great expectations for this technique. The synthesis of a complete gene for a tyrosine transfer RNA precursor from Escherichia coli by KHORANA and coworkers is certainly a strong impetus for the further exploitation of the possibilities for industrial production based on genetic engineering [40].

The reason for the rapid progress in the synthesis of polynucleotides is that in polynucleotide synthesis, in contrast to the synthesis of peptides, it is possible to combine non-protected fragments enzymatically in aqueous solution. The most important limiting factor in the synthesis of polynucleotides just now is the tedious preparation of the fragments, *i.e.* oligonucleotides. These are at present prepared by organic chemical synthesis in an organic medium. It would therefore mean a significant improvement, if an automated procedure were at hand. Various laboratories have investigated the possibility of carrying out the synthesis of oligonucleotides with the solid-phase technique, using the same type of resin ordinarily used in the synthesis of peptides, namely crosslinked polystyrene. The results however, have,

been negative. Recent experiments have nevertheless indicated that resin of the polyacrylamide-type are more advantageous [41]. Experiments carried out in our laboratory have confirmed this observation, as in the synthesis of pentathymidine-tetraphosphate it has been possible to obtain yields by the coupling of the single nucleotides of 84—90% [42]. We are therefore pursuing our efforts and hope that they will result in an automated synthesis of oligonucleotides based on the principles for automation already developed for the synthesis of peptides.

The initial studies of condensation of nucleotides to oligonucleotides were inspired by the achievements of the organic synthesis of peptides. It is indeed fascinating to realize that historically the experiment of CURTIUS in 1882 is thus linked to the modern understanding of the basic function of living matter.

References

[1] *Curtius, T.:* J. Prakt. Chem. **26,** 145 (1882).
[2] *Fischer, E.:* Berichte **40,** 1754 (1907).
[3] *Ryle, A. P., F. Sanger, L. F. Smith, R. Kitai:* Biochem. J. **60,** 541 (1955).
[4] *Meienhofer, J., E. Schnabel, H. Bremer, O. Brinkhoff, R. Zabel, W. Sroka, H. Klostermeyer, D. Brandenburg, T. Okuda, H. Zahn:* Z. Naturforsch. **186,** 1120 (1963).
[5] *Kung, Y., et al.:* Scientia Sinica **14,** 1710 (1965).
[6] *Merrifield, R. B.:* J. Amer. Chem. Soc. **85,** 2149 (1963).
[7] *Letsinger, R. L., M. J. Kornet:* J. Amer. Chem. Soc. **85,** 3045 (1963).
[8] *Sakakibara, S., Y. Kishida, K. Okuyama, N. Tanaka, T. Ashida, M. Kahudo:* J. Mol. Biol. **65,** 371 (1972).
[9] *Bayer, E., H. Eckstein, K. Hägele, W. A. König, W. Brünig, H. Hagenmaier, W. Parr:* J. Amer. Chem. Soc. **92,** 1735 (1970).
[10] *Hirt, J., E. W. B. de Leer, H. C. Beyerman:* The Chemistry of Polypeptides, Plenum Press, New York, 1973. pp. 363.
[10a] *Brunfeldt, K.:* In Peptides, 1972, North-Holland and American Elsevier Publishing Companies, Amsterdam—London and New York 1973, pp. 141.
[11] *Kaiser, E., R. L. Colescott, C. D. Bossinger, P. I. Cook:* Anal. Biochem. **34,** 595 (1970).
[12] *Felix, A. M., M. H. Jimenez:* Anal. Biochem. **52,** 377 (1973).
[13] *Schou, O.:* Acta Chem. Scand. **B 30,** 991 (1976).
[13a] *Udenfried, S., S. Stein:* In Peptides, Proc. 5th Amer. Pept. Symp., John Wiley and Sons, 1978, pp. 14.
[13b] *Burgus, R., J. Rivier:* In Peptides, 1976, Editions de l'Université de Bruxelles, Bruxelles, 1976, pp. 85.
[14] *Merrifield, R. B.:* Biochemistry **3,** 1385 (1964).
[15] *Bayer, E., G. Young, H. Hagenmaier:* Tetrahedron 4853 (1968).
[16] *Dorman, L. C.:* Tetrahedron Letters 2319 (1969).
[17] *Gisin, B. F.:* Anal. Chim. Acta **58,** 248 (1972).
[18] *Hodges, R. S., R. B. Merrifield:* Anal. Biochem. **65,** 241 (1975).
[19] *Brunfeldt, K., P. Roepstorff, J. Thomsen:* Acta Chem. Scand. **23,** 2906 (1969).
[20] *Brunfeldt, K., T. Christensen, P. Villemoes:* FEBS Letters **22,** 238 (1972).
[21] *Villemoes, P., T. Christensen, K. Brunfeldt:* Hoppe-Seyler's Z. Physiol. Chem. **357,** 713 (1976).
[22] *Schou, O., K. Brunfeldt, I. Rubin, L. Hansen:* Hoppe-Seyler' s Z. Physiol. Chem. **356,** 1451 (1975).
[23] *Brunfeldt, K., T. Christensen:* FEBS Letters **19,** 345 (1972).
[24] *Brunfeldt, K., T. Christensen, P. Roepstroff:* FEBS Letters **25,** 184 (1972).
[25] *Roepstorff, P., K. Brunfeldt:* FEBS Letters **21,** 320 (1972).
[26] *Brunfeldt, K., D. Bucher, T. Christensen, O. Schou, I. Rubin:* in Peptides 1974, John Wiley and Sons, New York and Israel Universities Press, Jerusalem, 1975. pp. 227.
[27] *Schou, O., D. Bucher, E. Nebelin:* Hoppe-Seyler's Z. Physiol. Chem. **357,** 103 (1976).
[28] *Loffet, A.:* Int. J. Protein Res. **3,** 297 (1971).
[29] *Gisin, B. F.:* Helv. Chim. Acta **56,** 1476 (1973).

[30] *Villemoes, P., T. Christensen, K. Brunfeldt:* Hoppe-Seyler's Z. Physiol. Chem. **357**, 713 (1976).
[31] *Halström, J., T. Christensen, K. Brunfeldt:* Hoppe-Seyler's Z. Physiol. Chem. **357**, 999 (1976).
[32] *Guarneri, M., R. Ferroni, G. Giori, C. A. Benassi:* in Chemistry and Biology of Peptides, Ann Arbor Science Publishers Inc., Ann Arbor, Michigan, 1972. pp. 213.
[33] *Brunfeldt, K., P. Roeptsorff, J. Halström:* U. S. Pat. 3.557.077, filed 1967, granted 1971.
[34] *Brunfeldt, K., J. Halström, P. Roepstorff:* Acta Chem. Scand. **23**, 2830 (1969).
[35] *Villemoes, P., T. Christensen, K. Brunfeldt:* to be published.
[36] *Christensen, T., P. Villemoes, K. Brunfeldt:* in Peptides, Proc. 5th Amer. Pept. Symp., John Wiley and Sons, 1978, pp. 569.
[37] *Gut, V., J. Rudinger:* in Peptides 1968, North Holland Publ. Co. Amsterdam, 1968. pp. 185.
[38] *Birr, C.:* in Peptides 1974, John Wiley and Sons, New York and Israel Universities Press, Jerusalem, 1975. pp. 117.
[39] *Atherton, E., R. C. Sheppard:* in Peptides 1974, John Wiley and Sons, New York, and Israel Universities Press, Jerusalem, 1975, pp. 123.
[40] *Belegaje, R., E. L. Brown, N. J. Fritz, M. J. Gait, R. G. Lees, K. E. Norris, T. Sekiya, T. Takeya, R. Contreras, H. Küpper, M. J. Ryan, H. G. Khorana:* Advances in Techniques used in Nucleoside and Nucleotide Chemistry ACS Series Academic Press New York, in press.
[41] *Gait, M. J., R. C. Sheppard:* Nucleic Acids Research 4, 1135 (1977).
[42] *Narang, C. K., K. Brunfeldt, K. L. E. Norris:* Tetrahedron Letters 1819 (1977).

ЗАМЕЧАНИЯ ПО ПОВОДУ АНАЛИЗА СИНТЕТИЧЕСКНХ ПЕПТИДОВ

К. Брунфельдт

Существует три принципиальных возможностей для аналитического контроля эффективности степени связывания и освобождения функциональных групп в процессе твердофазного синтеза пептидов: 1) анализ образцов; 2) определение количества образовавшихся полипептидных связей; 3) измерения в жидкой фазе. Эти три разных метода обсуждаются подробно.

MATHEMATICAL MODELLING OF A CONTINUOUS SETTLING APPARATUS

S. KATONA and P. FEJES
Applied Chemistry Department, József Attila University,
Szeged, Hungary

(Received September 28, 1977)

Initiated by the need to produce quartz-free bentonite as a filler substance for machine greases, the mathematical model of a continuously-operating settling apparatus has been elaborated, together with a computer programme to evaluate experimental data and compare them with the theoretical ones. Though the experimental flow pattern deviates to various extents from the ideal laminar flow used in the theoretical approach, the granulometric curves measured and computed on the product agree fairly well. The method described can be used for modelling and optimization of continuous settlers.

Bentonite is one of the most frequently occurring clay minerals; it is widely used in both its original and its modified, organophilic form in many fields of industry (food, textile, pharmaceutical, varnish and paint industries). Its role in oil production is gaining in importance, particularly in deep drilling.

Our task was to investigate the experimental possibilities of producing quartz-free bentonite as a filler for the production of machine greases by settling.

The experiments were carried out in a continuously-operating settling apparatus. The settling was desired to produce a fraction with radius under 2 μm which, as has been shown in separate experiments, is free of quartz. For the evaluation of the experimental data and the mathematical modelling of the apparatus a simplified model of the settling process was considered.

Principle of calculation

Let it be supposed that a liquid containing solid particles is flowing laminarly as a layer of thickness L on top of a static bulk liquid, as shown in Fig. 1. Within the layer the linear rate of flow decreases from its maximum value $v(L) \equiv v_{max}$ at L to $v(0) \equiv 0$ at $L=0$; accordingly, the path of a solid particle entering the continuous settler at ($h=0$, $l=L$) will be a parabola as long as the settling takes place in the moving medium, and a straight line, normal to the direction of flow, in the static bulk. If the overflow is taken only from the moving layer, a residence time $t^*(r)$ can be defined for every particle with radius r by

$$t^*(r) \equiv \frac{L}{v_{sed}(r)} \tag{1}$$

where v_{sed} is the rate of sedimentation, characterized by the following property: if the settling time t as determined by the applied input flow rate and the size of the settling apparatus is equal to or greater than $t^*(r)$, *i.e.* $t \geqq t^*(r)$, then the particle will settle; otherwise it leaves the settler in the overflowing liquid.

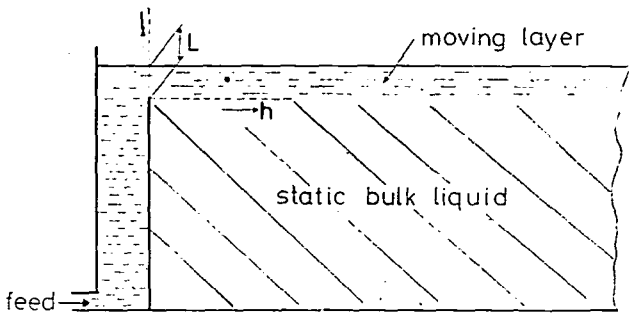

Fig. 1. Sketch of the settling apparatus

Now, in possession of the density function of the particle size distribution, $f(r)$, for the original suspension and assuming ideal functioning of the settler, it would be a very simple task to find the particle size distribution of the suspension in the overflowing liquid and that remaining in the settler as well. It can easily be shown that, taking the mean residence time $\bar{t}$ of the flow

$$\bar{t} = \frac{H \cdot L \cdot a}{w} \tag{2}$$

where H is the length,
a is the width of the settler and
w is the volumetric flow rate,
a sedimentation rate $\bar{v}_{sed}(r)$ and hence a particle radius $\bar{r}$ may be obtained *via* equ. (1). Particles having radii equal to or greater than $\bar{r}$ will settle, while the others will leave the settler. In non-interacting suspensions the rate of sedimentation $v_{sed}(r)$ is described best by Stokes' law [1].

Unfortunately, the density function of the residence time of flow in real settling apparatus, $E(t)$, deviates to various extents from that valid for ideal laminar conditions because the actual flow pattern is never free of small backward currents:

$$E(t) \neq E(t)_{id} \equiv \frac{2t_0^2}{t^3} \quad (t \geqq t_0)$$

where $t_0 \equiv \frac{L}{v_{max}}$ is the time necessary to reach the end of the settler with the maximum flow rate. Additionally, the input and output of the suspension correspond only approximately to the conditions set at the beginning. To overcome this difficulty the distribution of the residence time should be determined empirically. However, this semiempirical approach becomes so complicated that actual calculations have to be carried out using a computer.

Experiments and calculations

The experiments and calculations were performed according to the scheme shown in Fig. 2.

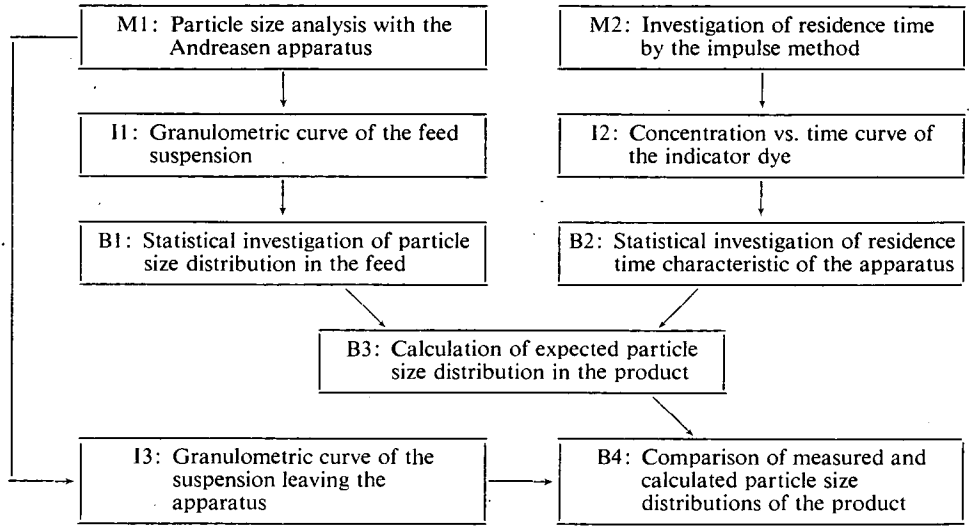

Fig. 2. Flow sheet

The flow-sheet contains the segments of the computer programme (B1, B2, B3, B4), the blocks of the input data (I1, I2, I3) and the symbolic blocks of the experimental methods (M1, M2).

As may be seen from the Figure, the *experimental work* consisted of two steps: *analysis of the particle size distribution* of the suspension fed into and leaving the apparatus, and the fluid mechanical description of the apparatus.

The granulometric curves $(Y_g(r))$ of the suspensions (I1, I3) were measured by means of Andreasen's static settling apparatus (M1) [2]. In block B1 the particle size distribution is calculated from the granulometric curves by the equation:

$$Y(r) = 1 - Y_g(r).$$

The density function of the particle size distribution according to mass, $f(r)$, is determined by numerical derivation, applying the Douglass—Avakian method [3]. (The Douglass—Avakian procedure fits a fourth-degree polynomial to seven points of a curve by the method of least squares and takes the derivative analytically.)

The *fluid mechanical study* of the apparatus comprised the other part of the experimental work. By measuring the residence time of the fluid flow, it was possible to determine empirically how closely the flow pattern in the apparatus approaches ideal laminar flow. For this purpose the impulse method was the most suitable (M2). Briefly, an aqueous solution of an appropriate dye (in our case erioglaucin A) is injected into the liquid at the place of input (the amount was M g), and the concent-

ration of the dye, $c(t)$, is measured in the overflowing fluid (I2). In segment B2 of the computer programme the calculation of the density function of the residence time distribution, $E(t)$, is carried out according to the formula:

$$E(t) \equiv \frac{w}{M} c(t).$$

The residence time distribution function, $G(t)$, is calculated by numerical integration according to the trapezoidal rule [3]:

$$G(t) = \int_{t_0}^{t} E(\tau)\, d\tau.$$

The mean residence time, $\bar{t}$, can also be calculated by numerical integration, applying Simpson's rule [3]:

$$\bar{t} = \int_{t_0}^{\infty} \tau E(\tau)\, d\tau.$$

By definition the average thickness of flow is calculated from equ. (2) using $\bar{t}$:

$$L = \frac{\bar{t} \cdot w}{H \cdot a}.$$

The time $t^*(r)$ necessary for particles with a radius between r and $r+dr$ to settle with a sedimentation rate v_{sed} in the moving layer can be calculated by means of Stokes' law:

$$t^* = \frac{9L\eta}{2r^2(\varrho_s - \varrho_f)g}$$

where ϱ_s is the density of the suspended solid particles,
ϱ_f is the density of the dispersion medium,
g is the gravitational constant,
η is the coefficient of internal friction of the medium.

In block B3, which is of key importance in the computer programme, the *expected* particle size distribution in the suspension leaving the apparatus is calculated.

The particles remaining in the flowing layer for time t, which is less than that needed to pass the distance L (*i.e.* $t < t^*$), will get into the fine fraction (product), their mass ratio* in it being $G(t^*) \cdot f(r)\, dr$. To obtain the total mass ratio in the overflow, this function has to be integrated numerically in some interval $(0, r_{max})$:

$$Q \equiv \int_{0}^{r_{max}} G(t^*(r)) \cdot f(r)\, dr.$$

The particles having an actual residence time $t \geqq t^*$ will leave the moving layer and settle in the static bulk liquid filling part of the settling channel. To get as good a value as possible for $G(t^*(r))$ at every point t^*, $G(t^*(r))$ is calculated most suitably by quadratic interpolation.

* The mass of suspension in unit mass of feed, both on a water-free basis.

The density function of the particle size distribution in the suspension leaving the settler, $\varphi(r)$, is determined by the relative mass of the fraction with particle sizes between r and $r+dr$:

$$\varphi(r) \equiv \frac{G(t^*(r))f(r)\,dr}{Q}.$$

An analogous calculation can be used for the determination of the particle size distribution for the suspension remaining in the apparatus.

The numerical integration of $\varphi(r)$ (*e.g.* using the trapezoidal rule) provides the particle size distribution function of the product:

$$\Phi(r) = \int_0^r \varphi(\tau)\,d\tau.$$

The granulometric curve is computed from:

$$\psi_g(r) \equiv 1-\Phi(r).$$

In the last segments of the computer programme, B4 and I3, the measured and calculated particle size distributions and the granulometric curves of the product are compared.

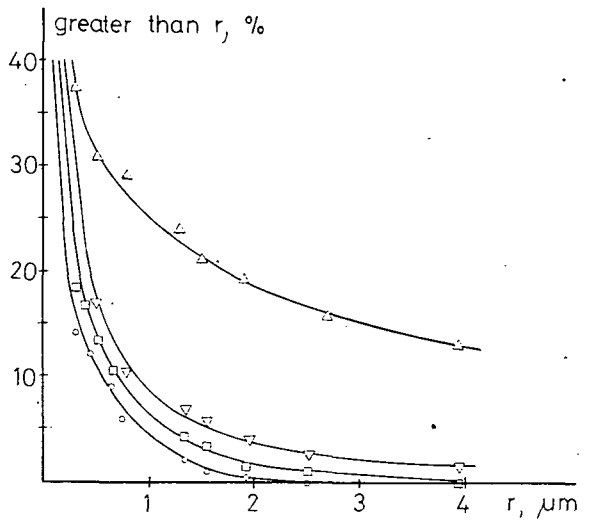

Fig. 3. Granulometric curves
of the suspension fed into and leaving the settler
—△—△—: suspension fed in
suspensions settled with various volumetric flow rates:
—▽—▽—: $w=4.66\cdot10^{-6}$ m^3 s^{-1}
—□—□—: $w=3.16\cdot10^{-6}$ m^3 s^{-1}
—○—○—: $w=1.08\cdot10^{-6}$ m^3 s^{-1}

Experimental results and their discussion

The experimental results are listed in Table I. It is seen from the accumulations in the settler at various flow rates that optimum separation could be achieved at the lowest input flow rate. The quality of fractionation is illustrated far more impressively in Fig. 3, where the granulometric curves of the product obtained at various flow rates are shown. In this fraction no quartz could be detected by X-ray or optical methods.

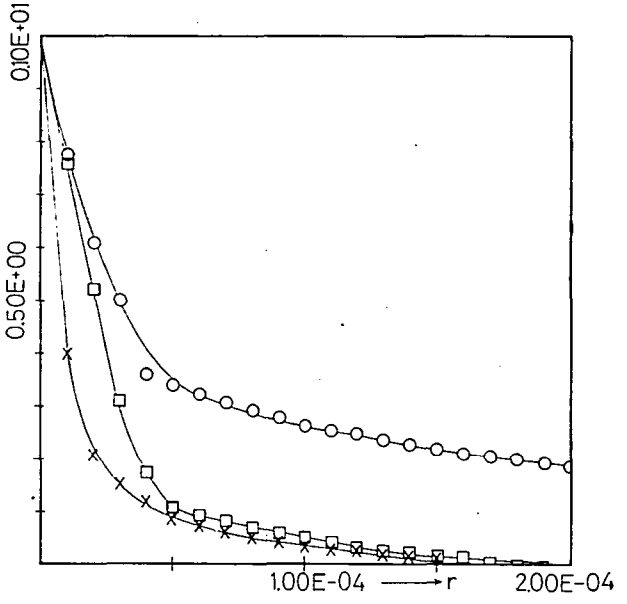

Fig. 4. Granulometric curves (results of the computerized approximation)
$w = 1.08 \cdot 10^{-6}$ m^3 s^{-1}
—○—○— : suspension fed in
—□—□— : calculated
—×—×— : measured

Figure 4 shows the results of the computerized approximation. The measured and calculated granulometric curves do not entirely coincide. This can be explained by the fact that the thickness of flow, L, as calculated from the mean residence time, $\bar{t}$, is an average value. In the calculation of the settling times t^* pertaining to the radii r of individual particles, *this* value was taken as the sedimentation height. As mentioned earlier, this is an idealized picture from which the true flow pattern in the apparatus shows considerable deviations. Nevertheless, the computerized approach is still statisfactory and can be used for the description of the settling process in a given apparatus.

The principle of calculation and the computer programme outlined above can be used for modelling similar settling problems, in the planning of settling apparatus, and for the optimization of the operational parameters of existing apparatus.

Table I

Experimental data

Volumetric flow rate [10^{-6} m^3 s^{-1}]	1.08	3.16	4.66
Mean residence time [s]	402.3	353.1	187.9
Mean thickness of flow [10^{-2}·m]	0.218	0.555	0.384
Reynolds number	42.34	116.2	175.0
Solid content of the suspension in the feed [10^{-4} kg m^{-3}]	1.006	1.006	0.926
Solid content of the suspension leaving the apparatus [10^{-4} kg m^{-3}]	0.766	0.826	0.805
Accumulation [10^{-4} kg m^{-3}]	0.240	0.180	0.121
Mass ratio leaving the apparatus [%]	76.1	82.1	86.9

References

[1] *Wolfram E.:* Kolloidika II/1. Egységes jegyzet (Colloid Chemistry II/1. University notes) Tankönyvkiadó Budapest 1969.
[2] *Batel, W.:* Einführung in die Korngrössenmesstechnik, Springer-Verlag Berlin 1971.
[3] *Sherwood, T. K., Reed, C. E.:* Applied Mathematics in Chemical Engineering, McGraw-Hill Book Co., Inc. New York 1939.

МАТЕМАТИЧЕСКОЕ МОДЕЛИРОВАНИЕ ОСАДИТЕЛЬНОГО ОБОРУДОВАНИЯ НЕПРЕРЫВНОГО ДЕЙСТВИЯ

Ш. Катона и П. Фейеш

Цель работы заключалась в получении суспензии бентонита без кварца, которая может использоваться в качестве наполнителя смазки. Разработана математическая модель непрерывного осадительного оборудования. Оценка результатов измерений, а так же их сравнение с рассчитанными данными были проведены на ЭВМ. Хотя экспериментально определенный характер потока различается более или менее от теоретически предполагаемого ламинарьного потока, измеренные и рассчитанные гранулометрические составы продукта довольно сходны. Описанный метод может использоваться для моделирования и оптималиэациия непрерывних осадительных оборудований.

INDEX

TOMI PRIORES

Acta Chemica, Mineralogica et Phyxica	Tom.	I,	Fasc.	1—2,	1928—29.
Acta Chemica, Mineralogica et Physica	Tom.	II,	Fasc.	1—2,	1932.
Acta Chemica, Mineralogica et Physica	Tom.	III,	Fasc.	1—3,	1934.
Acta Chemica, Mineralogica et Physica	Tom.	IV,	Fasc.	1—3,	1934.
Acta Chemica, Mineralogica et Physica	Tom.	V,	Fasc.	1—3,	1937.
Acta Chemica, Mineralogica et Physica	Tom.	VI,	Fasc.	1—3,	1938.
Acta Chemica, Mineralogica et Physica	Tom.	VII,	Fasc.	1—3,	1939.
Acta Chemica et Physica	Tom.	I,	Fasc.	1—2,	1942.
Acta Chemica et Physica	Tom.	II,	Fasc.	1—6,	1948—50.
Acta Physica et Chemica, Nova series	Tom.	I,	Fasc.	1—4,	1955.
Acta Physica et Chemica, Nova series	Tom.	II,	Fasc.	1—4,	1956.
Acta Physica et Chemica, Nova series	Tom.	II,	Fasc.	1—5,	1957.
Acta Physica et Chemica, Nova series	Tom.	IV,	Fasc.	1—2,	1958.
Acta Physica et Chemica, Nova series	Tom.	IV,	Fasc.	3—4,	1958.
Acta Physica et Chemica, Nova series	Tom.	V,	Fasc.	1—2,	1959.
Acta Physica et Chemica, Nova series	Tom.	V,	Fasc.	3—4,	1959.
Acta Physica et Chemica, Nova series	Tom.	VI,	Fasc.	1—4,	1960.
Acta Physica et Chemica, Nova series	Tom.	VII,	Fasc.	1—2,	1961.
Acta Physica et Chemica, Nova series	Tom.	VII,	Fasc.	3—4,	1961.
Acta Physica et Chemica, Nova series	Tom.	VIII,	Fasc.	1—2,	1962.
Acta Physica et Chemica, Nova series	Tom.	VIII,	Fasc.	3—4,	1962.
Acta Physica et Chemica, Nova series	Tom.	IX,	Fasc.	1—2,	1963.
Acta Physica et Chemica, Nova series	Tom.	IX,	Fasc.	3—4,	1963.
Acta Physica et Chemica, Nova series	Tom.	IX,	Fasc.	3—4,	1963.
Acta Physica et Chemica, Nova series	Tom.	X,	Fasc.	1—2,	1964.
Acta Physica et Chemica, Nova series	Tom.	X,	Fasc.	3—4,	1964.
Acta Physica et Chemica, Nova series	Tom.	XI,	Fasc.	1—2,	1965.
Acta Physica et Chemica, Nova series	Tom.	XI,	Fasc.	3—4,	1965.
Acta Physica et Chemica, Nova series	Tom.	XII,	Fasc.	1—2,	1966.
Acta Physica et Chemica, Nova series	Tom.	XII,	Fasc.	3—4,	1966.
Acta Physica et Chemica, Nova series	Tom.	XIII,	Fasc.	1—2,	1967.
Acta Physica et Chemica, Nova series	Tom.	XIII,	Fasc.	3—4,	1967.
Acta Physica et Chemica, Nova series	Tom.	XIV,	Fasc.	1—2,	1968.
Acta Physica et Chemica, Nova series	Tom.	XIV,	Fasc.	3—4,	1968.
Acta Physica et Chemica, Nova series	Tom.	XV,	Fasc.	1—2,	1969.
Acta Physica et Chemica, Nova series	Tom.	XV,	Fasc.	3—4,	1969.
Acta Physica et Chemica, Nova series	Tom.	XVI,	Fasc.	1—2,	1970.
Acta Physica et Chemica, Nova series	Tom.	XVI,	Fasc.	3—4,	1970.
Acta Physica et Chemica, Nova series	Tom.	XVII,	Fasc.	1—2,	1971.
Acta Physica et Chemica, Nova series	Tom.	XVII,	Fasc.	3—4,	1971.
Acta Physica et Chemica, Nova series	Tom.	XVIII,	Fasc.	1—2,	1972.
Acta Physica et Chemica, Nova series	Tom.	XVIII,	Fasc.	3—4,	1972.
Acta Physica et Chemica, Nova series	Tom.	XIX,	Fasc.	1—2,	1973.
Acta Physica et Chemica, Nova series	Tom.	XIX,	Fasc.	3,	1973.
Acta Physica et Chemica, Nova series	Tom.	XIX,	Fasc.	4,	1973.
Acta Physica et Chemica, Nova series	Tom.	XX,	Fasc.	1—2,	1974.
Acta Physica et Chemica, Nova series	Tom.	XX,	Fasc.	3,	1974.
Acta Physica et Chemica, Nova series	Tom.	XX,	Fasc.	4,	1974.
Acta Physica et Chemica, Nova series	Tom.	XXI,	Fasc.	1—2,	1975.
Acta Physica et Chemica, Nova series	Tom.	XXI,	Fasc.	3—4,	1975.
Acta Physica et Chemica, Nova series	Tom.	XXII,	Fasc.	1—4,	1976.
Acta Physica et Chemica, Nova series	Tom.	XXIII,	Fasc.	1,	1977.
Acta Physica et Chemica, Nova series	Tom.	XXIII,	Fasc.	2—3,	1977.

A kiadásért felelős: Dr. Tandori Károly
1977
A kézirat nyomdába érkezett: 1977. október. Megjelenés 1978.
Példányszám: 550. Ábrák száma 57. Terjedelem: 14 (A/5) ív
Készült monószedéssel, íves magasnyomással, az MNOSZ 5601—50/A szabványok szerint
77-4608 — Szegedi Nyomda — Felelős vezető: Dobó József igazgató